Low Temperature Spectroscopy of Photosystem II in Higher Plants

A thesis submitted for the degree of
Doctor of Philosophy of the
Australian National University

Lesley Debono

June 2009

Declaration

The work described in this thesis is my own, except where otherwise stated. None of my own work described in this thesis has been submitted for any other degree.

Lesley Debono

June 2009

Acknowledgements

I am grateful to the Australian National University for providing my PhD scholarship and making this research possible.

My sincerest appreciation goes to my supervisor Elmars Krausz for his guidance, patience and enthusiasm throughout my PhD candidature.

I am indebted to the Krausz group post-docs, students and staff for their invaluable assistance and friendship over the years, including: Barry, Sindra, Joe, Ronald, Keith, Maria and Peter. Thanks also to the extended 'PSII family' at ANU including all the members of the Pace and Wydrzynski research groups and overseas visitors with whom I have had the pleasure of interacting, both academically and personally.

Special thanks to Paul Smith for generously providing PSII samples and Ronald Steffen for help with the CCD spectrometer and copious feedback on the thesis (even while on the opposite side of the planet!)

I would not have made it without the love and support of my family and friends who have endured this journey with me. My heartfelt gratitude goes out to all of you.

Finally, to Krisztian and David thanks for all the coffees; although I look forward to catching up for a cuppa somewhere other than the RSC tea-room for a change!

"Success is the ability to go from one failure to another with no loss of enthusiasm." - Sir Winston Churchhill

Abstract

Photosystem II (PSII) is an assembly of several proteins responsible for harvesting light energy and splitting water to dioxygen in cyanobacteria, algae and higher plants. In this thesis, PSII enriched membrane (PEM) samples prepared from spinach were studied by low temperature (1.7 – 5 K) absorption and MCD spectroscopy.

The factors affecting sample optical quality were investigated from a theoretical point of view. Based on theory, work was done to develop practical methods to ensure PEM samples of high optical-quality were prepared so as to produce reproducible and high quality absorption data from spectra obtained at low temperature.

Cytochrome b_{559} (cyt b_{559}) is an important subunit of the photosystem II complex. A new methodology was developed to accurately quantify cyt b_{559} in PEM samples. For the first time, the spectroscopic technique of MCD was used to confirm that sodium dithionite treatment reduced all cyt b_{559} in PEM samples.

Illumination-induced difference spectra of PEM samples were studied. Illumination of PSII samples at cryogenic temperature is understood to result in the formation of a stable charged quinone species Q_A^- which electrochromically shifts the spectra of pigments in its vicinity.

The apparent variability of illumination-induced difference spectra in PEM samples was found to be artefactual and dependent on the stability of spectrometers utilised to obtain the spectra as well as sample quality. Improvements in spectrometer stability and sample preparation techniques allowed the determination of an illumination-induced difference spectrum free from artefacts. Calculations simulating the effect of Q_A^- on the pigments in PSII were performed to show how the difference

spectrum could be due to the shift of the spectra of all the pheophytin and chlorophyll pigments in the reaction centre (D1 and D2 proteins) of PSII. This result differs from similar analyses performed in the literature previously.

A novel transient feature was discovered in the PEM illumination-induced difference spectrum under certain illumination conditions and was hypothesised to be due to the formation of P_{680}^{+}. This hypothesis was evaluated by comparing experimental data to a model of the kinetics of the electron transfer processes that occur upon low temperature illumination of PSII.

List of Commonly Used Abbreviations and Symbols

ANU	Australian National University
ATP	adenosine triphosphate
Car	beta-carotene
CCD	charge-coupled device
Chl	chlorophyll
Cont	continuous illumination
cyt	cytochrome
D	secondary donor of PSII
D1/D2	the proteins comprising the reaction centre of PSII (subscript denotes pigment in relevant protein, e.g $Pheo_{D1}$ is the pheophytin in D1)
$\Delta\alpha$	the change in polarisability between the ground and excited state
ΔA	difference in absorbance
DDM	n-dodecyl β-D-maltoside
$\boldsymbol{E}_{eff}$	effective electric field vector
ε_{eff}	effective dielectric constant
EG	ethylene glycol
EPR	electron paramagnetic resonance
FWHM	full width at half-maximum
Gly	glycerol
HeNe	helium neon
HL	high-light illumination
LL	low-light illumination
MCD	magnetic circular dichroism
NADPH	nicotinamide adenine dinucleotide phosphate
OD	optical density
OEC	oxygen-evolving complex

P_{680}	primary electron donor in PSII
PEM	PSII enriched membrane fragment
Pheo	pheophytin
PSII	photosystem II
Q band	Low energy transition in chlorin-type pigments
Q_A / Q_B	plastoquinones in PSII
Q_x / Q_y	orthogonal components of the Q band along the x and y axes of the chlorin ring
RC	PSII reaction centre (the D1 and D2 proteins)
S/N	signal-to-noise
TDM	transition dipole moment
THDS	transient high-light difference spectrum
Y_Z / Y_D	tyrosine Z / tyrosine D
$\Delta\mu$	difference in ground state and excited state dipole moments

Chapter 1: Introduction

1.1 Photosynthesis

1.1.1 Significance

"Plants do photosynthesis, a complicated process, and without plants, we'd all be dead." – Professor Pamela C. Ronald

Photosynthesis is a process by which organisms convert solar energy into chemical energy. Photosynthetic organisms efficiently harness solar energy for their own growth and reproduction and simultaneously provide sustenance for virtually all other non-photosynthetic life-forms. The first organisms capable of oxygenic photosynthesis arose about 2.5 billion years ago. Over millions of years they have drastically altered the biosphere by shifting the atmosphere from a reducing to an oxidising regime and have thus profoundly affected the evolution all other life-forms on the planet.[1]

Considering the fundamental importance of photosynthesis to life and particularly the quality of life of humans, it is not surprising that scientists from many disciplines are interested in understanding the fundamental mechanisms of photosynthesis.

Elucidation of the molecular basis of photosynthesis has many current and potential practical applications. This understanding is, for example, inspiring synthetic chemists to create artificial assemblies based on the morphology of natural photosynthetic systems. This so-called artificial photosynthesis is currently an active area of research.[2-7]

A useful working definition of photosynthesis is that it "is a process in which light energy is captured and stored by an organism, and the stored energy is used to drive cellular processes."[1] The most common form of photosynthesis involves chlorophyll-type pigments and is carried out by oxygen-evolving species including higher plants, algae and cyanobacteria and non oxygen-evolving bacteria. Unless otherwise specified,

the processes described in this chapter are for higher plants as this work has been exclusively based on samples sourced from this class of organism.

1.1.2 General Overview of Oxygenic Photosynthesis

The overall reaction carried out by oxygenic photosynthesis can be elegantly summarised as follows:

$$n\mathrm{CO_2} + n\mathrm{H_2O} + \text{light} \longrightarrow (\mathrm{CH_2O})_n + n\mathrm{O_2}$$

where $(CH_2O)_n$ is a generic representation of carbohydrates.[†] The process is much more complicated than implied from the above reaction and it can be divided into four phases: i) the collection of light by 'antenna' systems ii) primary electron transfer in reaction centres iii) energy stabilisation by secondary processes and iv) synthesis and export of stable products.[1]

In the cells of higher plants, photosynthesis takes place in organelles known as chloroplasts. Proteins that carry out the first steps (i – iii) of light-capture and utilisation are embedded into the thylakoid membrane of chloroplasts. The relative size and location of plant cells, chloroplasts and the thylakoid membrane are shown in Figure 1.1.

The thylakoid membrane is an extensive and complex structure that is a lipid bi-layer, and hence is a hydrophobic environment. It partitions into two regions; densely stacked flattened sacs known as grana lamellae and unstacked stroma lamellae. The space within the thylakoid is known as the lumen while the exterior is called the stroma.[1]

[†] For example, when n = 6 this denotes the molecule glucose.

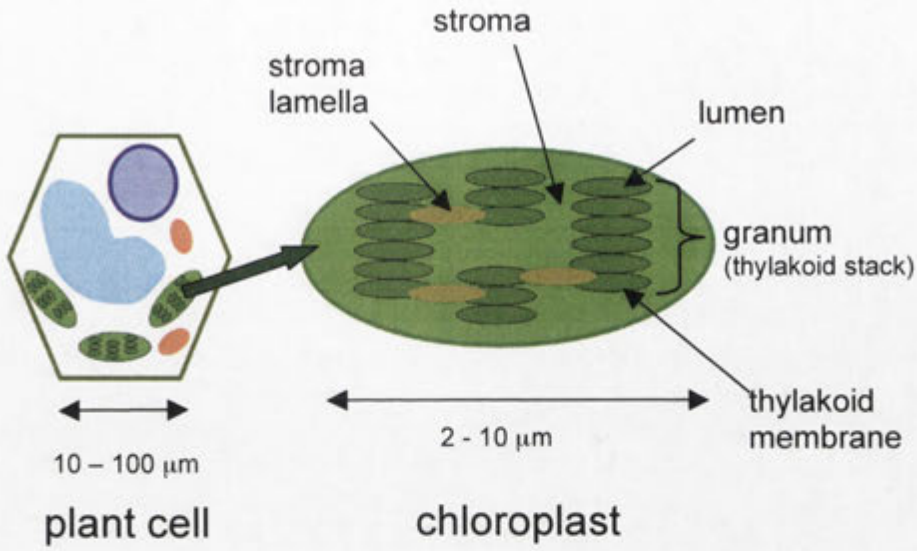

Figure 1.1 The location and structure of chloroplasts in higher plants. Chloroplasts are 2 – 10 μm in diameter and 1 μm thick.

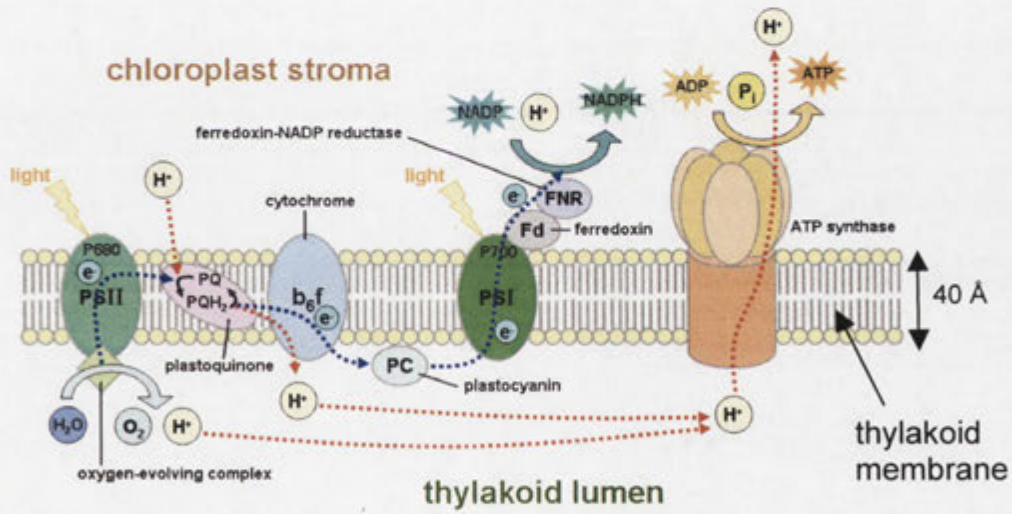

Figure 1.2 Stylised depiction of the thylakoid membrane and its embedded proteins.[60]

Figure 1.2 shows a stylised depiction of the proteins and the main biochemical reactions that occur in the thylakoid membrane. The embedded protein complexes are photosystem I, ATP synthase (both found in the stroma lamellae), photosystem II (found

in the grana stacks) and cytochrome b_6f (which is evenly distributed between the grana and stroma).

The energetics of photosynthesis can be understood via the 'Z-scheme' (see Figure 1.3), an energy diagram for electron transfer in oxygenic photosynthesis. The vertical scale depicts the capacity for each species to reduce the species on its right-hand-side, which is measured experimentally as midpoint redox potentials.[1]

Specific coupled pigments in the two photosystems known as P_{680} and P_{700}, in PSII and PSI respectively, absorb and are excited by light and this increases their capacity for reducing species. The Z-scheme does not however indicate that most light energy in plants is first absorbed by pigments embedded in proteins known as the antenna systems before being funnelled to P_{680} or P_{700} where photochemistry takes place. Antenna systems greatly increase the efficiency of plants by allowing a greater range of photons to be absorbed than could be collected by P_{680} and P_{700} alone. This is discussed further in the next Section.

Once P_{680} is excited to form P_{680}*, a cascade of electron transfer processes ensue, where the excited electron from P_{680}* reduces successive electron acceptors and consequently decreases its reductive capacity with each reduction. A second input of light energy in PSI raises the energy of the electron again and P_{700}* forms. A second series of electron transfers occurs until finally nicotinamide adenine dinucleotide phosphate ($NADP^+$) is reduced to form NADPH. Overall, NADPH has a reduction potential much higher than that of water (its ultimate electron source) due to the input of light energy into the system.[1]

As the above reactions take place, a proton (pH) difference is generated across the membrane as a consequence of water splitting and other biochemical reactions (see Figure

1.2). ATP synthase is a protein complex that manufactures ATP (adenosine triphosphate) by utilising the energy liberated by migration of protons from the lumen to the stromal side of the thylakoid membrane.

The high-energy compounds NADPH and ATP are utilised by enzymes in the chloroplast stroma to reduce carbon dioxide to sugars. These reactions form the biochemical pathway known as the Calvin-Benson cycle.[1]

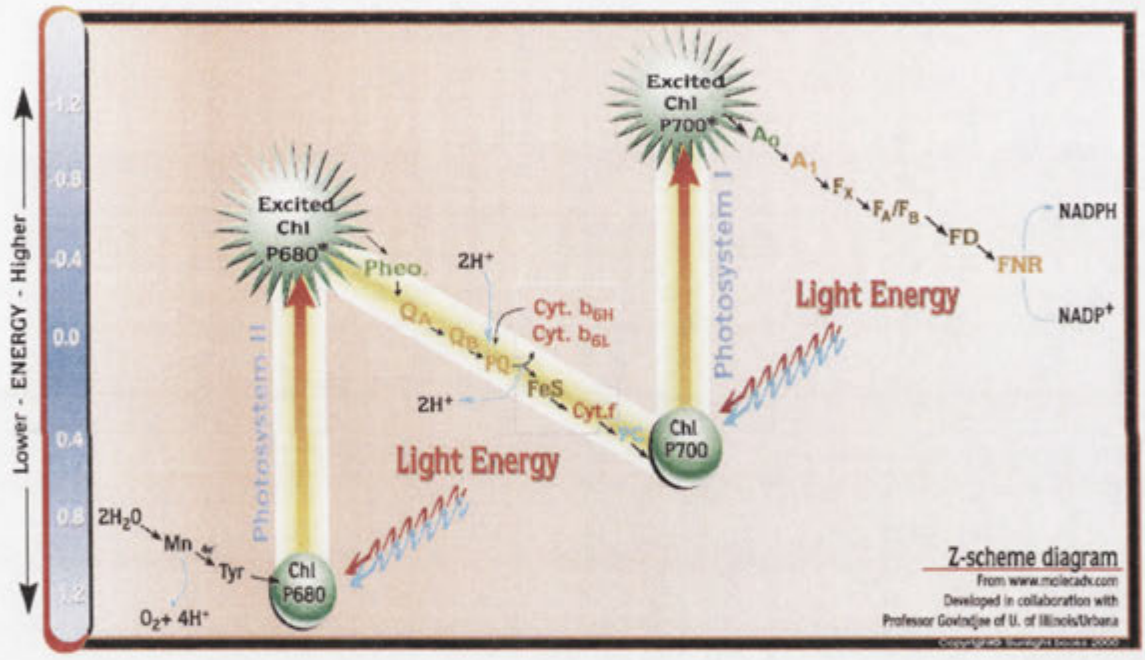

Figure 1.3 The Z-Scheme: Energy transfer in the thylakoid membrane.[8]

1.2 Photosystem II

1.2.1 Structure and Function

Photosystem II (PSII) is an assembly of proteins embedded into the thylakoid membrane of cyanobacteria, algae and higher plants. Comprising of as many as 28 proteins *in vivo* (some are exclusive to either cyanobacteria or higher plants), it has the unique ability in the natural world to split water into dioxygen and protons. Its function has been succinctly summarised by its technical designation: the water-plastoquinone oxidoreductase, that is, an enzyme that oxidises water and reduces plastoquinones.

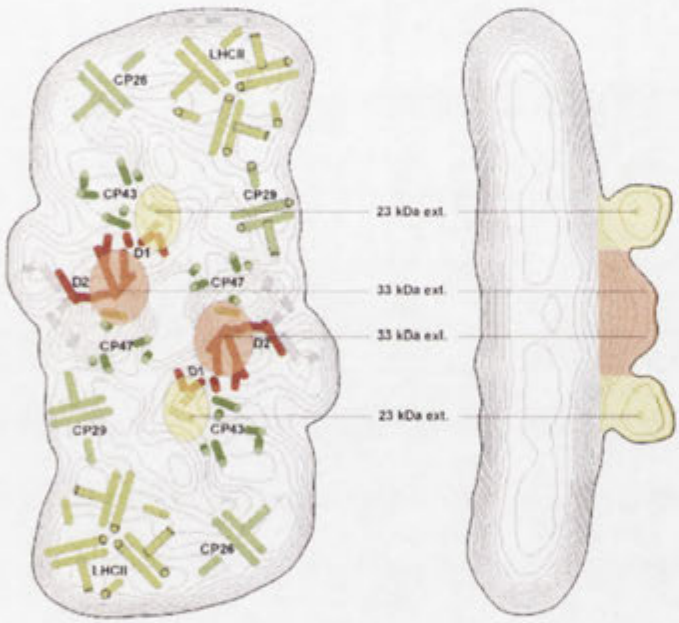

Figure 1.4 Arrangement of proteins in the PSII dimer.[9]

The supramolecular structure of PSII was first studied by electron microscopy at ~20 Å resolution[10,11] where it was argued that it is a dimer *in vivo*. The spatial arrangement of subunits in PSII is shown in Figure 1.4 and is based on the results of several experimental techniques including cryoelectron microscopy, structural data, sequence homologies and difference mapping.[9] The subunits are classified into groups according to their functionality, including antenna, extrinsic and reaction centre proteins.

The antenna proteins absorb photons and channel energy to the 'reaction centre' where photochemistry takes place. Absorption results in the electronic excitation of chromophores (mainly chlorophyll *a*, chlorophyll *b* and carotenoids) and due to weak coupling of the chromophores, the excited states migrate to the reaction centre.[1] In higher plants the antenna proteins include the outer light-harvesting LHCII (light harvesting complex of PSII), CP26, CP29 and inner light harvesting proteins CP43 and CP47, which are adjacent to the reaction centre.§

The extrinsic polypeptides are named after their masses and hence are known as the 33, 24 and 16 kDa proteins. Their role is to shield the manganese cluster from exogenous reactants in the aqueous phase of the lumen.[12] A number of other small polypeptides (with masses less than 10 kDa) are found in PSII with no known function.[12]

The PSII reaction centre includes the thylakoid membrane spanning proteins: D1, D2 and cyt b_{559}. The D polypeptides are analogous in structure and function to the L and M subunits in the bacterial reaction centre, the first photosystem to be characterised at high resolution with X-ray crystallography.[13] The D1 and D2 proteins are the site of the important electron transfer reactions and oxygen evolution (see Section 1.2.2).

1.2.2 The Reaction Centre

The reaction centre proteins are the 'scaffolding' upon which cofactor (non amino acid) molecules are specifically arranged to facilitate primary photochemistry. It consists of the nine porphyrin type molecules including six chlorophyll *a* (Chl *a*), two pheophytin *a* (Pheo *a*) and the heme of cytochrome b_{559} (cyt b_{559}). P_{680}, the primary electron donor, is currently understood to consist of four excitonically-coupled chlorophylls Chl_{D1}, Chl_{D2}, P_{D1} and P_{D2} and possibly includes some pheophytin contribution, although this is

§ CP is an acronym for 'chlorophyll protein' and is followed by apparent mass in kDa.

controversial.[12] The other cofactors include 2 β-carotenes, two plastoquinones Q_A and Q_B which are bridged by a non-heme iron and the oxygen evolving cluster (OEC) which consists of 4 manganese atoms, a calcium atom and possibly a chloride anion. There are two redox active tyrosine residues, labelled Y_Z and Y_D.

The reaction centre is divided into two halves, the acceptor ($Pheo_{D1}$, Q_A and Q_B) and donor (P_{680}, Y_Z, Mn cluster, secondary donors) sides.

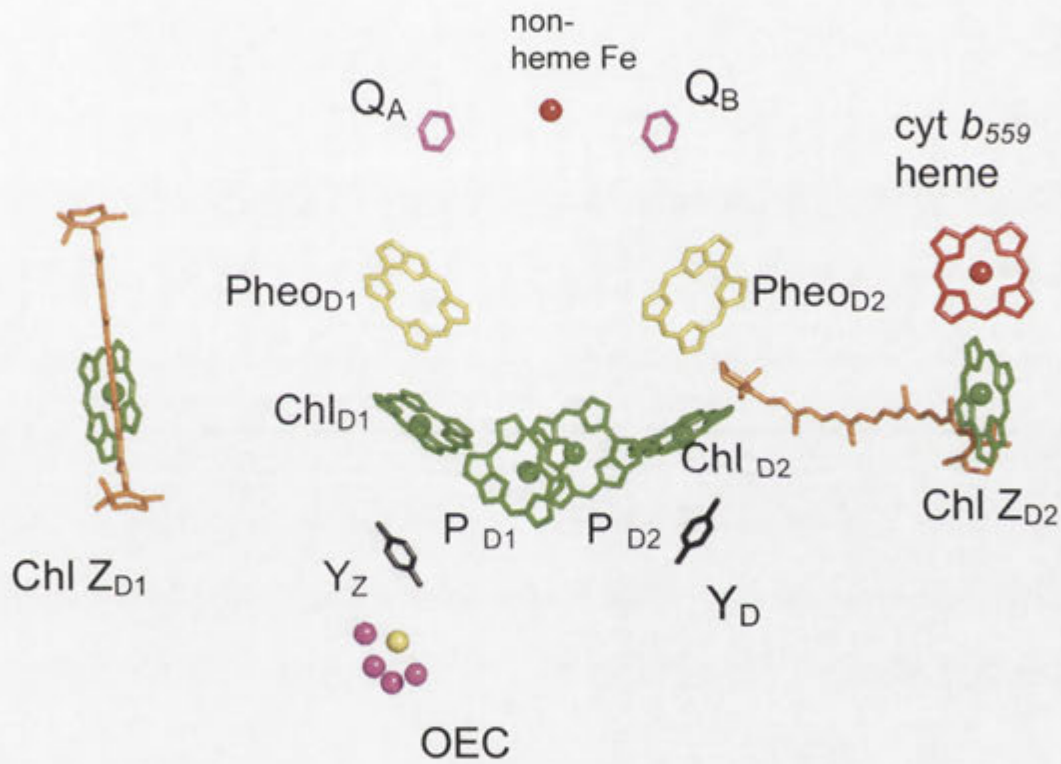

Figure 1.5 Cofactors in the reaction centre of photosystem II where the thylakoid membrane (not shown) would be in the plane of the page. The orange molecules are Car_{D1} (left) and Car_{D2} (right). From the Protein Data Bank Crystal Structure Coordinates file: 2AXT, published by Loll et al.[14]

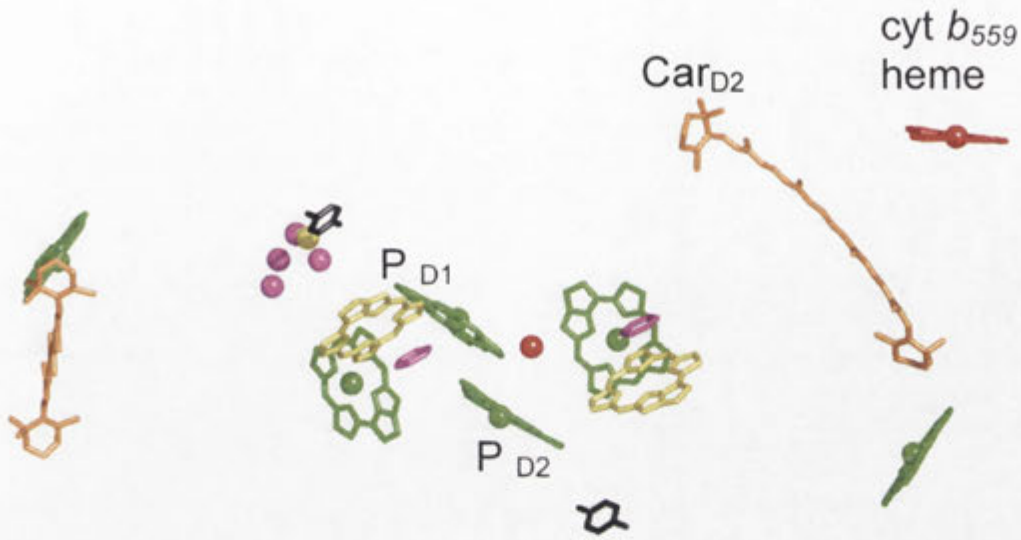

Figure 1.6 Top view of the PSII reaction centre cofactors (approximately viewing down the non-heme Fe - P_{D1} axis). Colour scheme is the same as in Figure 1.5.

Under physiological conditions electron transfer pathway occurs in PSII as follows. Photons[†] are absorbed by pigments in the antenna systems and these funnel energy to the reaction centre where a group of chlorophylls in the reaction centre known as P_{680}, is excited forming P_{680}*. Within tens of picoseconds P_{680}* donates an electron to $Pheo_{D1}$ to form the charge separated state $Pheo_{D1}^{-}/P_{680}^{+}$. The electron on $Pheo_{D1}$ shifts to Q_A within hundreds of picoseconds, forming Q_A^{-}, while P_{680}^{+} is stabilised by electron donation from one, or more, of a suite of possible donors. Under physiological conditions the electron donor to P_{680}^{+} is Y_Z and the electron transfer occurs on the order of nanoseconds to microseconds. Tyrosine Z^{+} is then reduced by the manganese cluster, which itself, in turn, catalytically oxidises water to form dioxygen. It is the high reduction

[†] In nature these originate from the sun, but can be of any origin as long as they are at an energy that can be absorbed by the antenna systems.

potential of P_{680}^{+}, unmatched in the biological world (estimated to be +1.12V[15] and +1.26V[16]), that facilitates the oxidation of water.

Q_A^- doubly reduces Q_B to form Q_BH_2 (a plastoquinol), which is exported from PSII via diffusion through the thylakoid membrane. The plastoquinol transfers electrons to the PSI photosystem via cyt b_6f where they ultimately reduce $NADP^+$ to NADPH.

Overall, in PSII, energy from sunlight is used to split water with the remainder, apart from heat, being stored in the bonds of Q_BH_2.

In intact PSII samples, a large fraction of cyt b_{559} is reduced, but at temperatures above ~200 K it does not contribute electrons (to a great extent) to the primary electron pathway, and is instead greatly out-competed by the OEC.[17,18] At cryogenic temperatures, or in samples in which the OEC has been removed, however, cyt b_{559} (or Chl Z) via Car^+ are the main electron donors in the photo-induced charge separation. These secondary-electron donors are thought to play an important supporting role to the primary pathway under physiological conditions.

1.2.3 Photosystem II Preparations

Advances in the understanding of PSII were concurrent with the developments in PSII isolation techniques. Emerson and Arnold showed experimentally that hundreds of chlorophyll molecules were involved in producing a single O_2 molecule.[19, 20] This lead to the idea of the existence of the 'photosynthetic unit'[21], the minimum entity capable of photosynthesis, which researchers soon began attempting to isolate experimentally.

A breakthrough occurred when Boardman and Anderson[22] separated digitonin-solubilised spinach chloroplasts into two fractions that were enriched in PSI and PSII. Over the years the experimental methodology was refined and culminated in the "BBY" preparation[23] (named after the initials of its makers), which has full O_2-evolving activity.

The BBY preparation has since been modified by numerous workers and has been invaluable to the study of PSII.

The majority of samples used in this work were a BBY-type preparation known as PSII enriched membrane fragments (PEMs) that were produced and provided by Paul Smith (ANU). Spinach leaves were blended, filtered and put through two centrifugation and homogenisation steps to form broken chloroplasts. This suspension was left on ice in the dark for an hour to allow the segregation of the thylakoid membrane into granal and stromal regions. The key step was the solubilisation of stromal regions with Triton X-100 detergent. After centrifugation the stroma-rich supernatant was discarded leaving behind a pellet containing thylakoid granal membrane regions. This pellet was further purified to remove starch and resulted in a preparation consisting of thylakoid membrane fragments enriched in PSII.

The samples were virtually free of PSI and cyt b_6f (which would have interfered with optical measurements of PSII) but intact enough to retain O_2 evolving and charge separation capacity and hence function as closely as possible to the native system.

1.3 Absorption Spectroscopy of PSII

1.3.1 Theory

1.3.1.1 Porphyrin-type Molecules

The UV-visible absorption spectrum of PEM samples is dominated by chlorophyll transitions, as there are approximately 200 Chl molecules per PSII complex. Chlorophylls, pheophytins and cytochromes all contain a macrocycle, which is structurally similar to porphyrin (see Figure 1.7, A). The spectroscopy of porphyrin-type molecules, such as those of interest in PSII, is understood in terms of the Gouterman Four Orbital Model.[24]

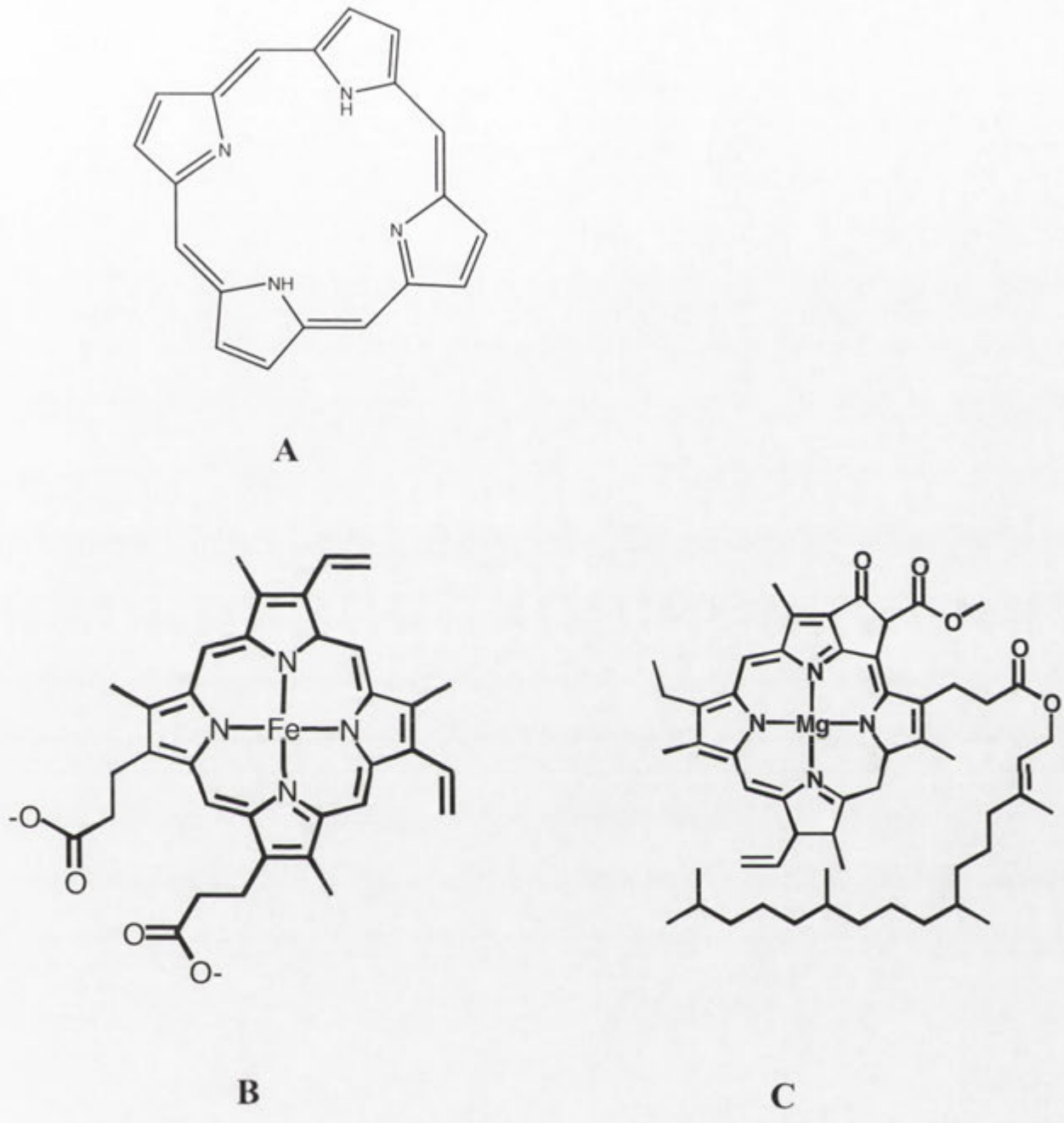

Figure 1.7 Structure of A) porphyrin, B) the cyt b_{559} heme and C) chlorophyll *a*. Pheophytin is identical to chlorophyll except there is no ligating magnesium atom.

Porphyrin-type macrocycles have a conjugated π bonding system in which $\pi \rightarrow \pi^*$ transitions can occur upon light absorption. The model stipulates that these transitions arise from electronic excitation from the two highest occupied molecular orbitals (HOMOs) to the two lowest unoccupied molecular orbitals (LUMOs) (see Figure

1.8). The two lowest-energy transitions are labelled the Q bands, and the two higher energy transitions are known as the B or Soret bands.

The Q band transitions are generally split into two components. These are identified as Q_x and Q_y as transition dipole moments are indeed approximately orthogonal. The Q_y transition is usually the lower-energy of the pair. The Soret bands have a mixed polarisation.

The model, as it is presented here, is simplified because it neglects contributions from higher-energy molecular orbitals (via configuration interaction). Additionally there are vibrational overtones overlaying the electronic excitations.

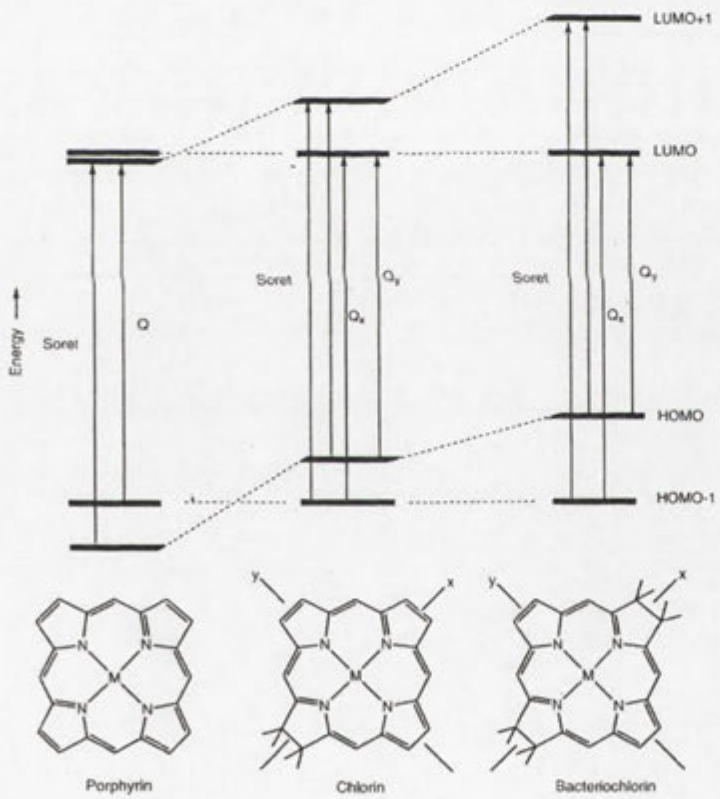

Figure 1.8 Gouterman 4 Orbital Model showing simplified electronic transitions of porphyrin, chlorin and bacteriochlorin (left to right). Diagram from Blankenship.[1]

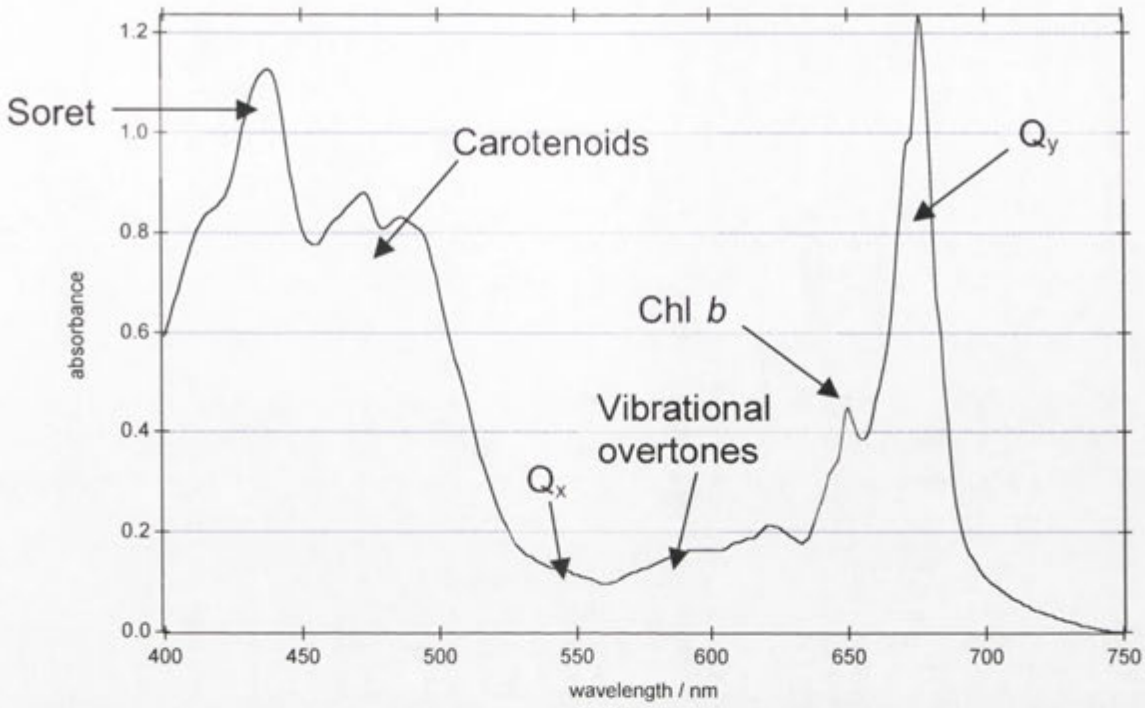

Figure 1.9 Typical PSII enriched membrane absorption spectrum at 1.7 K with main electronic transitions labelled.

1.3.1.2 Carotenoids

Carotenoids are long chain hydrocarbon molecules with a delocalised π electron system. Some contain oxygen atoms, usually in epoxide or hydroxyl groups. Carotenoids improve the efficiency of antenna systems by absorbing photons not harvested by chlorophylls, typically 400 to 500 nm and also function as photoprotectants.

The PSII core complex binds several β-carotenes and possibly small amounts of lutein.[12] While there is some uncertainty and variability in the total number of Car in PSII it has been established that there are two in the (D1/D2), and two or three each in CP43 and CP47 (reviewed by Tracewell et al.[25]) Seven carotenoids have been assigned in a crystal structure[26] in the reaction centre of PSII sourced from cyanobacteria but it was noted that some unassigned electron density could explain why the number is less than obtained by biochemical analysis (estimated as up to 8 carotenoids).

Of interest in this work was the β-carotene radical, which is formed by illumination of PSII. It is stable at low temperatures and has an absorption band at ~990 nm with FWHM of ~60 nm. Its extinction coefficient has been determined from studies of the isolated carotenoid.[27-29]

1.3.1.3 Magnetic Circular Dichroism

Circular dichroism (CD) spectroscopy is a technique where the difference between left (lcp) and right circularly polarised light (rcp) absorption is measured as a function of wavelength. When a magnetic field is applied to the absorbing sample, degenerate electronic energy levels can experience a Zeeman splitting and non-degenerate levels experience shifts. Field induced circular polarisations are induced in all transitions and the technique is called magnetic circular dichroism (MCD) spectroscopy.[30]

MCD spectroscopic signals are characterised as being either Faraday A, B or C terms. The origin of these terms can be illustrated considering a hypothetical atomic transition from a ^1S state to a ^1P state as follows. When a magnetic field is applied the ^1P state is split into two levels with $M_J = \pm 1$ (where M_J is the z component of total angular momentum) due to Zeeman splitting. Quantum mechanical selection rules stipulate that lcp light is absorbed at a lower energy than the rcp light, corresponding to transitions from the ground state to $M_J = -1$ and $M_J = +1$, respectively. Hence, when the absorbance of rcp light is subtracted from the absorbance lcp light, in a magnetic field, a sharp first-derivate type lineshape[1] is observed and this is know as a Faraday A term.

We now consider the case where the atomic states are inverted, that is, a transition from a ^1S state to a ^1P state. The splitting pattern and selection rules are the same as the case above but now the ^1P state will have higher population in the $M_J = -1$ level compared with the $M_J = +1$ level. Hence the absorption due to rcp light will be greater than that due

[1] Provided the Zeeman splitting is less than the linewidth of the transition.

to lcp and the difference spectrum will appear similar to the transition observed with no field. This type of transition is known as a Faraday C term. Unlike the A term, the C term is temperature dependent as the population of ^1P Zeeman sub-levels change with temperature and consequently the relative absorption intensity of lcp and rcp light varies.

A third parameter known as the Faraday B term arises of the mixing of energy levels by the application of a magnetic field. The B term is identical in lineshape to the C term but is not temperature dependent.

MCD is a powerful technique as it can distinguish the redox forms of cyt b_{559}. In a previous work[31] MCD spectra of the PSII samples used in this work were compared with those of isolated hemeproteins.[32] It was concluded there was low-spin cyt b_{559}, in both the Fe (II) and Fe(III) forms. Reduced (Fe(II)) cyt b_{559} has a strong, sharp Faraday A-term feature in the alpha-band region, with a characteristic derivative shape while the oxidised (Fe(III)) form has a temperature-dependent Faraday C-term exhibiting a 1/T temperature dependence. The C term is unaffected by diamagnetic species absorbing in the region (that is, Chl, Pheo, and Fe II cytochrome).

In this work, MCD was used to confirm that all cyt b_{559} in PEM samples is reduced when treated with excess sodium dithionite and hence provide a calibration peak for samples with 100% reduced cyt b_{559}.

1.3.2 Advantages of Cryogenic Temperature

There are several advantages for carrying out absorption spectroscopy at cryogenic temperatures.

As the temperature is decreased, spectral linewidths are generally narrowed due to the population of lower vibrational states of the ground states of electronic transitions. This narrowing increases the resolution of spectra. Furthermore, the S/N in spectra is

increased at low temperature allowing smaller changes between spectra to be detected than is possible at room temperature.

Electron transfer reactions can be studied virtually independently from chemical and physical effects that may dominate at higher temperatures. For example, the complex water splitting reactions that occur at room temperature cease to operate at cryogenic temperatures, allowing the electron transfer reactions to be studied in isolation. Low temperature studies can tease apart processes and thereby assist the understanding of processes that occur at physiological temperatures.

The corollary of the point made in the last paragraph is that physiological processes cannot be directly studied by cryogenic temperature experiments. Room temperature processes can be indirectly studied by exposing the sample to light or chemicals at room temperature and then rapidly freezing the sample to fix the sample in a particular state.

1.4 Cytochromes

1.4.1 Historical Overview

Cytochromes are a diverse class of proteins found in virtually all known life forms[33] and probably evolved hundreds of millions of years before photosynthesis. They are involved in a diverse number of fundamental processes including cellular respiration, photosynthetic electron transfer, anaerobic and chemosynthetic bacterial reactions.[34]

Cytochromes were discovered in the 1880s by MacMunn[35], an Irish doctor who practiced medicine in England. He recorded the absorption of cytochromes in insect tissues and established they were involved in respiration. In 1925 Keilin (originator of the word cytochrome) extended MacMunn's work and detected cytochromes in many plant species and hence established its universality among living things.[36]

Keilin and Hill chemically characterised cytochromes and discovered they contained the porphyrin moiety.[37] Williams was the first to give a detailed discussion of the link between the magnetic and optical properties of the metalloporphyrins.[38]

1.4.2 Properties

According to International Union of Biochemistry guidelines[39] cytochromes are defined as heme containing proteins (hemeproteins) that carry out electron (or proton) transfer which is associated with a reversible redox change between the Fe(II) and Fe(III) states of the heme iron. Hemeproteins that function as catalysts (for example, cytochrome P450[†]) are therefore not technically cytochromes.

Cytochromes are grouped into four main categories: a, b, c and d according to their heme type. The heme types vary in structure and covalent bonding to the protein. Cytochromes can be characterised further by the axial ligand coordination to the iron heme and sequence similarity between proteins.

The majority of cytochromes are found in membrane systems such as the mitochondrial inner membrane of eukaryotes or the thylakoid membrane of chloroplasts. There are several cytochromes associated with photosynthesis such as cyt c_6, cyt f, cyt M, cyt c_{549} reviewed by Kerfeld and Krogmann.[36]

1.5 Cytochrome b_{559}

Cyt b_{559} has been labelled an 'enigma' because despite being clearly fundamental to the functioning of PSII, its role is not well understood. Its role is a current topic in the literature five decades after its discovery. Cyt b_{559} is redox active, but it has been inferred that it does not participate in the primary electron-transfer reactions leading to water oxidation.

[†] A family of cytochromes ubiquitous to all life-forms.

1.5.1 Early Work

Photosynthetic cyt b_{559} was first described by Lundegardh in 1961[40] but was termed 'cytochrome b_3'. In 1969 Knaff and Arnon photooxidised cyt b_{559} in chloroplasts at low temperature (84 K).[41] Since only short-wavelength light could induce the oxidation this localised cyt b_{559} to PSII. Boardman and Anderson associated cyt b_{559} with 'system II'.[42] Furthermore, the fact that it could be oxidised at cryogenic temperature showed that electron transfer was occurring between cyt b_{559} and PSII reaction centre chlorophylls.

The methods required to isolate cyt b_{559} were pioneered by Garewal and Wasserman[43] but the results of that work have been interpreted as a "heterogenous mixture" rather than pure cyt b_{559}.[44] Improved purification methods were developed by Metz et al.[45] and Widger et al.[46] which allowed the identification and sequencing of the genes psbE and psbF[47, 48] responsible for the synthesis of the α and β polypeptide subunits, respectively.

1.5.2 Stoichiometry

There has been a long-standing controversy over the number of cyt b_{559} proteins per PSII reaction centre. One, two or an intermediate number† of cyt b_{559}s per RC have been reported in the literature. There are a number of variables that could explain the contradictory results and these are discussed in papers by MacDonald et al.[49] and Stewart and Brudvig.[50] Cyt b_{559} stoichiometry may vary depending on the organism, PSII preparation type, estimate of antenna size and cyt b_{559} extinction coefficient used. Both optical and EPR methods of quantification are hampered by interfering signals and may be inaccurate if the samples do not have a homogeneous distribution of centres.

† That is, an average between 1 and 2 cytochromes, corresponding to a mixture of PSII reaction centres containing 1 and 2 cyt b_{559} proteins.

The issue appears to have been resolved when the first X-ray crystal structure of PSII[51] revealed one cyt b_{559} subunit per RC, however the authors considered the possibility that a cytochrome could have been removed during sample preparation. Interestingly, there are two trans-membrane helices on the opposite (D1) side of cyt b_{559} in PSII, but there is no heme there. Faller et al.[52] proposed that the heme may have been lost over an evolutionary time-scale rather than during PSII isolation.

There is now a consensus that there is only one cyt b_{559} per RC as shown by subsequent PSII crystal structures.[14,26,53,54] Shen and Kamiya[12] presented evidence to show there was one cyt b_{559} per RC in their PSII samples (used to obtain their X-ray crystal structure) prior to and after crystallisation.

All the PSII crystal structures to date have been from thermophilic cyanobacteria. A recent and thorough study[55] has shown that both cyanobacteria and higher plant PSII have one cyt b_{559} per RC. There has been no evidence contradicting there being one cyt b_{559} per RC in the literature since the first PSII crystal structure was published.

1.5.3 Structure and Physical Properties

Cyt b_{559} is composed of two polypeptides labelled α and β that span the thylakoid membrane. The polypeptides are 9 and 4 kDa in weight respectively. Cyt b_{559} is named for its 'b-type' heme (that is, an iron chelate of protoporphyrin IX with no covalent bonds to the protein) and the reduced form of the cytochrome has its main (α) absorption band at ~559 nm. The α and β subunits each coordinate to the heme iron via a histidine residue.

Figure 1.10 Structure of cytochrome b_{559}. The α subunit and β subunits (blue and green peptides respectively) are shown ligating the iron heme (red) via histidine residues.

1.5.3.1 Optical Spectroscopy

Cytochromes have Soret and Q bands in the visible region (see Section 1.3.1.1). The Q band of the reduced form of cyt b_{559} two peaks has two peaks which are known as the α (~559 nm) and β (~530 nm) bands. Optical measurements are usually made on the α component of the Q band at ~559 nm because this transition has the least interference from other chromophores and a moderate extinction coefficient.[50] The FWHM of the α band is 10 – 12 nm at room temperature. The band narrows to ~5 nm and is shifted 2 – 3 nm to the blue at cryogenic temperatures.[56]

At room temperature cyt b_{559} is normally quantified from the chemically reduced (via dithionite)-minus-oxidised (via ferricyanide) spectrum.

1.5.3.2 Redox Properties

Compared to other b-type cytochromes, cyt b_{559} has an unusually high maximum reduction midpoint potential (E_m) of ~370 - 435 mV. A number of different forms of cyt

b_{559} with various E_ms have been documented[50], including high- (HP), intermediate- (IP) and low-potential (LP). The factors which influence the reduction potentials are not well understood[50] but are thought to include the membrane environment, hydrogen-bonding interactions with the heme, presence of the extrinsic polypeptides, detergents and cryoprotectants.

1.5.4 Function

Researchers have been postulating a function for cyt b_{559} in PSII since its discovery. It can be reasoned that it must have a beneficial function based on energetic and evolutionary arguments.

Cyt b_{559}, like all proteins, has a complicated biosynthesis pathway (involving several other proteins) that requires a considerable investment of energy. Cyt b_{559} is not likely to be an evolutionary remnant considering it has been conserved in PSII for approximately three billion years in cyanobacteria and in the 'higher' photosynthetic organisms. During this time, no organism has evolved a way to perform oxygenic photosynthesis without cyt b_{559}, implying that it is an indispensable component of PSII.

The experimental evidence that cyt b_{559} is integral to PSII is two-fold: i) in mutants that have had the cyt b_{559} genes deleted, PSII was not assembled[57] and ii) it is retained in the minimum assembly of proteins purified from PSII that can perform charge separation (along with the D1 and D2 polypeptides).[58]

The function is not likely to be purely structural because then there would not be any need for the construction and transport of the heme cofactor to its final position.

1.5.4.1 Protection from Photoinhibition

The important properties becoming clear about cyt b_{559} were that it was integral to PSII, had variable midpoint potential forms and could be reversibly oxidised and reduced.

Since it had been shown not to be involved in the primary electron pathway it was proposed that it is involved in a protection mechanism against photoinhibition.[50] Photoinhibition is the damage to photosynthetic capacity of organisms due to exposure to excess light. Photoinhibition is broad in scope (reviewed by Powles[59]) but here photoinhibition is limited to mean damage caused to PSII by visible light.

It is now becoming clear that cyt b_{559} (concomitant with other electron donors) is part of a secondary electron pathway in PSII whose purpose is currently under discussion.

1.6 Overview of Thesis

The preparation methods for PSII enriched membrane samples and a detailed description the two spectrometers used to analyse them are compiled in Chapter 2. The following chapter describes the typical experiments performed with the samples. Chapters 4 to 7 comprise the main body of work of the thesis including all experimental results and discussion of the results. Some theory is presented in the results and discussion chapters where the need arises.

Chapter 4 outlines the systematic work done to produce high optical-quality PEM samples. Chapter 5 describes the work on quantifying the important cyt b_{559} protein in PSII by absorption and MCD spectroscopy. Chapters 5 and 6 were concerned with assigning features in the illumination-induced difference spectra of PEM samples. In both chapters the spectroscopic assignments were facilitated by mathematical modelling. Finally, the conclusions drawn from the research conducted are outlined in Chapter 8.

1.7 References

[1] R. E. Blankenship, *Molecular Mechanisms of Photosynthesis*, Blackwell Science, **2002**.

[2] J. Barber, *Chemical Society Reviews* **2009**, *38*, 185.

[3] M. Yagi, A. Syouji, S. Yamada, M. Komi, H. Yamazaki, S. Tajima, *Photochemical and Photobiological Sciences* **2009**, *8*, 139.

[4] R. Lomoth, A. Magnuson, M. Sjoedin, P. Huang, S. Styring, L. Hammarstroem, *Photosynthesis Research* **2006**, *87*, 25.

[5] J. H. Alstrum-Acevedo, M. K. Brennaman, T. J. Meyer, *Inorganic Chemistry* **2005**, *44*, 6802.

[6] K. Szacilowski, W. Macyk, A. Drzewiecka-Matuszek, M. Brindell, G. Stochel, *Chemical Reviews* **2005**, *105*, 2647.

[7] A. Magnuson, S. Styring, L. Hammarstrom, Understanding Photosystem II Function by Artificial Photosynthesis in *Photosystem II: The Light-Driven Water:Plastoquinone Oxidoreductase* (Eds.: T. J. Wydrzynski, K. Satoh), Springer, Dordrecht, **2005**.

[8] W. Veit, Govindjee, *The Z-Scheme Diagram of Photosynthesis* <http://www.life.illinois.edu/govindjee/page3.html> **2010.**

[9] J. Barber, J. Nield, E. P. Morris, B. Hankamer, *Trends in Biochemical Sciences* **1999**, *24*, 43.

[10] M. Rögner, J. P. Dekker, E. J. Boekema, H. T. Witt, *Federation of European Biochemical Societies* **1987**, *219*, 207.

[11] J. P. Dekker, E. J. Boekema, H. T. Witt, M. Rögner, *Biochimica et Biophysica Acta* **1988**, *936*, 307.

[12] T. J. Wydrzynski, K. Satoh, (Eds) in *Photosystem II The Light-Driven Water:Plastoquinone Oxidoreductase,* Springer, Dordrecht, **2005**.

[13] J. Deisenhofer, O. Epp, K. Miki, R. Huber, H. Michel, *Nature* **1985**, *318*, 618.

[14] B. Loll, J. Kern, W. Saenger, A. Zouni, J. Biesiadka, *Nature* **2005**, *438*, 1040.

[15] B. A. Diner, F. Rappaport, *Annual Review of Plant Biology* **2002**, *53*, 551.

16] A. Cuni, L. Xiong, R. Sayre, F. Rappaport, J. Lavergne, *Physical Chemistry Chemical Physics* **2004**, *6*, 4825.

[17] P. Mathis, A. Vermeglio, *Biochimica et Biophysica Acta* **1975**, *369*, 371.

[18] J. C. de Paula, J. B. Innes, G. W. Brudvig, *Biochemistry* **1985**, *24*, 8114.

[19] R. Emerson, W. Arnold, *The Journal of General Physiology* **1932**, *15*, 391.

[20] R. Emerson, W. Arnold, *The Journal of General Physiology* **1932**, *16*, 191.

[21] H. Gaffron, K. Wohl, *Naturwissenschaften* **1936**, *24*, 81.

[22] N. K. Boardman, J. M. Anderson, *Nature* **1964**, *293*, 166.

[23] D. A. Berthold, G. T. Babcock, C. F. Yocum, *Federation of European Biochemical Societies Letters* **1981**, *134*, 231.

[24] M. Gouterman, *Journal of Molecular Spectroscopy* **1961**, *6*, 138.

[25] C. A. Tracewell, J. S. Vrettos, J. A. Bautista, H. A. Frank, G. W. Brudvig, *Archives of Biochemistry and Biophysics* **2001**, *385*, 61.

[26] K. N. Ferreira, T. M. Iverson, K. Maghlaoui, J. Barber, S. Iwata, *Science* **2004**, *303*, 1831.

[27] E. A. Dawe, E. J. Lan, *Journal of the Chemical Society, Faraday Transactions 1.* **1975**, *71*, 2162.

[28] P. Mathis, A. Vermeglio, *Photochemical and Photobiological Sciences* **1972**, *15*, 157.

[29] T. A. Moore, D. Dust, P. Mathis, J. C. Mialocq, C Chachaty, R. V. Bensasson, E. J. Land, D. Doizi, P. A. Liddell, W. R. Lehman, G. A. Nemethy, A. L. Moore, *Nature* **1984**, *307*, 630.

[30] P. N. Schatz, A. J. McCaffery, *Quarterly Reviews* **1969**, *23*, 552.

[31] P. J. Smith, S. Peterson, V. M. Masters, T. Wydrzynski, S. Styring, E. Krausz, R. J. Pace, *Biochemistry* **2002**, *41*, 1981.

[32] M. R. Cheesman, C. Greenwood, A. J. Thomson, *Advances in Inorganic Chemistry* **1991**, *36*, 201.

[33] F. S. Mathews, *Progress in Biophysics and Molecular Biology* **1985**, *45*, 1.

[34] R. Lemberg, J. Barrett, *Cytochromes*, Academic Press, London; New York, **1973**.

[35] C. MacMunn, *Philosophical Transactions of the Royal Society of London* **1886**, *177*, 267.

[36] C. A. Kerfeld, D. W. Krogmann, *Annual Review of Plant Physiology and Plant Molecular Biology* **1998**, *49*, 397.

[37] R. Hill, D. Keilin, *Proceedings of the Royal Society of London, Series B, Containing Papers of a Biological Character* **1930**, *107*, 286.

[38] R. J. P. Williams, *Chemistry Reviews* **1956**, *5*, 299.

[39] G. Palmer, J. Reedijk, *European Journal of Biochemistry* **1991**, *200*, 599.

[40] H. Lundegårdh, *Nature* **1961**, *192*, 243.

[41] D. B. Knaff, D. I. Arnon, *Proceedings of the National Academy of Sciences of the United States of America* **1969**, *63*, 963.

[42] N. K. Boardman, J. M. Anderson, *Biochimica et Biophysica Acta* **1967**, *143*, 187.

[43] H. S. Garewal, A. R. Wasserman, *Biochemistry* **1974**, *13*, 4063.

[44] W. A. Cramer, S. M. Theg, W. R. Widger, *Photosynthesis Research* **1986**, *10*, 393.

[45] J. G. Metz, G. Ulmer, T. M. Bricker, D. Miles, *Biochimica et Biophysica Acta* **1983**, *725*, 203.

[46] W. R. Widger, W. A. Cramer, M. Hermodson, D. Meyer, M. Gullifor, *The Journal of Biological Chemistry* **1984**, *259*, 3870.

[47] R. G. Herrmann, J. Alt, B. Schiller, W. R. Widger, W. A. Cramer, *Federation of European Biochemical Societies Letters* **1984**, *176*, 239.

[48] W. R. Widger, W. A. Cramer, M. Hermodson, R. G. Herrmann, *Federation of European Biochemical Societies Letters* **1985**, *191*, 186.

[49] G. M. MacDonald, R. J. Boerner, R. M. Everly, W. A. Cramer, R. J. Debus, B. A. Barry, *Biochemistry* **1994**, *33*, 4393.

[50] D. H. Stewart, G. W. Brudvig, *Biochimica et Biophysica Acta - Bioenergetics* **1998**, *1367*, 63.

[51] A. Zouni, H. T. Witt, J. Kern, P. Fromme, N. Krauss, W. Saenger, P. Orth, *Nature* **2001**, *409*, 739.

[52] P. Faller, C. Fufezan, A. W. Rutherford, The Side-Path Electron Donors: Cytochrome b_{559}, Chlorophyll Z and ß-Carotene in *Photosystem II: The Light-Driven Water/Plastoquinone Oxido-Reductase* (Eds.: T. J. Wydrzynski, K. Satoh), Springer, Dordrecht, **2005**.

[53] N. Kamiya, J.-R. Shen, *Proceedings of the National Academy of Sciences of the United States of America* **2003**, *100*, 98.

[54] J. Biesiadka, B. Loll, J. Kern, K.-D. Irrgang, A. Zouni, *Physical Chemistry Chemical Physics* **2004**, *6*, 4733.

[55] O. Kaminskaya, J. Kern, V. A. Shuvalov, G. Renger, *Biochimica et Biophysica Acta* **2005**, *1708*, 333.

[56] S. Okayama, W. L. Butler, *Biochimica et Biophysica Acta* **1972**, *267*, 523.

[57] A. Pascal, A. Telfer, J. Barber, B. Robert, *Federation of European Biochemical Societies Letters* **1999**, *453*, 11.

[58] O. Nanba, K. Satoh, *Proceedings of the National Academy of Sciences of the United States of America* **1987**, *84*, 109.

[59] S. B. Powles, *Annual Reviews of Plant Physiology* **1984**, *35*, 15.

[60] Light-dependent reactions of photosynthesis at the thylakoid membrane. <http://upload.wikimedia.org/wikipedia/commons/1/18/Thylakoid_membrane.png> **2007**

2 Materials and Instrumentation

2.1 Photosystem II Enriched Membrane Samples

2.1.1 ANU Preparation

The majority of samples studied in this work were prepared by Dr Paul Smith in the Department of Chemistry, ANU. The photosystem II enriched membrane (PEM) preparation method is briefly described in the literature[1] and detailed in Dr Smith's PhD thesis.[2] A detailed description of the steps in the preparation of PEM samples is outlined below and is followed by a summary in point form. The procedure used to make samples for this work varies slightly from that in Smith's thesis.

PSII enriched membrane sample-preparation details

Market spinach-leaves were deveined, washed and shredded by hand. The leaves were then blended with Buffer 1 (0.1 M sucrose, 0.05 M KH_2PO_4, 0.05 M Na_2HPO_4, 0.2M NaCl, 2 gL^{-1} bovine serum albumin (BSA), pH 7.5) in a Waring type blender. The resulting homogenate was filtered through muslin, which was squeezed by hand to remove excess liquid from the leaf fibre. The filtrate was then centrifuged at 5000 × g for 10 minutes using a SLA 1500 rotor.

The supernatant was discarded and the pellet homogenised in Buffer 2 (0.4 M sucrose, 0.015 M NaCl, 0.005 M $MgCl_2$, 0.05 M 2-[N-Morpholino] ethane sulfonic acid (MES), 0.005 M ethylene diamine tetra acetic acid (as disodium salt) (Na_2.EDTA), 2.5 g L^{-1} BSA, pH 6.0) and centrifuged at 6500 rpm in an SLA 1500 centrifuge for 10 minutes. The supernatant was decanted and discarded, the pellet homogenised in sufficient Buffer 2 to obtain a total chlorophyll concentration of approximately 3 g L^{-1}.

This homogenate was left at 4°C in the dark for an hour to allow the segregation of the thylakoid membrane into granal and stromal regions. Buffer 3 (Buffer 2 with 0.2 kg L^{-}

[1] Triton® X-100 detergent) was then added to obtain a detergent-to-chlorophyll ratio of ~20:1 (w/w). The solubilising thylakoid suspension was rapidly swirled to enhance mixing and centrifuged at 35,000 × g for 30 minutes, in a SS34 rotor. Before centrifugation, the thylakoid suspension was in contact with the Triton for a short time (about 2 minutes) so as to minimise membrane solubilisation and hence obtain maximum yield of granal membranes.

After centrifugation, the supernatant (rich in detergent-solubilised thylakoid stromal region membranes) was discarded leaving behind a pellet containing thylakoid granal membrane regions (rich in PSII) and starch. This pellet was homogenised in Buffer 4 (0.05 M NaCl, 0.005 M $MgSO_4$, 0.05 M MES, pH 6.0) and centrifuged at 3000 × g for one minute. The pellet, containing more than 90% of the starch content was discarded. The supernatant was transferred to a clean centrifuge tube and centrifuged at 35,000 × g for 30 minutes.

The supernatant was decanted and discarded. The pellet was suspended and homogenised in ~8 mL Storage Buffer (0.4 M sucrose, 0.015 M NaCl, 0.01 M $MgCl_2$, 0.02 M MES, pH 6.0). The homogenate was stirred vigorously by shaking in a Vortex shaker / stirrer. The volume of the final PSII containing suspension was adjusted to ~ 10 g L^{-1} total chlorophyll content. Aliquots of ~1 mL were placed in Eppendorf tubes and stored at -80°C.

PSII enriched membrane sample preparation summary:

1. Spinach leaves were blended with Buffer 1 and filtered. The homogenate was centrifuged (5000 × g) for 10 min.

2. The supernatant was discarded and the pellet was homogenised in Buffer 2 and centrifuged (5000 × g) for 10 min.

3. The supernatant was discarded and the pellet was homogenised in Buffer 2.

4. The homogenate was left on ice and in the dark for 1 hour with [Chl] ~ 3 g L^{-1} (allowing stacking and segregation of grana and stroma).

5. Buffer 3 was added (Triton detergent solubilisation), rapid mixing and centrifugation (35,000 × g) for 30 min.

6. The supernatant was discarded and the pellet homogenised in Buffer 4 centrifuged (3000 × g) for 2 min, pellet containing starch discarded. The supernatant was transferred to clean centrifuge tube and centrifuged (35,000 × g) for 30 min.

7. The supernatant was discarded and the pellet was homogenised in Storage Buffer and vortexed.

8. Aliquots (~1 mL) of PEM sample were stored at -80°C.

2.1.2 Uppsala University Preparation

Some samples were prepared by the Styring research group in Uppsala University, Sweden and brought to our lab by Dr Felix Ho. These were made in a similar way to Paul Smith's PEM samples although there were variations in the details of buffer composition and sample handling.

The difference between the two preparations, detectable by optical spectroscopy, was that the Swedish PEM had very little, or no, initially reduced cyt b_{559}. This was probably due to the minimal contact time of thylakoid with Triton detergent in the solubilisation step in the Smith preparation (2 minutes) compared with the Uppsala preparation (25 minutes).

Uppsala PSII enriched membrane preparation summary

1. Spinach leaves were blended in buffer (20 mM Tris-HCl (pH 7.8), 100 mM sucrose, 300 mM NaCl) and sodium ascorbate (2 g/L) and centrifuged (1500 × g) for 15 min.

2. The pellet was suspended in buffer (25 mM MES-NaOH (pH 6.1), 100 mM sucrose, 15 mM NaCl, 5 mM $MgCl_2$) and centrifuged (100 × g) for 2 min to remove excess starch.

3. The was supernatant transferred to new tubes and centrifuged (3100 × g) for 20 min.

4. The pellet was homogenised in MES buffer, incubated in the dark for 30 min under gentle stirring (the grana stacking step).

5. MES buffer containing 20% Triton was slowly added to homogenised sample while gently stirred, to a ratio of 20:1 Triton:Chl. This was allowed to incubate for 25 min in the dark, and then centrifuged (30,000 × g) for 25 min.

6. The pellet was suspended in MES buffer (without Triton) and centrifuged for 25 min.

7. The wash step was repeated.

8. The final pellet was dissolved and homogenised in storage buffer (25 mM MES-NaOH (pH 6.1), 400 mM sucrose, 15 mM NaCl, 3 mM $MgCl_2$).

2.2 Spectrometers

Two spectrometers were used to study PEM samples via absorption and MCD spectroscopy. They were developed from commercial and custom-made components by members of the Krausz group, at the Research School of Chemistry in the ANU.

2.2.1 Magnetic Circular Dichroism Spectrometer

The Magnetic Circular Dichroism (MCD) spectrometer measured absorption spectra. In some experiments, circular dichroism (CD) and magnetic circular dichroism (MCD) spectra were simultaneously collected. The system was primarily designed and developed by Prof. Elmars Krausz prior to the commencement of this project. Early in the project Dr. Barry Prince implemented software, written with Labview 7.0, to operate the monochromator and collect spectra.

2.2.1.1 Overview of Operation

A schematic of the MCD spectrometer is shown in Figure 2.1 and its operation is briefly described here. The interrogating white-light source was split into its component colours with a monochromator. From the exit slit of the monochromator, a light beam of a single wavelength was passed through the sample and imaged onto a photodetector. The light reaching the photodetector produced a voltage proportional to the light intensity and the voltage was extracted by a lock-in amplifier and recorded on a computer. By scanning the monochromator over a wavelength range and recording the light intensity at each wavelength, an absorption spectrum of a sample could be constructed.

To collect circular dichroism spectra, left and right circularly polarised (lcp and rcp) light was generated and the difference between the absorption of the two polarisations detected. A linear polariser and photo-elastic modulator were employed to generate the polarised light and, in a process known as heterodyning, two lock-in

amplifiers were used to measure the difference in intensity between the two polarisations. To measure MCD spectra, a magnetic field was applied to the sample via a superconducting magnet during the CD measurement.

2.2.1.2 Components of the MCD Spectrometer

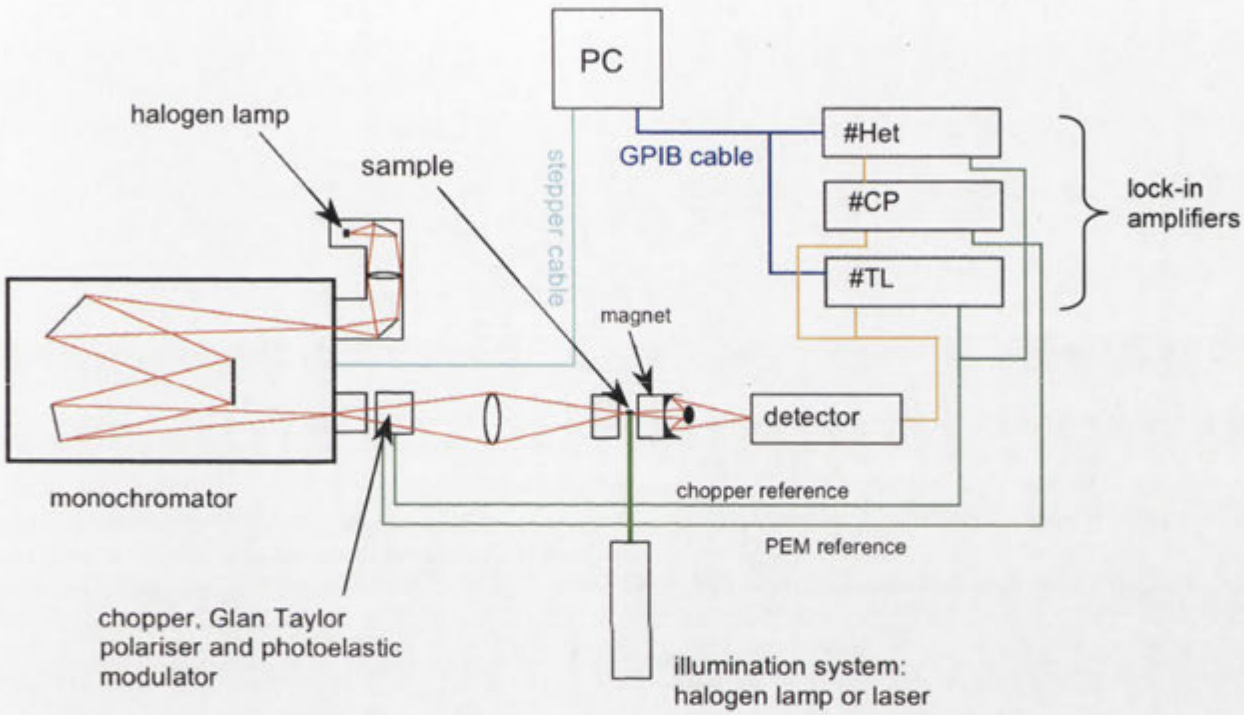

Figure 2.1 Schematic of the MCD spectrometer. Red line shows the path of light from halogen lamp to the detector.

Optics

The light source was a 250 W, 24 V Osram halogen tungsten-filament lamp connected to a stable power supply. It was enclosed in a specially built metal housing, fan-cooled and was run continuously during an experiment. A mirror was placed inside the housing to reflect otherwise unused light and hence maximise the number of photons reaching the sample and detector. This was done to maximise the signal-to-noise (S/N) ratio in absorption spectra.

Light was passed through a Spex 0.75M Czerny-Turner-type double monochromator (used as single monochromator) with a 1200 line/mm diffraction grating blazed at 500 nm. Two slits, situated at the monochromator entrance and exit had their widths adjusted to control the light intensity reaching the sample and resolution of the monochromator. The wavelength exiting the monochromator was selected by adjusting the angle of the monochromator's diffraction grating via a stepper motor interfaced to the computer.

The light exiting the monochromator was modulated at a frequency of 489 Hz with a New Focus Inc 3501 optical chopper. The light was passed through a Glan-Taylor linear polariser, and photo-elastic modulator, which together produced alternating lcp and rcp light for (M)CD measurements and a cutoff filter, which eliminated second order light (light at half the indicated wavelength) from the monochromator.

The Glan-Taylor polariser is composed of two right-angled prisms of calcite that are separated on their long faces with an air gap. When unpolarised light is passed through the polariser, s-polarised light (that is, light polarised perpendicular to the plane of incidence) is totally internally reflected at the air-gap resulting in only p-polarised light (light polarised parallel to the plane of incidence) being transmitted by the device. The transmitted light is thus linearly polarised.

When linearly polarised light is passed through a quarter-wave plate (an optically transparent rectangular bar of fused silica) with its electric vector **E** at 45° to the vertical, the E_x component of **E** phase shifts relative to the E_y component. The net result of this phase shift is that the electric field vector of light maps out a spiral about the optical axis and this is known as circularly polarised light.

A PEM consists of a fused silica bar, which is attached to a quartz piezoelectric transducer. As it is piezoelectric, an application of an electric field to the silica bar causes a change in the dimension in the material. The piezoelectric transducer is tuned to the resonant frequency of the longitudinal vibration of the silica bar. The bar's plane of vibration is aligned with the E_x component of light, and the velocity of E_x is alternately increased and decreased as the bar is compressed and stretched. This leads to alternating lcp and rcp being transmitted at the frequency of the vibration of the quartz bar (57 kHz).

Finally the light beam was directed with a lens into the sample chamber and then onto a photodetector. The light at the sample could be in either a focussed or defocused state, determined by the position of the lens.

External Light Sources

PSII samples were illuminated with either green (filtered white light from a halogen lamp) or red light (633 nm) from a helium-neon (HeNe) laser. An illumination was carried out by rotating the sample rod 90 degrees, removing a cap on the cryostat to allow light through quartz windows and onto the sample.

The green lamp consisted of a halogen lamp with a housing similar to that constructed for the MCD spectrometer and connected to a stable power supply. The light was directed through 10 cm of water (to filter infrared radiation) and a filter stack that passed green light before being focussed to an image of the lamp filament with a concave lens. The green light transmission profile was a skewed Gaussian with maximum fluence at 546 nm and FWHM ~56 nm. The lamp irradiance was measured to be 3.9 mW/cm^2. A HeNe laser was fitted with a lens to defocus the laser-beam and had an irradiance of approximately 5 mW/cm^2.

Cryogenic system

An Oxford Instruments Spectromag 4 (SM4) cryostat was used to cool the sample chamber and the superconducting magnet required for MCD measurements.

The cryostat is a cylindrical steel container with several levels of insulation including a high vacuum (~10^{-7} mbar) jacket (maintained by a JAVAC turbomolecular pump), liquid nitrogen jacket and "inner" and "outer" compartments. These compartments are pre-cooled with liquid nitrogen, which was then removed before filling the outer compartment with liquid helium. The bulk of liquid helium was stored in the outer compartment and a needle valve allowed transfer of a small amount of liquid to the inner compartment, which bathed the sample.

By vacuum pumping on the liquid helium in the inner compartment, a helium superfluid was formed which had a base temperature of 1.7 K. This was carried out prior to spectroscopic measurements to maximise S/N. The pumping on the He to below the lambda point of helium (2.17 K) was a practical consideration, namely to avoid the bubbles formed when liquid helium boils. These bubbles interfere with the measuring light and therefore decrease the S/N.

A sample chamber was attached to the bottom of the SM4 cryostat consisting of a copper radiation shield and quartz windows. There were also windows on the axis perpendicular to the spectrometer optical axis to allow the introduction of actinic light.

Sample Rod

PSII samples were loaded into quartz cells, which were mounted at the end of a custom-built sample rod. The sample rod was inserted into the sample chamber through the top of the SM4 cryostat and held the sample at the optical axis of the spectrometer. It was equipped with a temperature sensor (carbon resistor) and heater, both situated near the sample mount and wired up through the inside of the rod to two controllers.

An Oxford Instruments 3120 temperature controller measured the resistance (proportional to temperature) at the sample and allowed control of the heater. An Oxford Instruments 3400 DL resistance meter was required to measure temperatures below 4 K. The temperature was measured relative to a reference electrode placed in the liquid nitrogen jacket.

Using a plastic guide, the rod could be accurately rotated ninety degrees to facilitate sample illumination and rotated back to the initial position for a post-illumination spectrum.

Lock-in Amplifiers

Lock-in amplifiers are instruments used to filter out noise from an electronic signal. They operate by "locking in" to a signal modulated at a specific frequency while rejecting signals that are unmodulated or modulated at alternate frequencies.

In the MCD spectrometer, lock-in amplifiers served two purposes. The interrogating light from the lamp was modulated with an optical chopper at 489 Hz and detected with a Stanford Research Systems SR510 lock-in amplifier (marked #TL in Figure 2.1). Consequently, any stray light or other noise source, was ignored and this helped to improve the S/N in the absorption spectra collected.

The second use of lock-in amplifiers was to detect left- and right-circularly polarised light for (M)CD measurements. The photoelastic modulator produced the two polarisations of light alternating at 57 kHz and hence by detecting the signal with the lock-in referenced at the same frequency, labelled #CP (Princeton Applied Research Model 124A) the difference in intensity between the two polarisations of light was measured. The signal was then passed through another lock-in, labelled #Het (same model as the #TL amplifer), referenced to the chopper frequency.

Photodetectors

To perform an absorption measurement light intensity needs to be detected. Photodetectors fulfil this function by converting photons to a voltage or current that can be measured and recorded. Two types of detector were employed; a photomultiplier (PM) tube and avalanche photodiode. The detectors worked optimally in different regions of the electromagnetic spectrum and thus the wavelength range of interest in each experiment determined the choice of detector. The PM tube was used for visible measurements (400 – 750 nm) while the photodiode was employed for mid-visible to NIR measurements (500 – 1100 nm).

Photomultipliers

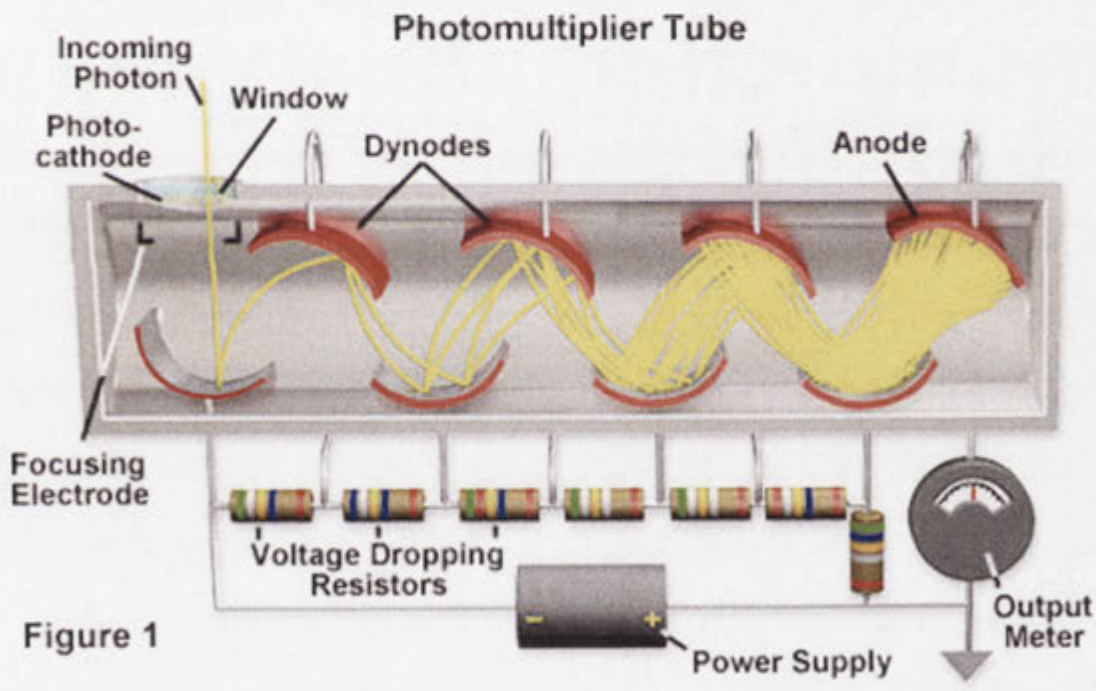

Figure 2.2 Schematic of a photomultiplier tube.[3]

A schematic of a photomultiplier tube is shown in Figure 2.2 and the principles behind its operation are described here. Photons impinge a photocathode at the front of the device and electrons are liberated due to the photoelectric effect. A focussing electrode directs the electrons to a positively charged electrode known as a dynode.

When electrons strike a dynode, further electrons are released due to secondary emission and these collide with the next dynode in the chain. The potential of each dynode is increasingly positive hence each collision produces more electrons than the previous one. The result of this arrangement is a multiplication of electrons reaching the anode compared with those initially ejected at the photocathode, typically by a factor of 10^6. An accumulation of charge on the anode results in a sharp current pulse that can be measured and is proportional to the number of incident photons.

A Hamamatsu R669 photomultiplier tube connected to a 412B high voltage power supply was used in this work.

Avalanche photodiodes

The avalanche photodiode is a type of light-sensitive diode; a component that permits electron flow in only one direction.

Photodiodes consist of a p-n junction, an interface of p- and n-type semiconductor materials, so-called because they possess excess positive and negative charge respectively. Photon absorption causes electron excitation and results in the formation of a positive electron-hole and mobile negative-charge. The mobile electron migrates to the p-region which gives rise to a current. The production of this photoinduced current, known as the photovoltaic effect, is exploited to make solar cells. Photovoltaics are not suitable for photodetection because the response is non-linear with respect to light intensity.

If a reverse-bias is applied to the photodiode it induces a very high resistance. A reverse-bias, in this context, is a constant voltage applied across the p-n junction where the negative and positive terminals are applied to the p- and n-regions respectively. Light absorption causes a drop in the resistance and hence light can be detected by monitoring the current of the device. If the reverse-bias is sufficiently high, free electrons can have

enough energy to liberate electrons from atoms in collisions. This process is known as avalanche breakdown and hence devices making use of this phenomenon are called avalanche photodiodes. The result of the avalanching process is the multiplication of photoelectrons and hence a dramatic improvement in the sensitivity of the detector.

Superconducting Magnet

The magnet consists of two Niobium-Titanium alloy coils, which sit in the outer compartment of the SM4 cryostat, about the sample compartment. To achieve superconductivity, they were first cooled to 4 K (by filling the cryostat with liquid helium) and then a current of 45.76 A was introduced into the coils resulting in a 5 T magnetic field. The coil arrangement, in which the coil separation is equal to the radii, is known as a Helmholtz pair and results in a uniform magnetic field between the coils.

Computer

A PC was used to control the spectrometer and record absorption spectra. It drove the stepper motor, which in turn adjusted the angle of the diffraction grating in the monochromator and therefore determined the wavelength range and the spacing and rate of data collection. The total light intensity (and difference in lcp and rcp light intensity) at each wavelength was recorded by reading the voltage from the #TL and #Het lock-in amplifiers connected to the photodetector.

2.2.2 Charge-Coupled Device Spectrometer

2.2.2.1 Overview of Operation

The charge-coupled device (CCD) spectrometer was named after its photodetector. It consisted of components arranged and synchronised to collect absorption spectra and was developed by Dr. Ronald Steffen.

A schematic of the main components and optical path of CCD spectrometer is shown in Figure 2.3. The spectrometer functioned as follows; white light from a halogen

lamp was focussed at the sample and split into its component wavelengths via a monochromator before finally being imaged on a CCD detector. The resulting electron count (proportional to light intensity) was recorded as a function of wavelength.

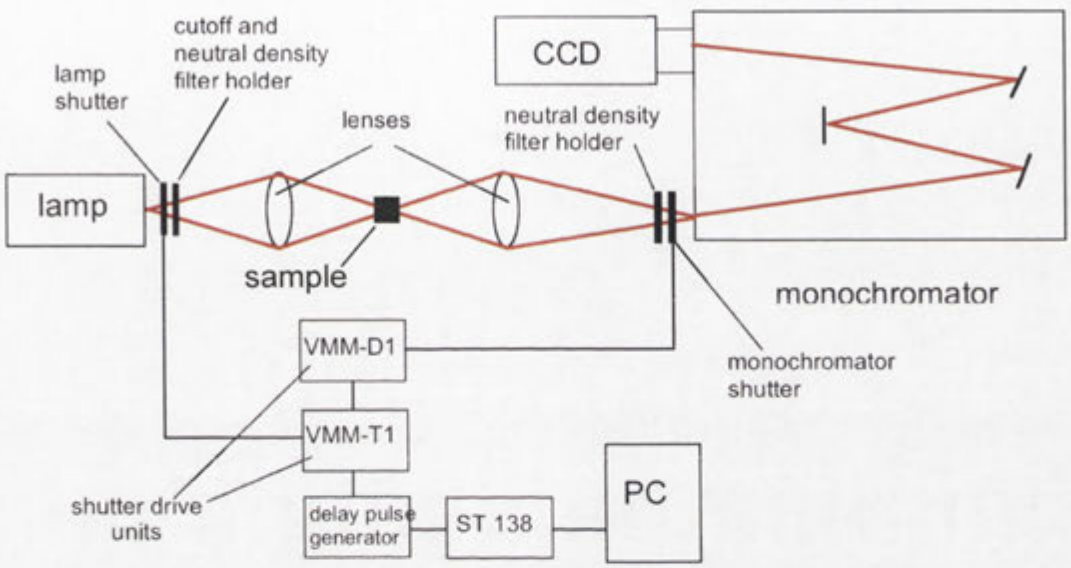

Figure 2.3 Schematic of the CCD spectrometer. The light path from the halogen lamp to CCD detector is depicted as a red line.

2.2.2.2 Components

Optics

A lamp housing with a cooling fan similar to that used in the MCD spectrometer was utilised. Light was focussed into a sample chamber and guided into a monochromator before being imaged on a CCD detector. The light wavelength, bandwidth and intensity were controlled with slits, shutters and filters depending on the requirements of the experiment being executed. The system was designed to exclude as much room light as possible.

The monochromator slit was set to a compromise width to balance between total-light throughput and spectrometer resolution. It was attenuated to a width below which the resolution of the sharpest spectral features typically observed was not improved.

Cutoff filters were used to block out infrared (1-69 Corning), ultraviolet (OG490 longpass) or visible light (RG645) depending on the wavelength range of interest in an experiment. The aim was to minimise the intensity of measuring light falling on the sample.

Neutral density filters placed before and/or after the sample were used to attenuate the light intensity at the sample and reaching the detector. By placing an OD 2 neutral density filter before or after the sample, low or high intensity light respectively (labelled LL and HL in this work) fell on the sample while maintaining a constant fluence at the CCD detector.

Cryogenics

A flow tube system with liquid helium was used to cool the sample to ~5 K. This consisted of a liquid helium dewar into which a heating resistor and specially designed quartz tube were inserted. The tube consisted of an outer vacuum jacket (pumped down each day with and oil diffusion pump before commencing an experiment) for insulation and an inner section in which sample mounted on a rod was inserted. It was silvered below the sample level to minimise heat loss. The resistor caused helium to boil off and cool the sample as it flowed past it

Shutters

The shutters (Vincent Associates model VS25S2S1) were controlled by separate drive units (Vincent Associates Single Channel Shutter Driver(/Timer) models VMM-D1 and VMM-T1 respectively). The drive units were connected to a (Stanford Research Systems model DG535).

To collect a single spectrum the delay/pulse generator was triggered. This produced a TTL pulse which activated the shutter drivers that, in-turn, simultaneously opened both shutters for 100 ms. Multiple spectra were collected by configuring the

delay/pulse generator to automatically trigger at regular fixed time intervals. The minimum time between spectra collection was 6 s due to the time taken to transfer the data of one spectrum from the CCD to the PC.

The interrogating light was used to illuminate the sample at the same time a spectrum was acquired. When taking multiple spectra the lamp shutter could be configured to remain open resulting in continuous illumination of the sample (spectral acquisition, however, was still limited to one spectrum per 6 s).

Temperature Sensor

The sample rod was equipped with an iron-gold thermocouple, which reported the temperature near the sample via a voltage read out on a voltmeter.

Charge-Coupled Device Detector

CCD detectors consist of light-sensitive elements (known as potential wells or pixels) arranged in a two-dimensional array. When a pixel is struck by a photon an electron is liberated via the photoelectric-effect. The number of electrons (charge) deposited on a pixel is therefore proportional to the number of photons (light intensity) incident with that pixel.

The CCD spectrometer was designed such that after the interrogating light had passed through the sample it was spatially resolved with a monochromator and hence each column on the CCD chip corresponded to a wavelength.

To maximise the S/N of a spectrum the number of electrons in each column was summed. This was achieved by "binning", that is, shifting all the electrons in a column down to the pixel in the last row. The charge was then shifted horizontally where it was converted to a voltage and recorded on the PC.

The CCD detector used was a liquid-nitrogen cooled Princeton instruments model EBHRST. It consisted of 1340 × 400 rows of pixels, each of which had dimensions of 20 × 20 μm.

Computer

Absorption spectra were recorded on a PC that was interfaced with the CCD detector via a ST 138 controller.

2.2.3 Comparison of MCD and CCD Spectrometers

Over the same time period it was possible to take many more spectra with the CCD rather than the MCD spectrometer because the CCD spectrometer could be prepared relatively quickly and spectra could be acquired relatively rapidly. Despite being more time consuming, the MCD spectrometer could facilitate experiments not possible on the CCD system.

The MCD spectrometer exposed the sample to very low fluence but took a significant time to collect a spectrum (typically 5 – 10 min). With the CCD system, the situation was reversed, that is, relatively high fluence impinged on the sample but spectra were collected in a very short time (100 ms). This meant that in the process of collecting a spectrum, the measuring light in the CCD spectrometer caused greater Q_A^- formation than in the MCD spectrometer. On the other hand the CCD could probe processes occurring on a much shorter time scale, that is, milliseconds versus minutes. The CCD could address kinetic processes occurring on the milliseconds (one spectrum) or seconds (several spectra) timescale compared to several minutes with the MCD system.

The MCD spectrometer could attain a lower temperature than the CCD system, namely 1.7 K as opposed to approximately 5 K. Furthermore, it was easier to maintain a higher temperature for annealing with the MCD system by raising the sample above the

liquid helium. In the CCD system, the temperature was raised by turning off the helium heater but it was difficult to maintain a constant temperature since it relied on manually turning on and off the heater and was affected by the backpressure in the helium return line.

2.3 References

[1] R. J. Pace, P. Smith, R. Bramley, D. Stehlik, *Biochimica et Biophysica Acta* **1991**, *1058*, 161.

[2] P. J. Smith, Australian National University **1996**.

[3] Photomultiplier Tube <http://www.astro.virginia.edu/class/oconnell/astr130/im/photomultiplier.jpg> **2010**

3 Experimental Methods

3.1 Preparation of Samples for Spectroscopy

PEM samples were obtained from storage (-80°C freezer) and left to thaw in the dark and on ice (typically for ~1 hour). Cryoprotectant (neat glycerol or a 1:1 (v/v) ethylene glycol/glycerol mix (EG/Gly)) and PSII Storage Buffer were combined in a 500 μL Eppendorf tube. When neat glycerol was used, it was diluted to 70% (v/v) in PEM storage buffer (see Section 2.1.1) so that it could be accurately transferred with a micropippette. The final cryoprotectant concentration was typically 40-45% (v/v).

Under dim green light the PEM sample was added to the cryoprotectant / buffer mixture in the Eppendorf tube. It was thoroughly mixed by repeatedly drawing the sample up and down in the micropipette and brief stirring (a few seconds) with a vortex.[†]

The sample was carefully loaded into a quartz cell so that bubble formation was avoided (or masked if unavoidable). It was dark adapted for ten minutes at room temperature, either in the sample lock of the MCD spectrometer or in the sample rod of the flow-tube system for CCD spectrometer. The sample was then rapidly frozen and aligned in preparation for absorption measurements.

[†] Vortexing was found to assist homogenisation as discussed in Chapter 4. Other homogenisation techniques were used and these are described where relevant.

3.2 Preparation of Spectrometers

3.2.1 MCD spectrometer:

3.2.1.1 Filling the SM4 cryostat

Precooling

The SM4 cryostat was evacuated and cooled with liquid nitrogen before filling with liquid helium. This was done to minimise the consumption of expensive helium, which would be vaporised until the cryostat reached 4.2 K and liquid started to collect.

The insulation vacuum was pumped down to at least 10^{-3} mbar. With the needle valve open, both the inner and outer compartments were pumped down. The turbo pump was turned on and stabilised to a pressure of 10^{-7} mbar at which point it was connected to the insulation vacuum.

The SM4 was filled with liquid nitrogen to cool it down to 77 K and was then removed by blowing nitrogen gas through the system. It was very important to thoroughly remove all traces of liquid nitrogen because in the subsequent helium fill, helium would be wasted freezing the nitrogen. Furthermore, pieces of solid nitrogen could potentially block the needle valve and hence require that the system be warmed up to room temperature and the precooling protocol restarted.

Once the SM4 cryostat was cooled to cryogenic temperature, the cryostat could most efficiently be utilised by maintaining the low temperature over weeks or months.

Helium Fill

A vacuum pumped transfer line was inserted into a helium dewar (maximum capacity of 38 L of liquid helium) so that a flow of helium gas could just be felt (indicating a positive pressure). The dewar was raised on a hydraulic jack and the transfer line was inserted into a port on the outer compartment of the SM4 cryostat. Helium gas was introduced into the helium dewar which pressurised it and thus forced liquid helium

into the cryostat. The liquid initially vaporised on contact with the SM4 until a temperature 4 K was reached and liquid began to collect. Filling continued until the cryostat was full of liquid helium, monitored by temperature sensors within the cryostat.

3.2.1.2 Sample checks

Samples were left to dark adapt in the spectrometer lock for 10 minutes and then rapidly frozen by lowering the sample rod down into the liquid helium over ~1 min. The sample was checked for bubbles by passing 800 nm light through the sample and viewing it, on the opposite side, with a infrared viewer. If bubbles were observed the sample was removed and a new sample prepared and loaded into the cryostat.

The transmission of the sample was checked at 750 nm by comparing the signal detected with and without the sample in the beam path. If the transmission was too low (less than ~20 %) this indicated high scattering and would result in poor spectra. In this case the sample was replaced.

3.2.1.3 Spectrometer Checks

Each day before measurements were carried out the MCD spectrometer performance was checked. The spectrometer components (slit widths, voltage on the PMT etc) were adjusted to specific values and with the lamp on the output voltage on the 'total light' lock-in was read. A reading that deviated from the predetermined value when the system was running optimally (new lamp etc) indicated that there was a problem with the system which would have to be rectified before commencing the experiment.

Once the sample had been verified as being of good quality (see Section 3.2.1.2) liquid helium was transferred into the inner compartment and pumped upon to reach the supercritical fluid. Once a resistance of 7 kΩ was reached on the temperature sensor a series of rescans were made until the baseline was flat and to check that the sample

absorption spectrum looked reasonable. At this point illuminations and measurements could proceed depending on the type of experiment being carried out.

3.2.1.4 Baseline spectra

An absorption spectrum was taken with an empty sample rod in the space where the sample was normally placed and this was known as the 'baseline' spectrum. Absorption spectra were produced by taking the negative log of the sample spectrum divided by the baseline spectrum over the same wavelength range.

3.2.1.5 Illumination Procedures

The sample was scanned at least twice to ensure the sample was of good quality and the spectrometer was stable. Typically a wide scan was performed (400 – 750 nm) followed by a narrower scan for the area of interest either Q_x (535 – 575 nm) or Q_y (650 – 720 nm). The sample was then illuminated with the green lamp. Several scans were made after illumination, covering the same wavelength range to compare with the pre-illumination spectra.

3.2.1.6 MCD Measurements

Slit widths were opened to 500 μm to maximise S/N as the difference between lcp and rcp light being detected was typically very small. To measure MCD, separate spectra (over the same wavelength range) were taken with the magnetic field set at +5 T and -5 T. By subtracting the spectra taken at -5T from that taken at +5T, a spectrum with effectively twice the MCD signal was obtained. This is because the MCD component of the spectrum is reversed when the magnetic field polarity is reversed while the CD and baseline components are relatively unaffected. This is illustrated in the equation below.

$$\begin{aligned} 5T\ \text{Spectrum} - (-5T\ \text{Spectrum}) &= (+MCD + CD + BL) - (-MCD + CD + BL) \\ &= 2MCD \end{aligned}$$

3.2.2 CCD spectrometer:

3.2.2.1 Flow-tube system

The outer compartment of the quartz flow tube was evacuated with an oil diffusion pump. A liquid helium dewar was aligned under the spectrometer sample chamber, a resistor connected to a power supply was placed in the dewar and the flow tube was carefully inserted into the dewar. The flow tube was attached to the helium return line and aligned so that the light focussed just above the tube's silvering, the coldest part of the flow tube.

A current was passed through the resistor causing helium to boil and hence cool the flow tube. A customised sample rod was inserted into the flow tube and the temperature was checked at the sample. The current was adjusted to achieve ~5 K at the sample rod.

3.2.2.2 Calibration of the CCD

The CCD was calibrated each day an experiment was to be run with a neon lamp. The monochromator slit was closed to 50 μm to resolve the sharp transitions of the neon lamp. Firstly the rotational alignment of the CCD was checked and adjusted if required. The main peaks spanning the wavelength range of the diffraction grating were then assigned their known accurate wavelengths and software calibrated the CCD based on this data.

With the sample rod in place the maximum intensity of the lamp image was set to 30,000 counts by adjusting the lamp slit. This ensured the light intensity at the sample was the same between different experiments. The middle two hundred rows of the CCD were used because the light intensity dropped markedly outside this range.

3.2.2.3 Measurement of Spectra

In a typical experiment the flow tube was positioned in the helium dewar in the CCD spectrometer and helium heater was turned on. The flow tube was left to cool to ~5 K as the PEM sample was prepared.

The CCD spectrometer was flexible; with a number of different possible experiments that could be conducted depending on the configuration and timing of the different components. The technical minimum limit of the spectrometer was collection of spectra every 6.3 s with a minimum 100 ms exposure of the CCD per spectrum.

During the 6.3 s between CCD exposure, the shutters could be either closed or open. The illumination with the closed shutters between CCD exposure were termed a 'flash' where the measurement light beam also functioned as the actinic light beam (the illumination time was therefore 100 ms). The set-up with open shutter illumination were termed 'continuous' illumination which could be any duration over 100 ms (seconds or minutes if required) but spectra could only be collected at intervals of 6.3 s with a 100 ms collection time. A combination of flashes and continuous illuminations could be incorporated into the same experiment.

Light intensity at the sample was either 'low light' (LL) or 'high light' (HL), with the latter being 100 times more intense than the former. The light intensity was determined by the position of an OD 2 neutral density filter, which could be placed before or after the sample. The total light received by the CCD detector was therefore approximately the same whether a LL or HL illumination was conducted.

In all experiments, a baseline LL 100 ms spectrum was taken in which the sample rod was in place in the flow tube without any sample. A HL baseline spectrum was

collected if needed. All spectra were referenced to the first 100 ms LL (or HL as appropriate) baseline spectrum.

4 Optimisation the Optical Quality of Photosystem II Enriched Membrane Fragment Samples

4.1 Introduction

In this PhD research project, photosystem II protein-complexes were studied by the technique of cryogenic-temperature absorption-spectroscopy. In general, when conducting absorption spectroscopy experiments, high-quality data can only be obtained from high optical-quality samples. A high optical-quality sample, for the purposes of this work, was one that was as homogeneous as possible, exhibited minimal light scattering and prepared at an appropriate optical density for the spectral feature(s) of interest. A sample of poor optical-quality produces data of limited value because i) its absorption behaviour can deviate from that predicted by the Beer-Lambert Law and ii) spectra from such a sample can have a reduced signal-to-noise ratio (S/N) which limits the amount of information that can be extracted from the spectrum.

The main factor that reduces optical quality is sample heterogeneity. Heterogeneity can arise from several sources such as bubbles, particulates and thylakoid-membrane-fragment aggregation. Depending on the nature of the heterogeneity, it can give rise to a number of spectral effects such as light scattering, the flattening effect and fringing.

Light scattering is a broad phenomenon that was particularly problematic for PEM samples and has thus been discussed in a section separate from heterogeneity. Light scattering is caused by heterogeneities such as aggregation and particulates and manifests itself in absorption spectra as an apparent increase in sample absorption.

The flattening effect, due to heterogeneity, is a reduction in peak absorption of a sample that occurs due to aggregation within the sample forming strongly light absorbing particles of significant size. The reduction of peaks in absorption is the 'flattening effect'.

Another factor that affects optical quality is the sample optical density.

There was a significant effort, throughout this PhD research project, directed at developing protocols to reproducibly prepare samples of good optical-quality. This was required to enable the collection of good quality data. The theoretical basis of the factors identified in contributing to the optical quality (optical density, heterogeneity and light scattering) are discussed in Section 4.2 and experiments characterising some of these factors are presented in Section 4.3. The experimental techniques employed to address the factors and hence improve PEM optical quality are outlined in Section 4.4.

4.2 Phenomena that affect PEM optical quality

4.2.1 Optical Density

The optical density (OD) of a sample is its absorbance at a specified wavelength. In an absorption experiment the absorbance, A, at wavelength λ is defined as

$$A(\lambda) = -\log_{10}(T) = -\log_{10}\left(\frac{I}{I_0}\right) \qquad \textbf{Equation 4.1}$$

where T is the transmission of light through the sample, I_0 is the incident light intensity, and I is transmitted light intensity.

In this work, a PEM sample's OD refers to the difference between the maximum absorbance value in the Q_y spectral region (~676 nm) and the absorbance value at 750 nm[†] (which is assumed to be zero absorbance in PEM samples). According to the Beer-Lambert Law, absorbance is directly proportional to concentration and hence the

[†] Single beam spectrometers were used in this work and these can only measure a relative absorbance.

OD is a useful measure of PSII concentration. The integrated form of the Beer-Lambert Law is

$$A = \varepsilon l c \qquad \textbf{Equation 4.2}$$

where A is the absorption, ε is the extinction coefficient, l is the pathlength of light through the sample and c is the concentration of the absorbing chromophore. Absorption is a dimensionless quantity hence the units of the extinction coefficient must be the inverse of the length × concentration units. Typically the non SI units of cm and M (mol/L) are used for length and concentration and hence this establishes the extinction coefficient units to be M^{-1} cm^{-1} or L $mol^{-1}cm^{-1}$.

It should be noted at this point that in absorption experiments it is the light extinction that is measured, that is, the decrease in light intensity after passing through the sample. The extinction is usually equated with the absorption of chromophores but can be affected by factors other than absorption such as light scattering and flattening. In PEM samples the fraction of apparent absorbance in the Q_y region due to scattering correction was typically 3 – 10%.[§] Flattening has been shown to cause a decrease in extinction of about a third (see Section 4.4.1 and Figure 4.3). The OD is therefore not a completely reliable measure of PSII reaction centre concentration.

The choice of OD for a sample to be analysed by absorption spectroscopy is always a compromise between two factors. The OD must be high enough so that absorption signals of interest appear well above baseline artefacts in the spectrum. If the OD is too high, however, insufficient light reaches the detector, leading to a decreased S/N ratio or even clipping of the most intense peaks. In addition, a high OD sample

[§] Based on a straight-line approximation of the scatter at ~750 nm in several samples.

cannot be as uniformly illuminated as a lower OD sample as a consequence of the Beer-Lambert Law.

An OD of about 1 was found to be ideal for PEM samples, as this resulted in a reasonable compromise between spectrum quality in the Q_x and Q_y regions. In some experiments a very high OD (more than ~2) sample was used to maximise the absorbance in the Q_x region. Spectral regions of OD more than 2 correspond to less than 1% of light passing through the sample and hence the data in such samples were unusable due to excessive noise.

4.2.2 Heterogeneity

A system is homogeneous if all parts of the system are identical. If this condition is not met, then the system is said to be heterogeneous. Based on this definition, everything except a perfect vacuum is heterogeneous at some level. A pure gas, which is normally considered homogeneous, for example, upon closer scrutiny is, in fact, composed of discrete atoms or molecules and is therefore heterogeneous at the molecular level. This simple example demonstrates that the degree of homogeneity of a system depends on the spatial level that one examines a system.

Hereafter, the terms "homogeneous" and "heterogeneous" are therefore defined as meaning homogeneous or heterogeneous at, or above, the scale of the wavelengths of light employed to analyse the PEM samples (~400 to 1000 nm). Since experiments were typically performed at temperatures of 5 K or less, heterogeneity arising from molecular fluctuations over time was minimal and certainly much less than contributed from the structure of PEMs.

Heterogeneity in PEM samples

The heterogeneity found in PEM samples can be divided into two classes: macroscopic and microscopic.

Macroscopic heterogeneity, that is, heterogeneity visible with the naked eye, in PEM samples arose from opaque particulates present in the bulk sample or air bubbles inadvertently introduced into the quartz cells during the sample loading procedure.

Microscopic heterogeneity is defined here as heterogeneity on the scale below detection by the naked eye. Given that chromophores, such as chlorophyll, are localised in PSII complexes, there will always be microscopic heterogeneity as long as the structure of the protein is maintained. Moreover, the thylakoid membrane fragments in which the PSII complexes are embedded tend to aggregate and form larger structures. Indeed, the structure and therefore the functioning of thylakoid membranes *in vivo* is dependent on this tendency. Spinach PSII is known to aggregate with increasing protein concentration.[1]

Aggregation is an effect that can sometimes translate into heterogeneity at the macroscopic level (see the experiment in Section 4.4.1). Aggregation in PEM samples can, however be minimised with the appropriate use of detergents. The localisation of chromophores leads to a phenomenon in absorption spectroscopy known as flattening and its origin and consequences are described below.

Heterogeneity may result in either a surplus (for example, if the sample has a bubble) or deficiency (in the case of large particles) of light reaching the detector than compared to a homogeneous sample.

The importance of preparing homogeneous samples

It was important to prepare homogeneous samples to maximise the quality and usefulness of the data obtained from the absorption experiments performed on PEM

samples. There are several potential negative consequences of analysing a heterogeneous sample.

A macroscopically heterogeneous sample is not physically well defined so its true absorbance profile cannot be determined. In terms of the Beer-Lambert law (see Equation 4.2) this translates to the pathlength *l* (sample thickness) being variable throughout the sample so the proportionality between absorbance and chromophore concentration does not hold. Hence, the lack of accurate absorbance information makes it impossible to systematically compare experiments performed on different samples since the basic assumption that chromophore concentration scales with sample OD becomes invalid.

The absorbance of heterogeneous samples can be very sensitive to their precise position in a spectrometer. If a heterogeneous sample physically shifts during the experiment, this can lead to a change in absorption and therefore, an apparent change in concentration. This occurs because the interrogating light will pass through a different area of the sample and since the sample is heterogeneous, it can have a different average concentration of chromophores in different parts of the sample.

Microscopic heterogeneity can manifest itself in a number ways in absorption spectra. A special case of microscopic heterogeneity, known as the flattening effect, is particularly relevant to biological samples and is discussed in the next Section. The most dramatic effect caused by microscopic heterogeneity is light scattering, which is explained from first principles in Section 4.3.3.

In many cases during the analysis of PEM samples by absorption spectroscopy, heterogeneity often prevents the interrogating light that enters the samples from reaching the detector. Light absorbed by macroscopic particles or scattered by microscopic structures reduces the S/N ratio in spectra and effectively means less information is

available about the system. In other words the spectrum appears "noisy" and lower in quality than had it been obtained from a more homogeneous system.

4.2.2.1 Theory of The Flattening Effect

A special-case of heterogeneity, relevant to PEM samples, arises when strongly absorbing chromophores are inhomogeneously distributed. In absorption measurements of such systems this type of heterogeneity gives rise to the 'flattening effect'[†] so-called because the light extinction observed is less than would be the case if the particles were homogeneously distributed. The effect was first described by Duysens in 1956[2] and hence sometimes referred to as Duysens flattening.

Duysens first considered a suspension of idealised non-scattering cubical particles of uniform size and thickness. From statistical considerations he derived equations that relate the absorbance of a suspension to that of a single particle. The equations contain, as parameters, the particle thickness and the surface area of all particles present to the incident beam. There was also a constant subtracted from absorbance values to correct for scattering. Duysens proceeded to generalise his equations to particles of non-uniform volume and thickness and of arbitrary shape. In the words of later researchers Duysen's equations "do not seem to be of a useful form".[3]

Bustamante and Maestre[4] extended and further generalised Duysen's work by means of the theory of fluctuations and obtained an expression for the degree of flattening expected in absorption measurements. They corrected the Duysen analysis by demonstrating that flattening is not, as he assumed, independent of the number of particles in suspension, due to the finite nature of the coherence area of light. They also showed that light-scattering effects are difficult to disentangle from flattening. Bustamante and Maestre's results are summarised below to describe the flattening effect.

[†] Known as the 'sieve effect' in the older literature.

The flattening effect can be conceptually illustrated by way of a thought experiment. Consider a cuvette containing a non-scattering chromophore solution that is illuminated with monochromatic light. The light can be mentally divided into a bundle of 'pencils' with each light pencil experiencing the local concentration of chromophores.

In a homogeneous sample the macroscopic transmission corresponds to the geometric mean of the transmittance of the light pencils. In a heterogeneous sample the macroscopic transmission corresponds to the arithmetic mean of the transmittance of the light pencils. It can be shown mathematically that when the two samples described above have the same total concentration of chromophores their mean transmissions are not equal. Furthermore, it can be shown by a statistical analysis that the absorbance of an inhomogeneously distributed suspension of chromophores is always less than that of a homogeneous solution. This is the theoretical basis of the flattening effect.

A mathematical expression relating the absorption of a heterogeneous suspension of particles in terms of its homogeneous state was derived from first principles[4]:

$$Abs_{susp} = Abs_{sol} - (2.303a^2l^2\langle(\partial c)^2\rangle/2) \qquad \textbf{Equation 4.3}$$

where Abs_{susp} is the absorbance of a heterogeneous suspension of particles, Abs_{sol} is the absorbance of the same suspension homogeneously distributed, a is the absorption coefficient and $\langle(\partial c)^2\rangle$ is the mean quadratic fluctuation of the concentrations (that is, a measure of the dispersion of the concentration values from its mean). At this point it is important to note that the extinction coefficient ε (from Equation 4.2) has been separated into two components a and s, the absorption and scattering coefficients respectively and are related by the expression $\varepsilon = a + s$. This expression reflects that the total extinction of incident light in an absorption experiment can be due to the absorption of light by molecules and/or the scattering of light.

An important point about Equation 4.3 is that flattening is proportional to the square of the absorption coefficient so flattening is predicted to be greater for highly absorbing regions in a spectrum compared to areas of low absorption.

The flattening effect can be greatly complicated when the sample extinction has a large scattering component. An expression for the total optical density OD_{TOT} of a sample including the contribution from light scattering was derived.[4]

$$OD_{TOT} = (a+s)cl\left\{1-\left(\frac{2.303(a+s)(1-q)}{2k\lambda^2}\right)\right\} \qquad \textbf{Equation 4.4}$$

Where a is the absorption coefficient, s is the scattering coefficient, q is probability of finding a particle in the volume defined by a light pencil, c is the mean chromophore concentration, l is the path length of a square cuvette and k is a constant.

From Equation 4.4 a number of important points are evident. The scattering contribution to the extinction, s, experiences a similar flattening to that of the absorption. The flattening term is proportional to $(a + s)^2$ which means there is a cross term ($\sim a.s$) corresponding to the interference of absorption and scattering terms. This means one cannot simply correct scattering contributions by subtractions of the form λ^{-n} ; a practice frequently carried out in the literature.

4.2.2.2 *Fringing*

Some spectra exhibited a sinusoidal interference pattern overlaying the spectrum. This was most probably due to 'fringing' which is an optical process due to the due to the interference between two parallel reflective surfaces. The effect is pronounced when there is a there is a gap between surfaces on the order of the wavelength of light. It occurred when using the sandwich type quartz cells, where after freezing, an air gap formed between the sample and quartz top window due to lifting of the cell.

The flat cell[5] eliminates the problem of fringing as it is a single piece of quartz with no parts free to move during the freezing process and hence no gap can form. Fringing has not been observed in experiments using flat cells.

4.2.3 Light Scattering

In an ideal absorption experiment, all the interrogating light that passes through the sample is collected by the detector. In that case, the light extinction is only due, and therefore equal to, the absorbance of the molecules in the sample. In practice, light can be scattered away from the path to the detector as it traverses the sample.

4.2.3.1 Theory of Light Scattering

Scattering is defined as a deviation from a straight trajectory of electromagnetic radiation due to one or more local heterogeneities in the medium through which the radiation passes. The scattering of electromagnetic waves is a widespread phenomenon and occurs in heterogeneous systems. All systems, apart from a vacuum, are heterogeneous on some level. Even pure gases, liquids and solids, which are normally considered to be homogeneous, are heterogeneous at the level of atoms and molecules. All media, therefore, scatter light.[6]

Matter is composed of electrons and protons, which are discrete electric charges. If an obstacle (which could be a single electron, atom, molecule, solid or liquid particle) is illuminated by an electromagnetic wave, electric charges in the obstacle are set into oscillatory motion by the electric field of the incident wave. Accelerated electric charges radiate electromagnetic energy in all directions and it is this secondary radiation that is called the scattered radiation. In addition to reradiating electromagnetic energy, the excited elementary charges may transform part of the incident electromagnetic energy into other forms of energy, as in the case of absorption.[6]

There are different types of scattering depending on the ratio of the wavelength of radiation being scattered to the dimensions of the scattering system. In this work, visible light with wavelengths of hundreds of nanometres was utilised with systems that ranged in dimensions from nanometres to micrometres. The relevant types of scattering are therefore Rayleigh and Mie Scattering; the former being applicable to structures much less than the wavelength of incident light, while the latter is applicable to structures on the order of, or larger than, the incident light.

Rayleigh Scattering

In this section the Rayleigh scattering equation is derived based on the approach outlined by Ware.[7] Consider a light wave that impinges on a particle and is scattered at an angle θ. The scattering process may be viewed physically through the oscillating dipole model. The incident light, which is assumed for simplicity to be plane polarised, possesses an oscillating field to which the scattering particle is subjected. The electrons in the particle will be displaced slightly by the electric field, creating induced positive and negative charge separation. The induced dipole p is proportional to the strength of the incident field E, and the constant of proportionality, α, is called the polarisability of the particle

$$p = \alpha E \qquad \textbf{Equation 4.5}$$

The incident field is oscillating at a very high frequency; the simplest representation of the field is of the form

$$E = E_0 \cos(\omega t - 2\pi x/\lambda) \qquad \textbf{Equation 4.6}$$

Where E_0 is the field amplitude, ω is the angular frequency of the light ($2\pi\nu$), x is the linear displacement along the axis of propagation and λ is the wavelength in the medium. The oscillating field causes the dipole to oscillate at the same frequency:

$$p = \alpha E_0 \cos(\omega t - 2\pi x/\lambda) \qquad \textbf{Equation 4.7}$$

The oscillating dipole reradiates light, which is called scattered light. The exact derivation of the scattered field requires complex mathematics but here it will be stated in its simplest form. An accelerated charge radiates light and similarly the field emanating from an oscillating dipole is proportional to its acceleration, d^2p/dt^2. A valid expression for the scattered field may thus be obtained by taking the second derivative of Equation 4.7 and introducing the geometric factor sin (γ/rc^2), where γ is the angle of the detection axis from the plane of polarisation of the electric field, r is the distance from the oscillating dipole and c is the speed of light. The result is

$$E_s = (-\omega^2 \alpha E_0 \sin\gamma / c^2 r)\cos(\omega t - 2\pi x/\lambda) \qquad \textbf{Equation 4.8}$$

Light detectors respond to the intensity of light, which is proportional to the square of the field. Thus by taking the ratio of the square of Equation 4.8 to the square of Equation 4.6, the scattered intensity (I_s) can be obtained.

$$I_s = \frac{16\pi^4 \alpha^2 \sin^2\gamma}{\lambda^4 r^2} I_0 \qquad \textbf{Equation 4.9}$$

This equation was derived by John William Strutt (who would later be known as Lord Rayleigh) in 1871. There is an implicit assumption in Rayleigh's equation that the scattering particle is much smaller than the wavelength of light. That is the entire particle experiences the same phase of the radiation at all times. It shows that scattering is more pronounced at shorter wavelengths due to the $1/\lambda^4$ dependence and is also strongly dependent on the particle size (α^2 dependence) since the polarisability of a particle is proportional to the number of its electrons and thus its mass.[7]

Equation 4.9 applies to a single small molecule suspended in space but is adequate for the purpose of qualitatively illustrating the light-scattering effect of particles in absorption spectra. Scattering in PEM absorption spectra was analysed qualitatively in Section 4.3.3.

To better describe the scattering arising from real systems, Equation 4.9 has been further developed. For example, modifications can be made to take into account particles suspended in a medium (such as a solution or glass), the non-ideality of solutions and the case where particles are on the order of, or larger than, the wavelength of incident light.

In the latter case, light can experience absorption, refraction, diffraction or phase retardation as it traverses a single particle. The most comprehensive theory to describe the intensity magnitudes (and angular profiles) was developed by Mie, who published his theory in 1908.[7] Mie scattering is discussed on the next page.

Resonance Enhanced Rayleigh Scattering

Rayleigh scattering applies only at wavelengths far from a molecular absorption band.[8] For wavelengths close to a molecular absorption band the scattering intensity deviates from the $1/\lambda^4$ dependence. This phenomenon is known as resonance enhanced Rayleigh scattering and is predicted by the same theory that predicts resonance enhanced Raman scattering. This is relevant to PEM samples because chlorophylls have intense absorption bands in the blue (Soret) and red (Q_y) wavelength regions.

For illustration, consider a sphere with radius r and refractive index n_{sph} (which is different from the refractive index of the surrounding medium, n_{med}) interacting with and scattering light of wavelength λ. If $r << \lambda$ then the cross sections for absorption and scattering are[6]

$$c_{abs} = (\pi r^2) 4x \,\mathrm{Im}\left(\frac{m^2 - 1}{m^2 + 2}\right) \qquad \textbf{Equation 4.10}$$

$$c_{sca} = (\pi r^2)\left(\frac{8}{3}\right)x^4\left|\frac{m^2-1}{m^2+2}\right|^2 \qquad \textbf{Equation 4.11}$$

where $x = \frac{2\pi r n_{med}}{\lambda}$ and $m = n_{sph}/n_{med}$

In a region near a spectral maximum the real part of m varies and the imaginary part of m increases, causing both the absorption and scattering cross-sections to increase. The scattering is, however, a much stronger function of m than the absorption cross section, so under certain conditions scattering at wavelengths in the absorption band will be observed despite increases in photon absorption.[9] This is the origin of resonance enhanced Rayleigh scattering.

Mie Scattering

Consider again, a light wave interacting with a spherical particle. The field of the incident beam is distorted by the presence of the scattering particle by an amount that depends primarily on the relative refractive index m. In Rayleigh's theory the effect of this distortion is neglected because only small values of m are considered (that is, the difference in refractive index of the particles and the medium is small and hence m approaches unity). Another factor which has also been neglected is the possibility of a phase shift of the scattered wave relative to the incident wave.[10]

Mie showed that if the field of radiation of a particle is represented by dipoles, quadrupoles and poles of higher orders, with the centre of the particle as the origin, that an exact and general solution of the scattering can be obtained for isotropic transparent spheres.[10] It is, however, an extremely complicated expression depending on three parameters; the complex relative refractive index, m, the radius and the wavelength. The total scattering S, for unpolarised light per unit intensity is given by

$$S = \frac{\lambda^2}{2\pi} \sum_{i=1}^{\infty} \left(\frac{a_i^2 + \rho_i^2}{2n+1} \right) \qquad \textbf{Equation 4.12}$$

where a_i is a function of $A = 2\pi r / \lambda$, ρ_i is a function of $2\pi rm / \lambda$ and n is the real refractive index.

Since, like most real systems of interest, the particles in PEM samples are not transparent or perfect spheres, the applicability of Mie scattering is limited and, at best, is a simple approximation.

4.3 Experiments

4.3.1 Aggregation Experiment

It was suspected that aggregation was occurring during the dark-adaptation time prior to spectroscopic measurements of PEM samples, so an experiment was conducted to investigate this possibility.

Experimental Method

PEM samples were diluted tenfold with PSII Storage Buffer (a typical dilution factor used in absorption spectroscopy measurements in this work) of which 20 μL was dropped on a microscope slide and observed under bright light. The effect of mixing and vortexing the samples was investigated.

Results and Discussion

It was observed that opaqueness visible to the naked eye occurred immediately or after a few seconds and this was ascribed to sample aggregation. Aggregation occurred in all eight samples tested, which were between ~10 and 20 months old and were sourced from different species (spinach, pea and brassica). One sample was made in an overseas laboratory (the Uppsala sample). Mixing or vortexing the samples did not prevent the aggregation.

It was found that aggregation in PEMs could be prevented by detergent (DDM) solubilsation or by a washing procedure outlined in Section 4.4.3.

4.3.2 Experiment to find minimum DDM concentration that prevents aggregation

Since aggregation was found to occur immediately after sample preparation (see preceding Section), an experiment was carried out to determine the minimum DDM concentration that prevented aggregation.

Experimental Method

Five Eppendorf tubes were prepared containing the same amount of PEM at a concentration typically used in spectroscopy. To each tube an aliquot of DDM was pippetted so that the final DDM concentration was between 0.1 and 0.5% w/v. The tubes were mixed with the pipette tip, left for 10 minutes at room temperature and vortexed. A 10 μL aliquot of sample was removed from the top of each tube and pippetted on a glass slide and observed.

Results and Discussion

The results are presented in Table 4.1 below. The samples were all initially homogeneous and light green in colour. In samples that exhibited aggregation, the droplet components appeared to separate out, with clumping of dark green particles localised in the centre of the droplet and decolourisation of the surrounding liquid.

% DDM(w/v)	*0*	*0.1*	*0.2*	*0.3*	*0.4*	*0.5*
observation	Immediate aggregation	Immediate aggregation	Immediate aggregation	No change	Slight aggregation	No change

Table 4.1 Observation of DDM treated PEM samples on glass slides.

The minimum concentration of DDM required to prevent aggregation was 0.3% w/v. This is comparable to a study by Hanley et al.[11] who treated PEM samples with

DDM to "improve the optical properties" and found a concentration of 0.5% w/v DDM was the lowest concentration that solubilised PSII.

Additionally, comparing their EPR and optical data of detergent treated and untreated PEM samples they found the reactions occurring were "essentially unaffected" by detergent. They were probably not concerned with the redox state of cyt b_{559} since their Mn depleted samples probably had cyt b_{559} initially oxidised and their optical experiments were done in the NIR region where cyt b_{559} does not absorb.

4.3.3 Qualitative Analysis of Light Scattering in PEM Samples

Although it is possible to extract physical information from scattering experiments this was not the focus of this PhD research project. Instead, the aim was to minimise light scattering by PEM samples, since scattering decreases the optical quality of absorption spectra. This was achieved by understanding the origins of scatter from a theoretical viewpoint (see Section 4.2) and qualitatively analysing scattering and non-scattering samples to be able to identify scatter and hence be able to evaluate the effectiveness of the techniques employed to minimise scatter. The qualitative analysis is presented below.

The absorption spectra of three PSII samples are presented in Figure 4.1.

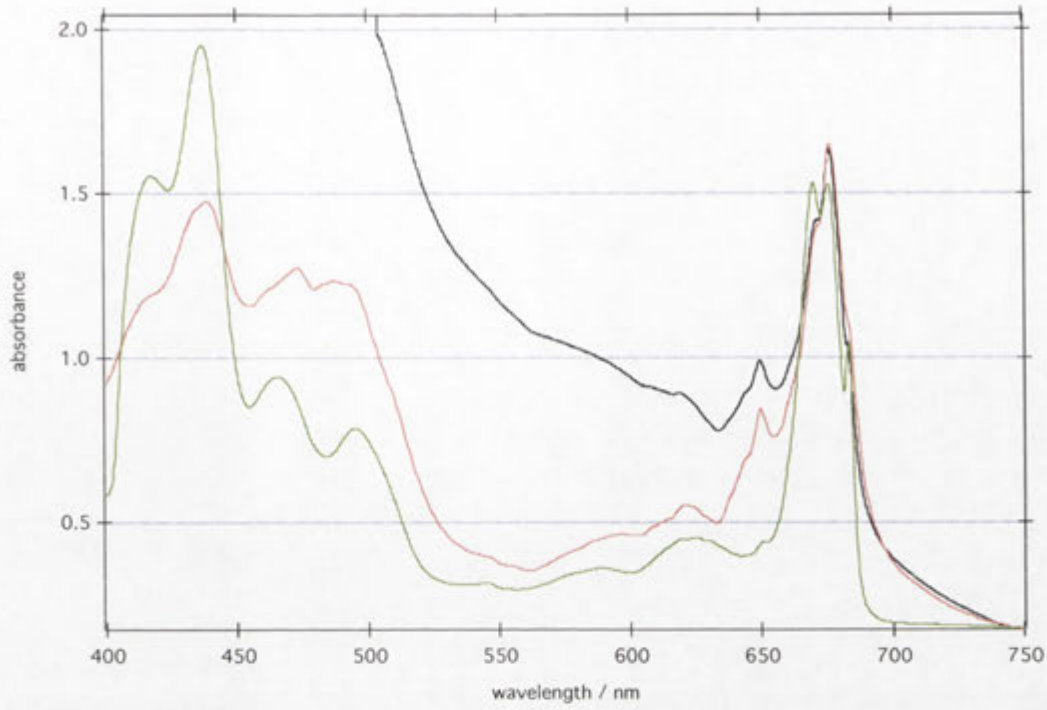

Figure 4.1 Example of light scattering in an absorption spectrum of a PEM sample. Sample details: CCD spectrometer, PEM (10 µL), glycerol (40 µL), store buffer (50 µL), dark adapted ~11 min, cooling to 5 K over 5 min, 1 LL flash. Comparison of a low scattering PEM (red trace), PSII core (green trace) and high scattering PEM sample (black trace).

The red trace is representative of a typical low-scattering PEM and the black trace is a PEM spectrum with high light-scattering. For comparison, a highly solubilised PSII core spectrum is shown in green. All the spectra were normalised to have approximately the same maximum absorption in Q_y.

At wavelengths less than about 650 nm the PEM high-scatter sample deviated markedly in extinction from the typical PEM sample, increasingly rapidly with decreasing wavelength. This illustrates that high-scattering samples are generally of limited value since no spectral features can be identified in this region, especially in the Soret region. In the Soret region, virtually no light can be accurately detected and the spectrum is therefore clipped. Although the difference spectra of such samples cancel out the scattering background, they are very noisy since very little light is reaching the detector.

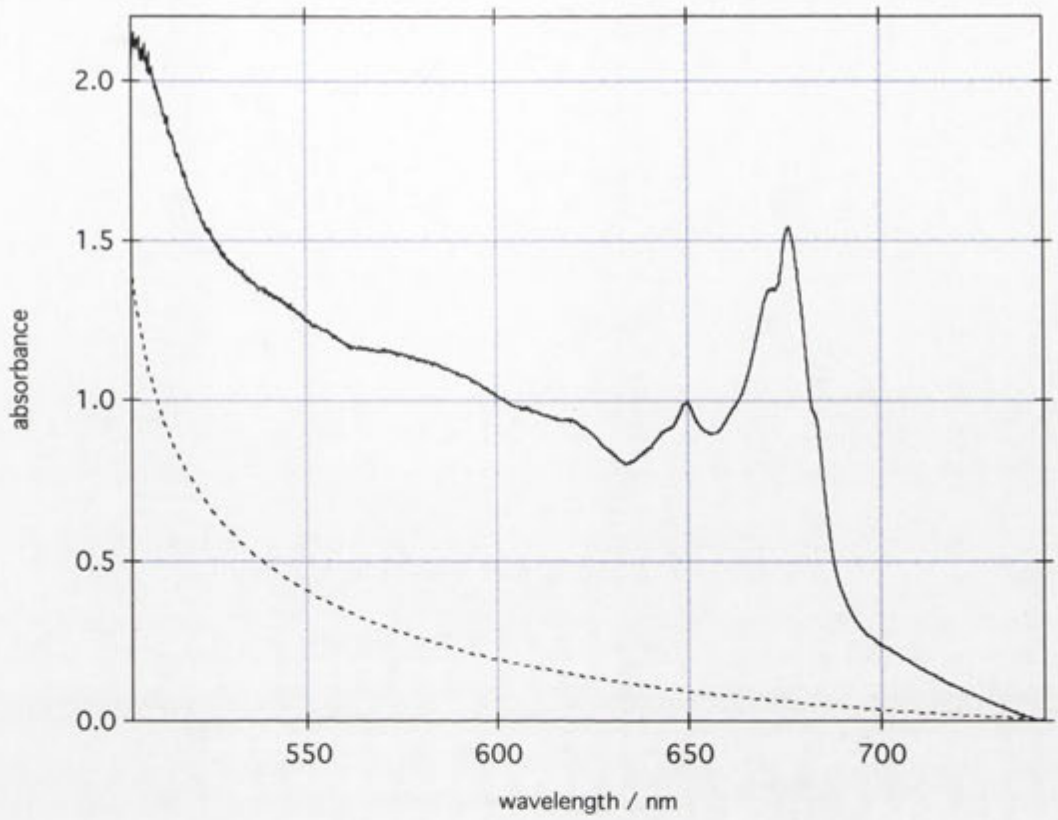

Figure 4.2 A fit of a baseline (dotted trace) to a highly scattering PEM sample (solid trace). The fit was applied to the I/I_0 trace of the PEM spectrum and converted to an absorption ($-\log_{10}$(fit)). The functional form of the fit was k / λ^4, where k is a constant.

The Q_x region (530 – 570 nm) is of special interest as it is the location of the pheophytin Q_x and reduced cyt b_{559} bands investigated in Chapter 5. In the Q_x region of the PSII core sample thes extinction was non-zero due to the absorption from adjacent carotenoid and chlorophyll bands. The low-scatter PEM sample was similar except for the presence of a sloping baseline. This slope was therefore due to scatter present in the PEM but not in core samples. The slope has been observed to differ markedly between PEM samples (for example, see Q_x spectra in Figure 5.11).

The (I/I_0) trace of the high scattering PEM spectrum from Figure 4.1 was fit to a function of the form $A = k / \lambda^4$. The fit was converted to an absorption trace and is shown in Figure 4.2. The underlying baseline was reasonably fit to the spectrum, hence indicating that the spectrum was likely subject to Rayleigh scattering, which has a λ^{-4}

dependence (see Equation 4.9). It is difficult to make an accurate fit of the scattering baseline in PEM spectra as one would have to distinguish between absorbing and scattering components. Furthermore, theory indicates that scattering is complicated by the flattening effect as well as resonance-enhanced Rayleigh scattering.

The scattering due to particles on the order of, or greater than, the wavelength of light is described by Mie scattering (see Equation 4.12).

Although structural data on the samples used in this work was not available, there is data on similarly prepared samples in the literature. Dimeric oxygen-evolving core-complexes from spinach characterised by electron microscopy and single-particle image-averaging analyses were found to have dimensions of about 17.2 nm × 9.7 nm with a maximum thickness of 9.1 nm.[12] In another electron microscopy study[13] PSII in spinach thylakoids were found to be roughly rectangular with dimensions of 17.6 nm × 14.1 nm and a thickness of ~8 nm. The dimensions reported in the two aforementioned studies can be assumed to be the lower limit of PSII particle size. Aggregates were observed with naked eye during the preparation of PEM samples in this work (see Section 4.4.1) and therefore must have been on the order of 50 μm or greater.

The above examples define the limits of the dimensions of microscopic particles that could be present in a PEM sample; from tens of nanometres up to the micrometre regime. In any given PEM sample there is probably a distribution of particles with dimensions ranging from nanometres to micrometres. Those in the nanometre range satisfy the Rayleigh equation, in that they are much smaller than the interrogating light, which is of the order of hundreds of nanometres. Particles with dimensions on the order of the wavelength of light or greater would then have scattering properties described by the Mie scattering theory. The form of the Mie scattering cannot be known since this depends on many factors including the size and shape of the scattering particles. Furthermore there

are other effects known to occur at areas of high absorption including the flattening effect (see Page 62) and resonance enhanced Rayleigh scattering (see Page 68).

4.4 Techniques for improving the optical quality of PEM samples

4.4.1 Detergent Treatment

The non ionic detergent n-dodecyl β-D-maltoside (DDM) is commonly used to solubilise PEM samples with aim of isolating the 'core' complex consisting of D1, D2, cyt b_{559}, CP47, CP43 and the 33 kDa extrinsic protein. The resulting preparations are known as "PSII core" preparations and those produced by Paul Smith[14] are an example. Since PSII core samples are known to exhibit minimal light-scattering (see the green trace in Figure 4.1) an experiment investigating the effect of DDM on the scattering of PEM samples was performed.

Experimental Method

An aliquot of a PEM sample was divided into two parts one of which was treated with DDM. The untreated (control) and treated samples were then analysed under identical conditions on the MCD spectrometer.

Bulk Sample: PEM, 45% EG/Gly, vortexed for 1 min and then split into two 100 μL lots (sample 1 and 2).

Sample 1: 5.25 μL (10% w/v) DDM added (final conc 0.5% w/v), vortexed ~30s, loaded into 200 μL sandwich type quartz cell, 10 min dark adapted. The percent transmission of the sample at 750 nm was 17%.

Sample 2: Left on ice, in the dark for 5.75 h (while first sample was being analysed), vortexed ~1min, prepared and analysed same way as Sample 1. The percent transmission of the sample at 750 nm was 19%.

MCD spectrometer protocol: Absorption of the Q_x and Q_y regions was measured, sample illuminated for 5 min with the green lamp. Absorption measurements were repeated.

Results and Discussion

The absorbance spectra of the two samples are shown in Figure 4.3.

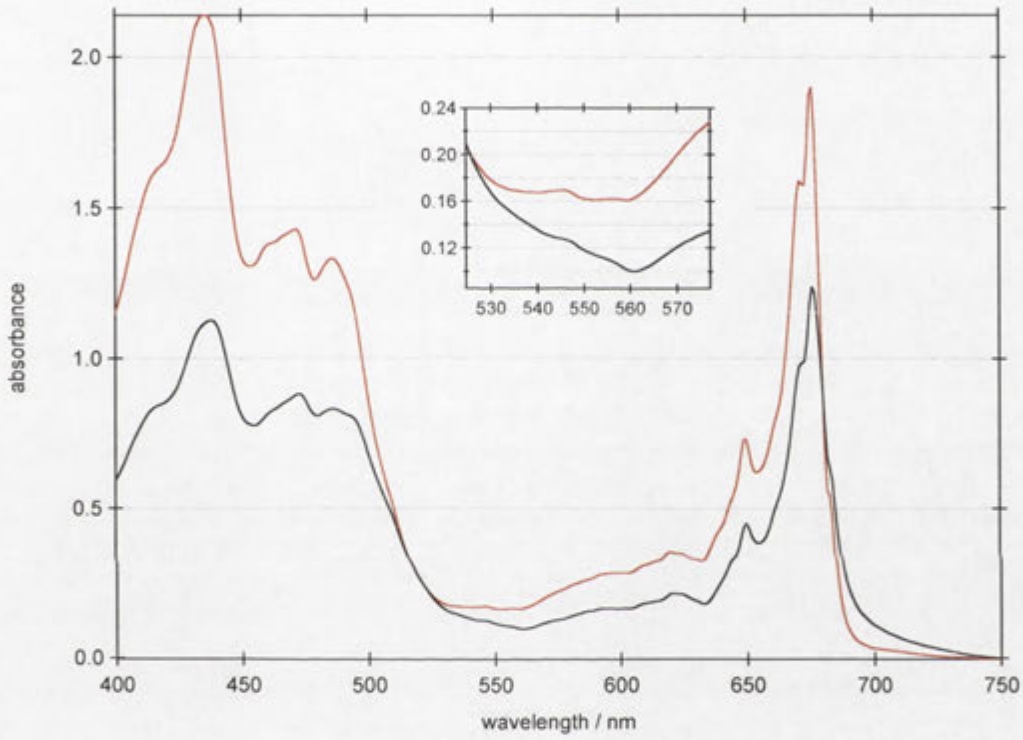

Figure 4.3 Absorption spectra of a DDM treated (red trace) and untreated (black trace) PEM samples. Spectra shifted so that zero absorbance is at 750 nm. T=1.7 K. Inset: Expansion of the Q_x region.

The most striking feature of Figure 4.3 was that the treated sample appeared to be 1.54 times more concentrated than the control based on the OD of the sample. This was interesting given that both samples were prepared from the same batch of PSII and made up to the same concentration.

The reason for the difference in OD was most likely due to the flattening effect; a phenomenon characteristic of samples where chromophores are spatially localised and which has been described on page 62. The hypothesis is as follows. The untreated sample was subject to the flattening effect whereas the detergent treatment solubilised thylakoid membrane particles resulted in a more homogeneous dispersion of chromophores and therefore a reduction in the flattening effect. This manifested itself as an increase in light extinction and hence an increase in the apparent absorption.

To test the hypothesis the treated spectrum was subtracted from the untreated spectrum, with the treated spectrum being scaled by a constant. Assuming there was no flattening the treated spectrum should simply be a scaled up version of the untreated spectrum and with an appropriate scaling factor, result in the zero spectrum (horizontal line equal to zero). It was impossible to find a constant such that the treated spectrum could be scaled and subtracted from the untreated spectrum. The scaling factor was varied so as to minimise the chl *b* feature at 650 nm and the resulting spectrum is presented in Figure 4.4 (red trace). The difference spectrum is consistent with flattening in the untreated sample because the greatest differences are seen at the regions of most intense absorption around the Q_y and Soret regions.[†]

The result is not definitive, however, because any scattering effects are also included in the difference spectra. The spectrum is, however, definitely more complicated than that expected by Rayleigh scattering alone, which would have a simple $1/\lambda^4$ form.

[†] Equation 4.3 showed that flattening is proportional to the square of the extinction coefficient of a chromophore.

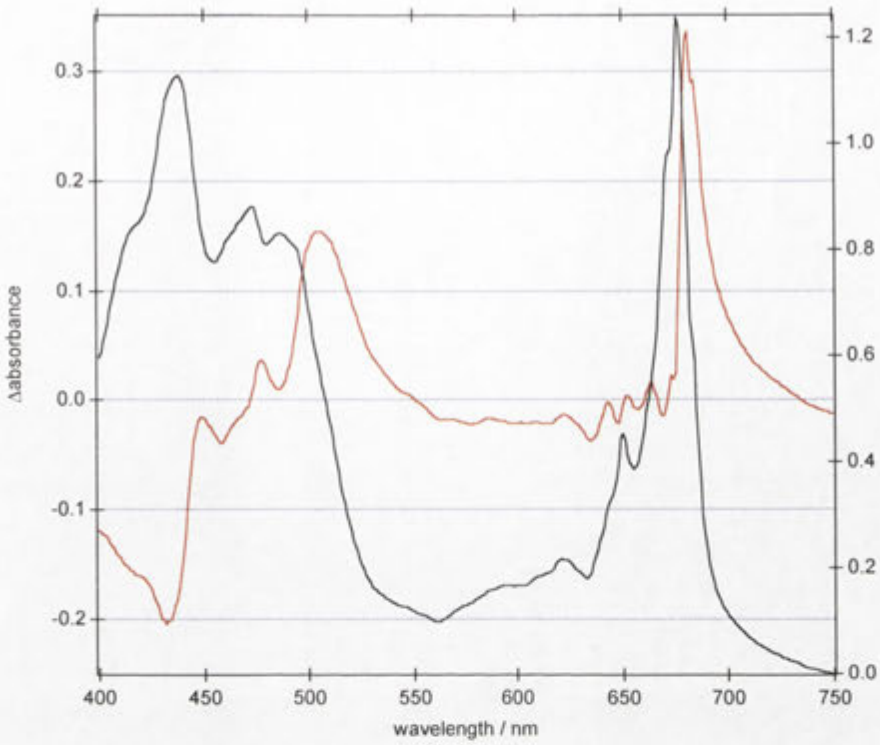

Figure 4.4 Red trace is untreated (black) minus 0.606 × DDM treated trace (not shown). Constant chosen to minimise difference at chl b peak at 650 nm. It was not possible to get zero spectrum subtracting one spectrum from the other.

A similar change in the magnitude of extinction to that seen in Figure 4.3 was observed by Jennings et al.[15] who investigated the effect of 0.06% DDM on the absorption spectra of PSII-Chl complexes. They stated that "in all cases, the detergent brought about a significant increase in optical density which varied between 20% and 40% at the absorption peak." The effect was greatest at the peak and decreases progressively at longer and shorter wavelengths, with decreasing optical density. They concluded the absorption effects were characteristic of the flattening effect[§] due to disruption of aggregated chl-protein complexes. They noted that in no case did DDM lead to significant changes in the absorption bands associated with the spectral forms.

The absorption spectra in this work were scaled to compare the scatter in the two samples (Figure 4.5) and it was evident in the treated sample there was an absorbance

[§] This was referred to in the paper by the original historical term "sieve effect".

decrease at ~690 nm, the lineshape was significantly flatter in the Q_x region and there was an apparently higher OD in the Soret region. These changes are consistent with the differences observed between a typical PEM and PSII core sample (see Figure 4.1) which has been analysed qualitatively in Section 4.3.3.

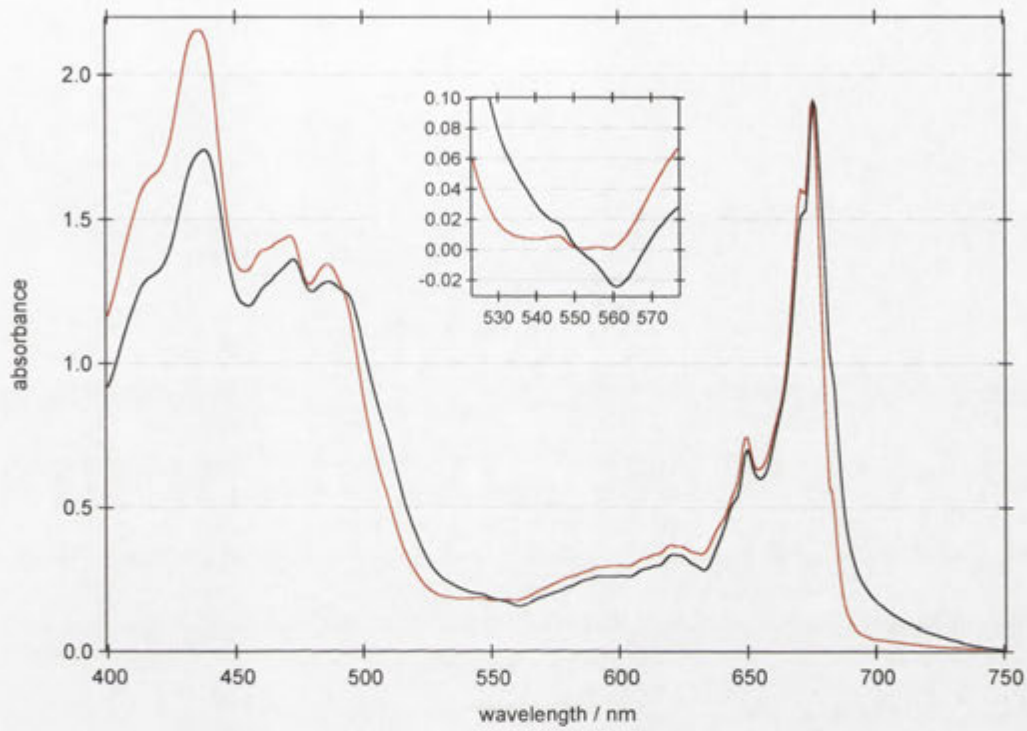

Figure 4.5 Same traces as in Figure 4.3 with untreated trace (black) scaled ×1.54. Inset: Expansion of the Q_x region.

The DDM treated and untreated illumination-induced difference spectra for the Q_x (Figure 4.6) and Q_y (Figure 4.7) regions are shown below. The Q_y electrochromic shift was 49% greater in magnitude in the treated sample than in the untreated sample. The $Pheo_{D1}$ Q_x shift, however, was identical in magnitude in both samples. A pronounced effect was observed in the Q_y region because, as seen in Figure 4.3, flattening is much more pronounced in the Q_y relative to the Q_x spectral region.

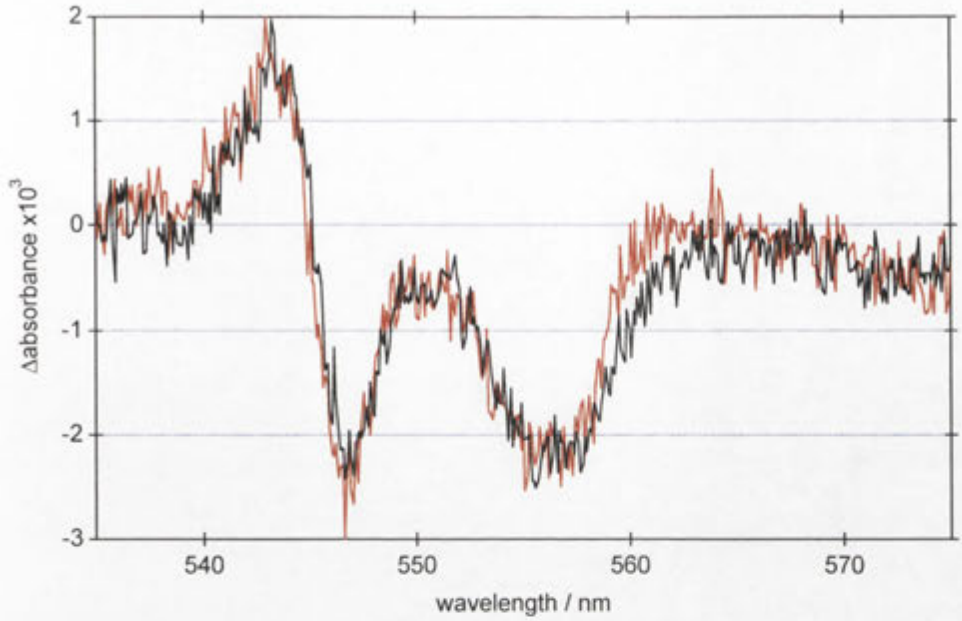

Figure 4.6 Dark-minus-illuminated spectra (Q_x region), 5 minute illumination of samples at 1.7 K by green lamp. Same samples as in Figure 4.3, DDM treated (red trace) and untreated (black trace).

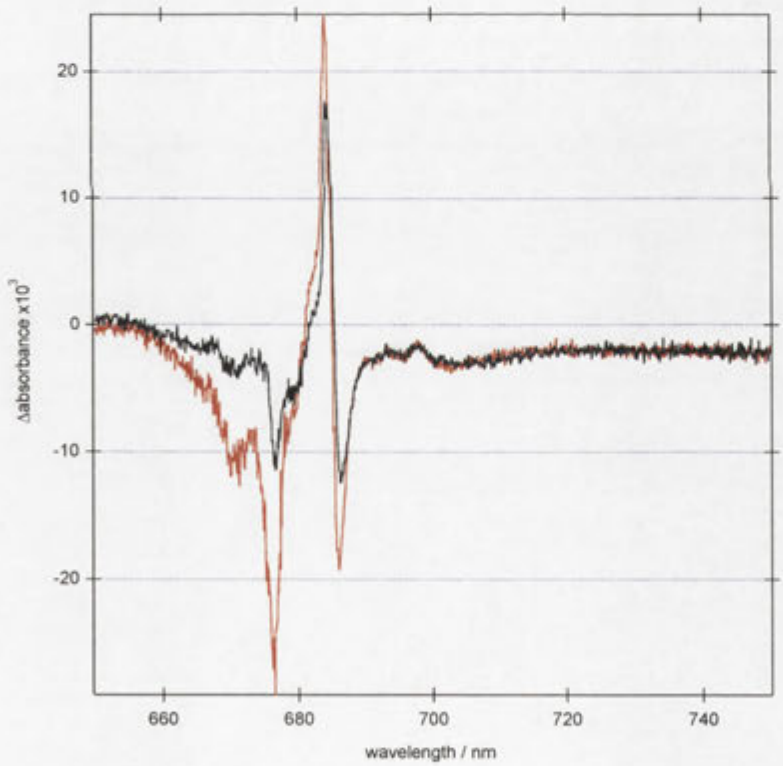

Figure 4.7 Untreated (black trace) and DDM treated (red trace) Q_y illumination induced difference spectra. Spectra were vertically offset for clarity. Treated Q_y shift is 1.49 × untreated Q_y shift.

4.4.2 Vortexing

The vortex mixer (or simply "vortex") is a bench-top laboratory device used to mix small vials of liquid. It consists of an electric motor with the drive shaft oriented vertically and attached to a cupped rubber piece mounted slightly off-centre. As the motor runs the rubber piece oscillates rapidly in a circular motion. When a vessel of liquid such as an Eppendorf micro test-tube is pressed into the rubber cup (or touched to its edge) the motion is transmitted to the liquid inside and a vortex is created which rapidly mixes the liquid.

The vortex would be expected to disperse PEM samples and the effect of vortexing on the scattering in the absorption spectra of such samples was investigated.

Experimental Method

In an experiment spectroscopically comparing two identically prepared PEM samples, one sample was vortexed for a minute and the other not vortexed. The sample details are as follows.

Sample 1: Spinach PEM, 41% EG/Gly (1:1), 200 μm sandwich-type cell, dark adapted for 10 min, sample vortexed for 1 min. Transmission at 750 nm was 21%, 5 min green illumination.

Sample 2: Made up in the same way as sample 1 (from the same PEM batch), transmission at 750 nm was 17%, no vortexing, sat on ice in the dark for 9.5 h (only mixed by manual stirring by pipette and drawing in and out of the pipette).

Both samples were analysed on the MCD spectrometer and both were illuminated for 5 min with the green lamp.

Results and Discussion

The absorption spectra of the two samples are shown in Figure 4.8. The results for the vortexed sample and its control are very similar to the DDM treated sample (see Section 4.4.1). The vortexed sample was apparently more concentrated than its control (a 1.32 fold increase). The spectrum of the control was scaled up to the OD of the vortexed sample (see Figure 4.9) and it was clear the vortexed sample had slightly less scattering than the control. If the Rayleigh scattering was very different between the samples one would expect a pronounced difference in the absorption at the blue end of the spectrum, however, this was not the case. The vortexing therefore probably dispersed aggregates into particles on the order of hundreds of nanometres or micrometre scale. The dispersion of the chromophores within the particles therefore resulted in a reduction of the flattening effect in the vortexed sample treated in a similar process to that which has been described for the DDM treated particles.

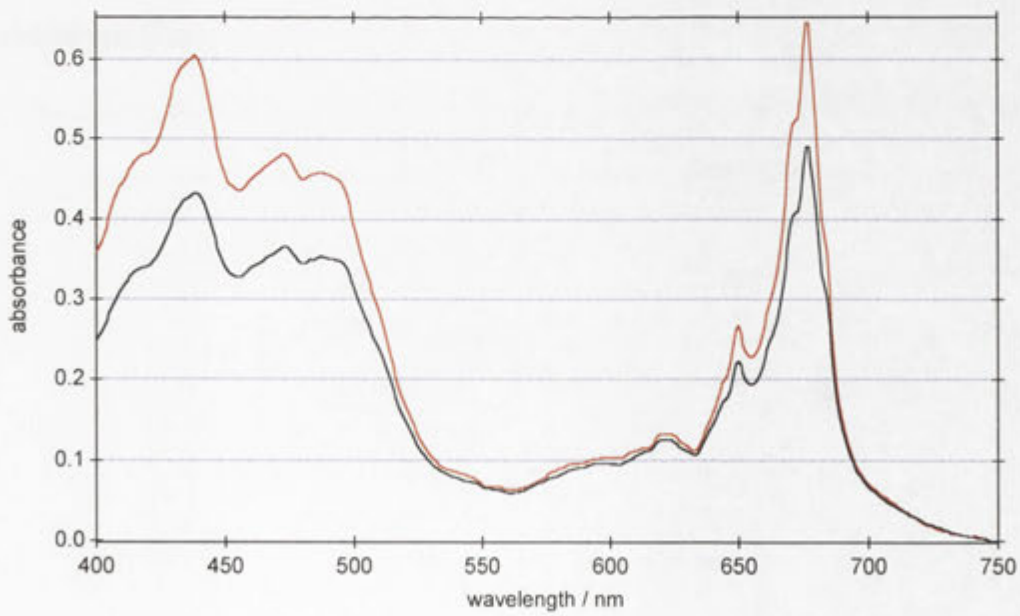

Figure 4.8 Absorption spectra of a vortexed (red trace) vs non-vortexed (black trace) PEM sample.

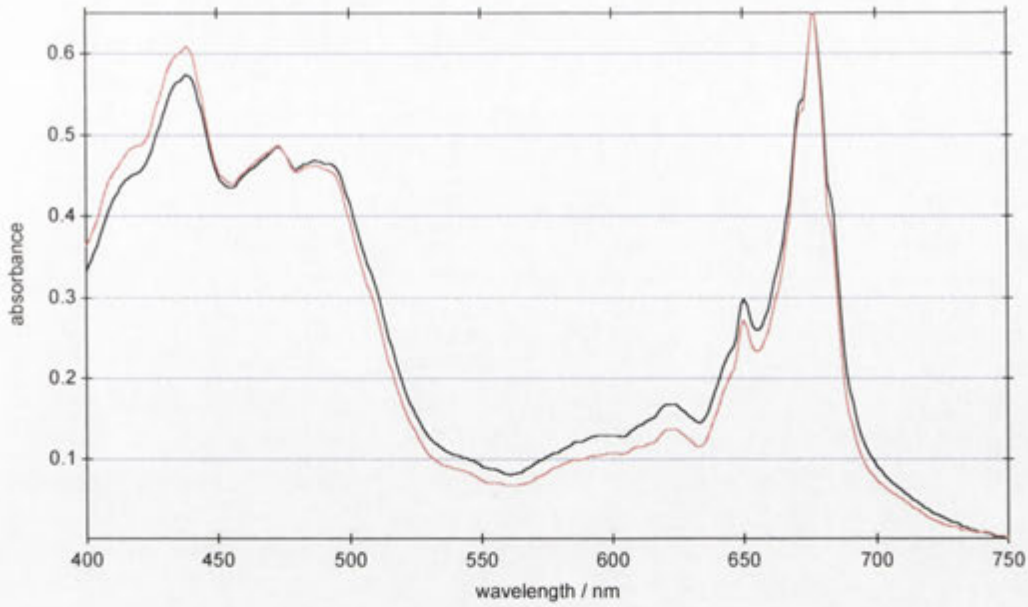

Figure 4.9 As for Figure 4.8 with vortexed sample scaled up

The Q_y shift of the vortexed sample (Figure 4.11) was increased (by 53%) compared to control while the pheophytin Q_x shifts (see Figure 4.10) were identical in the both the vortexed and control samples. This pattern of results was exactly mirrored in the DDM treated samples.

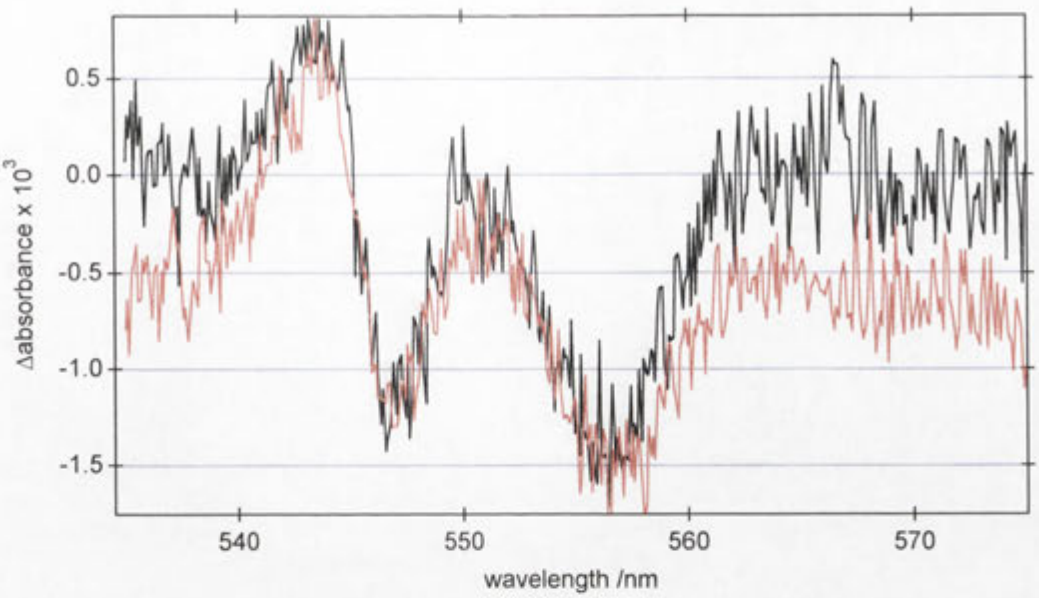

Figure 4.10 Comparison of the illumination-induced difference spectra of a vortexed (red trace, linearly corrected) and a non vortexed (black trace) PEM sample.

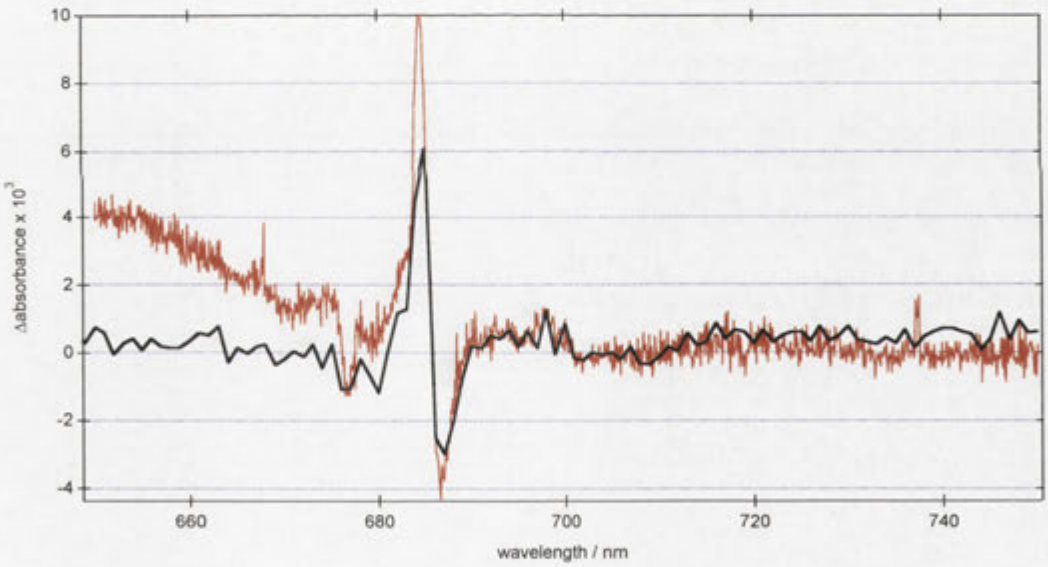

Figure 4.11 Q_y region after 5 min illumination. Untreated (black trace). Treated (red trace) Red trace is 1.53× black. The black trace is lower resolution than the red trace due to the accidental loss of the high-resolution data file. There is probably an under estimation of true shift magnitude due to the lower resolution.

The vortexed spectrum was subtracted from the control in the same way as for the DDM treated samples (see Section 4.4.1). The difference spectrum was qualitatively the

same, and hence supported the same conclusion; that flattening and scattering effects were modified by the vortexing. The fact that the difference spectra are quantitatively different supports the hypothesis that the DDM affects the particle size on a different scale to that achieved by vortexing, which is probably on the order of hundreds of nanometres or microns.

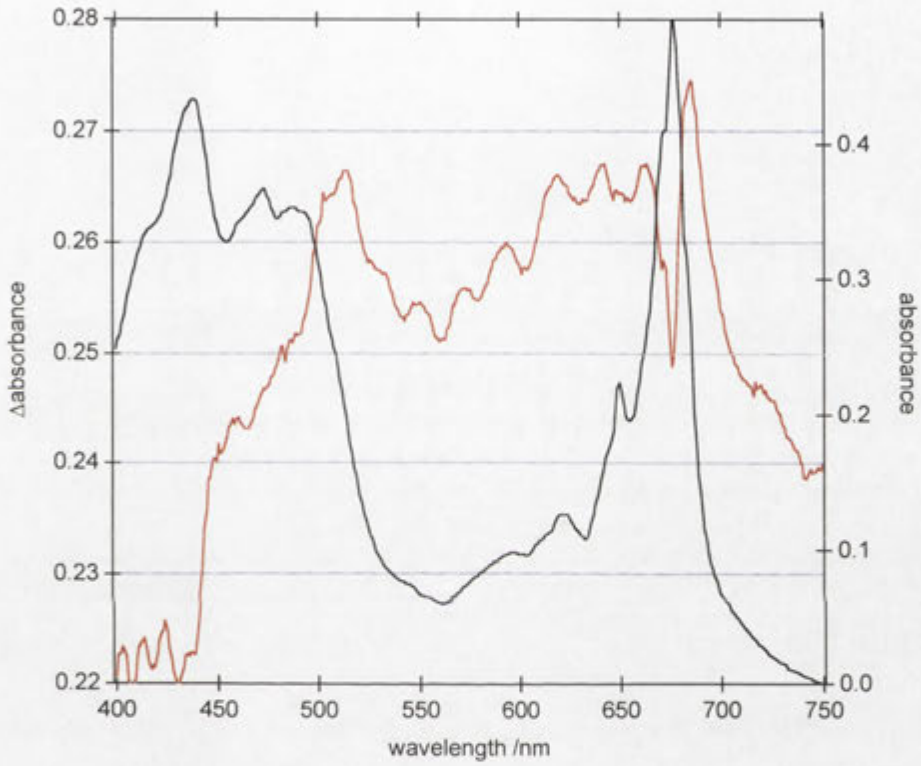

Figure 4.12 Red trace is untreated (black trace) minus 0.743 x vortexed trace (not shown). Constant chosen to minimise difference at chl b peak. It was not possible to get a zero spectrum subtracting one spectrum from the other.

4.4.3 Washing method

A washing method suggested by Paul Smith and performed by Nick Cox improved the quality of PEM spectra. They reproducibly had less scatter than previous samples. The washing method is outlined below:

Experimental Method

1. PEM of total Chl concentration ~10 mg/mL (~1 mL) was resuspended in 20 mL of Storage Buffer and cryoprotectant and homogenised.

2. The suspension was spun for 10 min at > 6000 rpm in RS32 type rotor.

3. The supernatant was then decanted and the pellet was collected.

4. Steps 1-3 were repeated on the final pellet.

Sample details

Untreated Sample: Analysed by MCD spectrometer. PEM (10 μL) added to 90 μL glycerol (40% in Storage Buffer). Final glycerol concentration = 36%, 225 μm cell, ~10 min dark adapted at room temperature in the lock, 10% transmission at 750 nm, OD 1.65.

Washed Sample: Analysed by MCD spectrometer. PEM washed (14 μL) added to 70% glycerol (26.3 μL). Final glycerol concentration = 30% 19.7 μL Storage Buffer 200 μm cell 15 min dark adapted at room temperature in lock, 42% transmission at 750 nm, OD 0.85 .

Results and Discussion

A comparison of the absorption spectra of a washed and untreated PEM sample is shown in Figure 4.13. To compare the spectra it was deemed most appropriate to scale them to same OD (that is at the absorption at 676 nm) as this is the region of minimum scattering according to experience and the Rayleigh theory of scattering. After scaling both spectra to the same OD, it was clear that the washed sample exhibited less scatter compared to the treated sample. This was probably due to the removal of scattering impurities.

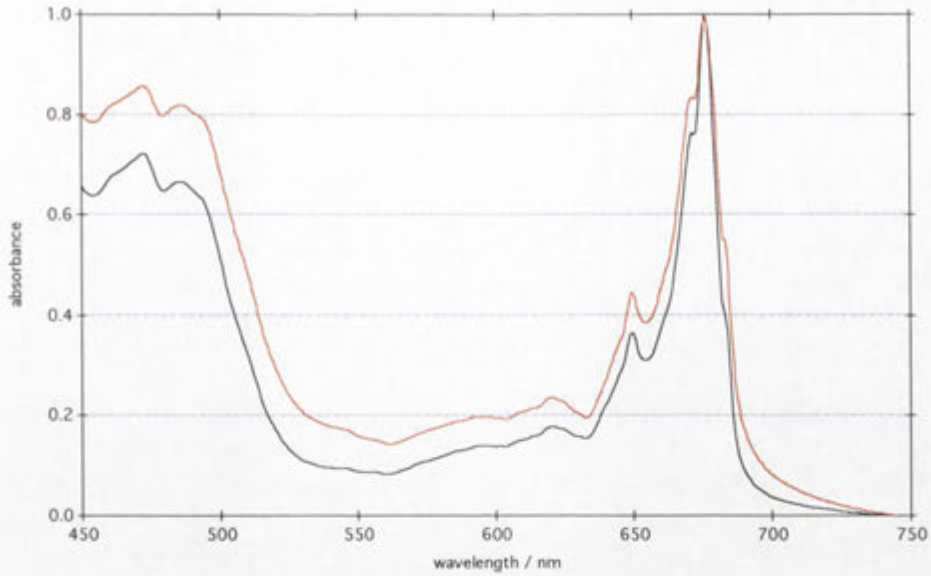

Figure 4.13. Comparison of the absorption spectra of a washed (red trace) vs untreated (black trace) PEM samples.

4.4.4 Freezing speed

The washed PEM samples (see section 4.4.3), prepared in flat cells sometimes exhibited spectra with high scatter in experiments on the CCD spectrometer. An experiment was conducted in which several PEM samples were prepared from the same bulk sample, on the same day and analysed on the CCD spectrometer. The effect of varying the cooling rate was observed.

Experimental Method

Sample 1: 15% washed PEM (6 μL), 30% glycerol, 20% EG (16 μL), 35% Storage Buffer (14 μL) loaded in a 200 μm flat cell. The sample was dark adapted for ~11.5 min at room temperature. During this time the He heater was switched on to cool the flow tube. After ninth minute the He heater was turned off and the sample rod inserted at approximately the tenth minute. The He heater was turned on and the sample was then cooled down to ~5 K over 5 min.

Sample 2: 40% glycerol, 15% washed PEM sample, 45% Storage Buffer. Loaded and cooled in the same way as Sample 1.

Sample 3: Same preparation and handling as Sample 2.

Sample 4: Same preparation as Sample 2 the He heater was not turned off once the flow tube pre-cooling started. (Hence the He cooling was increased compared to the Samples 1-3).

Results and Discussion

The results of the experiment are shown in Figure 4.14. When the sample was cooled as quickly as possible the light scattering was considerably reduced and the illumination-induced difference spectrum (black trace) was less distorted than for the highly scattering samples.

It was known that in the PEM samples prepared with EG/Gly cryoprotectant, fogging occurs if samples are maintained at 200 K.[16] Fogging occurs due to a phase transition in the glass and can render a sample nearly opaque and was therefore the likely cause of the light scattering in the slowly cooled samples.

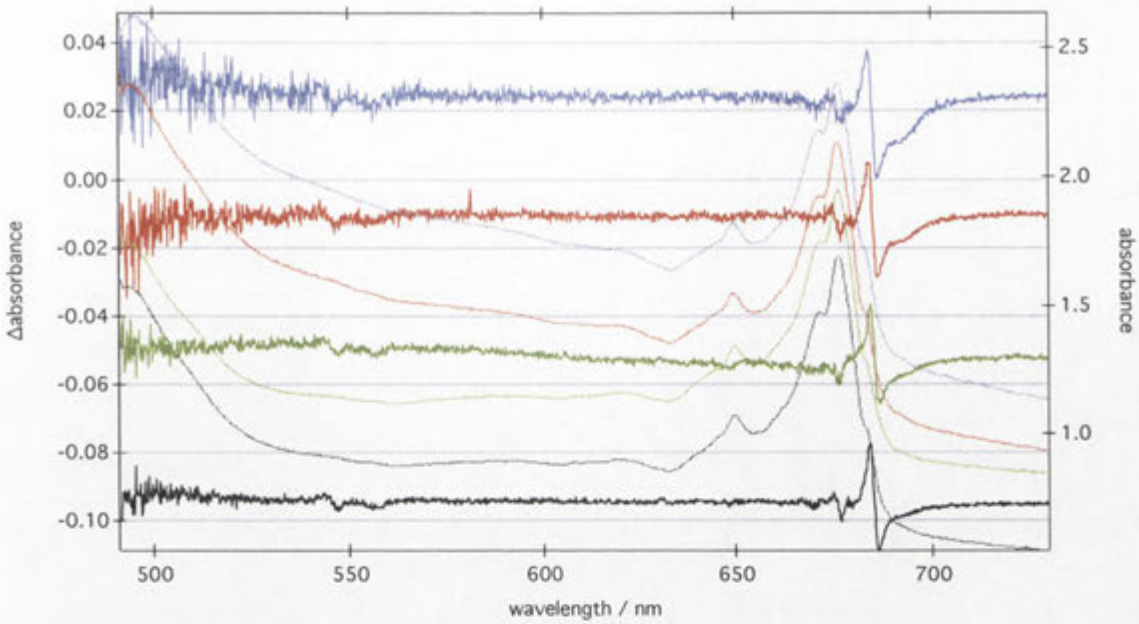

Figure 4.14 Four PEM samples, absorption (dotted lines) and illumination-induced difference spectra (solid lines). The difference spectra correspond to absorption spectra of the same colour. The black trace (sample 4) was a sample that was cooled more quickly than others. Absorbance spectra have not been shifted (true absorbance shown). Difference spectra shifted for clarity.

4.4.5 Homogenisation

If opaque particles were visible to the naked eye in a PEM sample they were dispersed with a glass homogeniser. A glass homogeniser consists of a test-tube shaped receptacle (mortar) and a tightly fitting glass rod (pestle) with a very narrow clearance (~0.1 mm). The sample is homogenised by placing it inside the test-tube and repeatedly forcing the rod in and out of the tube. Lateral forces arising due to the forcing of liquid between the mortar and pestle then disperse and homogenise particulates.

4.4.6 Managing Air Bubbles

Every sample was prepared with the aim of avoiding the introduction of air bubbles into the sample cell. This required care and experience to consistently achieve. Using the sandwich type sample holder, for example, it was found that using a specially built device that allowed the top window of the cell to be positioned at a shallow angle

greatly decreased the chances of obtaining bubbles. Sometimes bubbles were simply masked with a metal washer and analysed rather than expend time and PEM sample by attempting to produce bubble-free samples.

The flat cell type sample holder virtually eliminated the bubble problem because if any bubbles formed using these cells they could easily be forced out by introducing additional sample.

4.5 Discussion

4.5.1 Guide to preparing PEM samples of good optical quality

The main factors contributing to PEM sample optical quality were identified (see Sections 4.2 and 4.3) along with the techniques to address them (see Section 4.4). Based on the experiments described in this chapter and the experience gained preparing numerous samples, a guide to preparing optically good PEM samples is outlined below. It is organised chronologically considering each stage in the sample preparation process before spectroscopic measurement. The indicators of a sample's quality in terms of observations that can be made by the naked eye during preparation and of the resulting absorption spectra are presented.

4.5.1.1 Pre Freezing

In general, a PEM OD of about 1 was appropriate for analysing the entire visible spectrum. In experiments focussed on the Q_x region or the near-IR, a higher OD is appropriate but it should be noted that the Q_y data in such an experiment would be rendered unusable.

Opaque particulates should be avoided. They can be detected by diluting the PEM sample and spreading it on a glass slide or preparing a test sample in a quartz cell and examining by eye. The sample should appear as homogeneous as possible. Samples can

be made more homogeneous by using a glass homogeniser and vortexing. Washing the sample (resuspending the sample in buffer and centrifuging) is recommended as it has been shown to decrease scattering in absorption spectra. It probably does this by removing impurities and particulates, which would otherwise cause a decrease in the S/N ratio in spectra.

The potential for the aggregation of PSII membrane fragments in the PEM/buffer/cryogenic-agent mix during dark adaptation should be investigated. DDM was shown to prevent aggregation in samples during this time and washing the sample may also help. The dark adaptation should be less in duration than the time it takes for significant aggregation to occur.

Detergent can be used to solubilise PEM samples and hence minimise the problems due to aggregation such as scattering and decreased S/N ratio. The caveat that should be noted, however, is that DDM treated samples have cyt b_{559} partially oxidised compared to untreated samples (see Chapter 5). The minimum DDM found to prevent aggregation was 0.3% w/v.

A flat-cell type quartz sample holder should be used rather than the sandwich-type as they confer a number of advantages. The risk of fringing is eliminated and air bubbles can easily be forced out. A disadvantage of flat cells is that their sides are open to the atmosphere and hence sample loss could occur pre or post freezing.

4.5.1.2 During Freezing

The sample must be frozen quickly enough so that fogging does not occur. The consequence of fogging is a cloudy opaqueness in the sample cell and a pronounced scattering background in spectra

4.5.1.3 Post Freezing

One should check for bubbles and any other anomalies (such as fogging) before proceeding with spectroscopic measurements. This should be done under infra-red light (for example, 800 nm) and an infra-red viewer to ensure that Q_A^- formation is not induced in PSII centres before the sample is analysed. A measure of the transmission in a non-absorbing region of the spectrum (for example, 750 nm) is a useful diagnostic procedure to alert the experimentalist to a problem with the sample, such as fogging, may have occurred. As a rule of thumb, samples with a transmission of less than 20% at 750 nm were generally of poor optical quality.

4.6 References

[1] A. Zouni, J. Kern, J. Frank, T. Hellweg, J. Behlke, W. Saenger, K.-D. Irrgang, *Biochemistry* **2005**, *44*, 4572.

[2] L. N. M. Duysens, *Biochimica et Biophysica Acta* **1956**, *19*, 1.

[3] P. Latimer, C. A. H. Eubanks, *Archives of Biochemistry and Biophysics* **1962**, *98*, 274.

[4] C. Bustamante, M. F. Maestre, *Proceedings of the National Academy of Sciences of the United States of America* **1988**, 85, 8482.

[5] J. L. Hughes, E. Krausz Electronic Spectroscopy in *Application of Physical Methods to Inorganic and Bioinorganic Chemistry* Eds R. A. Scott, C. M. Lukehart, Wiley, New York, **2007.**

[6] C. F. Bohren, D. R. Huffman, *Absorption and Scattering of Light by Small Particles*, Wiley-VCH, Weinheim, **2004**.

[7] D. L. Rosseau, *Optical Techniques in Biological Research*, Academic Press, Orlando, **1984**.

[8] S. G. Stanton, R. Pecora, B. S. Hudson, *Journal of Chemical Physics* **1981**, *75*, 5615.

[9] R. F. Pasternack, C. Bustamante, P. J. Collings, A. Giannetto, E. J. Gibbs, *Journal of the American Chemical Society* **1993**, *115*, 5393.

[10] K. A. Stacey, *Light-Scattering in Physical Chemistry*, Butterworths Scientific Publications, London, **1956**.

[11] J. Hanley, Y. Deligiannakin, A. Pascal, P. Faller, A. W. Rutherford, *Biochemistry* **1999**, *38*, 8189.

[12] E. J. Boekema, B. Hankamer, D. Bald, J. Kruip, J. Nield, A. F. Boonstra, J. Barber, M. Rögner, *Proceedings of the National Academy of Sciences of the United States of America* **1995**, *92*, 175.

[13] W. V. Nicholson, F. H. Shepherd, M. F. Rosenberg, R. C. Ford, A. Holzenburg, *Biochemistry Journal* **1996**, *315*, 543.

[14] P. J. Smith, S. Peterson, V. M. Masters, T. Wydrzynski, S. Styring, E. Krausz, R. J. Pace, *Biochemistry* **2002**, *41*, 1981.

[15] R. C. Jennings, R. Bassi, F. M. Garlaschi, P. Dainese, G. Zucchelli, *Biochemistry* **1993**, *32*, 3203.

[16] S. P. Årsköld, V. M. Masters, B. J. Prince, P. J. Smith, R. J. Pace, E. Krausz, *Journal of the American Chemical Society* **2003**, *125*, 13063.

5 Quantification of Cytochrome b_{559}

5.1 Introduction

Cytochrome b_{559} (cyt b_{559}) is an important part of the PSII protein complex whose function in the photosystem is not fully understood. The reader is referred to Sections 1.4 and 1.5 of the Introduction Chapter for background information on cytochromes and cyt b_{559}.

A fundamental prerequisite for studying cyt b_{559} by optical spectroscopy is the ability to quantify the relative amounts of the different chemical (oxidised and reduced) forms of the heme. The methodology to quantify these forms of cyt b_{559} in PSII enriched membrane fragment (PEM) samples has not been adequately addressed in the literature.

Although the Beer-Lambert Law provides a straightforward relationship between the absorbance of a chromophore and its concentration, as has been demonstrated in Chapter 4, quantifying species by optical spectroscopy in PSII samples is far from trivial. Quantification of a chromophore by absorption spectroscopy requires two steps: the extraction of the peak from the spectrum and a calibration for concentration. Peak extraction methodology is complicated due to several factors including light scattering of the sample, (see Section 4.2.3) sample heterogeneity (see Section 4.2.2) and overlapping peaks in the spectrum.

5.1.1 Literature

The molar extinction coefficient of reduced cyt b_{559} has been determined from isolated cytochrome.[1,2] However, there is evidence that cyt b_{559} is perturbed when purified from PSII. For example, as the level of biochemical solubilsation of PSII increases; from thylakoid to PEM to PSII core, there is a gradual decrease in the proportion of cyt b_{559} initially present in its reduced form.

In a dithionite treated (D1/D2/cyt b_{559}) preparation the cyt b_{559} Q band, in a 4.2 K absorbance spectrum, was approximately twice the magnitude of the pheophytin peak.[3] In spinach sourced PEMs or PSII cores the cyt b_{559} peak is, at most, the same height as the pheophytin band. Studies carried out in our research group show that key spectral features in such purified preparations are "spectrally shifted and significantly inhomogeneously broadened"[4] compared to equivalent features in the more native (oxygen evolving) thylakoid, PEM and PSII core systems. The FWHM of the cytochrome α band at room temperature is broadened in isolated cyt b_{559}[2] (14.7 nm) compared with PEM samples[5] (10.7 nm).

The variability of cyt b_{559} properties with PSII preparation demonstrate that it would be flawed to apply the extinction coefficients obtained from highly purified systems to those of more native systems.

A cyt b_{559} extinction coefficient has been determined from a PSII enriched membrane sample[6] but this was done at room temperature and hence was not useful for application to the cryogenic studies carried out in this work.

5.1.2 Spectroscopy

The absorption spectrum of cyt b_{559} has been briefly described in the introduction chapter and will be presented in more detail here. Figure 5.1 is an absorption spectrum of cyt b_{559} isolated from higher plant PSII published in a paper by Babcock et al.[2] Dithionite treated (reduced) and ferricyanide treated (oxidised) cyt b_{559} are shown as dotted and solid lines respectively.

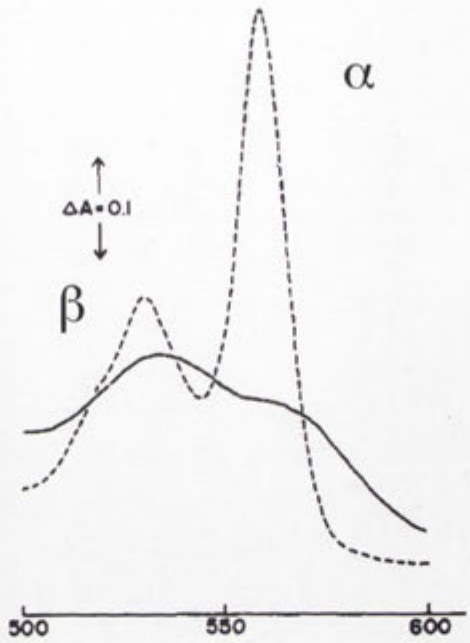

Figure 5.1 Literature absorption spectrum of the Q band of cyt b_{559} which consists of two peaks labelled α and β. The cyt b_{559} was isolated from higher plant PSII and spectrum measured at room temperature.[2] Dithionite treated (dotted trace) and ferricyanide treated (solid trace).

The spectra show that the oxidised and reduced forms of the cyt b_{559} are spectroscopically distinct. The two peaks of the reduced form are known as the α (~559 nm) and β (~530 nm) bands, which are components of the Q band (according to the nomenclature of the Gouterman Four Orbital Model).[7] A study of cyt b_{559} in higher plants[6] has confirmed that the extinction coefficient of the cyt b_{559} Q band is not dependent on the redox form (that is, the high, intermediate, or low potential forms) of the cyt b_{559} heme.

The Soret transition of cyt b_{559} (at ~430 nm) has a higher extinction coefficient than the Q band[5] but in PEM samples, the Soret spectral region contains overwhelming contributions from chlorophyll and carotene pigments. Additionally the sensitivity of the spectrometers is reduced due to the lower intensity of the tungsten lamp in that region. Hence the α component of the Q band was used to quantify cyt b_{559} in this work.

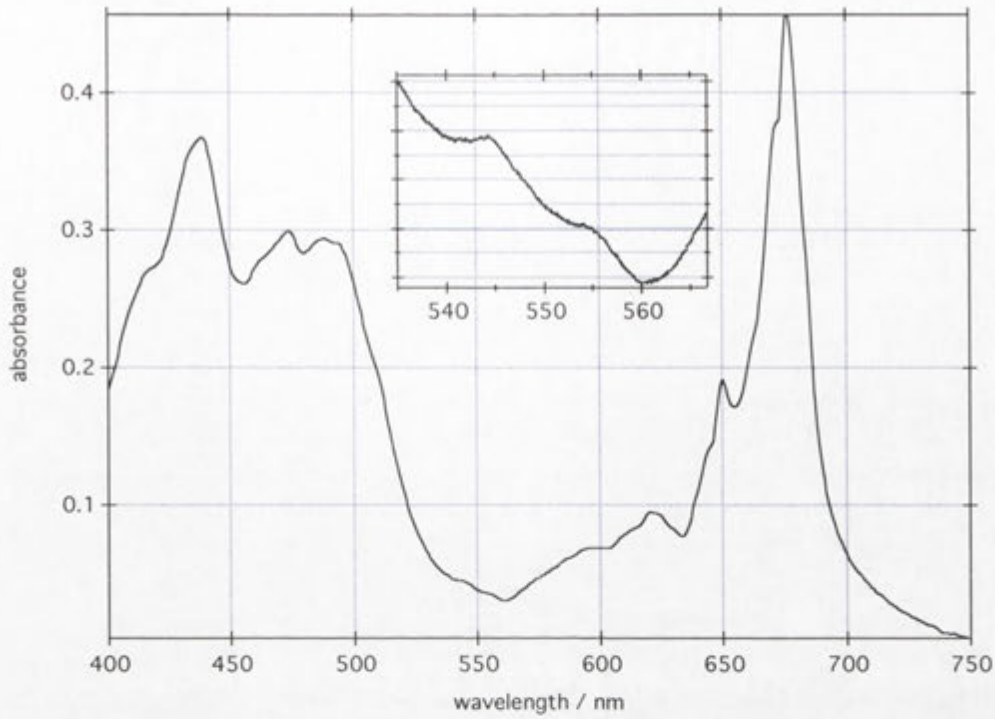

Figure 5.2 Low temperature (1.7 K) absorbance spectrum of dithionite-treated PEM sample. Inset: enlargement of reduced cyt b_{559} and pheophytin bands.

Figure 5.2 shows a dithionite treated PEM absorbance spectrum. The inset is an enlargement of the absorbance from cyt b_{559} at ~556 nm and the D1 and D2 pheophytins at ~545 nm. This figure highlights the relatively small magnitude of cyt b_{559} absorption compared to that of the other chromophores. The cyt b_{559} and pheophytin bands lie on a falling baseline (see Figure 5.2, inset), which is due to light scattering (see Section 4.2.3) by the sample.

5.1.3 Aim of this chapter

There is no estimate of the extinction coefficient for the reduced form of cyt b_{559} in PEM samples at cryogenic temperature in the literature (see Section 5.1.1). Hence the primary aim of the work presented in this chapter was to outline a method that can be used to quantify cyt b_{559} under such conditions. This is an important first step in enabling an understanding of the role of cyt b_{559} in PSII and, more generally, the electron transfer processes that occur in PEM samples at cryogenic temperatures.

5.1.4 Overview of Methodology

The Beer-Lambert Law states that the concentration of a species is linearly proportional to its absorbance (see Equation 4.2). The absorbance of reduced cyt b_{559} in a PEM absorbance spectrum cannot be directly determined since the chromophore's band shape is modified by scattering in the same spectral region (see Chapter 4), which manifests itself as a sloping baseline.

The baseline can be eliminated in an illumination experiment. In such an experiment two absorbance spectra are measured; one prior to, and one immediately after the sample is illuminated. By subtracting the pre- from the post-illumination spectrum, the baseline absorbance contributions cancel out, leaving only the spectroscopic changes due to the actinic light. In this work, this difference spectrum is referred to as the illumination-induced difference spectrum.

The changes that remain in the so-called (pheophytin) Q_x region are a negative peak (bleach) due to the oxidation of cyt b_{559} (loss of reduced cytochrome) and an electrochromic shift of a reaction centre pigment due to the effect of the electric field originating from Q_A^-. The peak position and width of cyt b_{559} can be accurately determined by a Gaussian fit of the negative peak. This knowledge can then be applied to extract the peak heights or areas of cyt b_{559} from absorbance spectra.

The absorbance band of cyt b_{559} alone is not useful without calibration against a known concentration of the cytochrome. To establish the maximum level of reduced cyt b_{559} (that is, every PSII centre having its cyt b_{559} in the reduced state), PEM samples were treated with sodium dithionite. This is a strong reducing agent commonly used for quantifying cyt b_{559} in PSII samples.[8] MCD spectroscopy was used, for the first time, to confirm that dithionite treated PEM samples had all of their cyt b_{559} reduced.

Finally, the fully reduced cyt b_{559} calibration had to be adjusted to account for the concentration of PSII centres in the sample. Two candidates for use as internal standards were investigated; the pheophytin Q_x absorption band at ~545 nm and the PSII Chl Q_y absorption band maximum height at ~676 nm.

The proportion of reduced cyt b_{559} was determined in a set of illumination experiments. Two separate quantifications were made per sample corresponding to the use of each internal standard. By comparing the data sets obtained by applying the two internal standards the best internal standard for cyt b_{559} quantification was selected.

The steps taken to develop a method for the quantification of reduced cyt b_{559} in PEM samples (at cryogenic temperatures, by absorption spectroscopy) are summarised below:

i) A method was developed for the extraction of cyt b_{559}, pheophytin and Q_y transition parameters from absorbance spectra (see Section 5.2).

ii) MCD spectra confirmed that dithionite treatment of PEMs results in a 100% reduction of cyt b_{559} (see Section 5.3).

iii) The analysis methods in (i) were used to characterise the spectroscopic parameters of dithionite-treated PEM samples with fully reduced cyt b_{559}. Two methods were devised (labelled Method 1 and Method 2) that utilised pheophytin and the Q_y maximum transition as internal standards respectively (see Section 5.4)

iv) A set of PEM samples were analysed in illumination experiments. The concentration of cyt b_{559} in each sample was determined before and after illumination with each of the two quantification methods. The two sets of resultant data were analysed and compared (see Section 5.5).

v) The cyt b_{559} quantification results derived from the superior method as judged in (iv) were then analysed.

5.2 Extraction of Spectroscopic Parameters

5.2.1 Cytochrome b_{559}

The peak position and width of cyt b_{559} were determined from illumination-induced difference spectra. A Gaussian function was chosen to fit the cyt b_{559} band and a typical fit of cyt b_{559} is shown in Figure 5.3. The residual trace (the difference between the data and Gaussian fit) appears to be random noise and hence confirmed that the choice of Gaussian was justified.

The fit was done using data points from ~552 to ~570 nm (the span of the residual trace) and was optimised such that the Gaussian's baseline coincided with the overall zero baseline of the data. In cases where the baseline was not flat, the difference spectrum was corrected by a linear subtraction before the Gaussian fit.

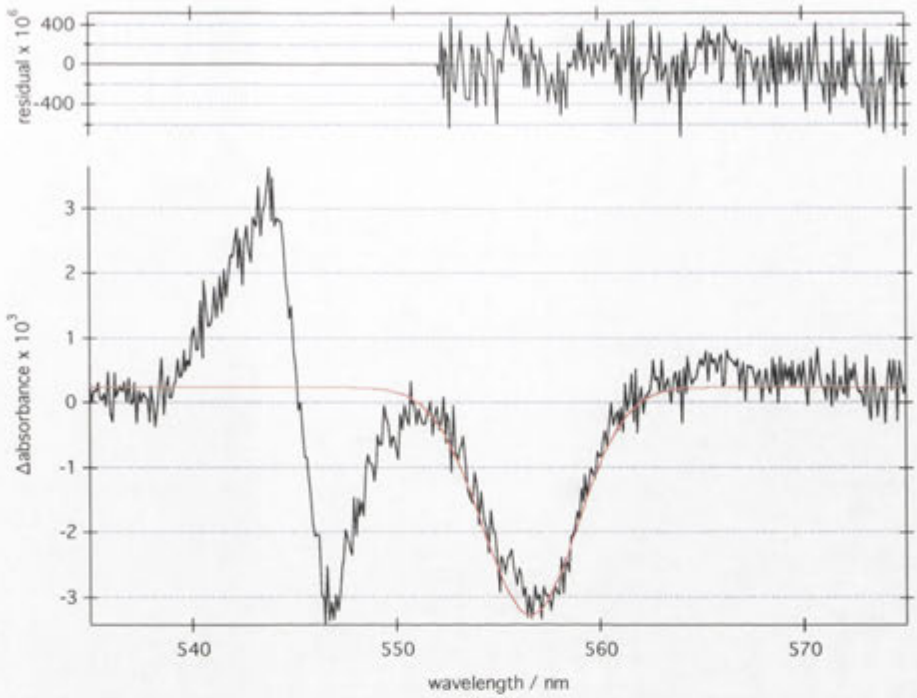

Figure 5.3 Gaussian fit of the cyt b_{559} bleach in a illumination induced difference spectrum. The residual trace associated with the fit is shown at the top and the span of the residual trace shows wavelength range used for the Gaussian fit.

An analysis of the cyt b_{559} peak width and position was carried out on sixteen illumination experiments. The average FWHM of oxidised cyt b_{559} was 5.85 nm with a standard deviation of 0.33 nm. The mean peak position was 556.4 nm with a standard deviation of 0.20 nm.

To extract cyt b_{559} from an absorption spectrum the FWHM from the corresponding illumination-induced spectrum was measured by a Gaussian fit (as in Figure 5.3). The peak in the absorption spectrum was then fitted with a Gaussian whose width was set to the value determined from the illumination-induced spectrum. An example of such a fit is shown in Figure 5.4. Note that the true baseline of the Gaussian is not visible due to the contributions from adjacent absorptions, but has been inferred from the fixed width Gaussian fit.

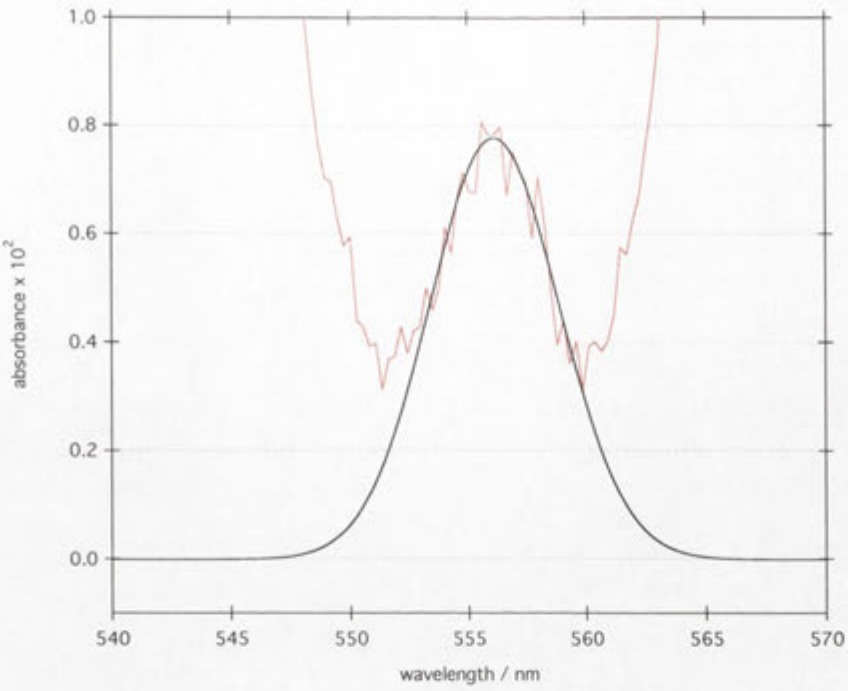

Figure 5.4 Gaussian fit (black trace) to the reduced cyt b_{559} peak in a dithionite treated PEM sample (red trace). The FWHM of the peak was fixed.

5.2.2 Pheophytin

In an illumination-induced difference spectrum there is a differential signal adjacent to the cyt b_{559} that is understood to be an electrochromic shift of the $Pheo_{D1}$ Q_x band by the electric field of Q_A^-.[9, 10]

The procedure to extract peak positions and widths of the pheophytin bands is much less straightforward than for cyt b_{559}. Assuming the shift is much less than the peak width, one can integrate the shift feature to elucidate the original peak lineshape. This results in a heavily distorted Gaussian band due to the cyt b_{559} bleach. This was done with a number of experiments to obtain a mean FWHM of $Pheo_{D1}$.

An attempt was made to use the Global Fit feature provided with Igor Pro software package to elucidate pheophytin positions and widths. Global fitting involves the fitting of a function to multiple data.

A global fit was carried out with the pre and post-illumination spectra from an illumination experiment. The function to be fitted to the data was the sum of three Gaussians to account for $Pheo_{D2}$, $Pheo_{D1}$ before illumination ($Pheo_{D1,dark}$) and $Pheo_{D1}$ after illumination ($Pheo_{D1,light}$). Restrictions were placed on the fit based on facts known about the system. These included setting the $Pheo_{D1,dark}$ and $Pheo_{D1,light}$ areas to zero in the post and preillumination spectra respectively, keeping all peak widths and the $Pheo_{D2}$ height constant. The peak width of $Pheo_{D1}$ was fixed at the estimate obtained by integrating the difference spectrum.

After applying all the conditions above, it was not possible to get reasonable fits for all the chromophores (for example, negative heights and poor fits were obtained). Relieving some of the restrictions did not improve the results. Since the aim here was to determine the area of the pheophytin band and not pheophytin peak positions and widths, a linear subtraction was made and the area between the line and the pheophytin band was measured (see Figure 5.5).

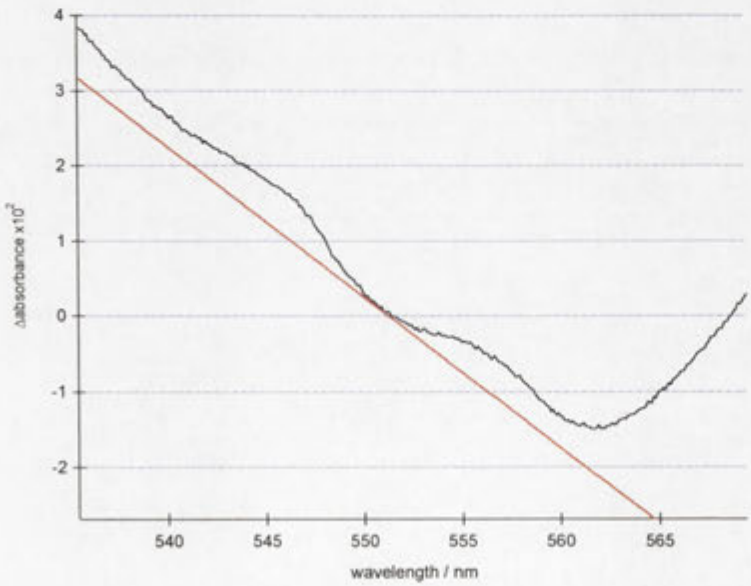

Figure 5.5 Method to obtain the area of pheophytin absorption. A linear baseline (green trace) was taken across the pheophytin band in a PEM absorption curve (black trace). The area between curve and baseline was measured.

5.2.3 PEM Chl Q_y Band

Another indicator of PSII centre concentration is the Q_y chlorophyll absorption band with maximum height at ~676 nm. Either the peak area or peak height of the Q_y could be measured to give the PSII concentration. Ideally the Q_y band area should be used for quantification because, unlike peak heights, area is invariant to temperature and subject to less error. However, in practice it is difficult to measure and compare the Q_y band area of PEM samples, as it was shown in Chapter 4 that different samples are subject to different amounts of light-scattering which affects the lineshape, and hence area of the band.

The peak height measurements will also be affected by light scattering but to a lesser extent than area measurements since scattering scales inversely to wavelength and hence is more pronounced at lower wavelengths. Although peak height is dependent on temperature it should be noted that the majority of samples in this work were either analysed at 1.7 or ~5 K and hence are comparable.

Given the problems with obtaining reliable peak area measurements the peak height measurement was selected as the most appropriate for quantification. The peak height was measured as the difference between absorbance at 750 nm and the maximum absorbance as shown in Figure 5.6. This was the standard method for determining PSII concentrations in this work.

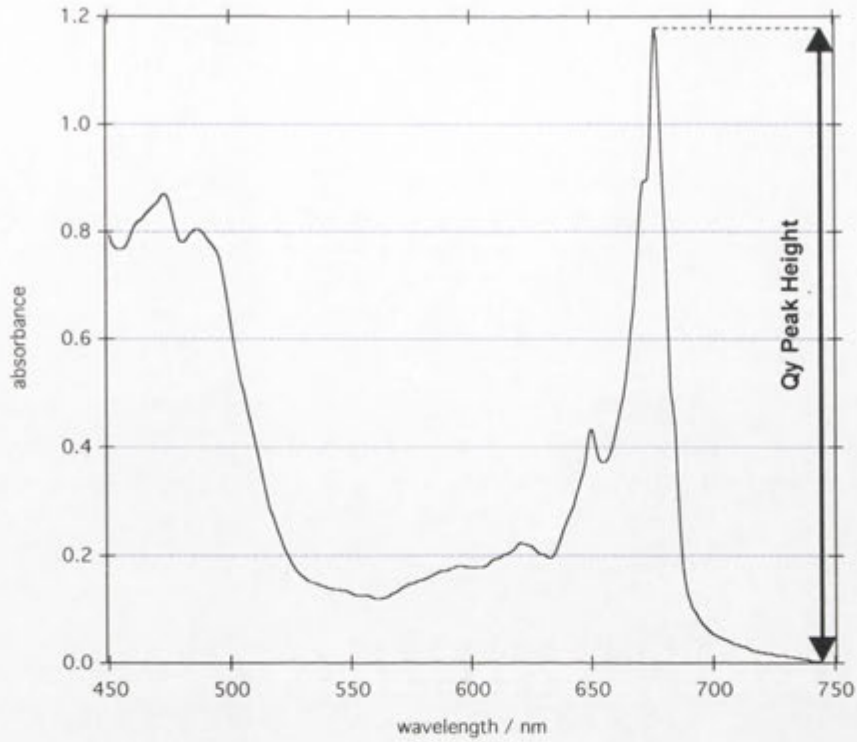

Figure 5.6 The Q_y peak height (also known as the sample OD) used to measure the concentration of PSII reaction centres in a PEM sample.

5.3 Dithionite treated PEM samples

5.3.1 MCD

A description of MCD and its application to quantifying cyt b_{559} has been presented in the Introduction Chapter, Section 1.3.1.3. MCD measurements were shown by Smith et al.[11] to be a potentially useful tool to confirm that all cyt b_{559} hemes in PEM samples can be reduced with dithionite treatment. Since MCD can detect both the oxidised and reduced forms of cyt b_{559}, the presence of the reduced form in the absence of the oxidised form indicates all cyt b_{559} must be reduced.

The MCD spectra from an untreated and dithionite treated PEM sample are shown in Figure 5.7. The spectra have been normalised by sample OD. The sharp Faraday A-term at 556.5 nm is characteristic of the reduced form of cyt b_{559}. As expected, the

dithionite treated sample has a larger A term than the untreated sample. The other MCD features are virtually identical.

The same samples were analysed for temperature-dependent Faraday C-terms by subtracting the MCD spectra taken at 1.7 K from spectra obtained at 60 K. These difference spectra are shown in Figure 5.8. Some oxidised cyt b_{559} was present in the untreated PEM sample, evidenced by the peak (similar in lineshape to the second derivative of a Gaussian) at 564.0 nm. The dithionite treated sample had no C-term visible which means none of the cyt b_{559} was oxidised. Hence, for the first time, MCD measurements confirmed that all cyt b_{559} in sodium dithionite treated PEM was in its reduced form.

Assuming that cyt b_{559} is fully reduced in the treated sample one can refer back to Figure 5.7 and by comparing the untreated and treated sample's A terms, calculate that in the untreated sample 26% of the cyt b_{559} was initially reduced.[†]

[†] This value was lower than quantified for PEM samples later in this chapter. This was expected due to high Q_A^- formation during the measurement of spectra caused by the necessity for the spectrometer slits to be wider in MCD experiments than in normal absorption experiments.

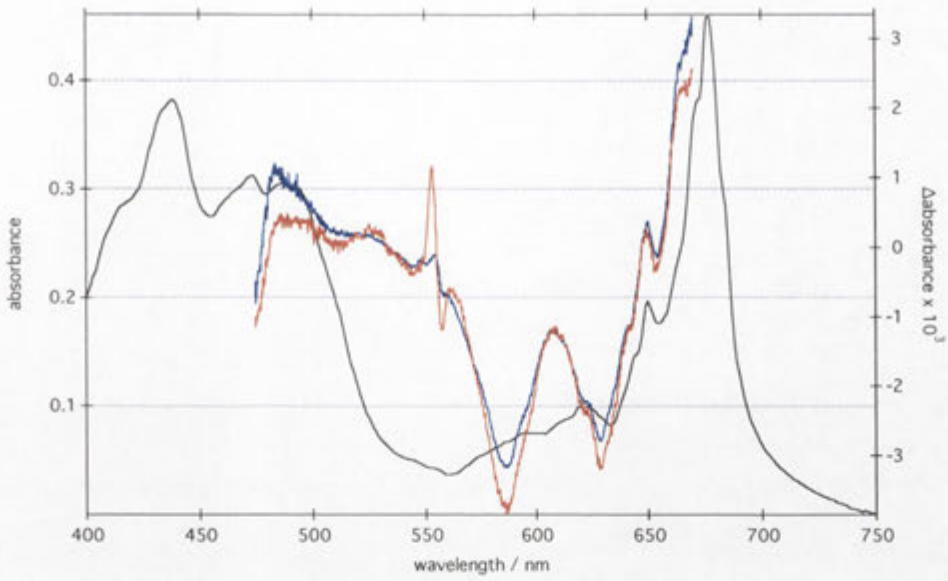

Figure 5.7 MCD Faraday A Terms of PEM sample at 1.7K. Blue trace: untreated, Red trace: dithionite treated. Left axis, absorbance of dithionite treated PEM. Right Axis: MCD.

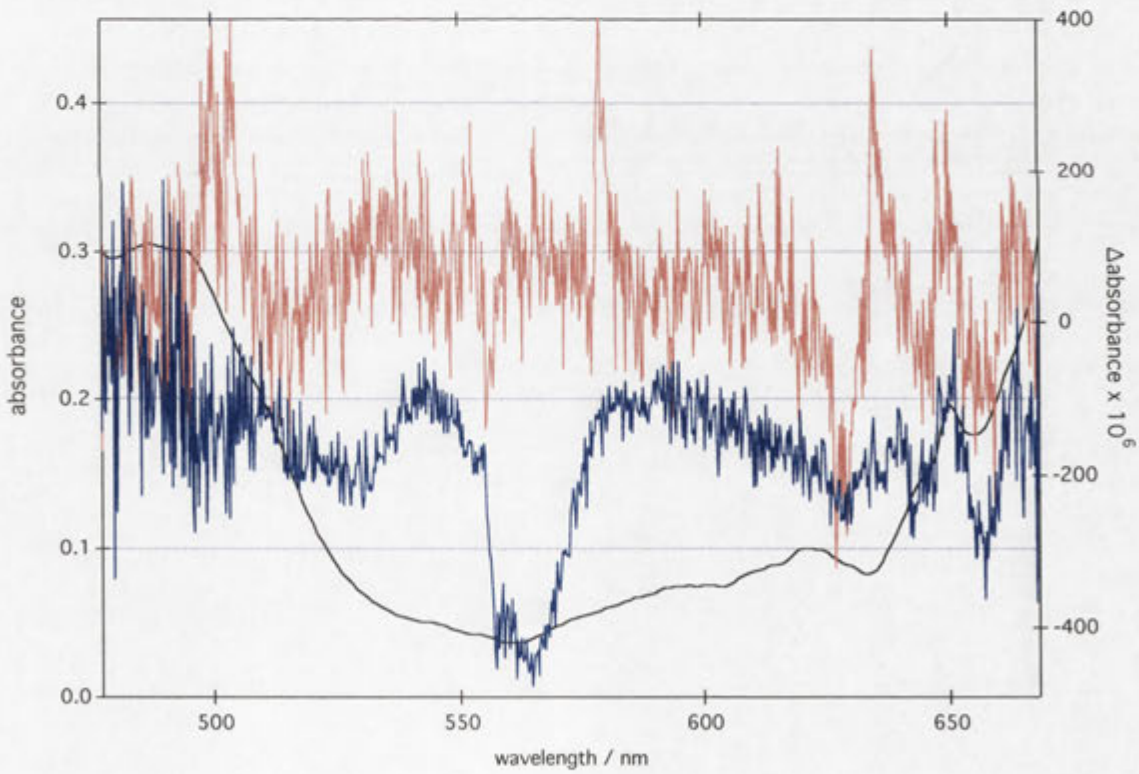

Figure 5.8 MCD Faraday C-terms. (60 K – 1.7 K spectra) of PEM samples. Dithionite treated (red trace), Untreated (blue trace), Absorbance (black trace).

5.4 Description of the Quantification Methods

Cyt b_{559} was quantified by two different methods. In both methods the cyt b_{559} peak area was extracted via the procedure outlined in Section 5.2.1.

Once a PEM sample is treated with excess dithionite, the cyt b_{559} remains locked in the reduced state. Theoretically one could first take the spectrum of an untreated sample, thaw the sample and recover it, treat it with dithionite and refreeze. However, from experience it would be almost impossible to do this because the second spectrum would invariably have different scattering characteristics to the first spectrum and would therefore not cancel out as has happens when the sample is reduced by (low temperature) light illumination alone.

An illumination-induced difference spectrum could not therefore be obtained for such samples. The FWHM of the dithionite treated cyt b_{559} band could not, therefore, be determined from illumination induced difference spectra as was done for untreated samples. The Gaussian fit to cyt b_{559} in dithionite-treated samples was therefore done with the average FWHM (5.85 nm) determined from sixteen illumination experiments (see Section 5.2.1.).

In both methods the ratio of the cyt b_{559} Q band area to an internal standard parameter was measured in a dithionite treated sample (which had all its cyt b_{559} reduced). Let this ratio be 'Y'. The ratio was then measured in the same way in the sample of unknown cyt b_{559}. Call this ratio 'X'. The percentage of reduced cyt b_{559} in the sample was therefore calculated via the simple formula 100% x (X/Y). The difference between the quantification methods was the internal standard used.

Quantification Methods

1) cyt b_{559} peak area to pheophytin peak area

The internal standard used was the pheophytin peak area extracted from absorption spectra by the method outlined in Section 5.2.2. Table 5.1 compares the ratios of cyt b_{559} area to pheophytin peak area in two different dithionite treated PEM samples. In samples of unknown cyt b_{559} concentration, the mean ratio (0.925) was used to evaluate the proportion of reduced cyt b_{559}.

2) cyt b_{559} peak area to Q_y height

The second method utilised the maximum Q_y absorbance in PEM samples at ~676 nm as an internal standard (see Section 5.2.3). The ratios of cyt b_{559}: PEM Q_y maximum peak height in two different dithionite treated PEM samples are listed in Table 5.1. (These were the same dithionite treated samples as above). In untreated samples the mean ratio (0.179) was used to evaluate the proportion of reduced cyt b_{559}.

Dithionite treated PEM sample	*Reduced Cyt b_{559} area / pheo area*	*Reduced Cyt b_{559} area / PEM Qy height*
1	0.907	0.195
2	0.943	0.162
Mean	**0.93**	**0.18**

Table 5.1 Ratios of reduced cyt b_{559} area to pheo area and PEM Q_y height in two dithionite treated samples (from Gaussian fits).

5.5 Results and Discussion

5.5.1 PEM Samples and Illumination Experiments

The cyt b_{559} quantification methods outlined in Section 5.4 were evaluated and compared by applying each method to absorption spectra from eleven illumination experiments. In each experiment the proportion of reduced cyt b_{559} was determined prior to and post illumination.

All experiments were performed on the MCD spectrometer at 1.7 K, with spinach PEM samples prepared by Paul Smith as outlined in Chapter 2 with analysed with the experimental methods outlined in Chapter 3. One PEM sample was analysed per experiment. Samples were made up with approximately 40% v/v cryoprotectant, being either neat glycerol or 1:1 (v/v) ethylene glycol:glycerol. All but one were illuminated with either 90 s helium-neon laser light diffused over the sample with a lens or 5 min green light from a tungsten lamp (using band pass filters) imaged onto the sample. One sample was illuminated with an argon laser (514.5 nm).

Samples from five separate batches are represented in the eleven experiments, where each batch of PEM was made on separate days.

5.5.2 Quantification Results

The cyt b_{559} quantification results are summarised in Figure 5.9 and Figure 5.10, which show the reduced cyt b_{559} quantified before and, remaining after, illumination respectively.

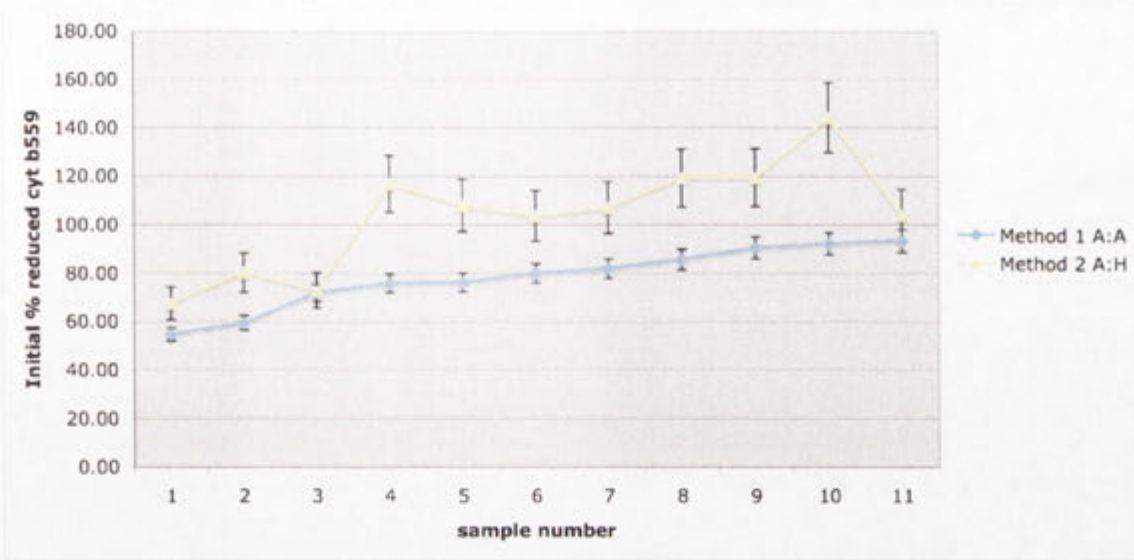

Figure 5.9 Quantification of the fraction of initially reduced cyt b_{559} in a number of untreated PEM samples by the two methods outlined in Section 5.4. Blue trace: Method 1 (cyt b_{559} area : pheophytin area). Yellow trace: Method 2 (cyt b_{559} area : PEM Q_y height). Samples are ordered by increasing percentage cyt b_{559} calculated by Method 1. Error bars: Method 1 = ±5% Method 2 = ± 10%

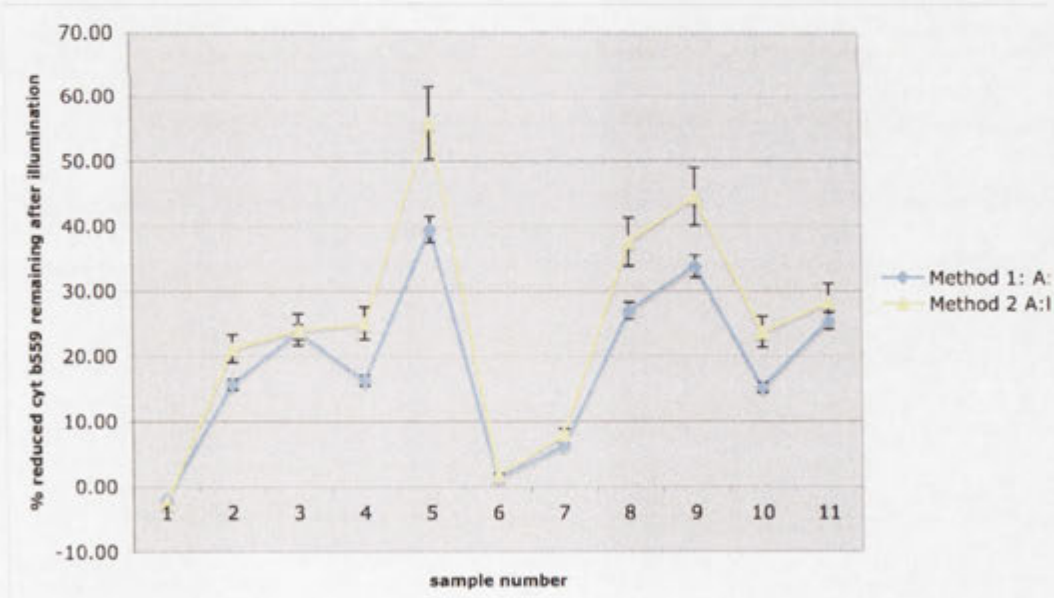

Figure 5.10 Reduced cyt b_{559} remaining after illumination by two methods of quantification. Sample numbers correspond to those in Figure 5.9. Error bars: Method 1 = ±5% Method 2 = ± 10%

5.5.3 Estimates of Uncertainty

The estimate of cyt b_{559} area had a very low uncertainty due to the accurate determination of FWHM from illumination-induced difference spectra and hence the confidence of the Gaussian fit. It was deemed to be negligible compared to other sources of uncertainty.

In Method 1, the two (cyt b_{559} : pheophytin) area ratios from the dithionite treated PEM samples are within 4%. The main contribution to uncertainty in Method 1 came from the determination of the pheophytin band area. That is, the choice of linear baseline applied to the pheophytin band was somewhat subjective. To estimate the magnitude of uncertainty introduced due to this, for each sample, a second baseline (slightly modified from the first but maintaining a reasonable fit) was applied and the resulting area was compared with the initial determination. It was found that two estimates differed by no more than ~10% and hence the uncertainty in fraction of reduced cyt b_{559} was estimated to be ± 5 %.

In Method 2 the uncertainty in measuring the PEM Q_y height was negligible as the noise was approximately 0.1% of the signal. The two cyt b_{559} area / PEM Q_y height ratios from the dithionite treated PEM samples were within ~20% and differed due to different scattering backgrounds. Hence this was the main contribution to the uncertainty in the reduced cyt b_{559} quantified by this method. It was thus estimated to be ± 10%.

5.5.4 Comparison and Evaluation of Quantitation Methods

Although both methods were generally in agreement on the relative amount of cyt b_{559} between samples (see Figure 5.9), Method 2 was clearly flawed as several determinations of the initial reduced cyt b_{559} were above 100%. Experiments seem to be subject to a serious systematic error.

The problem with Method 2 is inherent in the Q_y height measurement. It has been shown in Chapter 4 that PEM samples are prone to scattering and the extent varies between samples. Scattering results in an a change in the baseline shape and hence any difference in scattering between the dithionite treated and untreated PEM samples would result in a systematic error in the cyt b_{559} determination. This was consistent with the clear systematic overestimation of cyt b_{559} by Method 2.

The discrepancy in the value of the (cyt b_{559}: Q_y ratio) between the dithionite experiments also indicates this is the likely source of the problem as they clearly have different amounts of scattering. The ratio of (cyt b_{559} : pheophytin) areas in the dithionite treated samples, in contrast, were much more consistent with each other than the equivalent (cyt b_{559}: Q_y) height ratios (see Section 5.4), indicating the pheophytin area is less sensitive to differences in sample scattering.

By using the Q_y height internal standard it is implicitly assumed that the amount of chlorophylls per PSII reaction centre is the same between PEM batches, but it is known to vary between preparations. It is also subject to scattering contributions (see Section 4.2.3)

The pheophytin area is a more reliable internal standard in principle since it equates to two pheophytins and is not susceptible to the variability as is the case for Q_y height. The scattering at the Q_x pheophytin band region is essentially linear. It is not subject to significant resonance enhanced Rayleigh scattering as it is an area of low absorption.

The main problem with the pheophytin internal standard is accurately determining its area. There can be up to 10% variability due to the choice of linear baseline correction. Ideally the dithionite calibration should have similar scattering to the unknown sample.

This could be most easily achieved, by preparing a control PEM sample treated with dithionite to be analysed in parallel with the untreated sample.

Since the quantification of cyt b_{559} in PEMs is affected by the particular scattering characteristics of the sample, a molar extinction coefficient has not been determined.

5.5.5 Analysis of the Results obtained with Quantification Method 1

In the previous section it was established that Method 1 was the better of the two procedures for cyt b_{559} quantification. Thus, the results obtained by this method have been analysed.

The quantification data were sorted by several parameters to ascertain if a relationship existed between them and the proportion of cyt b_{559} initially reduced and oxidised by light. The parameters included PEM sample OD (Q_y height), cyt b_{559} peak area, transmission at 750 nm, amount of Q_A^- formation (measured by the $\Delta A/A$ ratio[†] in the Q_y region) and type of light source used in illumination. There was no correlation between any of those parameters and either the initial or post-illumination concentration of cyt b_{559}.

There was a discrepancy between the proportion of initially reduced cyt b_{559} between samples sourced from the same batch of PEM. Samples sourced from a PEM batch that has been analysed more than once are listed in Table 5.2. The samples highlighted in yellow are outliers with respect to the average amount of cyt b_{559} determined.

The absorbance spectra of the samples in Table 5.2 are shown Figure 5.11. The outliers highlighted in the table all have an absorbance spectrum with a different

[†] Where ΔA is the peak-to-peak height of the electrochromic shift at ~685 nm due to an illumination at cryogenic temperature and A is the maximum absorbance peak height in the Q_y region at ~676 nm.

scattering baseline. This demonstrates the sensitivity of Method 1 to the scattering in PEM samples. It reinforces the fact that it is best to minimise scattering in PEM samples (in both untreated test samples and dithionite treated). Failing that, it would be desirable to use a dithionite control with the same scattering baseline as the sample(s) to be analysed.

PEM Batch	*Sample #*	*% Cyt b_{559} initially reduced*
A	**1**	**59**
A	2	72
A	3	76
A	4	82
B	**1**	**55**
B	2	92
C	**1**	**76**
C	2	86
C	3	91

Table 5.2 Comparison of initially reduced cyt b_{559} in three batches of PEM sample calculated by Quantification Method 1 (see Section 5.4). Outliers with respect to the average amount of cyt b_{559} determined in a batch are highlighted in bold. Error for each determination was estimated to be ±5%.

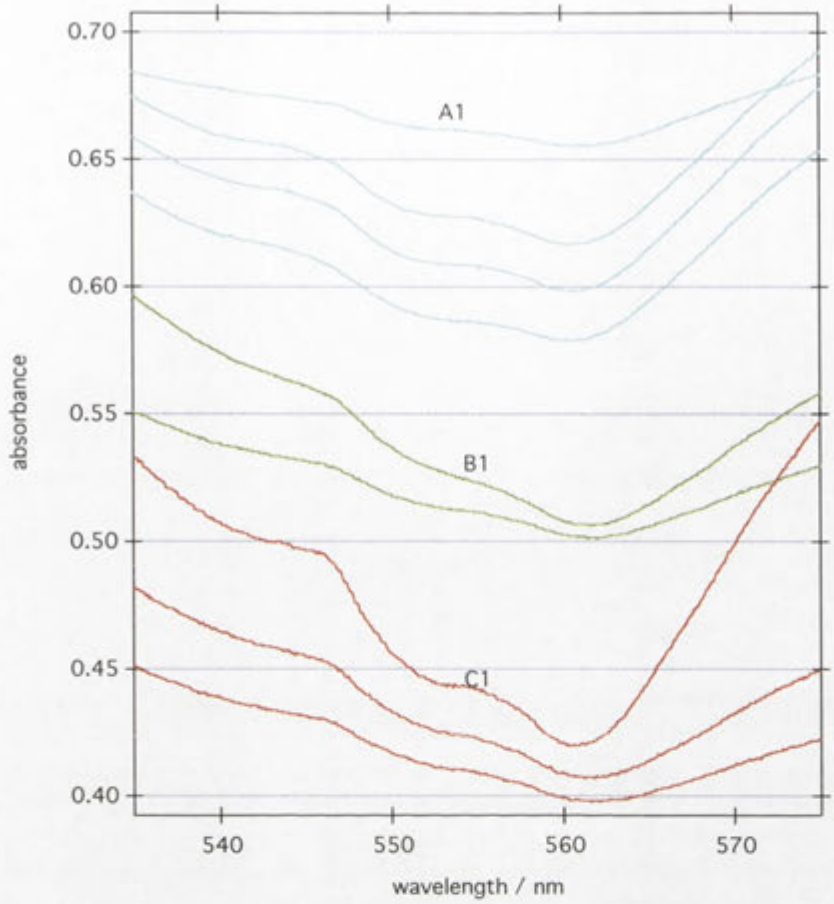

Figure 5.11 Pre-illumination absorbance spectra from PEM samples in Table 5.2. Samples are grouped by colour. Batch A (cyan traces), Batch B (green traces) and Batch C (red traces). The outlier samples highlighted in the table are marked A1, B1 and C1. Spectra are offset for clarity.

The initial reduced cyt b_{559} was found to be variable (55 to 93%) as was the fraction of cyt b_{559} photooxidised (48 to 100%). Excluding samples with high scatter the initial proportion of reduced cyt b_{559} was 72-92%. The proportion of reduced cyt b_{559} that was photooxidised did not correlate with the amount of cyt b_{559} initially reduced prior to illumination.

Although a small sample size, the data in Table 5.2 suggested the main source of variability in cyt b_{559} that is initially reduced was the sample preparation procedure. This is because (ignoring outliers due to scattering) the cyt b_{559} level varies more between sample batches than samples within the same batch. The variation in initially reduced cyt

b_{559} may be due to the details of sample preparation (for example, sample contact time with detergents) and the quality of plant material used in the procedure. This conclusion is supported by the fact that the initial oxidation state of cyt b_{559} is known to be progressively more oxidised as one analyses PSII material that is increasingly purified.

Additionally, sample handling immediately prior to spectroscopic analysis would also be expected to have an effect. This includes factors such as duration the sample was kept on ice, the extent of accidental light exposure etcetera. Sample handling procedures were kept as consistent as possible between samples.

5.6 Summary

Two methods were investigated to quantify cyt b_{559} in PEM samples. The cyt b_{559} peak area was compared to one of two internal spectroscopic standards: the pheophytin peak area (Method 1) or the Q_y peak height (Method 2).

Using MCD spectroscopy it was shown that dithionite treatment of PEM samples resulted in a reduction of 100% of cyt b_{559} proteins. In both methods, dithionite treated PEM samples were used to determine the parameter ratios corresponding to 100% reduction of cyt b_{559} and hence allowed the calculation the amount of cyt b_{559} in the untreated test PEM samples.

Method 2 was found to be flawed, as it implied some PEM samples had more than 100% of cyt b_{559} reduced (even taking into account the estimated error), and this was attributed to different scattering between the dithionite treated reference sample and test samples. Hence, only the results produced by Method 1 were further analysed.

Light scattering was identified as problem with obtaining reproducible results by Method 1, as it was noted that within three batches of PEM samples analysed, the outlier results corresponded to samples with a spectrum of significantly different scattering

baseline to the other samples. Excluding the outlier samples, the initial proportion of reduced cyt b_{559} in the PEM samples was 72 – 92%. The variation is thought to be due to arise from how the samples are prepared rather than any sample handling prior to spectroscopic measurement. The proportion of initially reduced cyt b_{559} that was photooxidised by illumination (50 to 100% with a mean of 77%) did not correlate with the amount of cyt b_{559} initially reduced prior to illumination.

5.7 References

[1] H. S. Garewal, A. R. Wasserman, *Biochemistry* **1974**, *13*, 4063.

[2] G. T. Babcock, W. R. Widger, W. A. Cramer, W. A. Oertling, J. G. Metz, *Biochemistry* **1985**, *24*.

[3] R. Jankowiak, M. Rätsep, R. Picorel, M. Seibert, G. J. Small, *Journal of Physical Chemistry B* **1999**, *103*, 9759.

[4] E. Krausz, J. L. Hughes, P. Smith, R. Pace, S. P. Årsköld, *Photochemical and Photobiological Sciences* **2005**, *4*, 744.

[5] C. A. Buser, L. K. Thompson, B. A. Diner, G. W. Brudvig, *Biochemistry* **1990**, *29*, 8977.

[6] O. Kaminskaya, J. Kern, V. A. Shuvalov, G. Renger, *Biochimica et Biophysica Acta* **2005**, *1708*, 333.

[7] M. Gouterman, *Journal of Molecular Spectroscopy* **1961**, *6*, 138.

[8] D. H. Stewart, G. W. Brudvig, *Biochimica et Biophysica Acta - Bioenergetics* **1998**, *1367*, 63.

[9] H. J. van Gorkom, J. J. Tamminga, J. Haveman, *Biochimica et Biophysica Acta* **1974**, *347*, 417.

[10] H. J. van Gorkom, *Biochimica et Biophysica Acta* **1974**, *347*, 439.

[11] P. J. Smith, S. Peterson, V. M. Masters, T. Wydrzynski, S. Styring, E. Krausz, R. J. Pace, *Biochemistry* **2002**, *41*, 1981.

6 Assignment of Spectral Features in Illumination-Induced Difference Spectra of PSII Enriched Membrane Samples

6.1 Introduction

Processes in the PSII protein complex were studied in this work by absorption spectroscopy. The illumination-induced difference absorption spectrum measured at low temperature provided a window into electron transfer events independently of processes, such as oxygen evolution, that dominate at physiological temperatures. A fundamental requirement to understand the electronic processes in PSII was therefore to first understand all the features in illumination-induced difference spectra, which since their discovery, have been the subject of much analysis and debate.

A challenge evident early on in this work was to obtain reproducible illumination-induced difference spectra. The first objective of this chapter was firstly therefore to understand and control the variability initially observed in illumination-induced difference spectra of PSII enriched membrane samples (PEMs). Once this had been achieved, our attention turned to identifying spectroscopic features, especially the hitherto unassigned 676 nm feature. In the process of achieving this aim, there was a rethinking of the origin of the main blue-shift feature at 685 nm.

6.1.1 PSII Illumination-Induced Difference Spectra: Literature Review

Upon illumination of higher plant chloroplasts with monochromatic light at wavelengths shorter than 700 nm a 'photoreactive component' in the absorbance spectra was discovered by Knaff and Arnon.[1] It was labelled C550 because it was a reversible absorbance change at 550 nm.

Van Gorkom proposed C550 "may be due to an influence of the semiquinone on the absorption spectrum of a reaction center pigment"[2] He proposed both the features at 550 and 685 nm "could be due to" a shift of a pheophytin *a* band. This proposal has not been subsequently challenged in the literature and hence remains the accepted explanation for the spectroscopic features observed. Furthermore, Van Gorkom's assignment is supported by the fact that all the crystal structures of PSII obtained thus far indicate that $Pheo_{D1}$ is the closest pigment to Q_A[3-7]. It will be shown in this chapter, however, that while the magnitude of electrochromic shifts of chromophore absorption bands in PSII are strongly dependant on the distance of the chromophore to Q_A, other factors such as the angle of the chromophores relative to Q_A and the effective dielectric constants, cannot be neglected.

The band that shifts at 550 nm is called the 'Q_x' band of $Pheo_{D1}$ according to the Gouterman four-orbital model[8], which is the framework on which our understanding of porphyrin-type absorbance spectra is based and this was discussed in Section 1.3.1. One of the first examples of the Q_x illumination induced difference spectrum in the literature can be seen in a study published by Butler in 1973 who made spectroscopic measurements on chloroplasts at 77 K[9] and is shown in Figure 6.1.

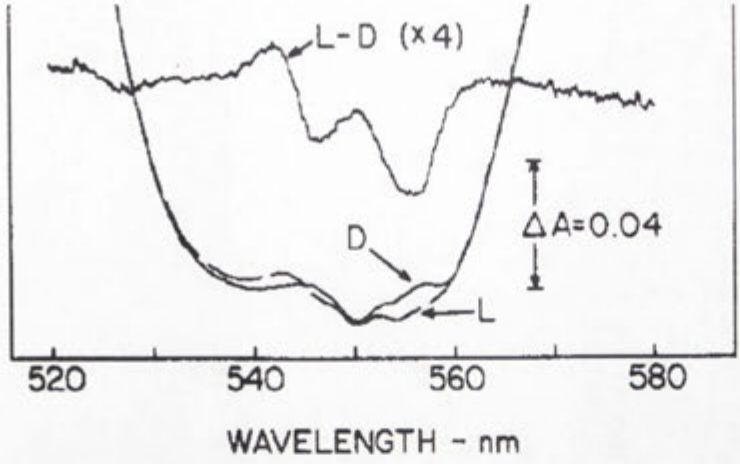

Figure 6.1 Q_x absorption spectra of chloroplasts at 77 K before (labelled D for dark) and after (labelled L for light) 30 s red light illumination. The illumination-induced difference spectrum is labelled L-D. From a study by Butler.[9]

There is a concomitant electrochromic shift in the Q_y region, which is more complex in form than the Q_x counterpart. There are differing interpretations of which pigments give rise to the electrochromic shift and these are discussed below. A specific problem for PEM preparations is that in the Q_y region of the absorbance spectrum there is a low S/N ratio due to spectroscopic contributions from approximately 200 Chls and 2 Pheos per reaction centre.[10] This makes the assignment of electrochromic shifts in this spectral region more challenging than the Q_x region.

A number of researchers have produced the Q_A^- - Q_A spectrum by low temperature illumination and attempted to explain their data terms of the electrochromic shift of pigments in the PSII reaction centre. The studies most relevant to this work are briefly summarised here.

Junge and coworkers analysed pea O_2 evolving PSII core particles by flash spectroscopy at room temperature.[11] Saturating exciting flashes were provided by a xenon lamp with FWHM of 10 μs. To produce the Q_A^- - Q_A spectrum the spectrum of the dark adapted spectrum was subtracted from the transient spectrum (taken 5 ms after the

first flash). The samples had DCBQ[†] (fluorescence quencher and electron acceptor) and DCMU[*] (to prevent electron transfer from Q_A to Q_B) added. The result is shown in Figure 6.2.

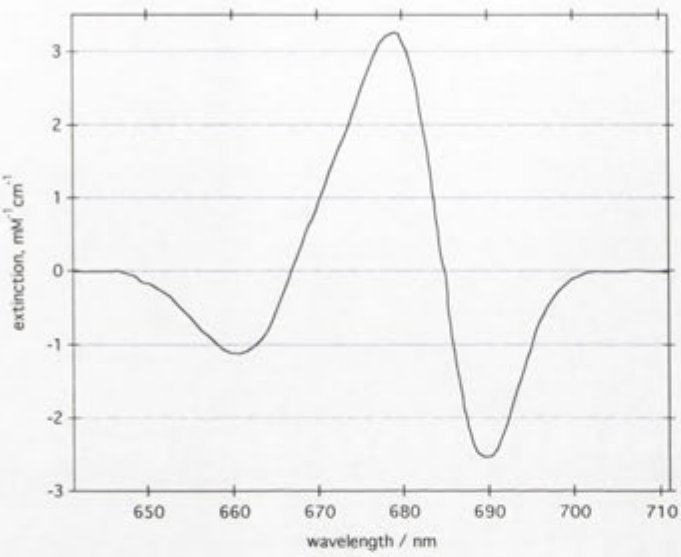

Figure 6.2 Spectrum of Q_A^- - Q_A digitised from the literature[11] Trace is a fit of 18 data points. See text for experimental details.

Diner and coworkers analysed Mn-depleted PSII from Synechocystis by low temperature (77 K) optical spectroscopy.[12] They formed the state Q_A^-/Chl Z^+/Car^+ by first pre-treating their PSII sample with an excess of $K_3[Fe(CN)_6]$ to fully oxidise Q_A and cyt b_{559} and then subjecting the sample to a continuous illumination white light (quartz halogen lamp) in a liquid nitrogen bath. The illumination-induced difference spectra from the wild-type and mutant cyanobacteria are shown in Figure 6.3.

[†] 2,6-dichloro-p-benzoqunione
[*] 3-(3,4-dichlorophenyl)-1,1-dimethylurea

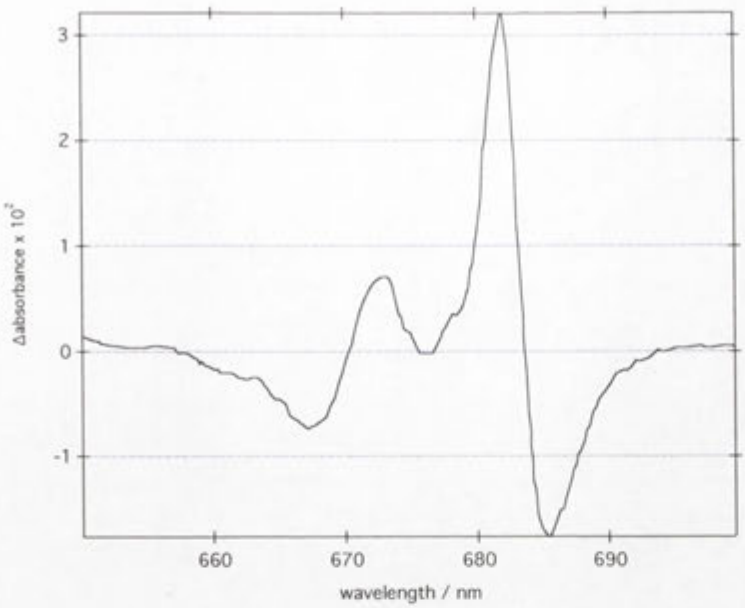

Figure 6.3 Digitised spectrum of the state Q_A^-/Chl Z^+/Car^+ in Synechocystis. See text for details.

Årsköld and coworkers analysed PSII enriched membrane fragments from spinach by low temperature optical spectroscopy (1.7 K).[13] They formed the Q_A^-/ Cyt b_{559}^+ state by green light illumination at 1.7 K. The illumination induced difference spectrum is shown in Figure 6.4.

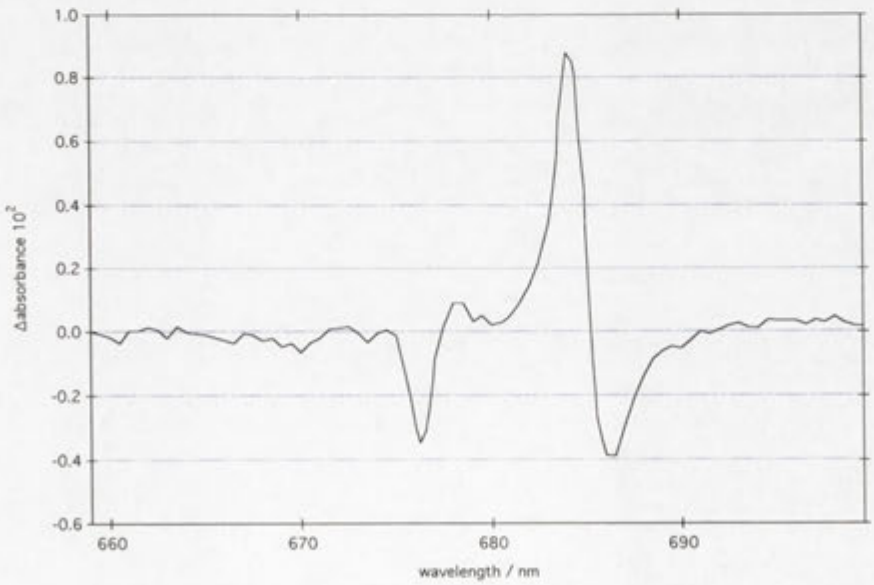

Figure 6.4 Digitised illumination induced difference spectrum[13]. See text for details.

In all the studies above major blue shift was observed in the illumination induced difference spectra together with some other minor features. These are summarised in the Table 6.1 below.

Study	*Major Blue Shift Feature / nm*		*Minor Features /nm*	*Illum. and spectrum temp.*	*Sample*	*Ilum. type*
	Maximum	*Minimum*				
Mulkidjanian et al. 1996[11]	680	690	min 660	RT	Pea PSII cores Mn	Short flashes, Xe lamp
Stewart et al. 2000[12]	682	685	max 673 min 668	77 K	depleted PSII from synecho cystis	White light, 70 mW/cm^2
Årsköld et al. 2003[13]	685	687	min 676	1.7 K	PEM from spinach	Green light, 1-2 mW/cm^2

Table 6.1 Summary of spectral details of the electrochromic shift and experimental parameters from studies in the literature that have formed Q_A^- in PSII by illumination.

6.2 Elucidation of the Illumination-Induced Difference Spectrum

6.2.1 Variability in Illumination-Induced Difference Spectra of PEMs

The reader is referred to Chapter 3 for experimental details on collecting illumination-induced difference spectra.

An example of the range of illumination-induced difference spectra of PEM samples obtained in this work is shown in Figure 6.5. Along with the main 685 nm blue shift there is a feature around the wavelength of 676 nm that sometimes appeared to be a bleach (red traces), growth (blue traces) or band shift (black trace). Table 6.2 outlines the

experimental details associated with each trace and are ordered identically as in Figure 6.5.

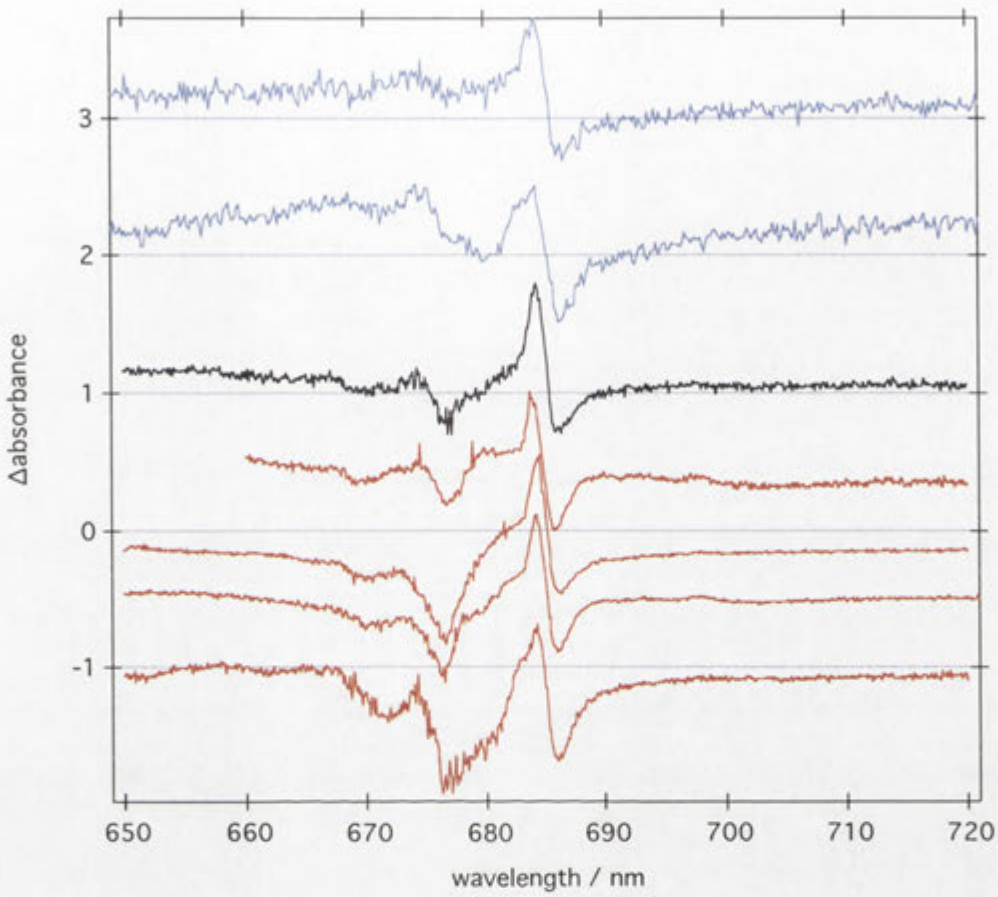

Figure 6.5 Examples of Q_y difference spectra highlighting the variability in the 676 nm feature. All spectra are normalised to the 685 nm shift. Spectra in which the 676 nm feature appears as a bleach are show in red, as a growth shown in blue and as a band shift in black.

Trace	*Spectrometer*	*PEM Sample Batch*	*Cryoprotectant*	*Cell pathlength / μm*	*OD*
1	CCD	a	40% Gly	50	0.66
2	CCD	a	40% Gly	50	0.10
3	MCD	a	37% Gly	225	1.0
4	MCD	b	35% (1:1 EG/Gly)	200	0.85
5	MCD	c	39% Gly	200	0.52
6	MCD	d	45% (1:1 EG/Gly)	200	1.90
7	MCD	a	36% Gly	225	1.65

Table 6.2 Experimental details of the samples used to obtain the light induced illumination spectra in Figure 6.5. The spectra are ordered identically to the figure. EG=Ethylene Glycol, Gly=Glycerol. Temperature of MCD and CCD experiments were 1.7 K and 7.1 K respectively.

The difference spectrum variability could not be correlated to any particular variable such as PSII sample batch, pathlength, PSII concentration (OD), cryoprotectant or illumination regime (see Table 6.2) and appeared to be random. Hence the variability was suspected to be artefactual, arising from the sample preparation and/or the spectrometer.

To investigate the hypothesis that the 676 nm feature was artefactual, the effect of a small change in concentration was simulated and compared with experimental data. This might be expected if there is an apparent change in concentration as discussed in Chapter 4. The simulation was carried out by scaling a post-illumination spectrum by a constant (sufficiently large to cause a change in the difference spectrum) and subtracting this from the pre-illumination spectrum. Without scaling, the 676 nm feature of the chosen illumination experiment data appeared as a shift (see black trace in Figure 6.5).

The simulation (see Figure 6.6) shows that the feature at 676 nm can appear as a bleach, growth or shift depending on the extent of the simulated concentration change. An important result highlighted by the simulation is that a change in absorbance of only 0.5% in a PEM sample can drastically modify the appearance of the difference spectrum at

maximum absorbance. According to the Beer-Lambert law, a 0.5% change in absorbance will occur if there is an identical per cent change in the pathlength, all else being equal.[†] Hence, for a pathlength of 200 μm (a typical cell pathlength used in this work) 0.5% is equivalent to a pathlength change of 1 μm.

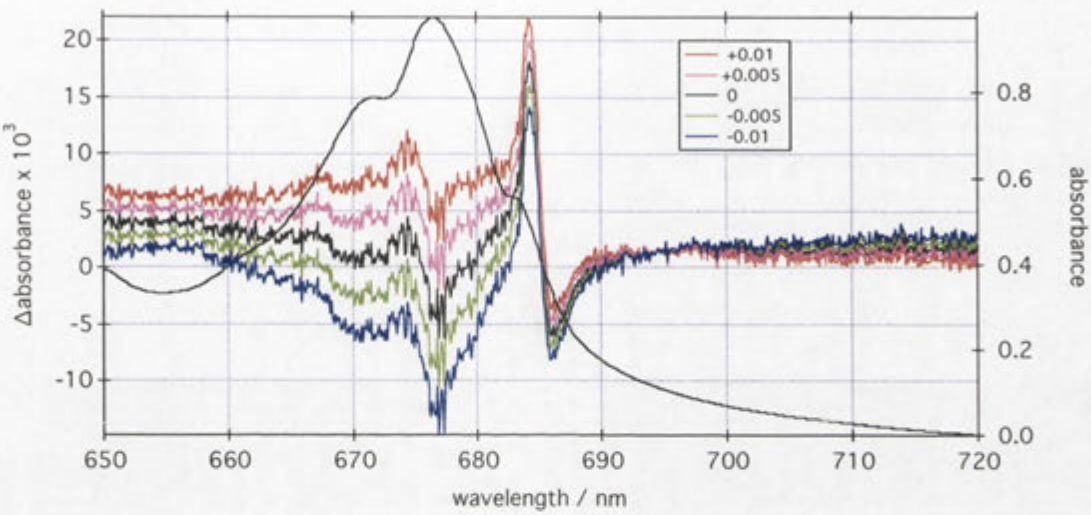

Figure 6.6 Simulation of the effect of an absorbance change in post-illumination spectrum on the illumination-induced difference spectrum. Absorbance changes of ±0.005 and ±0.01 were simulated. Difference traces were not shifted. Black trace is the absorption spectrum (right hand scale).

[†] The extinction coefficient or sample concentration were not expected to change during an experiment.

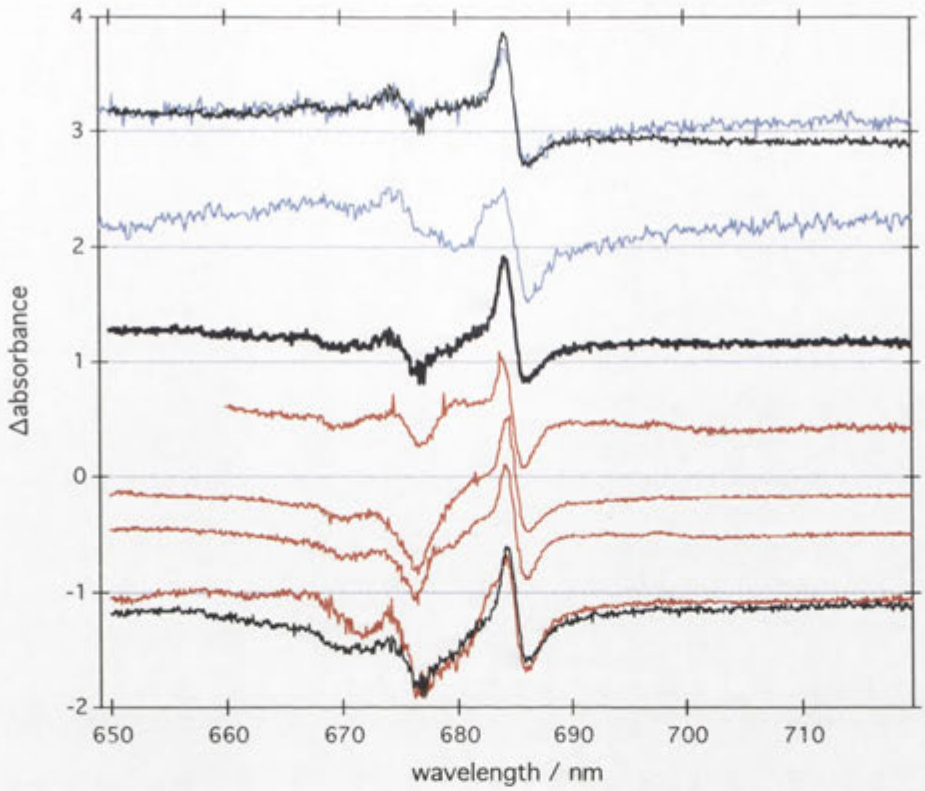

Figure 6.7 Examples of Q_y difference spectra probably affected by an apparent concentration change. All spectra are normalised to 685 nm shift. Spectra in which the 676 nm feature appear as a bleach are show in red and as a growth shown in blue. For comparison the bold black trace is the unaltered spectrum from Figure 6.6 with the +0.01 and -0.01 simulations shown as black traces in the upper and lower section of the graph respectively.

The simulation reproduces the range of Q_y difference spectra observed in the course of this study. This can be seen in Figure 6.7 where real spectra (blue and red traces), thought to be affected by an apparent concentration change, are compared with simulated spectra (upper and lower black traces) shown in Figure 6.6.

The randomness of the variations in the 676 nm feature pointed to the fact that the source of the variation was artefactual. The simulations above supported this idea by showing that the 676 nm variation could be explained by an overall apparent concentration change in the sample. This concentration change must have been apparent (such as due to sample movement and the heterogeneity of the sample) rather than real, since measurements were taken at cryogenic temperatures. Photobleaching can be ruled

out as the source of the concentration change since the PEM samples studied were subject to electromagnetic energy typically of the order of 5 mW with a duration of seconds to minutes.

It was therefore hypothesised that the apparent concentration change was due to a spectrometer issue(s) coupled with PEM sample heterogeneity. Sample heterogeneity was identified as being problem for PEM absorption spectra in Chapter 4. The mechanisms by which an apparent concentration change would occur are discussed in the next Section.

6.2.2 Artefacts in the Difference Spectra Due to the MCD and CCD Spectrometers

General Principles

The general mechanism by which an apparent concentration change would be observed in a difference spectrum is described here. In an illumination experiment two spectra are collected; one prior to- and one immediately after the illumination of the PEM sample. Ideally, the spectrometer operates in exactly the same way when obtaining each spectrum so that spectral changes observed are only due to the effect of illumination on the sample. In practice, a number of events can occur between (or during) the first and second spectrum that result in an apparent sample concentration change. The possibilities are listed here.

1) Movement of a heterogeneous sample

If the sample is caused to move relative to the spectrometer's optical path, then a different volume of the sample will be interrogated. Since PEM samples are known to be heterogeneous (see Chapter 4) the spectrum will indicate the sample concentration has changed compared to the pre-illumination spectrum.

2) Movement of optical components with a heterogeneous sample

This is identical to the scenario described in (1) except that it is the interrogating light position that moves in relation to the sample.

3) Pathlength change

If, after illumination, the sample is not the same position as before illumination (for example slightly rotated) the pathlength of the sample will change and thus affect the recorded concentration. This will result in an apparent concentration change even with a perfectly homogeneous sample.

4) Photon fluctuations

The spectrometer's light source could fluctuate in intensity over time resulting in an erroneous absorption reading and therefore an erroneous concentration determination.

The first three factors were the most likely to have caused an apparent concentration change. It should be noted that the simulation conducted in Section 6.2.1 showed that a pathlength change of 1 μm in 200 μm (that is, the equivalent of a concentration change of 0.5%) would be sufficient to make an observable difference in the 676 nm feature.

The last factor can be ruled out because of two reasons. Firstly, the MCD and CCD were both designed to be very stable with specific design features to ensure stability such as ultra-stable lamp power-supplies and the use of a chopper in the MCD to minimise detector offsets. Secondly, if (4) did occur, then gross changes would have been (and which sometimes were) observed in the baseline for example and in the routine checks performed on both spectrometers sans-sample prior to sample analysis (see Chapter 3). The problem could then be rectified before obtaining spectra from the PEM samples.

MCD Spectrometer

In the MCD spectrometer, factors (1) and/or (3) were probably the main cause of an apparent concentration change. In a typical experiment PEM samples were analysed, rotated 90° for illumination and then returned to their initial position for post-illumination spectrum collection. If the sample rod was not returned to its exact starting position after an illumination and the samples were heterogeneous it is conceivable that an apparent concentration change could be recorded. It is also possible the sample rod moved very slightly over the time periods required to obtain spectra (minutes timeframe).

The likelihood of sample movement was less in the CCD, compared with the MCD spectrometer, since the sample was usually illuminated over short time frames (tenths of a second to seconds) by the interrogating light and the sample rod did not need to be moved to allow illumination, as in the MCD system.

CCD Spectrometer

The alignment of the CCD-spectrometer optics was found to be altered by physical contact and temperature fluctuations in the laboratory. This equates to factor (2) above which could have caused a concentration change. Physical contact with the spectrometer (after the baseline spectrum was collected) was unavoidable as the sample rod had to be manually loaded.

There were two reasons that the CCD was more sensitive than the MCD spectrometer to physical contact and temperature. Firstly, the order of optical components was different in the two spectrometers. This meant that changes to the sample positioning in the CCD spectrometer affected the alignment of the input beam into the monochromator, while light in the MCD spectrometer entered the monochromator before reaching the sample. Secondly, the detector used on the MCD spectrometer

(photomultiplier tube) was relatively large compared to the CCD array used in the CCD detector and hence small deviation in light path could make a pronounced difference to CCD spectra. Furthermore, a lateral movement of the light path in the CCD would result in an incorrect measurement of wavelength since this was calibrated according the horizontal location upon the CCD array, while in the MCD this could not occur.

The stability problems in the CCD spectrometer (described in Section 6.2.2) have since been minimised or eliminated by Dr Steffen who continued to improve the system after the experimental component of this research work was completed. For example, the instrument was insulated from room temperature fluctuations using a foam box that enclosed the entire spectrometer. This spectrometer is referred to as the high-stability CCD system, on which some data was collected and generously provided for this work.

6.2.3 Elucidating the Artefact-Free Difference Spectrum

Since a range of illumination-induced difference spectra was produced, an important question arose: which of the spectra, if any, represented the actual Q_y illumination-induced difference spectrum, free from artefacts?

An illumination-induced difference spectrum of a PEM was measured by Dr Steffen with the improved high-stability CCD system. This spectrum, along with several Q_y difference spectra collected by the author on the MCD and CCD systems are shown in Figure 6.8. There is confidence that these represent the actual Q_y illumination-induced difference spectrum; as free as possible from artefacts caused by the sample or spectrometer. The reasons supporting this hypothesis are:

1) The spectra were obtained from different PEM illumination experiments sourced from different spinach batches, conducted on different spectrometers (MCD and

CCD) with different illumination regimes. It is therefore unlikely that there are any artefacts in the difference spectrum dependent on any of these factors.

2) The spectra are consistent with those obtained on the high-stability CCD system which was rigorously tested to ensure stability. This greatly diminishes the possibility that features in the difference spectra were due to a spectrometer artefact.

3) The CCD measurements were relatively fast (a minimum collection time of 100 ms per spectrum every 6.3 s was possible) and did not require sample movement for illumination as in the MCD. A single spectrum on the MCD took about 5-10 minutes to collect. There was therefore less chance that the sample would physically shift and give rise to artefacts with the CCD spectrometer.

4) Care was taken to ensure the PEM/buffer/cryoprotectant mixtures were prepared free from heterogeneity (applying the techniques learned from Chapter 4).

Since the experiments were conducted at temperatures of 5 K or less, the changes in the difference spectrum were due only to electron transfer in PSII and show that along with the major blue-shift type feature centred at 685 nm, there is also minor blue-shift feature at ~676 nm. This is hereafter referred to as the 676 nm feature. The 676 nm feature was always present in a cryogenic illumination induced difference spectrum of a PEM sample.

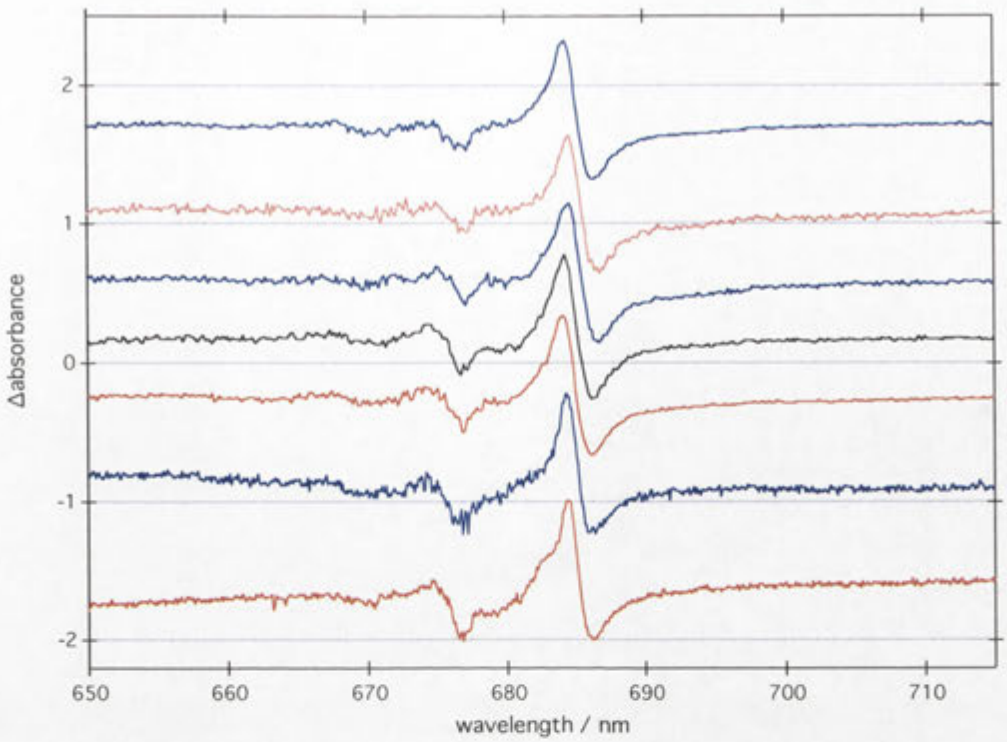

Figure 6.8 Comparison of Q_y Illumination-Induced Difference Spectra. Spectra are listed in the same order the samples listed in Table 6.3. Experimental details are listed in the Appendix in Table 6.10.

6.3 The 676 nm Feature

6.3.1 Properties

Along with the blue-shift at ~685 nm, illumination-induced difference spectra of PSII enriched membrane and core samples always contain a minor feature at ~676 nm. This minor feature was first thought to be a bleach at 676.6 nm, due to the spectrum published by our research group in 2003[13] shown in Figure 6.9. Subsequent repeated measurements and investigation (see Section 6.2.3 and Figure 6.8) confirm it is in fact a derivative-shaped feature centred at 675.6 nm. The apparent bleach was probably due to sample heterogeneity and/or a spectrometer artefact as has been discussed in the preceding Sections.

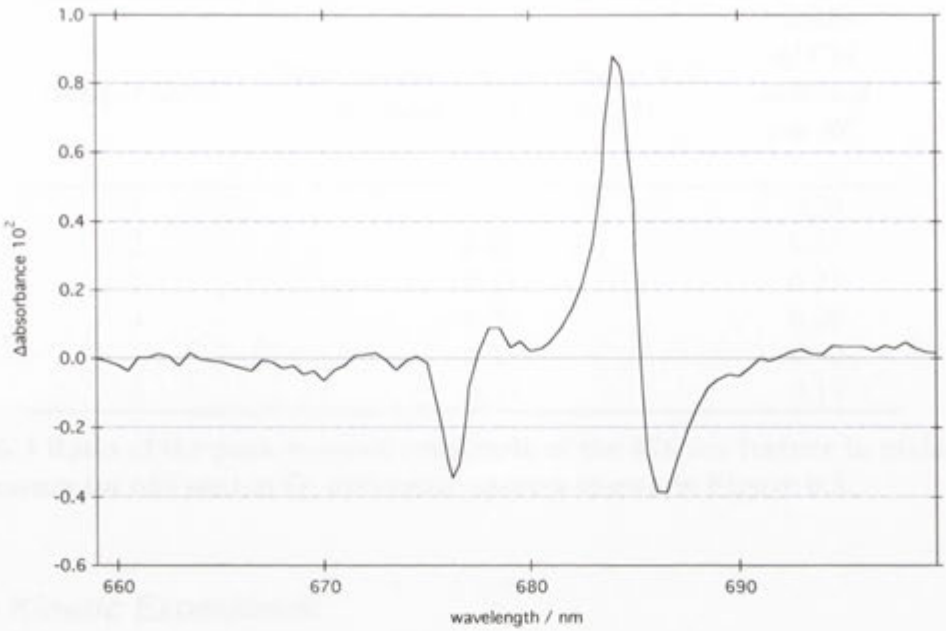

Figure 6.9 Illumination induced difference spectrum [13] of a PEM showing the 676 nm feature appearing as a bleach. 1.7 K.

The 676 nm feature has only been observed to form when samples are illuminated at cryogenic temperatures and always observed in conjunction with the 685 nm blue-shift.

In Table 6.3 a number of experiments are listed in which PEM samples which have been illuminated to have maximum Q_A^- formation† at cryogenic temperature. The ratio of the peak-to-peak amplitudes of the 676 nm feature to the peak-to-peak amplitude of the main Q_A^- shift at 685 nm ranged from 0.21 to 0.33. The amount of chlorophyll oxidised in each experiment was estimated from the signed area between the difference spectra trace and zero baseline and assuming the area in the Q_y region equates to 200 chlorophylls. The ratio of the amplitude of the two shifts was not dependent on the batch of PSII utilised, the amount of chlorophyll oxidised or the spectrometer used to analyse the sample.

† Indicated by a ΔA/A ratio of approximately 2.6 – 3.0%. This range has been determined from experience from dozens of measurements obtained in this work.

Sample batch	*Peak to-peak Height ratio of 676 nm:main Q_y shift ($\Delta A/A$)*	*Number of Chl oxidised per RC*
1	0.21	0.34
2	0.25	0.51
1	0.28	0.21
3	0.32	0.26
1	0.33	0.50
2	0.33	0.17

Table 6.3 Ratio of the peak-to-peak amplitude of the 676 nm feature to main shift feature (at 685 nm) in Q_y difference spectra shown in Figure 6.8.

6.3.2 Kinetic Experiment

An illumination experiment was performed on a PEM sample by Ronald Steffen.[§] The peak-to-peak magnitude of the 676 nm feature, Q_x and Q_y electrochromic shifts are plotted versus time (elapsed after the end of illumination) in Figure 6.10. The 676 nm and Q_x shift kinetic traces were scaled so that the maximum difference magnitude was the same as for the Q_y shift and were also smoothed for clarity.

The figure shows that the 676 nm feature grows at the same rate as the Q_x and Q_y electrochromic shifts.

[§] This was carried out on the high-stability CCD spectrometer.

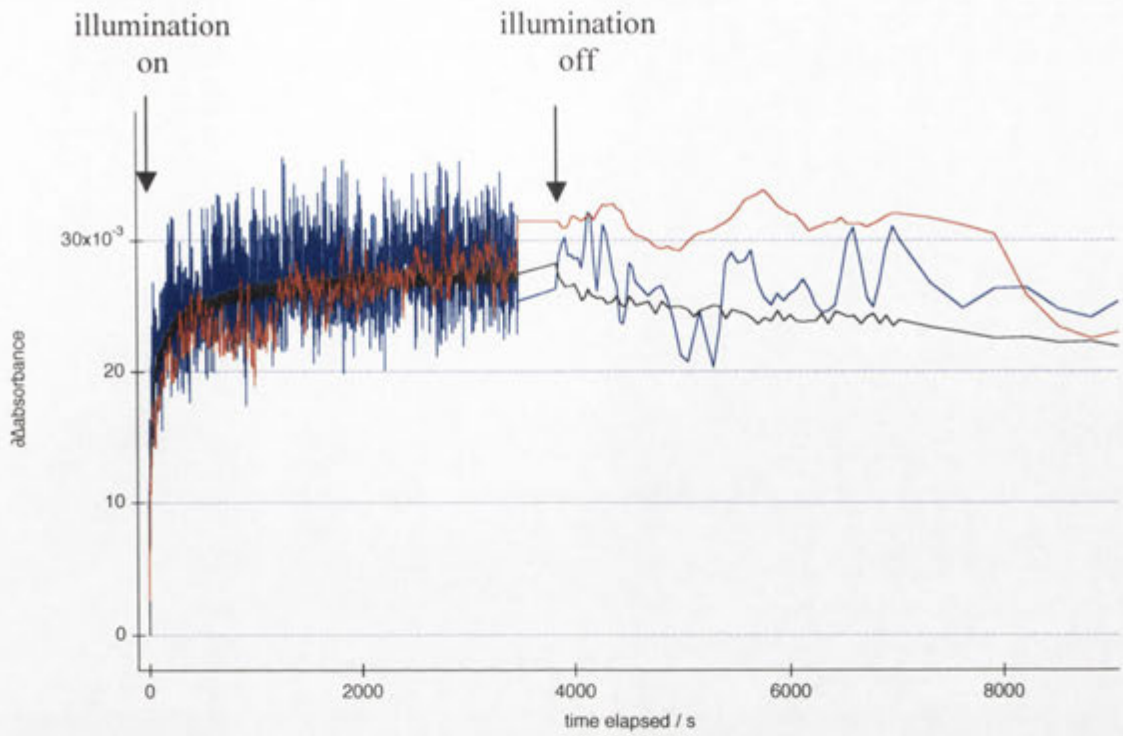

Figure 6.10 Kinetic trace of three features' peak-to-peak amplitudes in PEM illumination-induced difference spectra. Scaled 676 nm feature (red), Scaled Q_x pheo shift, 545 nm (blue trace), Q_y shift, 685 nm (black trace). 676 and Q_x shift smoothed with the Savitzky Golay algorithm (Smoothing parameters: 4th order, 25pts, End effect: bounce).

The analysis below was done on the data shown in Figure 6.10 before any scaling or smoothing was applied. The estimated uncertainties were based on the amplitude of the noise at the cessation of illumination.

All the spectral features reached their maximum amplitude at the end of illumination. The 685 nm feature was (76 ± 1)% of maximum peak-to-peak amplitude, approximately 1.1 hours after cessation of illumination. At the same point in time the 545 nm feature was (66 ± 10)% of its maximum peak-to-peak amplitude and the 676 nm feature was (72 ± 11)% of its maximum peak-to-peak amplitude.

The data suggests the 676 nm feature is electrochromic since it increased under illumination at the same rate as the Q_x and Q_y features, which have been established as being electrochromic shifts. The data points collected after the cessation of illumination

were too noisy to confirm that the 676 nm (or even the Q_x feature) decayed at the same rate as the Q_y shift feature.

6.4 The Origin of the 676 nm Feature

Based on the wavelength of the 676 nm shift in the spectrum, and assuming it is electrochromic in origin, it must be due to a charge affecting one or more pheophytin(s) and/or chlorophyll(s), as only these PSII pigments are known to absorb in this region of the spectrum. The charge could be located on an electron donor or acceptor molecule.

The experimental conditions giving rise to the 676 nm feature are known to form the state Q_A^- / D^+. In the following sections, two hypotheses are investigated and evaluated: i) the shift is due to the positive charge on a secondary donor and ii) the shift is due to the negative charge on Q_A^-.

6.4.1 Analysis of Hypothesis 1: The 676 nm feature is due to electrochromic shift due to a secondary donor

In an illumination experiment at cryogenic temperature, different secondary donors can be observed to donate to the primary electron donor P_{680}^+. The identity of the donating species depends on the experimental conditions and the PEM sample preparation details. See chapter 15 in the PSII monograph edited by Wydrzynski and Satoh.[14]

In this section each of the known electron donors to P_{680}^+ in PSII are considered in turn. The approach was to assume that the charged donor in question was giving rise to the 676 nm feature and the data was analysed to determine if it was consistent with that assumption.

Cytochrome b_{559} and the Manganese Cluster

In Figure 6.11 two difference spectra are shown from two different illumination experiments. The experiments were carried out by Dr Steffen, as my own annealing experiments at 180 K were affected by CCD instability; see Section 6.2.2.

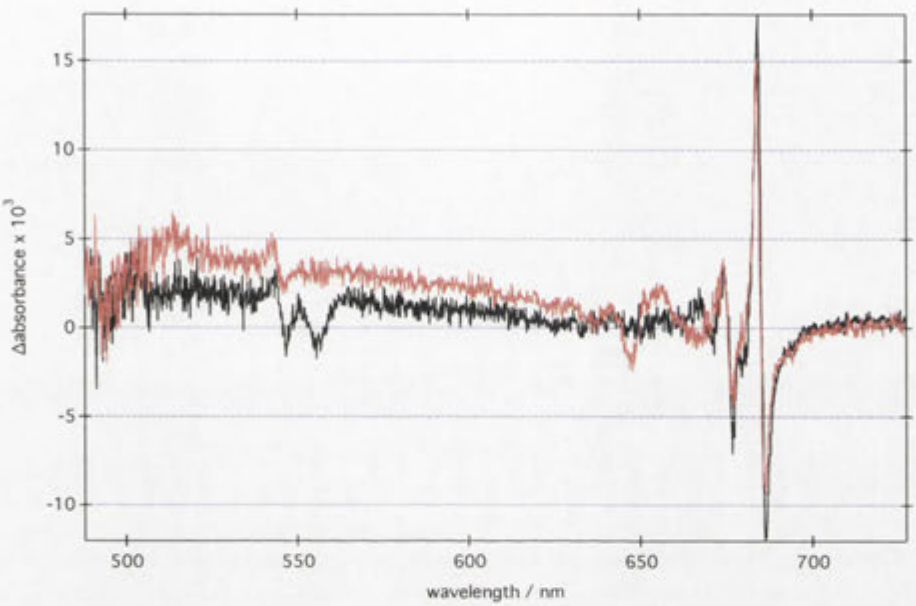

Figure 6.11 Illumination induced absorbance changes in PEMs from a 5 K (black trace) and 180 K (red trace) illumination. Both illuminations were a total of 5 ×100 ms white light flashes. All spectra were collected at 5 K.

The black trace is the difference spectrum resulting from a 5 K illumination of a PEM and the red trace from a 180 K illumination. All the absorption spectra in both experiments were collected at ~5 K. The traces are almost identical in the features due to the electrochromic shifts in the Q_x and Q_y regions. At 5 K the secondary donor is mainly cyt b_{559} as the bleach at ~559 nm, indicating cytochrome oxidation, is clearly visible (see Chapter 5). At 180 K the donor is principally the Mn cluster (S1 → S2 transition)[15] and no cyt b_{559} oxidation is discernable in the spectrum.

If the 676 nm feature was due to an electrochromic shift of a PSII pigment by oxidised cyt b_{559}, then the feature should be different in a sample in which the majority of donors are the Mn cluster. Since the 676 nm feature was identical in the two experiments,

this shows the feature is therefore not related to cyt b_{559}. Applying similar reasoning, the 676 nm feature also cannot be related to a charge on the Mn cluster.

The discrepancy between the traces at ~650 nm was reproducible after several freeze-thaw cycles and hence not an artefact. However, its origin is currently unknown. The pre-annealing spectra (not shown) showed changes that mimicked the derivative of the absorbance spectrum, that is, indicative of a small shift of the entire spectrum.

Carotenoid

The PEM samples from Uppsala University (see Chapter 2) had no (or very little) cyt b_{559} initially in the reduced state. In an illumination experiment with the Uppsula samples (see Figure 6.12) there was less than 20% cyt b_{559} oxidation observed in the Q_x region of the spectrum based on the noise and assuming 100% cytochrome oxidation gives a peak that is half the amplitude of the shift. The major electron donor was carotenoid as evidenced by the formation of Car^+ which has a characteristic peak at ~1000 nm (see Figure 6.13).

When the Q_y region is compared between the illuminated Uppsala PEM and the PEM preparations used in this work (see Figure 6.14), the two difference spectra are almost identical. Applying similar reasoning to that used in the preceding Section for cyt b_{559} and the Mn cluster, this experiment shows that a positive charge on a carotenoid donor can also be excluded as the source of the 676 nm feature.

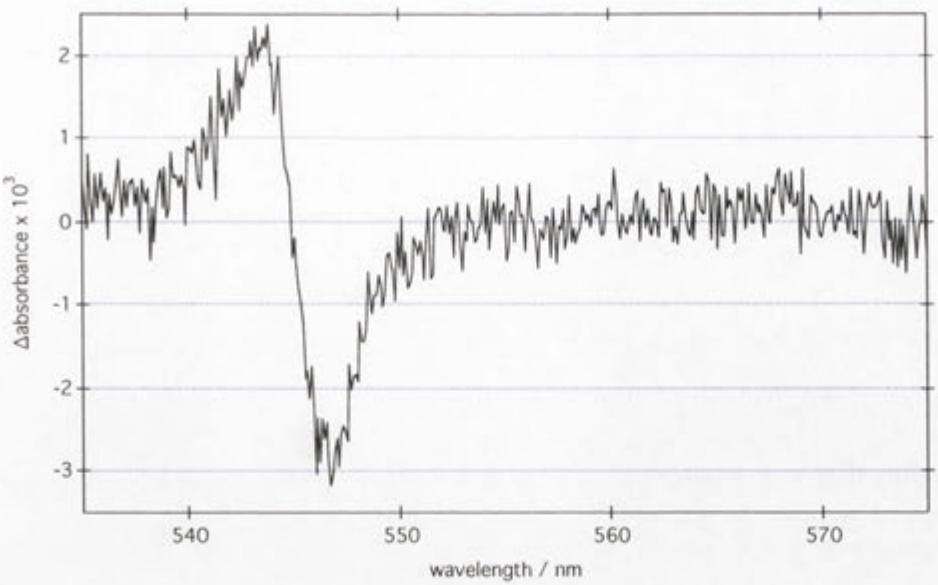

Figure 6.12 Absorbance change in the Q_x region due to a 1.7 K, 5 minute green illumination from a PEM prepared at Uppsala university.

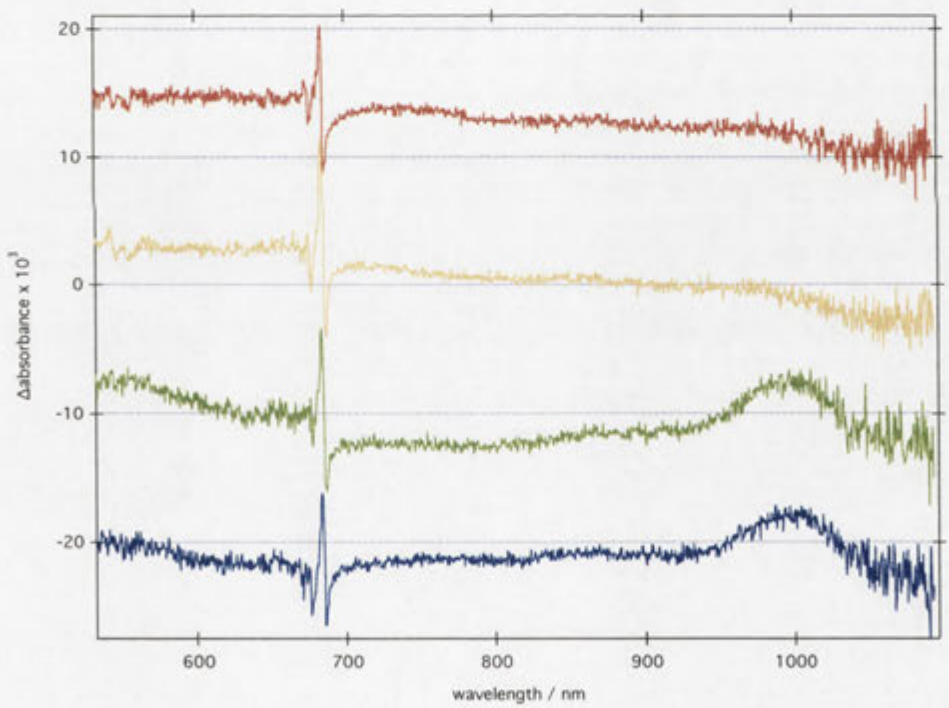

Figure 6.13 Comparison of illumination-induced differences spectra from ANU PEM samples (red and orange traces) and Uppsala PEM samples (green and blue traces).

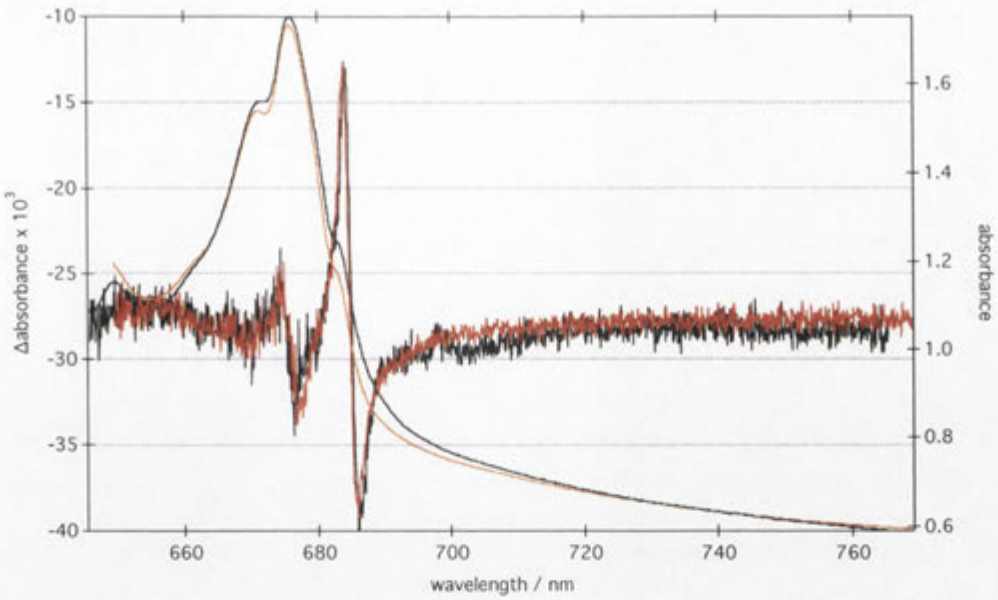

Figure 6.14 Comparison of the illumination induced difference spectra from two PEM samples. Red trace (Uppsala PEM, 20 LL flashes + 30 contiuous LL, no cyt b_{559} oxidation) and Black trace (ANU PEM, 98 continuous LL, mainly cyt b_{559} donation).

Tyrosine Z

PEM samples were analysed optically and by EPR, during cryogenic illumination.[16] The PEM samples were made by the same person (Dr Paul Smith) using the same methods as all the samples utilised in this work.

One of the findings of the study was that cryogenic illumination results in ~15% of PSII centres forming an EPR "split signal". The split signal was assigned to oxidised tyrosine Z (Y_Z) interacting by dipolar coupling with the S_1 state of the Mn cluster. The recombination of the Y_Z radical with Q_A^- was found to occur with a half life of ~150 s in the dark at temperatures below 20 K.

In the analysis of an illumination in Section 6.3.2, the 676 nm feature was found to decay to (72 ± 11)% of its maximum value after illumination after 2 h in the dark. Over this time (48 half lives) Y_Z is expected to fall to virtually zero. The 676 nm feature cannot therefore be due to the charge on oxidised Y_Z.

Tyrosine D

Tyrosine D (Y_D) is rapidly oxidised at room temperature and once oxidised, the tyrosine D radical is stable on the minutes to hours time scale. (See Faller[17] and references within).

The PEM samples in this work were always prepared in dim green light prior to their loading in the spectrometer. The 676 nm feature could not have arisen as a result of Y_D^+, since it would have already been photooxidised to a stable state before the sample illumination procedure.

Chlorophyll

If a chlorophyll cation (Chl^+) were formed during cryogenic illumination, then a bleach in the Q_y region of the spectrum should occur. Each of the samples shown in Figure 6.8 was analysed for the amount of Chl^+ formed and the results are listed in Table 6.3. The amount of Chl oxidation was estimated as follows.

The illumination-induced difference spectra were shifted such that the baseline went through zero Δabsorption. The area was measured between the zero line and the difference absorbance curve. The area over the same wavelength range was measured in the corresponding absorption spectra with a flat baseline extending from the red end. This was equated to be due to 200 Chl (the number of Chl per PSII reaction centre).

The area under the difference spectrum was divided by the area under the absorption curve and then divided by 200 to give the Chl absorbance. The ratio was underestimated due to the contribution of apparent absorbance from scatter, which was found to be on the order of about 3-10% (see Chapter 4).

An analysis of the area difference spectra in Figure 6.8, is presented in Table 6.3. The difference spectra equate to a loss of 0.095 – 0.51 chlorophyll per RC. This is interpreted as 9.5 – 51% of PSII centres having 1 chlorophyll molecule oxidised. There

appears to be no correlation between the estimated amount of chlorophyll photooxidised and the peak-to-peak amplitude of the 676 nm feature. Hence the 676 nm feature is not likely to be related to the formation of Chl^+.

Evaluation of Hypothesis 1

The experimental evidence suggests that the 676 nm feature is not caused by any of the known secondary electron donors in PSII. Hypothesis 1 therefore must be rejected.

6.4.2 Hypothesis 2: The 676 nm feature is due to an electrochromic shift of a pigment by Q_A^-

The analysis of spectra for the evaluation of hypothesis 1 showed that the 676 nm feature was not affected by the identity of the secondary electron-donor.

The acceptor molecule in all cases was Q_A^- so it was therefore consistent with the data to assume that the plastoquinone was the species responsible for an electrochromic shift at 676 nm. This proposition is labelled hypothesis 2.

6.4.2.1 Analysis of Hypothesis 2

It has been established that Q_A^- electrochromically shifts the $Pheo_{D1}$ Q_x band[2, 18] so it is reasonable to consider that the 676 nm feature may be also be due to an electrochromic shift of one or more PSII chromophores due to the negative charge localised on Q_A. Cyt b_{559} has no appreciable absorption features in this region. The only PSII reaction centre pigments that are known to absorb light in the vicinity of 676 nm are the pheophytins and chlorophylls.

To assess the validity of hypothesis 2, a study was done *in silico* simulating the expected electrochromic shift of all the chlorophyll and pheophytins in the PSII reaction centre due to the electric field from Q_A^- and comparing the simulated shifts to the experimental results.

6.5 Electrochromic Shift Simulations

6.5.1 Calculation of Expected Electrochromic Shifts of Chl and Pheo pigments in the PSII Reaction Centre due to Q_A^-

6.5.1.1 Theory of electrochromic shifts

Electrochromism is the phenomenon where the optical properties of molecules are influenced by an electric field. One consequence of an electric field on molecules is the shifting of their spectral bands, which is known as an electrochromic shift. The following theoretical analysis of electrochromic shifts is adapted from Liptay[19].

To illustrate the concept of the electrochromic shift, consider a molecule with two electronic states, the ground and an excited state. The permanent dipole moment in the ground and excited states are labeled $\boldsymbol{\mu}_g$ and $\boldsymbol{\mu}_a$[§] respectively. Now consider the molecule in the presence of an electric field. The effect of an electric field on the dipole moment is assumed to be negligible. In the presence of an electric field the energy of a molecule in the ground state (U_g^E)[†] is modified according to the magnitude of ground state dipole and electric field (***E***) vectors and their orientation relative to one another. Mathematically the ground state energy of a molecule in an electric field is given by

$$U_g^E = U_g - \boldsymbol{\mu}_g.\mathbf{E} = U_g - \mu_g E \cos\theta \qquad \textbf{Equation 6.1}$$

where θ is the angle between $\boldsymbol{\mu}_g$ and ***E***. The change in energy of the molecule depends on the scalar projection of the dipole moment on to the electric field vector (which is represented in the above equation as the dot-product).

Similarly the excited state energy in the electric field (U_a^E) is given by

$$U_a^E = U_a - \boldsymbol{\mu}_a.\mathbf{E} = U_a - \mu_a E \cos\theta \qquad \textbf{Equation 6.2}$$

[§] In this work, vector quantities are represented by bold symbols.
[†] The superscript 'E' on any parameter denotes that parameter in the presence of an electric field.

where all the symbols have the same meaning as in Equation 6.1 except that the subscript 'a' denotes an excited state, rather than ground state, parameter. In Equation 6.2 it has been assumed, that μ_a is parallel to μ_g (which is true for molecules with C_{2v} symmetry.)

The wavenumber energy of the transition between the ground and excited states v is given by the difference in energies

$$\nu = (U_a - U_g) / hc \qquad \textbf{Equation 6.3}$$

and in the electric field the transition energy is given by

$$\nu^E = (U_a^E - U_g^E) / hc \qquad \textbf{Equation 6.4}$$

Substituting the energy terms from Equation 6.1 and Equation 6.2 into Equation 6.4 we have

$$\nu^E = (U_a - \mu_a E\cos\theta - U_g + \mu_g E\cos\theta) / hc$$

$$= (U_a - U_g - E\cos\theta\,(\mu_a - \mu_g))/ hc$$

$$= \nu - (E\cos\theta\Delta\mu) / hc \quad \text{(substituting Equation 6.3)}$$

$$\nu^E - \nu = \Delta\nu = (-1/hc)(E\,\Delta\mu\cos\theta) \qquad \textbf{Equation 6.5}$$

Where the difference in ground state and excited state dipole magnitudes was substituted with $\Delta\mu$ and the difference in transition energy due to the electric field was substituted with Δv. The latter parameter represents the magnitude of the electrochromic shift due to the electric field.

The electrochromic shift is illustrated by means of an energy diagram in Figure 6.15. A hypothetical molecule is considered with two electronic states, a ground and

excited state. In the absence of an electric field there is a transition from the ground to excited state with energy *hcv*. In the presence of an electric field which is orientated anti-parallel to μ_g (and also μ_a which is assumed to be parallel to μ_g here) the energies of both the ground and excited states is increased (since cos(180°) = -1, see Equation 6.1 and Equation 6.2). Since $\mu_a > \mu_g$, the difference between the energy levels is greater in the electric field compared to without field. In a spectrum, this results in the transition band moving to higher energy. This band shift, which can be to either higher or lower energy, is known as an electrochromic shift.

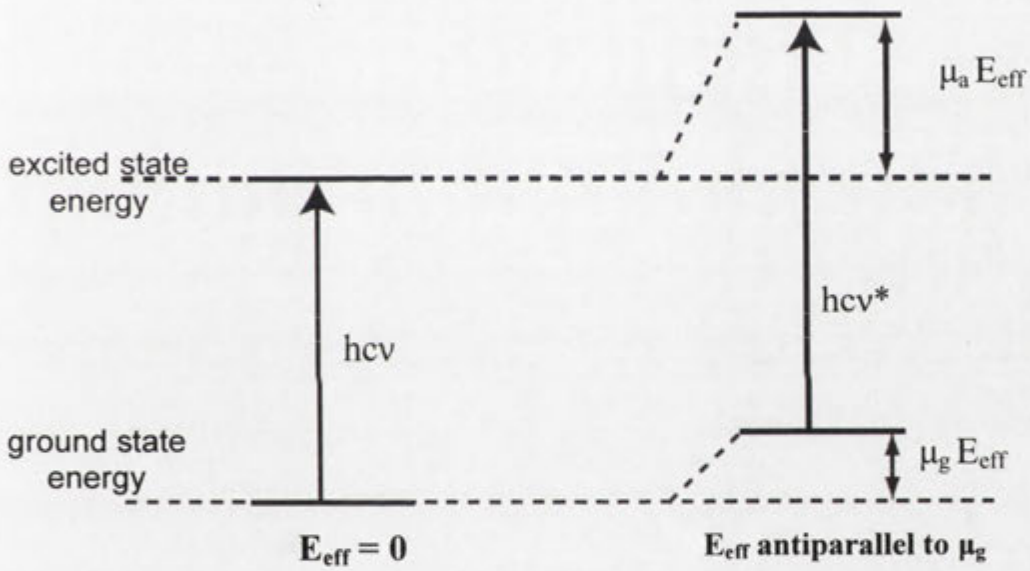

Figure 6.15 The electrochromic shift illustrated in an energy level diagram (see text). Since $\mu_a > \mu_g$, hcv* > hcv.

As a final step, if the polarisabilty of the molecule is taken into account in Equation 6.5[20] we obtain:

$$\Delta\nu = -\frac{1}{hc}\left(|\Delta\boldsymbol{\mu}||\boldsymbol{E}_{eff}|\cos\theta + \frac{1}{2}\Delta\alpha E_{eff}^{\ 2}\right) \qquad \textbf{Equation 6.6}$$

where,

$\Delta\alpha = \alpha_e - \alpha_g$ is the change in polarisability between the ground and excited state. The effective electric field vector $\boldsymbol{E}_{eff}$ is introduced here and explained below.

If $\Delta\nu$ is positive this indicates that $\nu^E > \nu$, that is, the band is shifted to higher energy, which is known as a blue shift. Conversely, a negative $\Delta\nu$ indicates a red electrochromic shift.† The sign of $\Delta\nu$ is only dependant on θ as all the other variables are positive.

Equation 6.6 applies to systems where the absolute axis directions are known. Discussion about the general equation for electrochromic shifts is given in the Appendix of this chapter (Section 6.7.1).

We now consider the source of the electric field in a PSII reaction centre, that is, the electron on Q_A^-. Assuming the electron is a point charge, the strength and direction of the electric field ($\boldsymbol{E}$) at a distance r can be calculated with Coulomb's law;

$$\boldsymbol{E} = \frac{e}{4\pi\varepsilon_0 r^2}\boldsymbol{r} \qquad \textbf{Equation 6.7}$$

where,

ε_0 is the permittivity of a vacuum, e is the charge of electron and $\boldsymbol{r}$ is the unit vector from charge to the molecule of interest.

The amino acids in the space between Q_A^- and the pigments in PSII can reduce the electric field strength at those pigments. This is known as 'charge screening' and is caused by the induced or permanent dipoles on amino acids orientating so as to terminate some of the field lines coming from Q_A^-. The effective dielectric constant accounts for the decrease in electric field strength at a pigment due to charge screening.[21] Mathematically,

† So-called because blue light is of higher energy than red light.

$$\mathbf{E_{eff}} = \mathbf{E} / \varepsilon_{eff} \qquad \textbf{Equation 6.8}$$

where ε_{eff} is the effective dielectric constant and $\boldsymbol{E_{eff}}$ the effective electric field vector experienced at the pigment of interest.

6.5.2 Electrochromic Shift Simulations Methodology

The electrochromic shifts expected from Q_A^- on the 6 Chl and 2 Pheo in the PSII reaction centre were calculated by Equation 6.6 with the electric field strength and direction at each chromophore was calculated by Equation 6.7 and Equation 6.8. Each chromophore was modeled as a Gaussian band and shifted by the calculated amount. The net result was obtained by summing all the shifts. The reasoning behind the choice of parameter values and the simulation results are presented below.

6.5.3 Choice of Parameter Values for Simulation

The simulations required estimates for all the parameters in Equations 6.6 , 6.7 and 6.8. As a starting point, the most applicable literature data was used to determine the value of each parameter used in the calculation of $\Delta\nu$ according to Equation 6.6. These include both calculated and experimentally determined parameters.

Spatial arrangement

The spatial arrangement of pigments in PSII was required to calculate the distance between Q_A^- and each pigment as well as the angle between $\Delta\boldsymbol{\mu}$ and $\boldsymbol{E_{eff}}$. The spatial arrangement of the pigments was obtained from the most recent PSII crystal structure[7] with the protein data bank accession code 2AXT. The structure was obtained from a cynaobacterium, *Thermosynechococcus elongatus* at a resolution of 3.0 Å, the highest resolution structure of PSII obtained to date.

The charge on Q_A^- was assumed to be located in the middle of the quinone head group and the $\Delta\boldsymbol{\mu}$s of the chlorin type pigments were assumed to be point-dipoles in the

plane of the ring. Their direction was taken to be from the centre of the macrocycle to a pyrrole nitrogen. The reasoning behind the choice of which nitrogen each chromophore dipole pointed to is discussed below.

Effective dielectric constant (ε_{eff})

Stark spectroscopy experiments on bacterial reaction centres showed that ε_{eff} can vary markedly between the active and inactive sides of the reaction centre.[22] Since there was no ε_{eff} estimate available for the plant PSII reaction centres, a default value of 1 was used as a starting point for the calculations here.

Change in polarisability ($\Delta\alpha$)

In isolated chlorophyll the change in polarisability has been estimated utilising Stark spectroscopy by Krawczyk.[23] The results from the study are summarised in Table 6.4. As a first approximation the value of $\Delta\alpha = 2$ Å^3 was used for all the electrochromic shift calculations. This value was also used by Mulkidjanian et al.[11] in their determination of the arrangement of pigments in PSII core particles from electrochromic difference spectra.

It should be noted that if $\Delta\alpha = 2$ Å^3, this makes a relatively small contribution to the calculated shift (typically 5 – 10%). Only if the angle between $\Delta\boldsymbol{\mu}$ and $\mathbf{E}_{\mathbf{eff}}$ is close to 90° does the term ($\frac{1}{2}\ \Delta\boldsymbol{\alpha}\ E^2$) in Equation 6.6 tend to dominate the calculated electrochromic shift.

A Stark-effect study on D1/D2/cyt b_{559}[24] showed that the Stark spectra resemble the second derivative of absorption spectra. This means that the Stark spectrum of the PSII reaction centre is dominated by $\Delta\boldsymbol{\mu}$ and it this is consistent with the relatively small magnitude of $\Delta\alpha$ assumed here.

Chl species, solvent/ligand, temperature	$\Delta\alpha$ (Å^3)	
	Q_x	Q_y
Monosolvate[‡], ethylbenzene/ butylbenzene (1:1, v/v) / triethylamine (0.25 M), 118 K	~13	2.2
Monosolvate, solvent: isopropanol, 155 K	~5	1.5

Table 6.4 Change in polarisabilities in the Q_x and Q_y regions. From Krawcyzk.[23]

Chlorophyll and Pheophytin $\Delta\mu_y$ Magnitudes

A study of D1/D2/cyt b_{559} reaction centres with Stark spectroscopy found that $\Delta\mu_y$ = 1.6 D[†] for Chl and $\Delta\mu_x$ = 0.6 D for Pheo.[24] The value of 1.6 was assumed for the $\Delta\mu_y$ of Chl and the $\Delta\mu_y$ of Pheo was assumed to equal the $\Delta\mu_x$ value of 0.6 D.

Chlorophyll $\Delta\mu_y$ Orientation

It is useful at this point to introduce the nomenclature for porphyrin rings that is used in specifying the $\Delta\mu$ orientations. Figure 6.16 shows a simplified structure of a chlorin which can represent pheophytin or chlorophyll. The pyrrole rings are labeled with Roman numerals I to V and the corresponding pyrrole nitrogens are labeled N_I to N_{IV}. All dipoles are assumed to lie in the plane of the chlorin ring.

According to the Gouterman four-orbital model the *x* axis is defined as the vector joining N_{II} and N_{IV} and the y axis is along the vector joining N_I and N_{III}.[25]

‡ A monosolvate has 1:1 stoichiometry of solvent to molecule.
† Debye

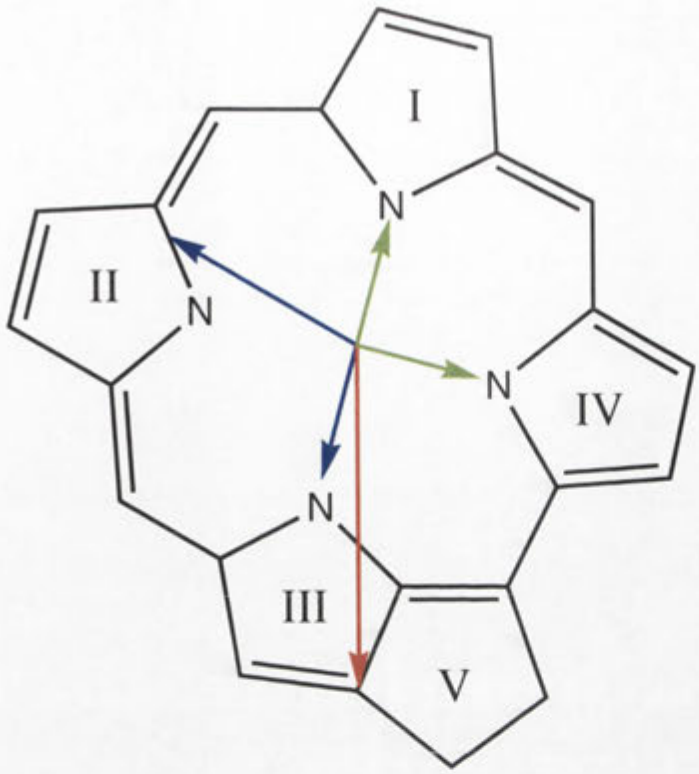

Figure 6.16 Summary of the Δμ and transition dipole moment orientations in Chl *a* and Pheo *a* from the literature. Red Vector: Pheo *a* Q_y TDM[26]. Blue Vectors (ring III) Chl *a* Q_y TDM[26] and bacterio chl *b* transition dipole[25] (ring II) bacterio chl *b* Q_x transition dipole.[25, 26] Green Vectors (ring IV) $Pheo_{D1}$ $\Delta\mu_y$[13](ring I) $Pheo_{D1}$ $\Delta\mu_x$.[13] Note: Arrows are only indicative of vector directions, their lengths do not indicate vector magnitudes.

The transition dipole moments (TDMs) of isolated chlorophyll *a* have been determined experimentally by van Zandvoort et al.[26] They embedded pigments in a nitrocellulose film to ensure no intermolecular energy transfer took place and the concentrations of the pigments were sufficiently dilute to ensure they were monomeric. The Q_y TDM of Chl *a* was found to lie along its N_I - N_{III} axis, pointing towards ring III and the Q_x Chl *a* TDM was not shown.

The TDM orientation determined by van Zandvoort et al. is consistent with a theoretical determination in which the dipole velocity method was used to calculate the transition dipoles of bacteriochlorophyll *b*.[25] The Q_y transition dipole moment was

predicted to point at N_{III}, while the Q_x moment pointed to the midpoint of the nitrogen on N_{II} and the carbon bonded to it (away from the 5th ring).

Krawczyk determined that the $\Delta\mu_y$ of Chl *a* in solution lies at an angle of 20° to the Q_y electronic transition moment.[23] This suggests $\Delta\mu_y$ lies 20° from the ring I-ring III axis and Mulkidjanian et al. interpreted the direction to be 20° towards the centre of ring V.[11]

To simplify the calculations carried out in this chapter, it was assumed that the Chl *a* $\Delta\mu_y$ pointed at N_{III}. This approximation, which deviates 20° from the value determined by Krawcyk, would slightly alter the magnitude of the calculated electrochromic shifts but not affect their direction (in terms of blue or red shift).

Pheophytin $\Delta\mu_y$ Orientation

In the study cited above, van Zandvoort et al.[26] also determined the Q_y transition dipole moment of isolated pheophytin *a*. It pointed from the centre of the pheophytin to the most distant shared carbon atom of ring III and V (see Figure 6.16).

Peterson Årsköld et al.[13] concluded that $\Delta\mu_x$ of $Pheo_{D1}$ points to N_I. This corresponds to a rotation of approximately 90° compared to the vector calculated for Chl *a*[25] and is inconsistent with the Pheo *a* TDM determined experimentally.[26] This discrepancy is resolved below by analysing experimental data from this work and preliminary calculations.

In the Q_x region of an illumination-induced difference spectrum, only the pheophytins and cyt b_{559} absorb light. They give rise to the C550 feature, an electrochromic blue-shift (see Section 6.1.1) and the cyt b_{559} bleach (due to cytochrome photooxidation). The C550 feature may have a minor overlap with cyt b_{559} but it is clearly a blue shift.

The expected direction of the electrochromic shift can be calculated using Equation 6.6 requiring only the angle between the electric field and $\Delta\boldsymbol{\mu}$ vectors. This is because the sign of $\Delta\nu$ is only dependent on the angle between the vectors. These preliminary calculations show a blue shift of the pheophytin band occurs if $\Delta\boldsymbol{\mu}$ points at N_I or N_{II} and red shifts if it points to N_{III} or N_{IV}. Therefore, since the $Pheo_{D1}$ Q_x band blue-shifts, $\Delta\boldsymbol{\mu}_x$ must point at N_I or N_{II}.

Using the parameters determined thus far, the expected electrochromic shift for the two possible dipole orientations was calculated (see Figure 6.17). Shifts of 59 cm^{-1} and 12 cm^{-1} were obtained for the dipoles pointing at N_I and N_{II}, respectively. A pheophytin peak was simulated shifting both of the calculated energies and compared with the experimental shift feature to determine which was most likely to be correct. This was done as follows.

A Q_x difference spectrum was shifted vertically such that its baseline went through zero Δabsorbance. It was then integrated and the resultant peak was fitted to a Gaussian function. The FWHM was of the fitted band was found to be 4.9 nm, which is comparable to the literature value of 7 nm.[27]

The area of the fitted peak was measured and equated to be the area of 1 Pheo (scaled to the sample OD). A peak at 545 nm was simulated (with a Gaussian FWHM = 4.9 nm and area of 1 Pheo) to shift 12 cm^{-1} and 59 cm^{-1} and this was compared to the shift from experiment (the results are shown Figure 6.17). The calculated peak wavelength shift was almost the same for the two simulations but the experimental peak-to-peak height was much closer to the 12 cm^{-1} rather than the 59 cm^{-1} shift. It was therefore concluded that the experimental data supports a $\Delta\boldsymbol{\mu}_x$ pointing at N_{II} and $\Delta\boldsymbol{\mu}_y$ at N_I or N_{III}, following the convention in the literature that $\Delta\boldsymbol{\mu}_x$ is perpendicular to $\Delta\boldsymbol{\mu}_y$. Initially $\Delta\boldsymbol{\mu}_y$

was assumed to point at N_{III} since this is more consistent with the literature determination of the Pheo *a* and Chl *a* $\Delta\mu_y$'s.

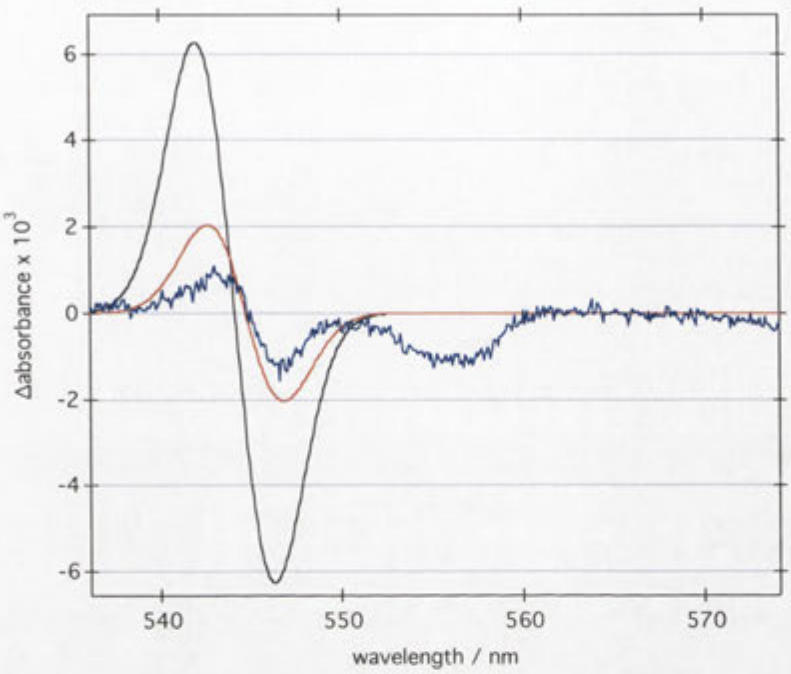

Figure 6.17 Simulation of two shifts corresponding to the two possible orientations of $\Delta\mu_x$. Black trace: 59 cm^{-1} shift, Red trace: 12 cm^{-1} shift, and Blue trace: Experimental Q_x illumination induced difference spectrum. All spectra scaled to the shift of one Pheo per PEM sample OD.

The direction of the shifts calculated here was consistent with literature INDO/s calculations of the electrochromic shift due to a charge affecting bacteriochlorophylls *a*, *b* and *g*, bacteriopheophytins *a* and *b*, and chlorophyll *a*.[28-30]

Chlorophyll and Pheophytin Q_y Band Positions and Widths

The final step was to estimate the peak positions and linewidths of the pigments and apply the calculated electrochromic shift. The shift of each pigment was calculated by subtracting the final band position from the initial band positions. The overall lineshape expected in a difference spectrum was constructed by summing all the individual electrochromic shifts.

Based on literature information, the pigments' bandwidths and areas were simulated as follows in calculations. The Chl *a* bands were assumed to have a Gaussian-shaped band with FWHM of 350 cm^{-1} (16 nm) based on a study by Altmann et al[31] where Chl *a* was doped in poly(vinyl butyral) at 2.0 K. The Pheo widths were set to 2/3 of the Chl width based on room temperature spectra,[25] which was valid for low temperature spectra since the dipole strength is independent of temperature. The area of the Pheo bands was set to be half of the Chls, as the dipole strength of pheophytin has been estimated to be half that of chlorophyll.[13]

The magnitude of the area was estimated by measuring the area of all Chls and dividing by 200. This was compared with integrating a Q_x illumination induced difference spectrum to obtain the area of a single $Pheo_{D1}$.

All pigments were assumed to absorb at 678 nm except the two Chl Z pigments which peak at 672 nm based on a Stark study of D1/D2/cyt b_{559} reaction centres.[24]

Parameter	*Value*	*Unit*	*Reference*
Atomic Coordinates	n/a	n/a	Loll et al.[7]
ε_{eff}	1	dimensionless	Default value of unity since none available (see text).
$\Delta\alpha$	2	$Å^3$	Krawczyk[23]
Chl $\Delta\mu_y$ Magnitude	1.6	Debye	Frese et al.[24]
Chl $\Delta\mu_y$ Direction	points at N_{III}	n/a	Zandvoort et al.[26] and Krawczyk[23]
$Pheo_{D2}$ $\Delta\mu_y$ Magnitude	0.6	Debye	Frese et al.[24]
$Pheo_{D2}$ $\Delta\mu_y$ Direction	points at N_{III}	n/a	Zandvoort et al.[26]and Krawczyk[23]
$Pheo_{D1}$ $\Delta\mu_y$ Magnitude	0.6	Debye	Frese et al.[24]
$Pheo_{D1}$ $\Delta\mu_y$ Direction	points at N_{III}	n/a	Based on calculations and reasoning on page 154 in this chapter. N_{III} chosen of the 2 possibilities N_I and N_{III} (as its consistent with literature value).

Table 6.5 Summary of parameter values used for simulation of the electrochromic shift of chlorophyll and pheophytin bands due to Q_A^-.

6.5.4 Simulation Results

The result of the first simulation iteration is shown in Figure 6.18. The calculations show that all pigments in the PSII reaction-centre are expected to be shifted. Although a large red-shift is expected for $Pheo_{D1}$ (solid blue trace) the contribution from all the pigments summed together (black trace) result in a blue-shift.

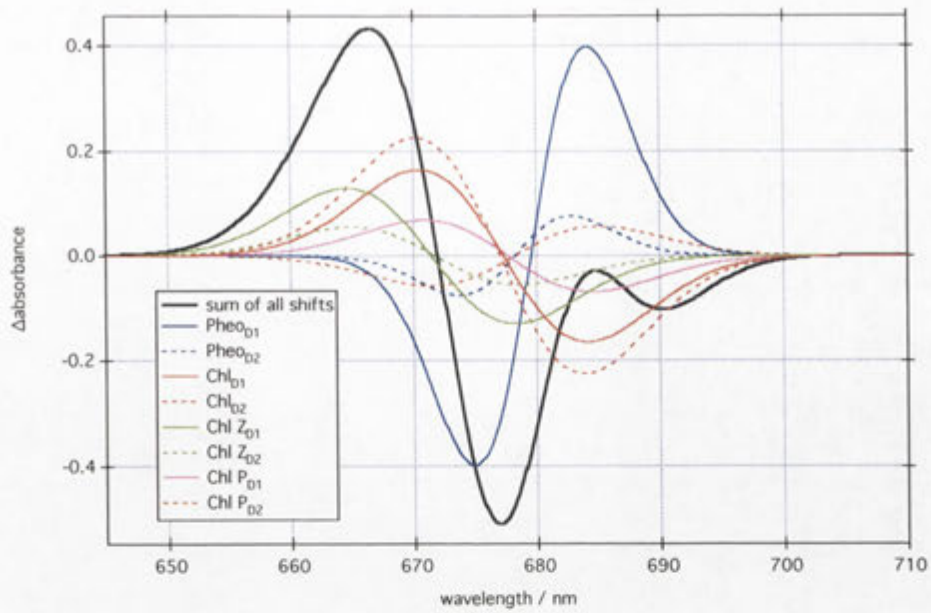

Figure 6.18 Simulation 1 Electrochromic Shifts due to Q_A^- in PSII. Parameters used are listed in Table 6.5 and Table 6.6.

It is clear that the overall shift is not consistent with experiment as the linewidth of the shift feature (~11 nm) is much broader than observed in experiments (~2 nm). This discrepancy can only be due to an incorrect estimate of the peak widths. Our research group has estimated the Pheo Q_y to have a FWHM 3.2 nm[13] but this is assuming the blue shift in Q_y is only due to $Pheo_{D1}$, an assumption not being made in this work. However, since no other data is available, this value was applied and the shifts simulated again (see Figure 6.19).

Parameter	*Value*	*Unit*	*Reference*
Band positions (except Chl Zs)	678	nm	Frese et al.[24]
Chl Z band positions	672	nm	Frese et al.[24]
Chl Band widths (simulation 1)	~17 (350)	nm (cm^{-1})	Altmann et al.[31]
Pheo Q_y Band width (simulations 2,3,4)	3.2 (~65)	nm (cm^{-1})	Peterson Årsköld et al.[13]
Chl Band width (simulations 2,3,4)	4.8	nm	1.5 × Pheo width in RT spectrum Scheer[25]
Pheo area	½ of Chl Area	n/a	Pheo has ½ dipole strength of Chl[13]
Chl area	1	n/a	Arbitrary value. Area was corrected for comparison with experiments. See text.

Table 6.6 Band positions, widths and areas used in the electrochromic shift calculations. Values are for all simulations unless otherwise stated.

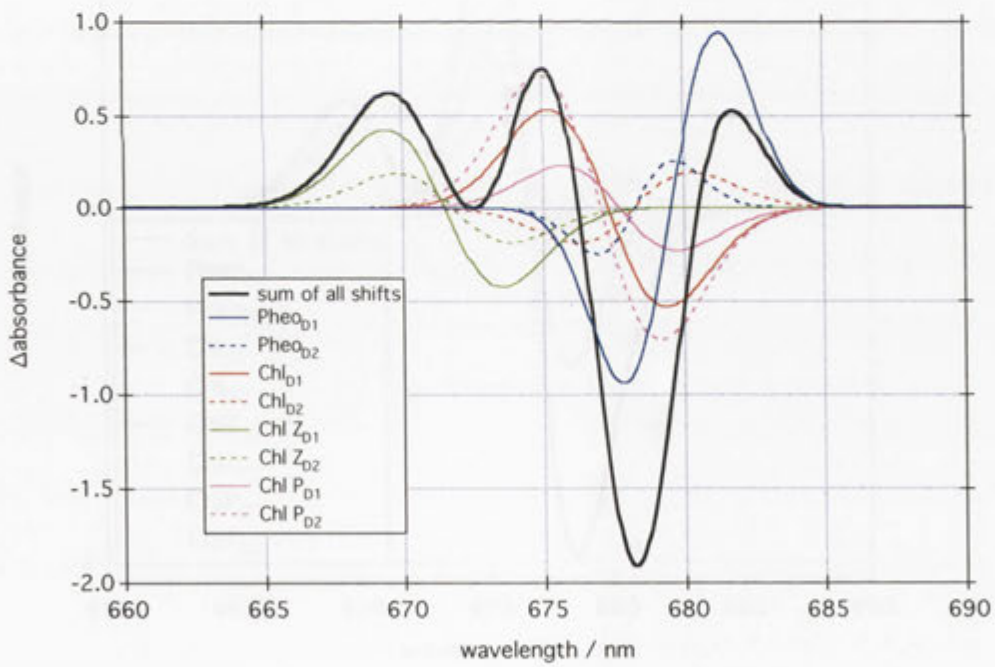

Figure 6.19 Simulation 2. The same parameters were used as for Simulation 1 except the FWHM of Pheo = 3.2 nm and the Chl widths were scaled accordingly as they were in Simulation 1.

In the second simulation the shift-feature widths were consistent with the width of the main 685 nm shift observed experimentally but resulted in a complicated lineshape not consistent with experiment. The $Pheo_{D1}$ contribution is a large red-shift based on the $\Delta\mu_y$ pointing to ring III. When determining the direction of $\Delta\mu_y$ (see page 154) two alternatives were consistent with the Q_x shift corresponding to the $\Delta\mu_y$ pointing to N_I or N_{III}. The latter alternative was simulated first since this was consistent with the direction determined in the literature. However, given that the simulation is not consistent with the experimentally observed difference spectrum, the other alternative ($\Delta\mu_y$ pointing to N_I) was simulated (see Figure 6.20).

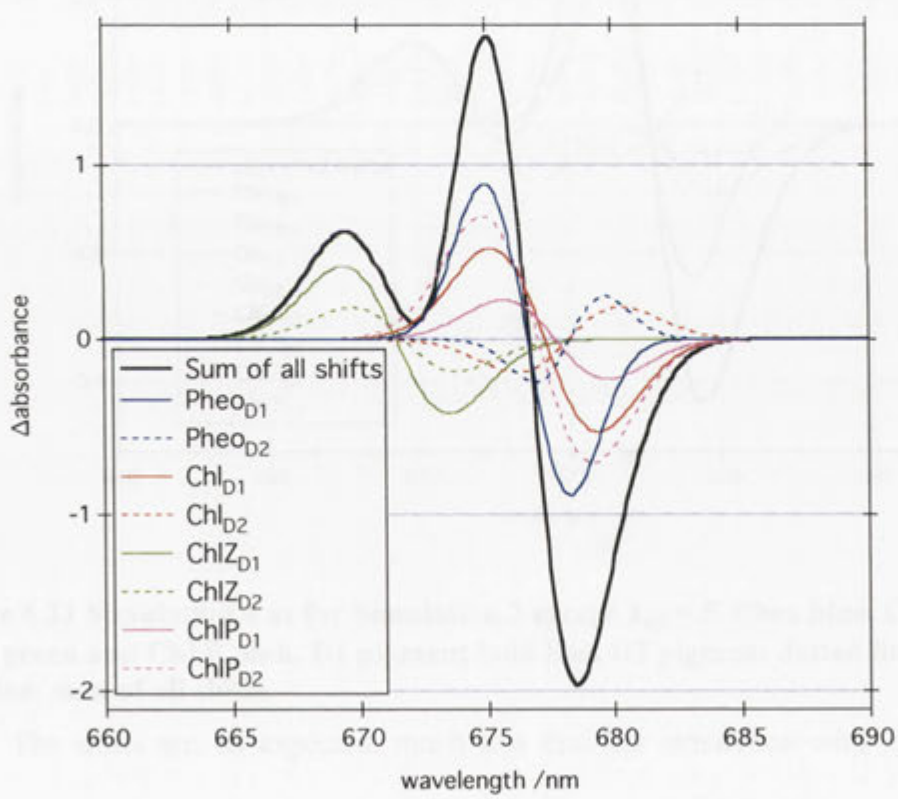

Figure 6.20 Simulation 3, parameters as for Simulation 2 except $Pheo_{D1}$ $\Delta\mu_y$ points to N_I.

Simulation 3 resembled the experimental data to a greater extent than the preceding simulations as it appears as an asymmetric blue shift with a small feature adjacent to the blue of the shift. The alternative $\Delta\mu_y$ for $Pheo_{D1}$ meant that its band was blue-shifted and together with the other strong blue-shifts (on Chl_{D1}, Chl P_{D1} and Chl P_{D2}) resulted in an overall blue-shift spectrum.

Finally, the shifts were simulated with the effective extinction coefficient set to 5 for all pigments (see Figure 6.21).

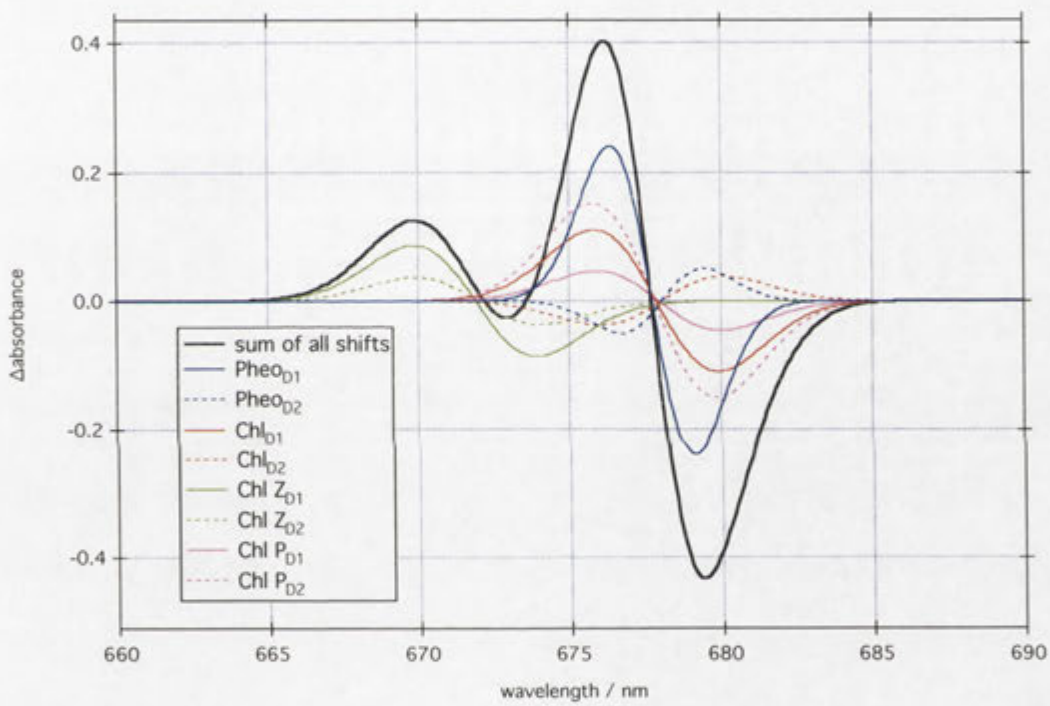

Figure 6.21 Simulation 4 as for Simulation 3 except ε_{eff} = 5. Pheo blue, Chl red, Chl Z green and Chl P pink. D1 pigment bold line, D2 pigment dotted line. Black bold line: sum of all shifts.

The shifts are, as expected, much less than for simulation with ε_{eff} = 1 in the preceding simulations. This results in an overall reduced peak-to-peak magnitude of the blue shift.

Peak Area Scaling

The simulated electrochromic shifts were scaled for comparison to the experimental spectrum. This was done by determining the area of absorbance in the Q_y region and equating it to 200 chlorophylls. The Chl area of the simulations were then adjusted to the value determined from experiment. The area of the PEM spectrum between 630 and 730 nm was measured and divided by 200 Chl and the OD, to determine an approximate area for 1 Chl per RC. The average area of 1 Chl was 0.0198 (from a sample of 5 spectra). The Chl area in the simulation was scaled to this value.

6.5.4.1 Summary of Simulation Results

The parameters used in each simulation are summarised in Table 6.7 below and the resultant spectral simulations are shown together in Figure 6.22.

Simulation No.	*Parameters*
1	See Table 6.5 and Table 6.6 (larger FWHM)
2	As for Sim 1 but FWHM Pheo = 3.2 nm (and Chl scaled accordingly smaller FWHMs)
3	As for Sim 2 $Pheo_{D1}$ $\Delta\mu_y$ point to N1
4	As for Sim 3 but $\varepsilon_{eff} = 5$

Table 6.7 Summary of parameters used in each electrochromic shift simulation.

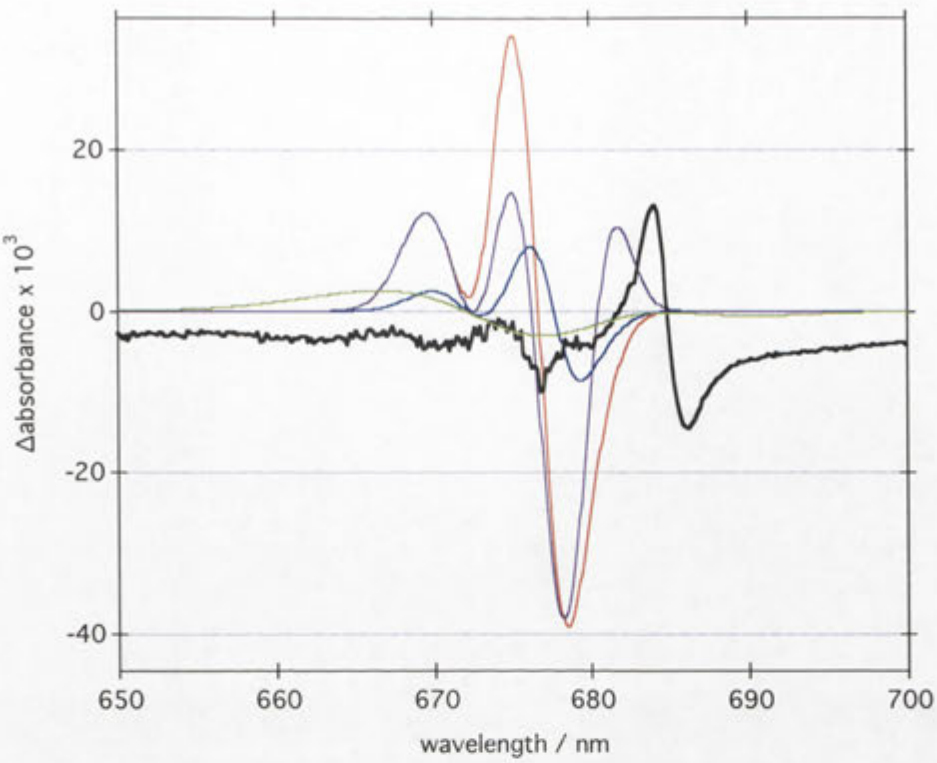

Figure 6.22 Comparison of the four Simulations of electrochromic shifts (green, purple, red and blue traces are Simulations 1, 2, 3 and 4 respectively) in PSII and a typical Q_y difference spectrum (black, baseline offset vertically for clarity). All scaled on a per OD basis as described in the text.

6.6 Discussion

In the first half of this chapter the true illumination-induced difference spectrum of PSII enriched membranes was determined. It was then shown by kinetic experiment that the 676 nm feature in that spectrum was consistent with being an electrochromic shift. A systematic study of several experiments showed that a positive charge on a known secondary donor is not the cause of the 676 nm feature. It was therefore concluded that the cause of the electrochromic shift was the electric field of Q_A^-. The expected electrochromic shifts were simulated by calculations that modelled the interaction between the PSII pigments' change in dipole moments and the electric field due to Q_A^-.

Electrochromic-Shift Simulations

The electrochromic-shift simulations were a tool to test if the 676 nm feature could be an electrochromic shift of pigments by the electric field of Q_A^-. Due to the extrapolation of data from systems other than intact PSII, such as D1/D2/cyt b_{559} preparations, and the simplicity of the model, the simulations can only give an indication of the origin the 676 nm and main 685 nm features. That is, they can only show what is possible and rule out impossibilities but not provide a definitive confirmation of the proposed hypothesis. The results of Simulations 1 and 2 showed that there were some problems with the input data (for example linewidths) and perhaps the complexity of the model.

General observations

The most interesting finding evident in the simulations was that Q_A^- is predicted to electrochromically shift all the Chl and Pheo Q_y bands (of which there are eight in total) in the PSII reaction centre to a significant and similar extent. This is a novel result. Previous studies have assumed that three or four pigments shift in PSII[11,12] based on

analogous experiments with bacterial reaction centres. Peterson-Årsköld et al. have assigned the 685 nm shift to only $Pheo_{D1}$.[13]

The calculations performed here show in fact that if Q_A^- can electrochromically shift $Pheo_{D1}$ then one must consider that all pigments in PSII should undergo an electrochromic shift of similar magnitude. The $Pheo_{D1}$ shift is just one component of the 685 nm shift.

In Table 6.8 below, the factors contributing to the ability of Q_A^- to electrochemically shift all chromophores in the PSII reaction centre are summarised. The chromophores are ordered by ascending distance from Q_A and the relative electric field strength due to Q_A^- was calculated by taking the inverse square of the distances and expressing these in terms of the closest chromophore $Pheo_{D1}$, where the magnitude was set to 1. This calculation alone shows there is potential for significant contributions from the other chromophores to the shifts in an illumination induced difference spectrum, with several chromophores experiencing 20 – 30% of the field at $Pheo_{D1}$.

Equation 6.6 states that the electrochromic shift is proportional to the product of the effective electric field, $\Delta\mu$ and $\cos(\theta)$. A relative electrochromic shift magnitude was calculated for each chromophore, again normalising to the largest shift due to $Pheo_{D1}$, which was set equal to 1. The expected electrochromic shift is increased for most of the chromophores. This is due in part to the larger $\Delta\boldsymbol{\mu}$ assumed for the pheophytins relative to chlorophylls and the angle between chromophore $\Delta\boldsymbol{\mu}$ and the electric field vector.

Chromophore	*Distance from Q_A^- / Å*	*Relative electric field strength at chromophore due to Q_A^-*	*θ / degrees*	*Relative electrochromic shift magnitude**
Pheo $_{D1}$	13.07	1.000	138.3	1.000
Chl $_{D1}$	22.83	0.328	113.9	0.474
Pheo $_{D2}$	23.43	0.311	63.3	-0.187
P $_{D1}$	26.98	0.235	103.9	0.202
P $_{D2}$	27.21	0.231	143.4	0.662
Chl $_{D2}$	29.77	0.193	76.5	-0.161
Chl Z $_{D1}$	32.37	0.163	131.2	0.383
Chl Z $_{D2}$	46.58	0.079	125.6	0.164

Table 6.8 Electrochromic shift parameters for chromophores in the PSII reaction centre. See text for details of calculations. *Calculated with Δμ directions used in Simulations 3 and 4. Positive number indicates a blue shift.

The results of the calculations do not contradict the fact (assumed in previous studies and this work) that the 685 nm shift amplitude is proportional to the amount of Q_A^- formed.

Spectral location of electrochromic shifts

In Simulation 3 the main blue-shift was transposed to the red by ~8 nm compared to experiment. This is because the literature value of the initial pigment peak positions were based on a study of D1/D2/cyt b_{559} preparations and the pigments in these preparations are known to be blue shifted compared to PEM and cores.[10] There is no consensus on the Q_y band peak positions and widths in PSII, especially in PEM type samples where peaks are not clearly resolved and there is high 'spectral congestion'. Clearly, comparison of the experimental difference spectrum with the calculations (see Figure 6.22) suggests that all the peaks should be shifted to the red compared to the estimate from D1/D2/cyt b_{559} preparations. The lineshape would be approximately the same for peaks located more to the red since the energy difference of peaks (in the

absence and presence of an electric field), at such a similar energies will equate to very similar wavelength shifts.

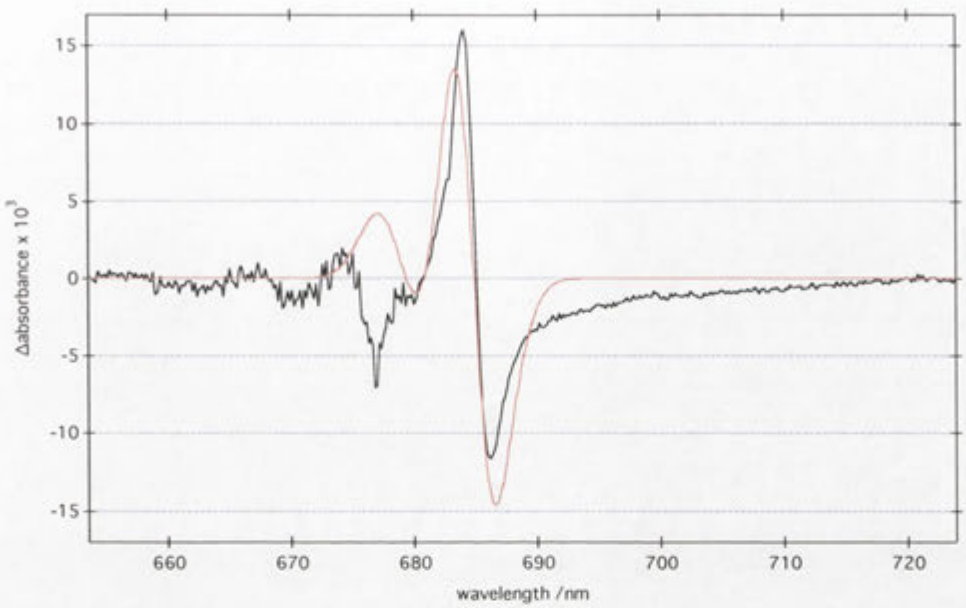

Figure 6.23 Electrochromic Shift Simulation 4 (red trace) compared to experimental illumination-induced difference spectrum (black trace). Simulation 4 was shifted to overlap the experimentally observed electrochromic shift at 685 nm and scaled to approximately the same peak-to-peak magnitude.

Difference Feature Lineshapes

According to the simulation the 685 nm feature is composed of multiple red and blue shifts of different peak-to-peak magnitudes which sum to produce a net blue shift. Six of the eight pigments in the PSII reaction centre are predicted to blue shift.

The 685 nm shift is asymmetric. A plausible reason for the asymmetry is that the observed shift is composed of multiple shift features. Since the pigments most likely shift from different initial positions and certainly to different extents, it is reasonable to expect the resultant shift will be asymmetric.

Origin of the 676 nm feature

The simulations were originally conducted to determine the possible origin of the 676 nm feature. The simulations show that it is possible that if one or more pigments

originated far enough in wavelength from the main electrochromic shift at 685 nm, this could give rise to a shift type feature observed in experiments. The minor feature adjacent to the main 685 nm shift was due to blue shifts of both Chl Z molecules. This assignment is unlikely to be correct for a number of reasons but does show a possible explanation for the origin of the 676 nm feature.

In Simulation 3 (Figure 6.20), for example, there are a number of pigments that blue shift and are approximately 1/3 the magnitude of the main electrochromic shift. Any one (or a combination of these and possibly red shifts) could contribute to the observed 676 nm blue shift that is approximately 25 – 40% the magnitude of the main shift.

The origin of the 676 nm feature cannot be definitively proved by simulations at the current time since the peak positions of individual chromophores in higher plant PSII is not known.

Dielectric constant

There is no data available on the effective field strength in plant or cyanobacterial PSII. A Stark study of bacterial reaction centres showed that it can vary considerably within the reaction centre depending on the side of reaction centre and the pigment.[22] For example, in bacterial reaction centres, which formed the $P^+Q_A^-$ state, the (functional) L branch[§] ε_{eff} was found to be 3.3 – 5.9 and 2.5 – 5.1 at the BPheo and BChl pigments respectively, where the range reflects the uncertainty in the calculations. The equivalent ε_{eff} ranges on the M (non-functional) branch were 0.9 – 1.7 and 0.7 – 1.8. This dielectric asymmetry was thought to arise from small contributions from several amino acids in the reaction centre.

[§] The L and M proteins in photosynthetic bacteria are analogous to the D1 and D2 proteins in PSII respectively.

The overall peak-to-peak magnitude produced by Simulation 4 (ε_{eff} = 5) was more consistent with experimental data than Simulation 3 (ε_{eff} = 1) indicating that the ε_{eff} in PEMs is more likely to be closer to a value of 5 rather than 1. There is the possibility, however, that ε_{eff} is highly dependent on location within the protein complex, as is the case for bacterial reaction centres.

Comparison with previous interpretations

In the Section 6.1.1 three studies were summarised in which the authors produced Q_A^- by illumination. Each group observed a blue shift at about 680 nm but interpreted their result differently. The Junge group assigned the shift to three chlorophylls species (P_{D1}, P_{D2} and Chl_{D1}) and $Pheo_{D1}$.[11] The Diner group assigned it to the two pheophytins and two chlorophylls.[12] Both groups used data from experiments done on photosynthetic bacteria as a starting point for making their assignments. The structure of photosynthetic bacteria was the best available model at the time since the crystal structure of an oxygen evolving PSII (from cyanobacteria) was not solved and published until 2001.[3] The Diner group utilised mutants in which the amino acids near P_{D1} and $Pheo_{D1}$ were changed. They concluded that four pigments must shift based on analogy to the bacterial photosystem, the changes in the spectra of the mutant PSII and the fact that a 4-band shift best fit their data.

The Krausz group first assumed that the shift corresponded to only one pigment and concluded it was therefore due to $Pheo_{D1}$, the closest pigment to Q_A^-.[13] Unconventional $\Delta\mu$ directions were proposed for $Pheo_{D1}$ to explain the observed blue shift, rather than the red shift expected.

The advantage of the methodology here was that there were, as far as possible, no constraining assumptions made before modelling. There were assumptions made over several iterations however to ensure the data was reproduced. The modelling was of

course not definitive considering that many variables were not precisely known for the system being studied. Nevertheless, assuming all the parameters were reasonable estimates, then the key result is likely to be valid. Namely, all the chlorophyll and pheophytin pigments in plant PSII undergo electrochromic shifting due to Q_A^- resulting in an overall blue shift centred at about 685 nm.

In a recent study Cox et al.[32] have been able to advance our understanding of the illumination-induced difference spectrum of PSII. Their calculations were based on simultaneously fitting absorption difference spectra where $Pheo_{D1}$ had been reduced and circular dichroism difference spectra. Multiple data sets were obtained from different PSII containing species and they included coupling between pigments based on a recent estimate published by Raszewski et al.[33] Their simulation of the Q_A^- - Q_A spectrum in spinach was in good agreement. The 676 nm feature was modelled more accurately than in this work and in agreement with this work it arises from the electrochromic shift of pigments in the PSII reaction centre due to Q_A^-.

6.7 Appendix

6.7.1 General Equation for Electrochromic Shifts

For an isolated absorption band in a non-orientated, immobilised sample when $\Delta\nu$ (the electrochromic shift) is smaller than the inhomogeneous line width, the change in absorption as a function of frequency $\Delta A(\nu)$ upon application of an electric field **F** is given by[34]:

$$\Delta A(\nu) = (f\mathbf{F})^2\{A_\chi A(\nu) + (B_\chi \nu/15hc)d[A(\nu)/\nu]d\nu + (C_\chi \nu/30h^2c^2)d^2[A(\nu)/\nu]d\nu^2\}$$

Equation 6.9

where

f is the local field correction,

A_χ depends on the transition polarisability and hyperpolarisability,

$B_\chi = \frac{1}{2}\{5Tr(\boldsymbol{\Delta\alpha}) + (3\cos^2\chi - 1)[3\,(\mathbf{p}.\boldsymbol{\Delta\alpha}.\mathbf{p}) - Tr(\boldsymbol{\Delta\alpha})]\}$,

$C_\chi = |\boldsymbol{\Delta\mu}|^2[5 + 3(\cos^2\zeta - 1)\,(3\cos^2\chi - 1)]$.

ζ is the molecular angle between $\boldsymbol{\Delta\mu}$ and transition moment **p,** and χ is the experimental angle between **F** and the electric vector of the linearly polarised light used to probe ΔA.

It has been found that a second derivate lineshape dominates the Stark effect for the Q_y absorption bands in wild-type PSII reaction centres.[22] In terms of Equation 6.9 this means that the electrochromic shift of Q_y absorption bands is dominated by the third term which means ΔA is mainly dependent on $\boldsymbol{\Delta\mu}$.

6.7.2 Summary of Experimental Parameters

PEM batch	*OD*	*Cell pathlength /μm*	*Cryoprotectant (% glycerol)*	*Spectrometer*	*ΔA/A (%)*
1	1.67	190	37%	CCD	2.59
2	1.15	190	40%	CCD	2.97
1	1.14	200 (flat cell)	40%	CCD	2.74
3	~1.83	190	40%	CCD	2.73
2	1.0	225	37%	MCD	~2.4
1 (washed)	~0.85	200	30%	MCD	2.78

Table 6.10 Experimental parameters for samples in Table 6.3.

6.8 References

[1] D. B. Knaff, D. I. Arnon, *Proceedings of the National Academy of Sciences of the United States of America* **1969**, 63, 963.

[2] H. J. van Gorkom, *Biochimica et Biophysica Acta* **1974**, *347*, 439.

[3] A. Zouni, H. T. Witt, J. Kern, P. Fromme, N. Krauss, W. Saenger, P. Orth, *Nature* **2001**, *409*, 739.

[4] N. Kamiya, J.-R. Shen, *Proceedings of the National Academy of Sciences of the United States of America* **2003**, 100, 98.

[5] J. Biesiadka, B. Loll, J. Kern, K.-D. Irrgang, A. Zouni, *Physical Chemistry Chemical Physics* **2004**, *6*, 4733.

[6] K. N. Ferreira, T. M. Iverson, K. Maghlaoui, J. Barber, S. Iwata, *Science* **2004**, *303*, 1831.

[7] B. Loll, J. Kern, W. Saenger, A. Zouni, J. Biesiadka, *Nature* **2005**, *438*, 1040.

[8] M. Gouterman, *Journal of Molecular Spectroscopy* **1961**, 6, 138.

[9] W. L. Butler, *Accounts of Chemical Research* **1973**, 6, 177.

[10] P. J. Smith, S. Peterson, V. M. Masters, T. Wydrzynski, S. Styring, E. Krausz, R. J. Pace, *Biochemistry* **2002**, *41*, 1981.

[11] A. Y. Mulkidjanian, D. A. Cherepanov, M. Haumann, W. Junge, *Biochemistry* **1996**, *35*, 3093.

[12] D. H. Stewart, P. J. Nixon, B. A. Diner, G. W. Brudvig, *Biochemistry* **2000**, *39*, 14583.

[13] S. P. Årsköld, V. M. Masters, B. J. Prince, P. J. Smith, R. J. Pace, E. Krausz, *Journal of the American Chemical Society* **2003**, *125*, 13063.

[14] T. J. Wydrzynski, K. Satoh, (Eds) in *Photosystem II The Light-Driven Water:Plastoquinone Oxidoreductase,* Springer, Dordrecht, **2005**.

[15] L. K. Thompson, G. W. Brudvig, *Biochemistry* **1988**, *27*, 6653.

[16] N. Cox, F. M. Ho, N. Pewnim, R. Steffen, P. J. Smith, K. G. V. Havelius, J. L. Hughes, L. Debono, S. Styring, E. Krausz, R. J. Pace, *Biochimica et Biophysica Acta - Bioenergetics* **2009**, *1787*, 882.

[17] P. Faller, R. J. Debus, K. Brette, M. Sugiura, A. W. Rutherford, A. Boussac, *Proceedings of the National Acadamy of Science of the United States of America* **2001**, *98*, 14368.

[18] H. J. van Gorkom, J. J. Tamminga, J. Haveman, *Biochimica et Biophysica Acta* **1974**, *347*, 417.

[19] W. Liptay, *Angewandte Chemie International Edition* **1969**, 8, 177.

[20] T. Kakitani, B. Honig, A. R. Crofts, *Biophysical Journal* **1982**, *39*, 57.

[21] N. Dashdorj, W. Xu, P. Martinsson, P. R. Chitnis, S. Savikhin, *Biophysical Journal* **2004**, *86*, 3121.

[22] M. A. Steffen, K. Lao, S. G. Boxer, *Science* **1994**, *264*, 810.

[23] S. Krawczyk, *Biochimica et Biophysica Acta* **1991**, 1056, 64.

[24] R. N. Frese, M. Germano, F. L. d. Weerd, I. H. M. v. Stokkum, A. Y. Shkuropatov, V. A. Shuvalov, H. J. v. Gorkom, R. v. Grondelle, J. P. Dekker, *Biochemistry* **2003**, *42*, 9205.

[25] H. Scheer (Ed), *Chlorophylls* CRC Press, Boca Raton, **1991**.

[26] M. A. M. J. V. Zandvoort, D. Wrobel, P. Lettinga, G. V. Ginkel, Y. K. Levine, *Photochemistry and Photobiology* **1995**, *62*, 299.

[27] S. R. Greenfield, M. Seibert, M. R. Wasielewski, *Journal of Physical Chemistry B* **1999**, *103*, 8364.

[28] L. K. Hanson, J. Fajer, M. A. Thompson, M. C. Zerner, *Journal of the American Chemical Society* **1987**, *109*, 4728.

[29] L. K. Hanson, M. A. Thompson, M. C. Zerner, J. Fajer, in *NATO Advanced Research Workshop on the Structure of the Photosynthetic Bacterial Reaction Center* (Eds.: J. Breton, A. Vermeglio), Plenum Press, New York, **1987**, pp. 355.

[30] J. Fajer, L. K. Hanson, M. C. Zerner, M. A. Thompson, in *The Photosynthetic Bacterial Reaction Center II: Structure, Spectroscopy and Dynamics* (Eds.: J. Breton, A. Vermeglio), Plenum Press, New York, **1992**, pp. 33.

[31] R. B. Altmann, D. Haarer, I. Renge, *Chemical Physics Letters* **1993**, *216*, 281.

[32] N. Cox, J. Hughes, R. Steffen, P. Smith, A. Rutherford, R. Pace, E. Krausz, *Journal of Physical Chemistry* **2009**, *Submitted.*

[33] G. Raszewski, B. A. Diner, E. Schlodder, T. Renger, *Biophysical Journal* **2008**, *95*, 105.

[34] J. Amesz, A. J. Hoff, in *Advances in Photosynthesis* (Ed.: Govindjee), Kluwer Academic Publishers, **1996**.

7 The Transient High-Light Difference Spectrum

7.1 Introduction

It was found that when PEM samples were exposed to certain illumination conditions at cryogenic temperatures, a novel illumination-induced difference absorption spectrum was produced. This spectrum was labelled the 'transient high-light difference-spectrum' (THDS). Dr Ronald Steffen first discovered the spectrum in PSII spinach core samples that he analysed with the CCD spectrometer.

The THDS was hypothesised as being due to the formation of the P_{680}^{+} / Q_A^{-} state because it was consistent with studies in the literature. The plausibility of the proposed assignment was tested using a mathematical model in which the kinetics of illumination induced electron transfer in PSII reaction centre were simulated. The model predicted the concentration of reaction centre electronic-states due to different illumination conditions and these results were compared with experimental data.

7.2 Experimental Results

The standard procedures followed when carrying out measurements on the CCD spectrometer are outlined in Chapter 3.

7.2.1 The Transient High-Light Difference-Spectrum

The simplest experiment in which THDS was observed was as follows. A PEM sample was loaded into the CCD spectrometer and under cryogenic temperatures (~5 K) exposed to a 100 ms low-intensity white light (LL) flash, left in the dark for 6 s and then exposed to another 100 ms high-intensity white light (HL) flash. The illumination and dark times were the shortest durations that could be used at the time due to the technical limits of the CCD spectrometer. The 6 s dark time was required for data transfer from the

CCD detector to the computer. It has been shown in subsequent experiments that the transient signal can be produced with a dark time of less than 6 s.

Subtraction of the LL from the HL transmission spectrum typically produced a difference spectrum (the THDS) similar to the red trace shown in Figure 7.1. The blue trace in Figure 7.1, in comparison, is the typical difference spectrum that was observed in 5 min illuminations carried out in the MCD spectrometer with the 'green light lamp' and using single-flash or continuous-LL illumination in the CCD spectrometer. This difference spectrum has been discussed and analysed in Chapter 6.

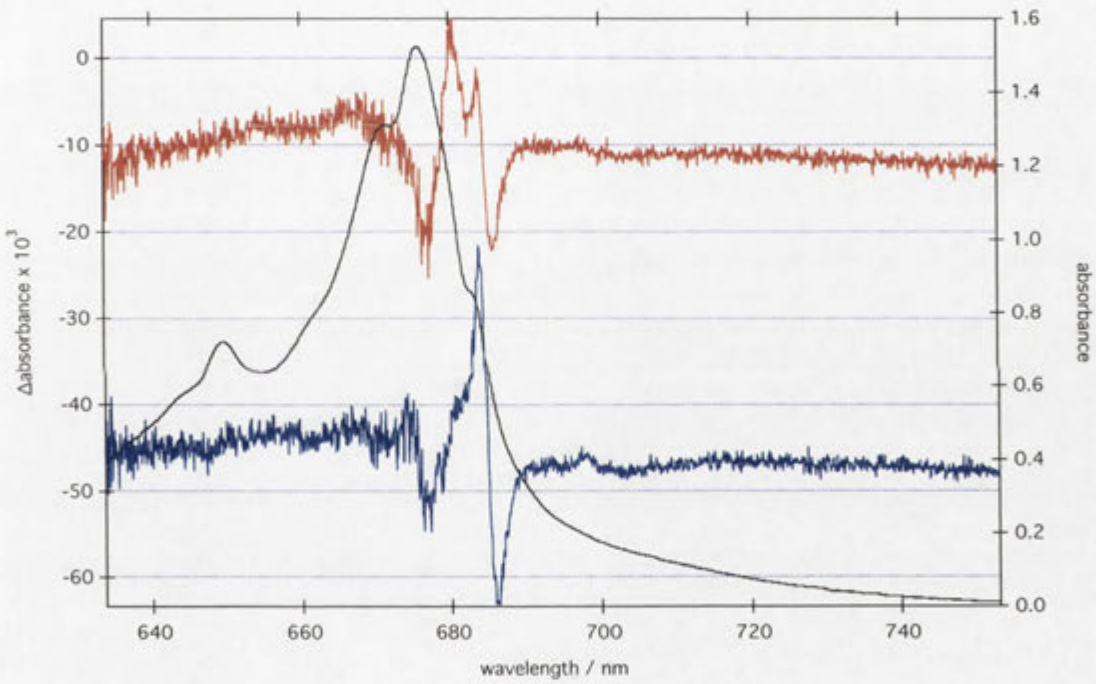

Figure 7.1 Transient High-Light Difference Spectrum (red trace) compared with a typical stable Illumination Induced Difference Spectrum (blue trace).

Experimental Details: PEM sample was dark adapted at room temperature for 10 min, cooled to ~5 K for 10 min in the CCD spectrometer. Illumination regime: 100ms LL flash, 6.3 s dark time, 100 ms HL flash. Sample was illuminated with continuous HL for 6.3 s and a second HL flash was taken. HL flash minus LL flash (red trace). Second HL flash minus LL flash (blue trace).

The THDS had a feature consistent with the first-differential of a Gaussian with a positive peak at ~680 nm with a negative partner at ~677 nm. The differential feature will be referred to as the '680 nm feature' from this point. The 680 nm feature is seen in conjunction with the electrochromic shift of PSII reaction centre pigment due to Q_A^- centred at ~685 nm.

7.2.2 Alternating Low-Light and High-Light Flashes

An experiment was carried out flashing a PEM sample with alternating 100 ms LL and HL flashes every 6.3 s for ~300 s. Selected difference spectra from the experiment are shown in Figure 7.2, where all spectra had the first LL flash subtracted. The red traces correspond to the LL flashes (LL flash 3,5,7 and 46* are shown) and the blue traces correspond to the HL flashes (HL flash 2,4,6,8 and 47 are shown).

* This is not an odd number due to an accidental double LL flash.

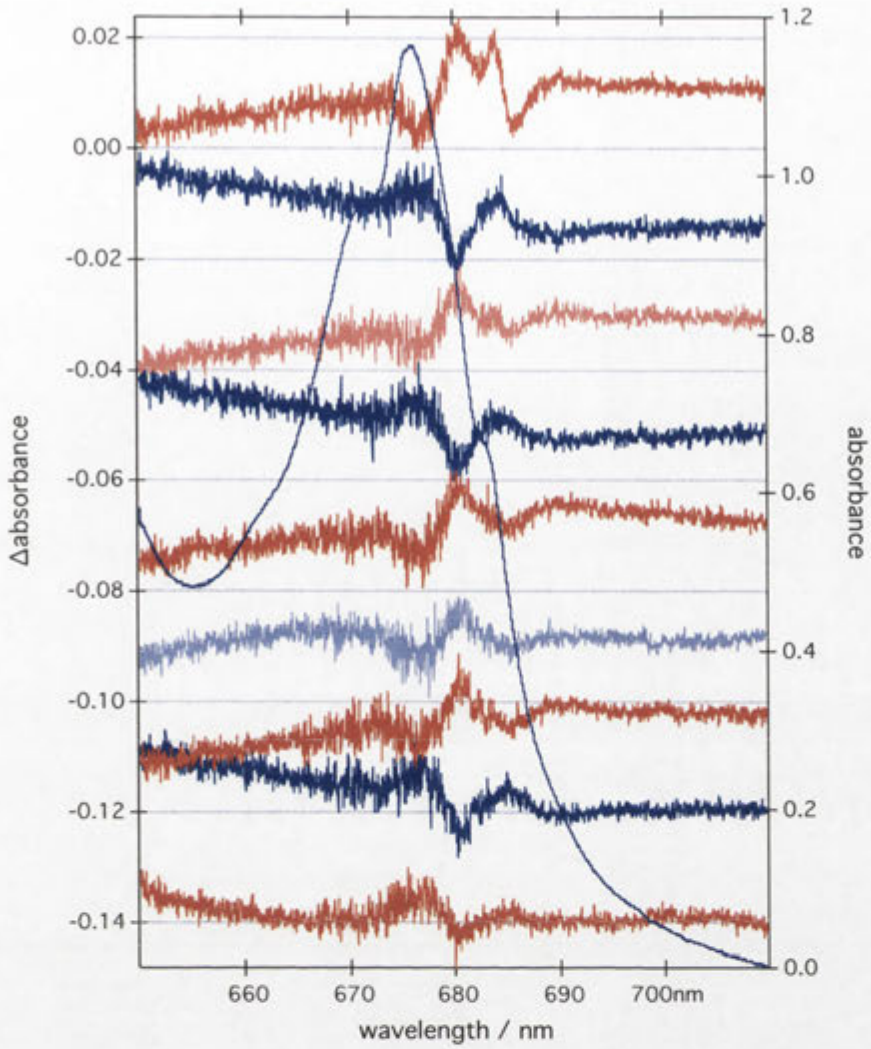

Figure 7.2 A PEM sample exposed to alternate LL and HL 100 ms white-light flashes with 6.3 s dark time between each flash. Black traces: Absorption spectrum. Red traces: LL flash spectra subtracted from the first LL flash. (Flashes 3,5,7 and 46 are shown from top to bottom). Blue traces: HL flash spectra subtracted from the first LL flash. (Flashes 2,4,6,8 and 47 are shown from top to bottom). Difference spectra have been offset for clarity.

In Figure 7.3, data from the difference absorption spectra shown in Figure 7.2 are plotted with respect to time. The black trace is the δΔA (change in absorption difference) between 684.0 nm and 686.6 nm (that is, the peak-to-peak absorption difference of the electrochromic blue-shift due to Q_A^-). The blue and red points are the δΔA corresponding to the difference in ΔA between 680.3 nm and 650.69 nm (that is, the peak-to-peak

absorption difference of the 680 nm feature). The blue and red traces correspond to HL and LL flashes respectively. All the 680 nm data was averaged from 10 points about the wavelengths indicated to minimise the effect of noise.

The electrochromic shift due to Q_A^- increased over time, reaching a steady-state level after ~16 flashes (~100 s elapsed time). With respect to the first LL flash, the 680 nm feature forms with a HL flash, is absent in the next LL flash, but recovers to approximately the same level in the next HL flash and so on, over the entire course of the experiment. The LL and HL flash differences both fluctuate about their respective means (represented as dotted lines in the figure) over the entire duration of the experiment. The magnitude of the fluctuations is consistent with the level of noise in the difference spectra. Since the 680 nm feature is absent from the LL flashes, this indicates that it completely decays within 6.3 s in the dark.

7.2.3 Effect of Low-Light illumination Before a HL Flash

To investigate the relationship between the THDS and the stable secondary donor difference-spectrum (for example. Figure 7.1, blue trace) PEM samples were exposed to different durations of continuous LL before a 100 ms HL flash (see Figure 7.4). When the PEM sample was exposed to continuous LL illumination (~8 s (blue trace) or ~630 s (red trace)), a subsequent HL flash did not produce the 680 nm transient. A shorter continuous LL illumination (~1 s, green trace), did not prevent the 680 nm transient feature forming after subsequent HL illumination.

When PEM samples were subject to continuous HL illumination the 680 nm feature decayed within 6.3 s. For example, in the experiment shown in Figure 7.1 there was a LL flash, 6.3 s dark time, a HL flash (680 nm feature is seen, red trace) and the

continuous HL is left on. In the next spectrum (after 6.3 s of continuous HL, blue trace) there is no 680 nm feature.

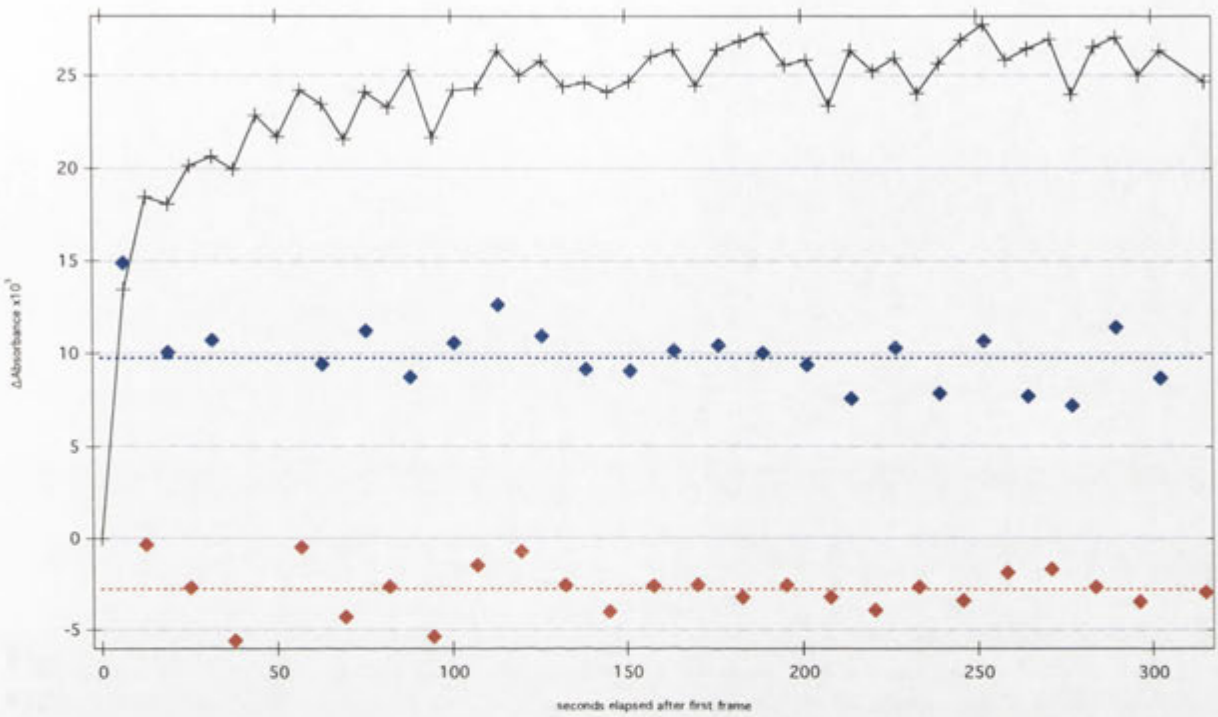

Figure 7.3 Kinetic traces from experiment shown in Figure 7.2. Black trace: difference between 684.0 and 685.6 nm in difference spectra. Blue diamonds: difference between 680.3 and 650.7 nm in difference spectra (HL). (Average of 10 points about the wavelength indicated). Red diamonds as for blue but LL flashes. Dotted lines are average absorbance differences for LL and HL data.

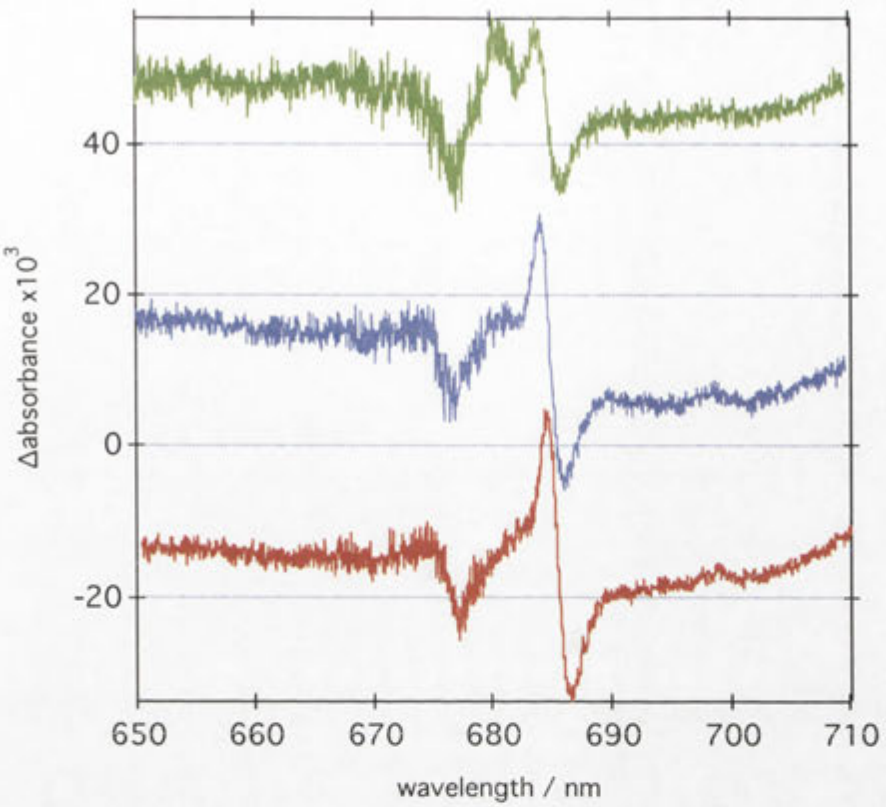

Figure 7.4 Illumination induced difference spectra from three PEM samples exposed to different durations of continuous LL illumination before a HL flash. All spectra are the HL flash minus the first LL flash. Green trace: LL flash, 6.3 s dark, 1.1 s continuous LL, 5.2 s dark, HL flash. Blue trace: LL flash, 8-9s continuous LL, 3-4s continuous HL. Red trace: 100 continuous LL, 1 HL flash.

The 680 nm feature could not have been observed with the MCD spectrometer, because if it was formed, it would have decayed within the timescales of those experiments (with data collection times of about 5 to 10 min).

7.3 Kinetic modelling

The plausibility of the assignment of the 680 nm transient feature was investigated by comparison to a mathematical model, which simulated the kinetics of charge transfer in PSII reaction centres.

The model consisted of a set of differential equations describing the formation and decay of the electronic states in PSII, based on the experiments in Section 7.2. Kinetic

data obtained from the literature was used to assign rate constant values in the model. The equations were then solved numerically with a computer program (Scicos – a block diagram simulator/modeler) under various simulated illumination conditions and compared with experimental data.

The model consisted of three electronic states labelled A, B and C. State A was the dark state where Q_A, P_{680} and the secondary donor (D) were uncharged. The secondary donor may have been cyt b_{559}, carotenoid or another donor, depending on the specific sample. No distinction was made between the donors in this model. State B was the primary charge separated state and state C represented the secondary charge separated state where the positive charge has migrated from P680 to a secondary donor. In summary:

state A = $Q_A/P_{680}/D$,

state B = $Q_A^-/P_{680}^+/D$ and;

state C = $Q_A^-/P_{680}/D^+$

The experiments in Section 7.2 established the following: i) State B is a transient species that can only be formed under sufficiently high light intensity conditions. (see experiment in Figure 7.2) and ii) State C is stable over the time scale of the experiment (refer to experiment in Figure 7.4). The model outlined below is consistent with these experimental observations.

When the sample is illuminated, state A is converted into state B representing the charge separated state Q_A/P_{680}^+. This charge separation process occurs on a picoseconds timescale and hence the formation of B is rate limited by the number of photons absorbed per time unit. When the system is in state B it can either reform state A or the charge separated state C. In other words when P_{680}^+ forms it can either oxidise Q_A or a secondary

donor. It is has been observed that a component of 685 nm electrochromic shift feature (the experimental measure of state C) decays with a half-life on the minutes timescale after the cessation of illumination. Since the decay is insignificant on the timescale of the experiments (milliseconds) it was ignored and state C was assumed to be stable.

The relationship between the states is given by a set of differential equations specifying the rate of formation and decay of the three states.

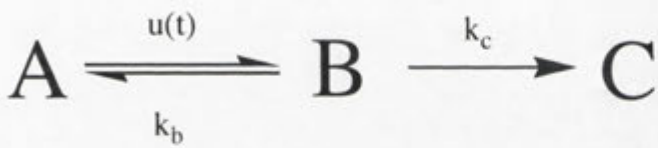

Figure 7.5 Schematic of the PSII reaction centre electron transfer kinetic model. State A = $Q_A/P_{680}/D$, State B = $Q_A^-/P_{680}^+/D$ and State C = $Q_A^-/P_{680}/D^+$.

The rate of formation of A is proportional to the concentration of B and decreased proportionally to the concentration of A and the light intensity. Mathematically this is expressed as:

$$d[A]/dt = -u(t)[A] + k_b[B]$$

The rate of formation of B is proportional to the concentration of A and light intensity and decreased proportionally to the concentration of B present. Mathematically:

$$d[B]/dt = u(t)[A] - k_b[B] - k_c[B]$$

The rate of formation of C depends only on the concentration of B present. Mathematically:

$$d[C]/dt = k_c[B]$$

The function u(t) converts state A to B when a PSII reaction centre absorbs a photon. In the experiments simulated here, light intensity is constant over time so u(t) is simply a constant. This number corresponds to the number of photons absorbed per

reaction centre per ms (since the rate constants are in ms) that give rise to the charge separated state P_{680}^{+}/Q_A^{-}.

The rate constants in the model were obtained from the literature. The recombination of P_{680}^{+}/Q_A^{-} (that is, the decay of state B to A in this model) in PSII enriched membranes from spinach at 20 K was found to occur with a half-life of 3 ms[1], so $k_b = 0.231\ ms^{-1}$.†

The secondary donor is known to reduce P_{680}^{+} with a half-life of 20 ms[2] (calculated taking into account the average half life donations from Car and Cyt b_{559} of 25 ms and 15 ms respectively) which is the observed rate constant associated with the formation of D^{+}. The internal half life, (formation of state C from state B) was set so that formation of D^{+} had a half-life of 20 ms. The half life was therefore 10 ms and hence the value of k_c was set to $0.0693\ ms^{-1}$.

7.3.1 Estimate of Photons incident on the sample

The kinetic model of illumination induced charge transfer in PSII reaction centres requires an estimation of the number of photons per unit time absorbed by the sample that induce primary charge separation (that is, convert state A into state B). This rate is simply the value of the function u(t).

The power of the lamp image that would normally be focussed on the sample in a HL experiment was measured with a power meter by Ronald Steffen. The power was measured as a function of slit width and showed a linear relationship between lamp power and slit width (see Figure 7.6). This graph gave the total power that would be incident at the sample neglecting losses due to the quartz flow tube and sample cell surfaces.

† Since $t_{1/2} = \ln 2 / k$

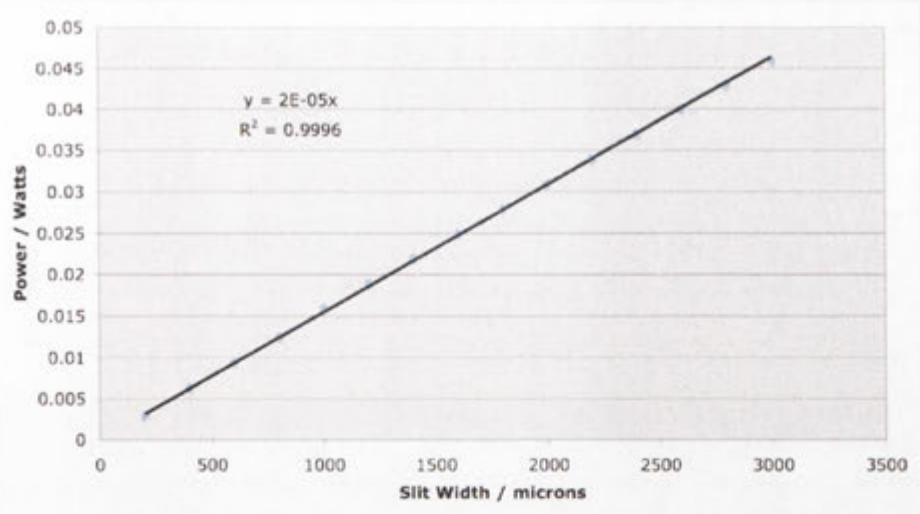

Figure 7.6 Power vs Lamp Slit of the CCD Spectrometer

For the purposes of the model, the total power was corrected to account for the proportion of total incident photons that were absorbed by a PSII reaction centre (and hence induced primary charge-separation).

The proportion of absorbed photons was calculated by multiplying the lamp spectrum (normalised to a total area of 1) by a typical PEM absorption curve that had been converted to a 1-Transmission (1-T) curve (see Figure 7.7). The area under the product of these two curves represents the proportion of lamp intensity (photons) that were absorbed by the sample.

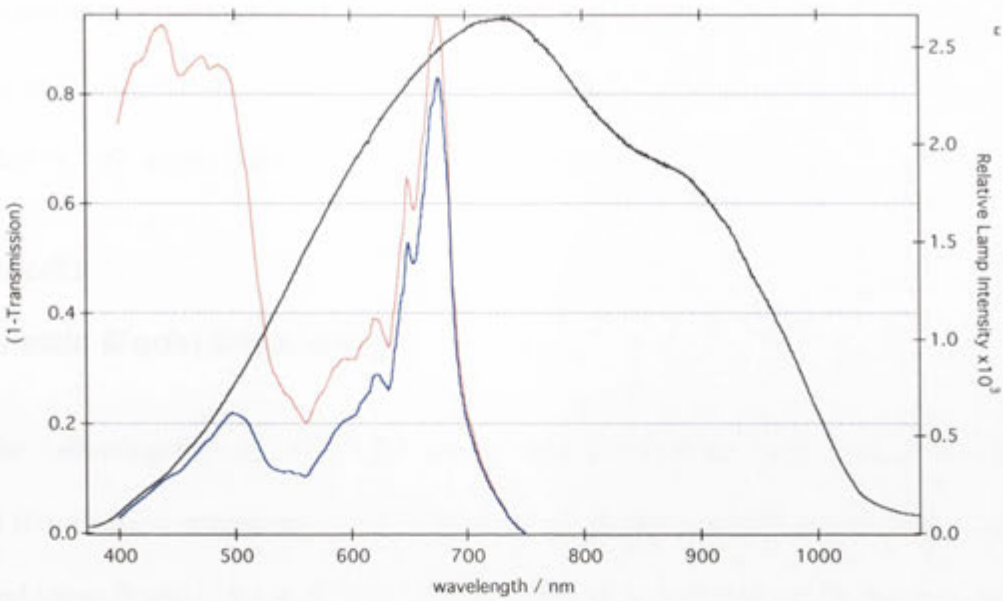

Figure 7.7 Spectra used to estimate the number of photons absorbed by a PEM sample. Black trace: CCD lamp spectrum (normalised to a total area of 1), Red trace: (1-Transmission curve) spectrum of a PEM and Blue trace: Black × Red traces.

The power was converted to the number of photons by first assuming all photons were of the same energy. From the (1-T) x lamp spectrum graph, each photon wavelength had an associated intensity. The weighted average wavelength was calculated as follows: $\lambda = \sum(\text{wavelength} \times \text{intensity}) / \sum(\text{intensities})$. This wavelength was calculated to be 607.085 nm. The number of photons was calculated by dividing the total energy absorbed by the energy of a 607.085 nm photon.

The concentration of RCs was calculated from the maximum OD in Q_y, the extinction coefficient calculated previously in our group for PEMs[3] and the pathlength of the cell. The number of RCs illuminated was estimated from the volume of the cell that was illuminated.

Finally, the number of photons absorbed (and therefore that induced charge separation) per RC, per unit time was calculated. This number reflected the number of

photons absorbed in the high-light illumination configuration which had no attenuating filter between the light source and sample. For the low-light illumination case, the number was divided by 100, as the light was attenuated by an OD 2 neutral-density filter.

7.4 Results

7.4.1 Kinetic Model Simulations

The following figures show the results from running the model under different simulated illumination conditions. The initial state of all the simulations was with state A set to 1 and states B and C set to 0, representing 100% of centres initially in the dark state. The sum of the three states was normalised, that is, always summed to 1.

The first two figures (Figure 7.8 and Figure 7.9) show the relative concentration of states over a period of 100 ms. To compare this data with the CCD experiment, which collects and integrates all photons over 100 ms, the areas under the curves were calculated and tabulated.

Figure 7.10 shows the result of simulating a 5 minute continuous LL illumination with the RC model.

7.4.2 100ms illumination simulation (LL)

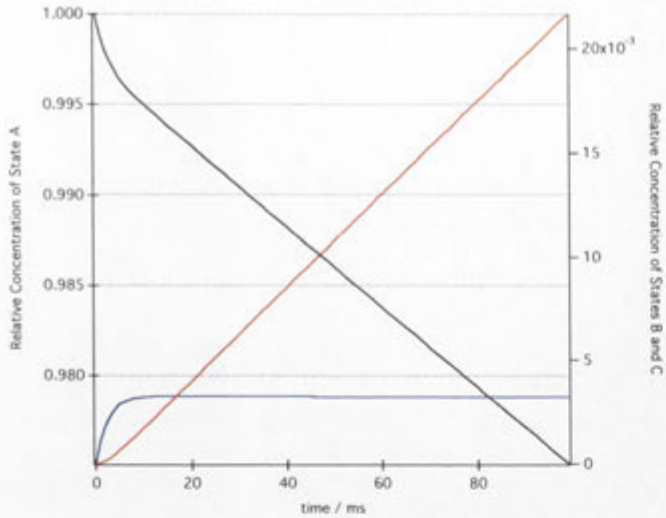

Figure 7.8 Simulation of a 100 ms low-light flash. (u(t) = 0.001 absorbed photons/reaction centre/ms, $k_b = 0.231ms^{-1}$, $k_c = 0.0693ms^{-1}$)

Relative concentrations of State A (black), State B (blue), State C (red).

7.4.3 100ms illumination simulation (HL)

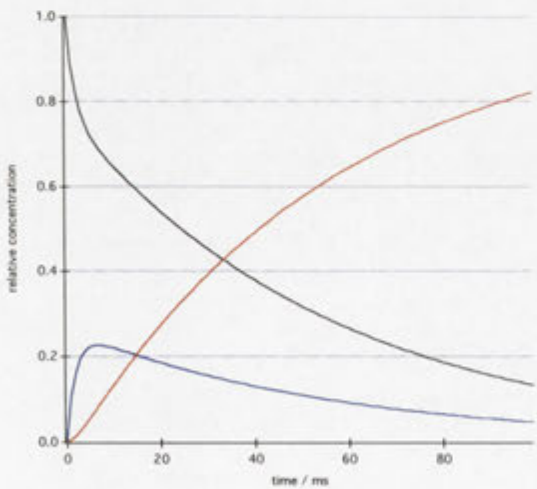

Figure 7.9 Simulation of a 100 ms HL flash. u(t) = 0.1 absorbed photons/reaction centre/ms. Other parameters and traces as for Figure 7.8.

7.4.4 5 minute LL illumination

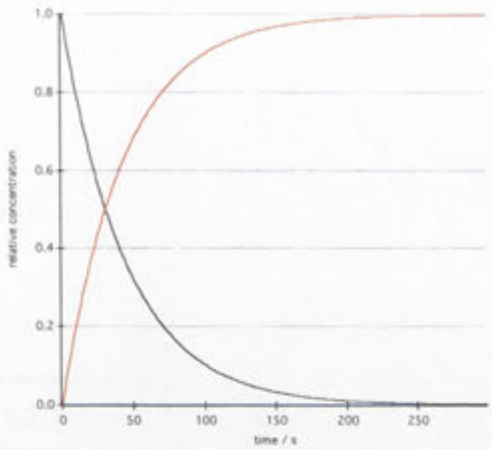

Figure 7.10 Simulation of continuous 5 min LL illumination. Parameters and traces as for Figure 7.8.

After 5 minutes of continuous LL illumination, state C (Q_A^- / D^+) reaches its maximum level.

In Table 7.1, data from several 'low intensity' and 'high intensity' light illumination-induced experiments are listed, with one experiment per row. For each experiment the number of photons absorbed that gave rise to Q_A^- formation (that is, the function u(t)) was estimated according to the method outlined in Section 7.3.1. The estimated u(t) value was entered into the kinetic model outlined in Section 7.3 to estimate the relative amounts of State A, B and C formed in each experiment over the 100 ms duration of the illuminations. An estimate of the amount of state C formed in each experiment (obtained from the difference spectra) was included for comparison.

Illumination type	*Photons/RC/ ms (u(t))*[§]	*Calculated % Q_A^- D^+ (C)*[†]	*Experimental % Q_A^- D^+ #*	*Calculated % Q_A P (A)*[†]	*Calculated % Q_A^- P^+ (B)*[†]
100 ms LL	0.00132	1.41	<6.28‡	98.2	0.418
	0.00365	3.81	6.28	95.1	1.12
	0.00435	4.51	5.40	94.2	1.32
	0.00511	5.25	5.86	93.2	1.54
100 ms HL	0.380	74.6	55	11.3	14.1
	0.308	72.2	50	13.8	14.0
	0.281	71.0	48	15.1	14.0
	0.281	71.0	50	15.0	14.0
	0.522	77.5	47	8.27	14.2

Table 7.1 Experimental and simulated data for several PEM illumination experiments on the CCD spectrometer. [†]Area under curve over 100 ms. [§]Calculated for each sample according to the method in Section 7.3. (using a typical PEM aborption curve scaled to the relevant OD in Q_y for calculation of (1-T)*Lamp spectrum). Constants used in model: $k_b = 0.231\ ms^{-1}$, $k_c = 0.0693\ ms^{-1}$. ‡Below the detection limit of the experiment. #Calculated by measuring the peak-to-peak height of the 685 nm blue shift in the difference spectrum divided by the OD the sample (max absorbance– 750 nm absorbance). Divided by the ratio obtained from several samples illuminated for 5 min. (avg max ratio=2.9%)

In the illumination experiments conducted, the kinetic model predicted ~1.4 – 5.3 % of PSII centres would form the secondary charge separated state Q_A^- / D^+ after 100 ms of LL illumination. This was comparable with the estimated 5.4 – 6.3% Q_A^- formation estimated from spectra in the experiments. After 100 ms of HL illumination, the model predicted ~73% Q_A^- / D^+ formation, which is not consistent with the results observed experimentally (47 - 55%).

In agreement with experiment, in the 5 min LL simulation the amount of State B (Q_A^- / P_{680}^+) formed was insignificant as virtually all that formed was converted to state C. It was therefore confirmed that the model is valid over the minutes well as the millisecond timescale.

Further experimental details for each sample can be found in the Appendix.

7.5 Discussion

7.5.1 Assignment of 680nm Transient Feature

The 680 nm transient feature was assigned to the formation of P_{680}^{+} / Q_A^{-} by comparison to the study by Hillmann et al.[1] In this study, PEM fragments from spinach were flashed with 532 nm light from a frequency-doubled Nd:YAG laser at 20 K. Before cooling, cyt b_{559} was preoxidised with $K_3[Fe(CN)_3]$ to prevent the oxidation of the heme during illumination.

They reported that at temperatures less than 200 K, P_{680}^{+} / Q_A^{-} decays mainly by charge recombination with half-life of about 3 ms. (This was consistent with results of previous studies in the literature). Hence, to construct an absorbance difference spectrum due to P_{680}^{+} / Q_A^{-}, in a saturating laser flash experiment they plotted the amplitudes of the 3 ms phase at wavelengths from 665 to 695 nm. The resulting spectrum (see Figure 7.11, black trace) was interpreted as the sum of a bleaching band at 685 nm (due to the bleach of P_{680} in forming P_{680}^{+}) and an electrochromic red-shift centred at 680 nm. Interestingly, the decay kinetics of the P_{680}^{+} / Q_A^{-} and the $P_{680}^{+}Q_A^{-}/P_{680}Q_A$ difference spectra were, according to the authors of the paper[1], "virtually identical in the PEM fragments as the PSII core complexes from Synechoccus".

In Figure 7.11 a typical THDS from this work was overlayed on top of the $P_{680}^{+}Q_A^{-}/P_{680}Q_A$ difference spectrum from the Hillmann paper. The spectra were normalised to the peak-to-peak height of the 680 nm feature and align almost exactly. The electrochromic shift centred at 685 nm, arising from the charge on Q_A^{-}, however, is not present in the Hillmann data. This was because in their experiment, $P_{680}^{+}Q_A^{-}$ was formed exclusively (cyt b_{559} was preoxidised), whereas in this work some of the centres formed the state $P_{680}^{+}/Q_A^{-}/D^{+}$ where a secondary donor was oxidised during the 100 ms flash (the majority of centres having cyt b_{559} as the secondary donor). It is therefore reasonable to

expect the electrochromic shift pattern due to Q_A^- perturbing nearby pigments would be affected by the presence of P_{680}^+ and hence the spectra at ~685 nm to be different to the $Q_A^-/P_{680}/D^+$ spectrum.

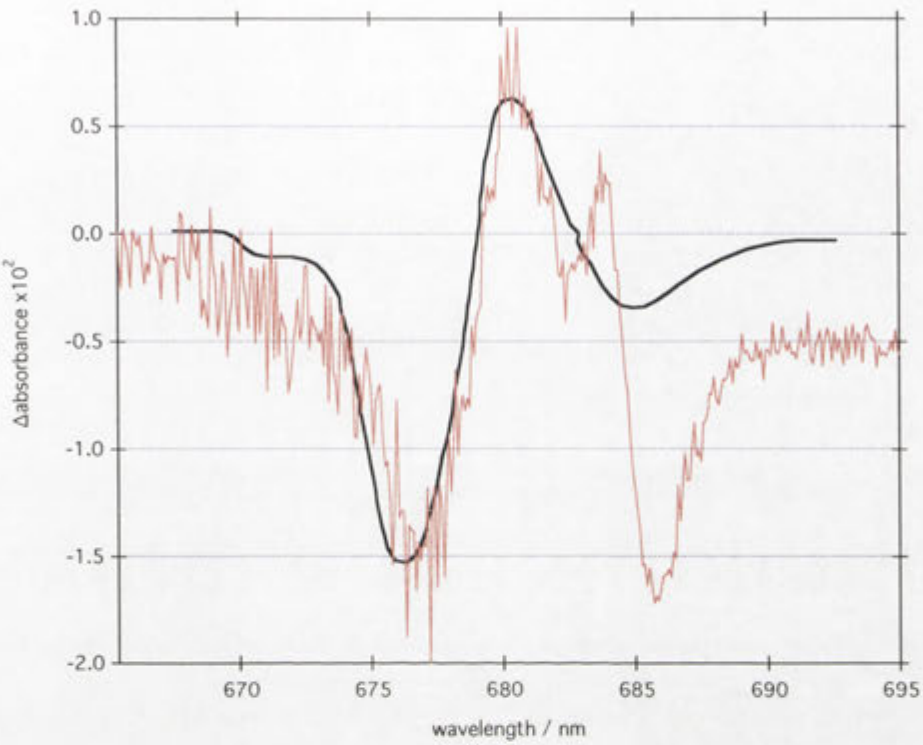

Figure 7.11 Comparison of the THDS feature (red trace) with a literature spectrum of Q_A^-/P_{680}^+ in PEM samples from spinach at 20 K [1] (black trace). See Section 7.5.1 for details of the literature experiment.

7.5.2 Comparison of the Kinetic Model with Experiments

The kinetic model predicted the relative amounts of the three electronic states in PSII reaction centres. The calculated concentrations of interest were states B and C, however, only state C could be estimated from the spectra produced by the experiments. The maximum amount of state C was quantified from several experiments measuring the ratio of the of the 685 nm shift feature peak-to-peak magnitude to the maximum absorbance at 676 nm, assuming zero absorbance at 750 nm. Hence, the validity of the kinetic model was evaluated by comparing the predicted and experimentally determined concentration of state C.

100 ms LL Flash

Considering the various uncertainties in the calculations, the kinetic model estimate for the concentration of D^+ was very good. The agreement was, however, less accurate than the results suggest since the concentrations of state C determined by experiment do not include Q_A^- formation that occurred during the first reference LL flash. That is, the experimental values are an underestimate of the actual amounts of state B and C formed.

100 ms HL Flash

The kinetic model overestimated the formation of D^+ in all HL illumination experiments by about 20 to 30%. Assuming that the basic assumptions of the model are correct, the discrepancy suggests that k_c and/or u(t) may be overestimated and/or k_b is underestimated. The calculations for LL illumination suggested that u(t), k_b and k_c were over- or underestimated in the opposite direction compared with the calculations for the HL illuminations. This result would suggest that at least two of the parameters have incorrect values or that the model is too simple to describe the electron transfer in PSII reaction centres.

The literature value of k_c was based on the assumption of equal donation from carotenoid and cyt b_{559} donors and also the magnitude of k_b. A recent paper has analysed similar PSII preparations to those used in this work with absorbance spectroscopy and EPR.[4] They found that the main electron donors under the conditions of their (and therefore this work's) experiments were cyt b_{559} (~30 50% of centres), an organic donor (possibly amino acid side-chain, ~30% centres) and a tyrosine related species (~15% centres). Chlorophyll and carotenoid electron donation combined accounted for less than 5% of all reaction centres. The k_c value is therefore most likely different from that used in

the kinetic model developed here, depending on the donation rates of the non-cytochrome donors.

The above point highlights the fact that PSII centres are not kinetically identical, with the centres possessing distributions of values for k_c and most likely for k_b and u(t). The variation in u(t) would take in to account, for example, inactive or damaged reaction centres that absorb light which does not lead to charge separation.

Even if all centres had the same secondary electron donor to P_{680}^+, there would still be a distribution of reaction rates for the electron transfer processes in PSII reaction centres. This is because each protein complex can assume a large number of conformations, each with a different energy and therefore each possessing different reaction rates.[5] This variation could be due to different distances between chromophores in different reaction centres, for example. When protein samples are rapidly cooled to cryogenic temperature the range of conformations at room temperature is frozen in place.

To improve the kinetic model developed here, one would need to take into account the heterogeneity of PSII reaction centres, in terms of both the secondary electron donors and the conformational sub-states of its constitute proteins.

7.5.3 The 680 nm feature

Comparing the pooled LL and HL experiment data, the model predicted that ~12 - 34 times more P_{680}^+ should be formed during a HL versus a LL flash. Taking into account this is qualitative data, based on the discussion in Section 7.5.2, this demonstrates it is plausible that P_{680}^+ would only be detectable in a HL rather than a LL flash, as the spectra indicate. The extinction coefficient of the P_{680}^+ spectral feature would need to be known in PEM systems to confirm this.

The differential molar extinction coefficient of the 675 nm bleaching band (that is, the negative component of the 680 nm feature) was quoted as being ~250,000 M^{-1} cm^{-1} under saturating conditions[1] but this was for Synechococcus cores rather than spinach so it is probably not applicable to this work. An extinction coefficient can however be calculated for spinach PEMs from Figure 7.11 and the data provided in the Hillmann paper†. The peak-to-peak absorbance difference was 0.035, l = 1 cm and [Chl] = 14.5 μM. So ε (Chl) = A / l c = 0.035 / 1 × 14.5 × 10^{-6} = 2413.8 $M^{-1}cm^{-1}$ Assuming 192 Chl per RC, ε (P_{680}^{+}) = 12.57 $M^{-1}cm^{-1}$.

Applying this extinction coefficient to the HL spectrum in Figure 7.1 [P_{680}^{+}] = 3.278 × 10^{-6} M = 57% of the total number of RCs. This is not consistent with the model prediction of ~14% of centres expected to form P_{680}^{+}. This could be due to their PEM samples having a different number of Chl per RC (PEM samples are known to vary in this ratio). The more likely possibility is that the difference spectrum is in fact more complicated than the simple analysis of two first-derivative type features.

The calculations in Chapter 6 suggest that the 685 nm electrochromic feature is composed of the shifts of the six chlorophylls and two pheophytins in the PSII reaction centre. An added complexity is that the four central chlorophylls (Chl_{D1}, P_{D1}, P_{D2} and Chl_{D2}) are likely to be electronically coupled due to their close proximity.

Electronic (Förster-Dexter, often called exciton) coupling arises when two or more molecules are close enough to each other so that their electric fields perturb each other. Their transition dipoles interact causing excitations to be delocalised over the group of molecules. The observable result is a splitting in the absorbance bands and shift of intensity depending on distance and geometry of the chromophores.[6]

† The extinction coefficient could be calculated from the Hillmann experiment since they used saturating laser flashes (meaning all PSII centres formed Q_A^-) and therefore the concentration of P_{680}^{+} could be equated to the concentration chlorophyll per PSII.

Formation of P_{680}^{+} would therefore perturb the degree of coupling amongst the chlorophylls and the illumination absorbance difference spectrum would therefore contain changes due to the perturbation in coupling in addition to the electrochromic effects.

7.6 Appendix

7.6.1 Experimental Details for CCD 100 ms Flash Experiments

The Q_A^- formation was estimated from the equation $(\Delta A/OD) / (\Delta A/OD)_{max}$ where ΔA is the peak-to-peak height of the electrochromic shift at ~685 nm due to an illumination OD is the maximum absorbance peak height in the Q_y region at ~676 nm and $(\Delta A/OD)_{max}$ is the average maximum observed $(\Delta A/OD)$ in PEM sample = 2.39% and equated to all PEM reaction centres forming Q_A^-.

PEM Batch	*OD*	*Lamp slit / μm*	*Q_A^- formation (%)*
A	0.53	85	< 6.28
B	1.30	365	6.28
B	1.14	355	5.40
B	0.72	355	5.86

Table 7.2 Experimental details for LL flash experiments.

PEM Batch	*OD*	*Lamp slit / μm*	*Q_A^- formation (%)*
B	1.51	350	55
B	0.78	350	50
B	1.49	320	48
B	1.60	320	50
A	1.32	320	47

Table 7.3 Experimental details for HL flash experiments.

7.6.2 Calculation of Photons Absorbed per Reaction Centre per Unit Time

For each illumination experiment the following parameters were calculated

1. Number of PSII Reaction Centres illuminated

$[RC] = A_{max} / (\varepsilon_{max}.l)$

where
[RC] = concentration of PSII reaction centres
A = optical density at 676 nm (maximum absorbance)
ε = molar extinction coefficient at 676 nm[3]
l = pathlength

V (illuminated volume) = (depth × height × width) illuminated

Number of RCs illuminated = $[RC].V.N_A$

where N_A is Avogadro's number

2. Photons absorbed per unit time

Power at the PSII sample (P) = k_1 × slit width (k_1 is a constant established with a power meter)

Power absorbed by the PSII sample (P_A) = P × k_2 (k_2 is constant established by multiplying (1-Transmission curve) × lamp spectrum)

Power that induced Q_A^- formation (P_T)= P_A× 0.50 (assuming quantum efficiency for Q_A^- formation is distributed equally among RCs with values of 1, 0.5 and 0.01 (unpublished result from Joseph Hughes).

Number of photons absorbed and induced Q_A^- formation per 100 ms = (P_T × 100 ms) / Mean Energy per Photon

3. Mean Energy per Photon

$E_m = hc/\lambda_{avg}$ (mean energy per photon)

where
c = speed of light
h =Planck's constant
λ_{avg} weighted wavelength of a photon
(from the lamp spectrum, $\sum$(wavelength × intensity) / $\sum$(intensities)

7.7 References

[1] B. Hillmann, J. K. Brettel, F. v. Mieghem, A. Kamlowski, A. W. Rutherford, E. Schlodder, *Biochemistry* **1995**, *34*, 4814.

[2] P. Faller, A. Pascal, A. W. Rutherford, *Biochemistry* **2001**, *40*, 6431.

[3] S. P. Årsköld, V. M. Masters, B. J. Prince, P. J. Smith, R. J. Pace, E. Krausz, *Journal of the American Chemical Society* **2003**, *125*, 13063.

[4] N. Cox, F. M. Ho, N. Pewnim, R. Steffen, P. J. Smith, K. G. V. Havelius, J. L. Hughes, L. Debono, S. Styring, E. Krausz, R. J. Pace, *Biochimica et Biophysica Acta - Bioenergetics* **2009**, *1787*, 882.

[5] G. Palazzo, A. Mallardi, A. Hochkoeppler, L. Cordone, G. Venturoli, *Biophysical Journal* **2002**, *82*, 558.

[6] C. R. Cantor, P. R. Schimmel, *Biophysical Chemistry Part II: Techniques for the Study of Biological Structure and Function*, W. H. Freeman and Company, San Francisco, **1980**.

8 Conclusions

The optical quality of PEM samples was understood in terms of chromophore concentrations (optical density), light scattering and the flattening effect. It was difficult to separate these effects in spectra but there appeared to be a strong Rayleigh scattering component in some samples. Practical methods for improving PEM sample optical quality were established, including: vortexing, homogenisation, a sample 'washing' method, detergent treatment and varying the freezing speed. All methods but the last were aimed at increasing homogeneity of the sample. Freezing samples quickly reduces fogging, a process that occurs when the glassy matrix undergoes a phase transition to a more crystalline phase.

It was found that light scattering and the flattening effect need to be minimised in samples as they can significantly change the apparent optical density of samples. Experiments in this work showed that light scattering can comprise ~3 10% of the maximum Q_y peak height in PEM spectra. It was shown that with detergent treatment and vortexing that flattening can suppress the maximum absorption peak height by as much as 30 to 50 %. It should be noted that detergent can affect the proportion of cyt b_{559} initially reduced in the samples.

A method to quantify the amount of initially reduced (and photooxidised) cyt b_{559} in PEM samples was developed. For the first time, the technique of MCD confirmed that excess sodium dithionite treatment leaves all cyt b_{559} hemes in the reduced state and therefore was a suitable method for calibrating the area of 100% heme reduction.

The cyt b_{559} quantification method was found to be strongly affected by scatter and hence, if this method is to be used successfully, the scatter in dithionite treated reference samples and untreated PEM samples needs to be comparable. An analysis of

several PEM samples by the quantification method suggested that 70 – 90% of PSII complexes have their cyt b_{559} initially reduced. There was no clear correlation between the amount of cytochrome initially reduced and the amount photooxidised by light and this question certainly deserves further attention. It appeared from the results that the amount of initially reduced cyt b_{559} in PEM samples was more dependent on the initial production of the sample rather than the handling immediately prior to spectroscopic analysis. Specifically, the contact time with detergent is an important factor, with longer contact times resulting in less cyt b_{559} being reduced.

The illumination-induced difference spectrum of PSII is a useful diagnostic for PSII samples as well as providing an insight into the electron transfer reactions that PSII has evolved to carry out. Armed with the knowledge of how to produce high optical quality samples, a systematic effort was made to determine the true illumination-induced difference spectrum free from spectral and sample artefacts.

The 676 nm feature was shown to be electrochromic, by comparison with the Q_x and Q_y shift features. The next task was to identify the source of the feature at 676 nm. Careful comparison of several experiments in which different secondary donors were formed by illumination at low temperature showed that the neither feature, nor in fact the whole spectrum was not dependent on the particular donor utilised by the system. Therefore it was concluded that Q_A^- was responsible for electrochromicially shifting one or more pigments and giving rise to the 676 nm feature.

A simulation of the effect of the Q_A^- on the pigments in PSII was carried out. The simulations suggested that Q_A^- electrochromically shifts all the chlorophyll and pheophytin pigments in the reaction centre of PSII; eight pigments in total. The major blue-shift feature at ~685 nm in the illumination-induced difference spectrum has not been interpreted this way before in the literature, rather it was thought to be due to one,

three or four pigments. The simulations were a first exploratory step in explaining the illumination-induced difference spectra. One weakness is the lack of specific data for the excitation energy for pigments in PSII, meaning that assumptions had to be made based on data obtained from other systems or, where no data was available, estimates were made so as to produce the best possible fit to experimental results. It has come to our attention that advancements have been recently made in this area in a study using a greater pool of diverse data (incorporating data from different species and circular dichroism measurements) as well as a more sophisticated model involving the coupling between pigments.

Finally, a novel feature in PEM spectra labelled 'the transient-high light difference spectrum' was tentatively assigned to P_{680}^{+}. The assignment was supported by comparison with a literature spectrum and calculations in this work simulating the expected relative concentration of P_{680}^{+} in low-light and high-light experiments. The method for forming the P_{680}^{+}/Q_A^{-} state described here is simpler than that described in the literature and may therefore be a useful method for studying this species in future.

Biochimica et Biophysica Acta 1787 (2009) 882–889

Contents lists available at ScienceDirect

Biochimica et Biophysica Acta

journal homepage: www.elsevier.com/locate/bbabio

The S_1 split signal of photosystem II; a tyrosine–manganese coupled interaction

Nicholas Cox [a], Felix M. Ho [b], Naray Pewnim [a], Ronald Steffen [c], Paul J. Smith [a], Kajsa G.V. Havelius [b], Joseph L. Hughes [c], Lesley Debono [c], Stenbjörn Styring [b], Elmars Krausz [c], Ron J. Pace [a,*]

[a] Department of Chemistry, College of Science, Australian National University, Canberra, ACT 0200, Australia
[b] Department of Photochemistry and Molecular Science, Ångström Laboratory, Uppsala University, P.O. Box 523, SE-751 20, Uppsala, Sweden
[c] Research School of Chemistry, Australian National University, Canberra, ACT 0200, Australia

ARTICLE INFO

Article history:
Received 10 September 2008
Received in revised form 26 March 2009
Accepted 30 March 2009
Available online 9 April 2009

Keywords:
S_1 split signal
Carotenoid
Chlorophyll
Cytochrome b_{559}
Pheophytin
Tyrosine
Exchange coupled interaction

ABSTRACT

Detailed optical and EPR analyses of states induced in dark-adapted PS II membranes by cryogenic illumination permit characterization and quantification of all pigment derived donors and acceptors, as well as optically silent (in the visible, near infrared) species which are EPR active. Near complete turnover formation of Q_A is seen in all centers, but with variable efficiency, depending on the donor species. In minimally detergent-exposed PS II membranes, negligible (<5%) oxidation of chlorophyll or carotenoid centers occurs for illumination temperatures 5–20 K. An optically silent electron donor to $P680^+$ is observed with the same decay kinetics as the S_1 split signal. Cryogenic donors to $P680^+$ seen are: (i) transient ($t_{1/2}$ ~ 150 s) tyrosine related species, including 'split signals' (~15% total centers), (ii) reduced cytochrome b_{559} (~30–50% centers), and (iii) an organic donor, possibly an amino acid side chain, (~30% centers).

1. Introduction

Photosystem II (PS II), a pigment–protein complex found in higher plants, algae and cyanobacteria, is responsible for the catalytic conversion of water to molecular oxygen in oxygenic photosynthesis. Initial charge separation occurs upon excitation of P680 – a chlorophyll assembly bound to the D1 and D2 protein subunits – resulting in the transfer of an electron to the neighboring pheophytin ($Pheo_{D1}$) and subsequently to plastoquinone co-factors Q_A and Q_B. Electrons for the re-reduction of $P680^+$ are sourced from the oxygen evolving complex (OEC) via the redox active tyrosine residue 161 (Y_Z) of the D1 protein. The OEC, which is the water-binding site of the PS II protein, is then in turn re-reduced by electrons released upon the oxidation of water. This generates molecular oxygen and protons (for review see [1]).

Whilst the above pathway for electron donation to $P680^+$ is the most efficient one under physiological temperatures, this is not so under cryogenic illumination conditions (<20 K), where the metastable states of the OEC, so called S-states, can be trapped for spectroscopic investigations. For example, in PS II material poised in the dark stable S_1 state, secondary donor pathways normally associated with photo-protection under physiological conditions can compete with the Y_Z/OEC donation pathway in a majority of centers. This is also true for Mn-depleted and OEC inhibited samples. Possible secondary donors include cytochrome b_{559} [2,3], carotenoid [4–8] or peripheral chlorophyll (chl_Z) associated with the reaction center [9–11]. However in a fraction of centers electron donation is still thought to come from the physiological pathway discussed above. Here though the electron hole is trapped on the intervening oxidized Y_Z. This radical magnetically interacts with the OEC resolving a 'split signal' [12–20]. Nugent et al. [12] first observed a new 'split like' EPR signal induced in intact PS II samples by visible light illumination of the S_1 state at <20 K. Petrouleas et al. [19,20] demonstrated that direct excitation of the Mn cluster via near infrared illumination (NIR) at liquid helium temperatures of intact cyanobacterial PS II poised in the S_2 state generates a resonance resembling that reported by Nugent et al. [12]. The NIR-induced signal was shown to be stable (at temperatures <20 K) and had near-Curie temperature dependence (4–10 K) [19].

Very recently, Styring and co-workers [21,22] have extended the study of intermediate turnover states in functional PS II, generated by cryogenic illumination by visible and NIR light. This has identified 'split' type signals arising from PS II poised initially in the S_0, S_1 and S_3 states. Although the established protocol of direct cryogenic illumination with visible light does not generate a split signal from S_2, such a species does appear to be formed from S_3, by a NIR-induced back

Abbreviations: EPR, Electron Paramagnetic Resonance; PS II, Photosystem II; OEC, Oxygen Evolving Complex; Q_A, primary plastoquinone A acceptor of PS II; Y_Z, tyrosine Z or residue 161 of the D1 polypeptide of PS II; Y_D, tyrosine D or residue 161 of the D2 polypeptide of PS II; Pheo, pheophytin; CW, continuous wave; ZFS, zero field splitting; MA, modulation amplitude; NIR, near infrared; chl, chlorophyll; Tris, Tris(hydroxymethyl)aminomethane; PpBQ, Phenyl-p-benzoquinone

* Corresponding author. Tel.: +61 2 6125 4546; fax: +61 2 6125 8997.
E-mail address: ron.pace@anu.edu.au (R.J. Pace).

0005-2728/$ – see front matter © 2009 Elsevier B.V. All rights reserved.
doi:10.1016/j.bbabio.2009.03.023

reaction [23] analogous to that used by Koulougliotis et al. (above) for generation of an S_1 split signal from S_2. Similarly an S_2 split signal has been generated upon flash advancement in the 77–190 K range and rapid cooling to 10 K or by cryogenic illumination in methanol treated samples [23].

In this report, we have studied the S_1 split signal in higher plant PS II membrane preparations via both optical and EPR techniques. Optical measurements enabled us to quantitatively monitor Q_A formation as well as chlorophyll, carotenoid and cytochrome b_{559} oxidation. EPR and optical measurements made on parallel samples permitted us to quantitatively observe the development of paramagnetic species in the $g\sim2$ region as well as cytochrome oxidation. Together they allow conclusions to be drawn as to the relative donor contributions involved in cryogenic turnover of intact PS II membranes. Importantly, these measurements demonstrate that there is an 'optical silent' electron donor with the same decay kinetics of the S_1 split signal.

2. Materials and methods

2.1. PS II membrane particles

All procedures were performed between 2 and 4 °C under dim green light. The PS II membrane particles were prepared as per the procedure of Bricker et al. [24] with modifications as per Smith et al. [25] and stored in 15 mM NaCl, 10 mM $MgCl_2$, 20 mM MES (pH 6.0) (NaOH), 400 mM sucrose and 1 M glycine betaine at −88 °C until use. PS II samples used in this study experienced very short contact times with detergents during solubilization of the thylakoid membranes. Careful washing removed unbound chlorophyll without degrading the sample. The number of chlorophylls per reaction center is estimated to be 200–220 [26]. Samples were stored at ~10 mg/mL (chl) and had a typical oxygen evolving capacity of 500–800 μmol O_2/(mg chl/h).

2.2. EPR sample manipulations/experimental procedure

Unless otherwise stated, EPR and optical measurements were performed in the same glassing/cryoprotectant medium, containing 40% glycerol. Samples were washed into our PS II storage buffer (as above), diluted with 40% glycerol, and the sample concentration was adjusted to 2.5–3.5 mg chl/mL for EPR and 1 mg chl/mL for optical measurements. Similarly, formate-treated membranes were washed into the same storage buffer with added glycerol which was first flushed with argon, and 10 mM added sodium formate.

Sample loading into quartz EPR tubes was performed under dim green illumination, the samples then degassed at 4 °C using a rotary vacuum pump for 1–2 min and filled with Ar to minimize O_2 signals. This was followed by >10 min dark adaptation at ~4 °C before freezing to ~200 K (CO_2/ethanol) and subsequently to 77 K (liquid N_2). Samples were used immediately or within 24 h.

For split signal induction at cryogenic temperatures, samples were illuminated with a 125 W halogen lamp in the EPR cavity. The light beam was first passed through a water filter (path length 10 cm) and an interference filter centered at 690 nm with spectral width 10 nm, then defocused (20 mm diameter spot) directly onto the front EPR cavity grate. Recent studies in our laboratories have shown that illumination at this wavelength generates efficient P680 turnover at cryogenic temperatures [27].

EPR measurements were performed with a Bruker ESP300E spectrometer with an Oxford ESR9 liquid helium flow cryostat. A gold-chromel thermocouple directly below the sample position was used for temperature measurement. Linearity of the thermocouple reading was checked over the 5–20 K range by direct double integration of the dark stable Y_D· radical signal (also known as Signal II_{slow}) under non-saturating conditions, demonstrating the Curie behavior of the signal.

2.3. Optical sample manipulations/experimental procedure

Optical spectroscopy was performed on a custom built CCD-based spectrograph consisting of a tungsten–halogen lamp (Osram, 250 W) as a light source, a Spex 1704 0.75 m monochromator and a Princeton instruments nitrogen-cooled CCD camera (LN/CCD-1340/400-EHRB) as a detector. All lenses and windows were made of fused quartz. The sample was located in a custom built 200 μm path length cell, cooled to 5 K by means of a helium flow tube system.

Samples were loaded into the optical cells under dim green light, and then transferred to the spectrometer using a custom built light-tight lock. The lock attached directly to the He gas flow tube, eliminating stray light exposure of the sample. Samples were dark-adapted at room temperature in the lock for approximately 10 min, after which the samples were rapidly cooled to 5 K in complete darkness to ensure good glassing and low scatter.

For measurements covering the range between 500 nm and 730 nm, a 150 lines/mm grating blazed at 600 nm was used. For the range 500 nm to 1100 nm, a 50 lines/mm grating blazed at 800 nm was used. Exposure of CCD and sample was controlled by two shutters (Uniblitz VS25S2S1) synchronized with the CCD camera. Each single spectrum was acquired in a 100 ms exposure of the CCD. A single measurement induced photochemistry in less than 3% of the sample.

3. Results

3.1. Optical spectroscopy

3.1.1. Observation of Q_A reduction/donor oxidation by optical spectroscopy

Fig. 1A shows the optical absorption spectrum of the dark-adapted PS II membrane fragments over the 500–1000 nm region recorded at

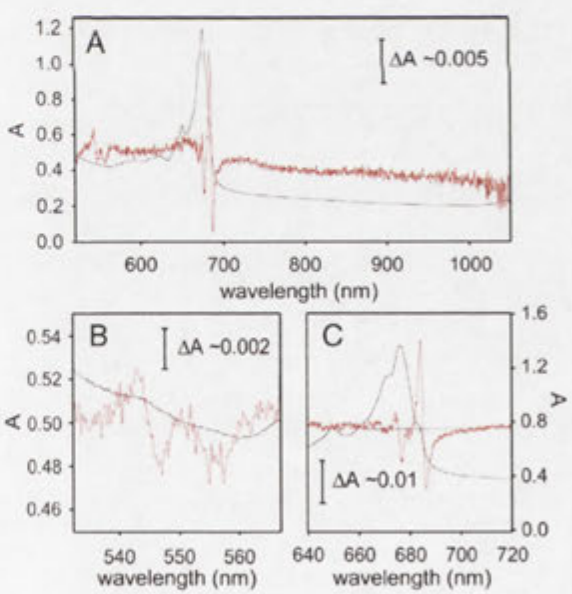

Fig. 1. Optical spectra of dark-adapted (10 min, see Materials and methods) PS II membrane particles in 40% glycerol cryoprotectant at 5 K. Black lines: absorption spectra; thin red lines: cryogenic light induced difference spectra (light-minus-dark, 5 min illumination, ~1 mW/cm^2). A: Complete Vis/NIR region where cryogenic donors/acceptors of PS II would be observed. Includes regions where chlorophyll (850 nm) and carotenoid (980 nm) radicals absorb. B: optimized spectrum of the chlorin Q_X region where the pheophytin (550 nm) and cytochrome b_{559} (557 nm) bands are readily observed. The cytochrome b_{559} band is seen as a bleach in the turnover spectrum. C: the optimized spectrum of the chlorin Q_Y region. Here Q_A−induced electrochromism of $pheo_{D1}$ is seen. Taking the zero difference base-line (thin straight line) as indicated, the turnover pattern in the 660–700 nm region is conservative, within the uncertainty of the data.

5 K. The major absorption features, between 600 and 700 nm, occur in the region of the lowest energy electronic transitions of chlorophyll and pheophytin (Q_Y transitions, Fig. 1A, C, thick solid lines). Additional bands between 560–640 nm comprise the Q_Y vibrational side structure. Two smaller features appear around 540–560 nm (Fig. 1A, B, thick solid lines). These arise from absorption by $Pheo_{D1}$ and $Pheo_{D2}$ (Q_X, second lowest transition) and reduced cytochrome b_{559}. As a consequence of the CCD detector sensitivity profile, the signal-to-noise ratio drops significantly beyond 1000 nm.

Upon cryogenic illumination (5 min green light, 1 mW/cm^2), two derivative band shift features appear in the light-minus-dark difference spectrum (red thin lines). These are centered at 684 nm and 545 nm (Fig. 1A, B, C), and have been attributed to electrochromic shifts of the Q_Y and Q_X bands of pheophytin/chlorophyll associated with the reaction center. These shifts are caused by the presence of the now negatively charge Q_A [28]. Therefore, the amplitudes of the shifts can be used to determine the extent of Q_A reduction, and hence sample turnover.

It can be seen in the difference spectrum of the Q_Y region (Fig. 1C) that there is also an additional shift feature centered at 674 nm. The amplitude of this shift is approximately 20–25% the dominant Q_Y shift. The origin of this shift is currently under investigation, and we presently do not assign this feature.

The only other optically observed change originating from a donor to $P680^+$ in the visible–NIR region is that from cytochrome b_{559} oxidation (Fig. 1B). In its reduced form it appears as a weak absorbance band centered around 557 nm in our samples (as confirmed by full chemical reduction of cytochrome b_{559} by dithionite; Supporting information S1). Upon illumination at 5 K this feature bleaches, giving rise to a trough in the difference spectrum (Fig. 1B, red thin line).

No spectral features above 700 nm were observed in the light-minus-dark difference spectrum, the region where absorptions by oxidized secondary donors have previously been observed (Fig. 1A). Absorbance bands at 850 nm associated with chlorophyll oxidation were not detected in the difference spectrum of any sample. Although there is a structured mix of negative and positive features in the difference spectrum in the 660–690 nm region, possibly reflecting electrochromism in coupled pigment systems, no significant net bleach was observed (Fig. 1C). This suggests negligible (<5% of reaction centers) oxidation of chlorophylls, including the chlorophyll Chl_Z [2]. In addition, no bands were observed in the 950 nm region where the carotenoid cation radicals would absorb. The large extinction coefficient (130,000–216,000 M^{-1} cm^{-1}, [4,8] and references therein) of this species allows us to exclude it as all but a trivial donor side contribution (<1% of reaction centers) in our samples.

3.1.2. Quantification of Q_A formation/re-oxidation and cytochrome b_{559} oxidation by optical spectroscopy

The amount of Q_A reduction can be estimated from the electrochromic shift feature in either Q_X or Q_Y as observed in the difference spectrum, scaled to the total absorption intensity of the Q_Y band (Fig. 1, [28]). The maximum amplitude of either shift was obtained after 5 min of illumination (1 mW/cm^2, see Materials and methods). This was taken to represent Q_A reduction in 100% of centers.

Q_A decay, as observed by either the Q_X or Q_Y shift features, occurs at cryogenic temperatures in all intact PS II preparations regardless of the illumination procedure (Fig. 2).[1] Approximately 15% of the Q_A formed decays (i.e. re-oxidized) with $t_{1/2}$ ~ 100–200 s (which is on a timescale consistent with the decay of the EPR split signal; see below). A slower decaying component is also observed with $t_{1/2}$ ~ 40–60 min in approximately ~25% of centers. The remaining Q_A formed does not re-oxidize within the timeframe of the experiments (>100 min).

[1] A more detailed discussion of decay rates and donor evolution will be given in a following article.

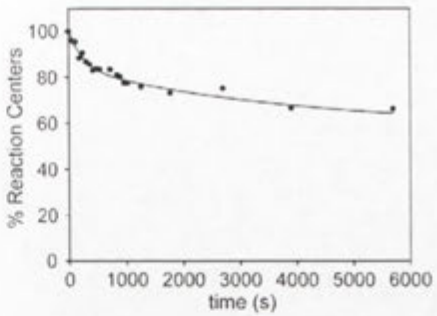

Fig. 2. Typical time course of Q_A decay after saturating illumination (5 min ~ 1 mW/cm^2, Materials and methods) at 2 K, as estimated optically from the Q_X $pheo_{D1}$ shift (Fig. 1B). Data were fitted using a double exponential function. Some sample specific variation is seen in the fitting parameters, but these are consistently within the ranges given in Table 1. The $t = 0$ in the figure is when illumination was terminated.

As noted above, cytochrome b_{559} was the only donor co-factor the oxidation of which could be optically observed upon cryogenic illumination. It was also found that once oxidized, cytochrome b_{559} did not re-reduce ('rollback') during subsequent dark adaptation at 5 K. In fact, the original amount of reduced cytochrome b_{559} was not fully recovered by any annealing procedure. Therefore, this donor cannot account for any of the transiently reduced Q_A that decayed after illumination ceased. Given that neither chlorophyll nor carotenoid appear to be significant donors in this highly intact membrane system, and the fact that one component of the Q_A decay kinetics is on a timescale similar to that observed for EPR split signals, a reasonable suggestion is that at least some of the missing transient donor population is Y_Z. This would appear optically in the UV region (<300 nm). However, our present experimental arrangement does not access this region with sufficient sensitivity to reliably detect one tyrosine oxidation against the protein–pigment background.

To quantify the amount of cytochrome b_{559} that was oxidized by illumination, the amount of reduced cytochrome b_{559} originally present in the dark-adapted PS II sample was first estimated. This was done by comparing the intensity of the reduced cytochrome b_{559} absorption at 557 nm (normalized to the pheophytin (Q_X) absorption at 545 nm) in untreated PS II samples and in samples where all the cytochrome b_{559} present had been chemically reduced by dithionite treatment (Supporting information S1). It was found that cytochrome b_{559} was normally in its reduced form in more than 50% of centers in our PS II samples. After cryogenic illumination, it was found that cytochrome b_{559} oxidation was not complete, and never exceeded 50% of the PS II centers. Typically, cytochrome b_{559} was oxidized by cryogenic illumination in approximately one-third of the PS II centers in the sample.

In summary, while Q_A reduction and re-oxidation could be readily observed by optical spectroscopy, generally only ~30% of the donors could be assigned from readily accessible optical features (Fig. 1A). Optically observed donors and acceptors (under saturating illumination conditions) are summarized in Table 1.

3.2. EPR spectroscopy

3.2.1. Q_A reduction-decay as monitored by EPR spectroscopy

The extent of Q_A formation can also be observed in EPR through the Q_AFe^{2+} EPR signal in PS II that has been treated with formate [29]. Fig. 3A shows the induction and loss of this signal upon cryogenic illumination of our dark-adapted PS II samples, as measured at the 3680 G peak (g ~ 1.84, signal maximum; see Fig. 3B).

The formation of Q_A by illumination was at least bi-exponential in character (black dash lines). It was found that maximum intensity of the Q_AFe^{2+} signal was achieved within ~10 min, and further illumination did not lead any significant increase.

Table 1
Optical and EPR observed donors and acceptors.

Acceptor/donor	% of RC Optical	% of RC EPR[a]
Q_AQ_A total decay	~40%	–
(After 40 min)	~30%	~30% (~25%)[b]
Fast ($t_{1/2}$~100-200 s)	~15%	<20% (<17%)
Slow ($t_{1/2}$~40-60 min)	~25%	10–30% (9–25%)
Stable	~60%	–
(After 40 min)	~70%	~70% (60%)
Cytochrome b_{559}	30–50%	30–50%
Chlorophyll	<5%	?
Carotenoid	<1%	?
Split signal	–	~15%
g~2 radical		
Total	–	20–30%
$t_{1/2}$~40 min		10–15%
Stable		10–15%

[a] Complete turnover by cryogenic illumination is difficult in EPR samples due to inefficiencies in sample illumination within the EPR cavity and the highly dispersive nature of the kinetics of Q_A formation at 5 K [41]. Total quantification of all EPR donors generally does not exceed 85% of all centers as determined by Y_D- signal integration.
[b] Estimated Q_A decay (at a percentage of total centers). Calculated by multiplying the observed Q_A decay by 0.85.

The decay trace (Fig. 3A, solid red line) is biphasic over 40 min at 5 K and the components that are lost amount to ~30% of total Q_A generated. The measurement time was too short to resolve each Q_A decay component precisely and stability limitations of the instrument made longer measurements unreliable. However, an (upper bound) estimate of the magnitude of the fast component could be made from the loss of Q_A signal intensity after ~20 min dark adaptation (Fig. 3B, dashed red line) compared to that under saturating illumination (10 min, Fig. 3B solid line). The Q_A re-oxidation was found to be ~20% of the total Q_A generated.

To rule out changes in Q_A induction, decay or absorption behavior due to the presence of formate, control optical measurements were performed and compared to those presented above (Figs. 1 and 2). No significant changes were observed (data not shown).

Interestingly, it was found that once a sample has been exposed to saturating illumination, the fast re-oxidizing Q_A could be repeatedly re-reduced by the application of short illuminations (10 s) after allowing the sample to dark adapt for 10–20 min. In this way, the decay rate of the fast component could be extracted (Fig. 3C, open circles). It was observed that the decay of the Q_A signal was then mono-exponential, giving a $t_{1/2}$ of ~150 s. This could then be compared to the decay of the EPR split signal induced in the same sample, as measured at the low field peak (see below for details). Control experiments showed that the induction of the split signal was not affected by the presence of formate (Supporting information Fig. S7). The split signal decay kinetics is overlaid in Fig. 3C, and it is very similar to that of the Q_AFe^{2+} signal. A single exponential fit of the split signal decay kinetics yields a $t_{1/2}$ of ~160 s. This correspondence in decay rates demonstrates a direct relationship between the decay of these two signals, and suggests that the radical responsible for the split signal is the same as that responsible for the fast component of the Q_A decay kinetics.

3.2.2. Resolution of different donors to $P680^+$ as observed by EPR spectroscopy

Complementary to the optical spectroscopy experiments described above, parallel EPR experiments were performed to observe EPR-visible radical species that were generated by low temperature illumination of PS II membranes. Overall, three signals were found.

Cytochrome b_{559} oxidation was evidenced by the well-characterized feature at $g\sim3$, corresponding to the g_z component of this radical (Fig. 4A). This signal was found to slowly accumulate with illumination time, with maximum signal intensity being reached after hour(s) long illumination. The cytochrome signal was stable once generated at

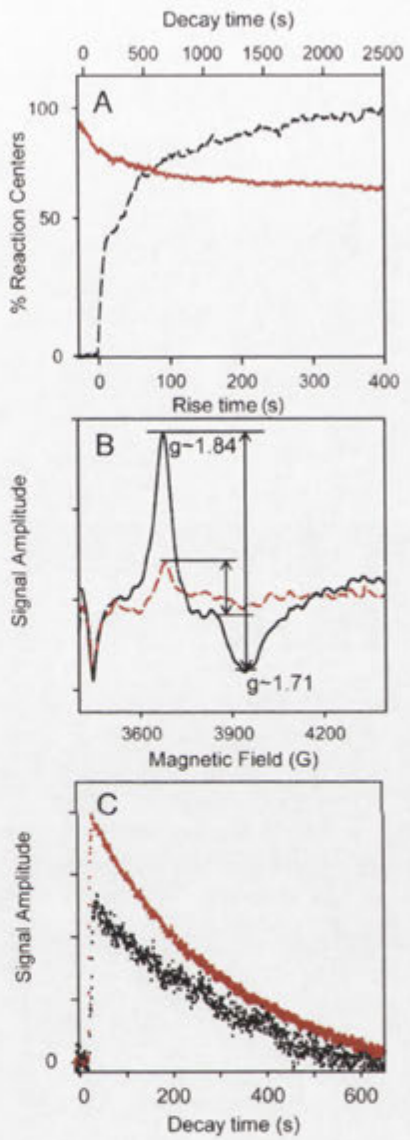

Fig. 3. Comparison of $_{QA-}$ and split signal decay kinetics as observed by EPR spectroscopy. (A) Time course of Q_AFe^{2+}, $g\sim1.84$ EPR signal intensity in PS II membranes (40% glycerol) treated with 25 mM sodium formate. Dashed black line: signal generation at 5 K as a function of the illumination time. Illumination starts time = 0. Solid red line: signal decay as a function of dark adaptation time at 5 K. Q_AFe^{2+} signal monitored at field of signal maximum ($g\sim1.84$). Illumination ended at time = 0. (B) (Under illumination) minus (pre-illumination) difference spectrum (solid black line) and (under illumination) minus (20 min post illumination) difference spectrum (dashed red line) of the Q_AFe^{2+} resonance (same sample as A). (C) Split signal decay kinetics (filled red circles) overlaid on fast Q_AFe^{2+} decay kinetics (open circles; see text for details). Both observed in the dark immediately following 10 s illumination at 5 K (same sample as A; both signals measured in the presence of formate). The sample had experienced a saturating illumination and 10 min dark adaptation prior to the 10 s re-illumination (fast rise region). The Q_AFe^{2+} decay curve is an average of three successive measurement cycles. The induced split signal was measured at the $g\sim2.035$ shoulder (see Fig. 4B). Total Q_AFe^{2+} levels were estimated by a difference of the signal intensities at the $g\sim1.84$ and $g\sim1.71$ field positions, acquired in separate kinetic scans EPR parameters. (A and B): Microwave power 16 mW; frequency, 9.44 GHz; modulation amplitude, 32 G; time constant 2.6 s. (C): Microwave power, 6 mW (split), 16 mW (Q_A-); frequency 9.44 GHz, modulation amplitude, 10 G (split), 32 G (Q_A-); time constant, 0.5 s.

<20 K, and showed no decay upon subsequent dark adaptation. By comparing the increase in amplitude of this feature to that observed in a fully oxidized standard, an estimate was made of its donor contribution (with appropriate scaling via $Y_{D^\cdot}$). It was found that the amount of illumination-induced cytochrome b_{559} oxidation was typically 30–50%. This is consistent with the optical experiments above; where cytochrome b_{559} was also found to be stably induced by illumination in 30–50% of the PS II centers present (Table 1).

At the $g\sim2$ region, two other signals with different decay kinetics could be observed. The faster decaying signal gave a $t_{1/2}\sim100$–120 s, while the slower decaying signal was found to decay with $t_{1/2}\sim40$–60 min, though a stable, non-decaying component of this signal was also observed.

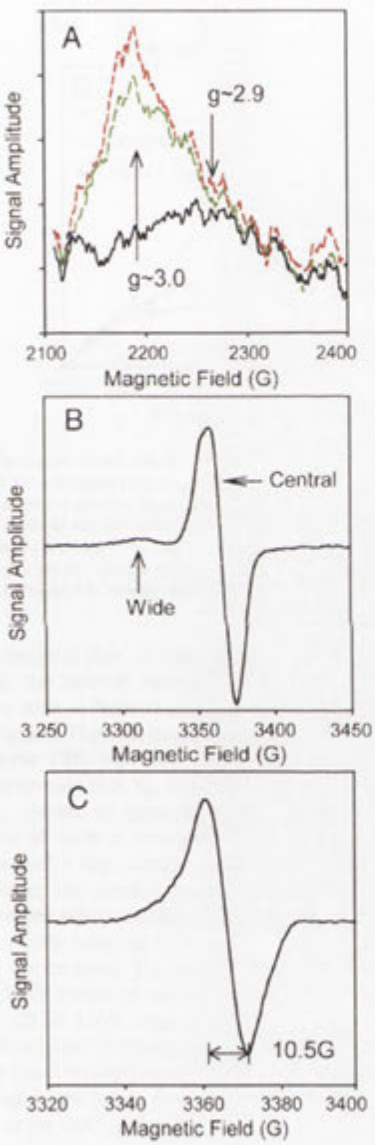

Fig. 4. EPR observed cryogenic donors to $P680^+$ produced by illumination at 5 K in 40% glycerol cryoprotectant. A: g ~ 3 (g_x) turning point of the oxidized cytochrome b_{559} (8.5 K). Solid black line:—pre-illumination; long green dashed line:—after 10 minutes illumination; short red dashed line:—after 1 h illumination. B: split signal observed under illumination at 5 K (both $Y_D^\cdot$ and 10.5 G radical subtracted). Labeled are the two main features associated with the signal when generated by visible illumination: a derivative centered at g ~ 2.0 and an absorption feature with maximum at g ~ 2.035. This appears to be the low field edge of a broad derivative like feature, the up-field negative component of which is partly overlaid by the prominent g ~ 2 peak. C: featureless, slowly decaying radical (g ~ 2, 10.5 G wide) generated upon illumination. EPR parameters: microwave power (A) 6 mW, (B) 50 μW, (C) 5 μW; frequency 9.44 GHz; modulation amplitude (A) 20 G, (B) 10 G, (C) 4 G.

In order to extract the spectral shape of the faster decaying signal, a difference spectrum was calculated from the signal taken under continuous illumination and that taken after the illuminated sample had been allowed to dark adapt for 10 min (Fig. 4B). This represents the component which decays within the first 10 min after illumination. This procedure minimized the contribution from the slowly decaying species whilst still allowing observation of the fast decaying signal with good signal-to-noise levels. The faster decaying signal was found to correspond to the S_1 state split signal, as previously reported [12,21], exhibiting both an assumed split derivative ($g\sim2.035$, wide component) and a simple derivative feature centered at $g\sim2.0$ (central component). The high field edge of the wide component appears only partially resolved as it overlays the more intense central component. Double integration of the total signal (scaled to $Y_{D^\cdot}$) yields an intensity of ~15% of centers.[2] It was further found that short illuminations (~1 min) were sufficient to generate the maximum signal, that the signal could also be re-generated at temperatures <20 K repeatedly without loss (its intensity was reproducible to within 10% over 5 successive illumination/decay cycles, with each cycle lasting more than 1 h in total).

Finally, in order to focus on the slowly decaying radical, a difference was taken between the spectrum of the sample before illumination and that of the sample after illumination and a subsequent ~15 min period of dark adaptation. This dark adaptation period allowed the fast decaying signal to decay away, so that the resulting difference spectrum consists only of the slowly decaying component of the total illumination-induced signal. This protocol also cancels out any contribution from the stable $Y_{D^\cdot}$ radical. The resulting signal (Fig. 4C) is a featureless radical centered at $g\sim2.0024$ with a width of 10.5 G. Its total donor contribution (scaled to Y_D) is typically 20–30%. As with cytochrome b_{559} oxidation, it slowly accumulated with illumination time, achieving maximum signal intensity after hour(s) long illumination.

Apart from their decay kinetics, the two signals found in the $g\sim2$ region also differed from each other in their relaxation behavior, with the faster decaying split signal also being the faster relaxing of the two species (the signals shown in Fig. 4B and C were measured under their respective non-saturating conditions). This is explored further below.

3.2.3. *Identifying distinct components of the split signal by $P_{1/2}$ studies*

When examining the split signal (Fig. 4C) at a single applied microwave power, its spectral shape was found to be similar to those examples reported previously [12,21,30,31]. The spectral shape of the split signal was also independent of the presence or absence of exogenous electron acceptors (e.g. PpPQ). Only minor variations in the relative intensity of the wide and central components were observed between samples, probably reflecting changes in the relative microwave saturation properties of different components of the signal (see below). Contribution from the narrow, more stable radical signal is minimized through the subtraction protocol described above. As previously reported [12,30], neither component of the split signal was generated in material lacking the manganese cluster (e.g. via Tris or NH_2OH treatments; data not shown), whereas a central component remained in the presence of methanol [32]. The use of 40% glycerol (v/v) as a cryoprotectant did not affect split signal yields.

[2] Assuming the broad split signal arises from a weak interaction between a spin 1/2 radical and some higher spin center of which the effective Zeeman energy (reflected by the g value) differs from that of the radical by substantially more than their interaction energy, then this estimation is valid. That is, the radical's absorption is simply spread over a wider field range, but the total transition intensity is unaltered in first order.

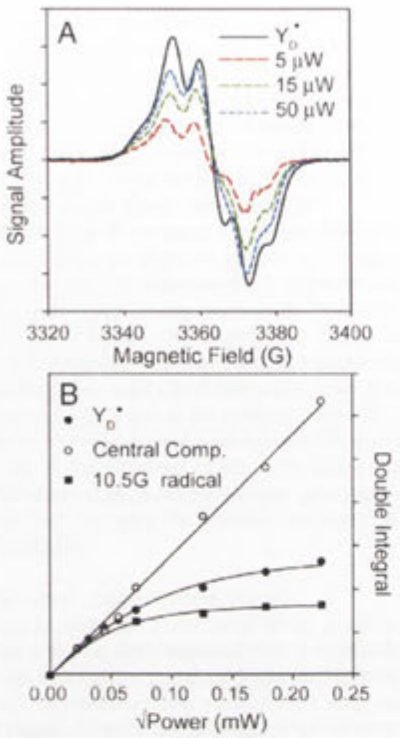

Fig. 5. Characterization of the central component of the split signal. (A) The central component of the split signal (Fig. 3B, $g \sim 2.0$) observed at low modulation amplitude and various microwave powers. Superimposed is the scaled $Y_{D^\bullet}$ spectrum (solid line). (B) The signal intensity as a function of the square root of the microwave power at 5 K of (i) 10.5 G radical (filled squares), (ii) $Y_{D^\bullet}$ (filled circles), and (iii) central split signal component (open circles). Sample conditions and EPR parameters as in Fig. 4C except: modulation amplitude, 4 G; sweep width is 100 G.

It was observed that, at low microwave powers and modulation amplitudes, the central component of the split signal could be resolved to give a hyperfine structure indicative of an oxidized tyrosine (Fig. 5A). This was the case even where methanol was present in the sample (4%; data not shown). This is in agreement with literature proposals that Y_Z. is the radical species that interacts with the $CaMn_4$ cluster to give the split signals, and recent similar observations of such a tyrosine-shaped component in split signal when measured at high temperatures (~100 K) [33,34].

In addition, the central component was found to be a faster relaxing species when compared to the slower relaxing $Y_{D^\bullet}$, or the even more slowly relaxing 10.5 G radical. The signal was unsaturated at 50 μW. By contrast, $Y_{D^\bullet}$ was found to give a $P_{1/2}$ of ~10 μW, consistent with literature values [35]. The $P_{1/2}$ of the 10.5 G radical was lower still, at 5 μW, suggesting that it may arise from an organic radical well removed from any fast-relaxing paramagnetic center in PS II. Thus the faster relaxation rate of the central component of the split signal is again evidence that it represents $Y_{Z^\bullet}$, situated in close proximity to the $CaMn_4$ cluster.

Finally, as compared to $Y_{D^\bullet}$, the central component of the split signal may have an altered hyperfine pattern and a possible shift in apparent g value. Since this difference was seen at all powers up to 50 μW, it is unlikely to result from contamination by other radical species.

Significantly, it was found that the spectral shape of this tyrosine-like central component was essentially constant over the microwave power range used (Fig. 5A), suggesting that the pattern is homogeneous with no interference from an underlying, slowly relaxing component (i.e. Y_D). The spectral shape was also preserved across a range of temperatures (5 K–20 K, Supporting information S4). This provides confirmation that the subtraction procedure for obtaining the split signal was successful in minimizing contributions from both the stable 10.5 G radical, and that the resolved tyrosine structure is not simply a saturation artifact of the large Y_D background due to enhancement of $Y_{D^\bullet}$ relaxation rate upon split signal induction (i.e. the influence of another paramagnetic center in the vicinity of Y_D).

4. Discussion

4.1. Quantitative analysis of turnover

4.1.1. Carotenoid/chlorophyll oxidation

Our optical measurements essentially exclude chlorophyll or carotenoid pigment oxidation following cryogenic turnover in the S_1 state of PS II in plant membranes, as prepared here [26]. Significant donation from either of these species does not occur upon low temperature illumination in this PS II preparation, either transiently or statically, irrespective of split signal intensity. However, as we will discuss elsewhere (see author's note), this result is dependant on the details of the PS II membrane preparation procedure used and is probably influenced to some extent by the illumination regime employed. The results seen here appear to represent one limit of a spectrum of behaviors that plant PS II preparations can exhibit.

The lack of carotenoid oxidation seen here contrasts with earlier studies where the pigment has been shown to be the dominant electron donor in higher plant PS II at liquid He temperatures. In these circumstances the cytochrome b_{559} center was pre-oxidized [6]. We find that a significant yield of photo-induced carotenoid oxidation occurs in PS II membrane samples subject to further detergent treatment during preparation, such that cytochrome b_{559} is almost totally oxidized before cryogenic illumination. Nevertheless, we are unable to achieve more than ~50% of cryogenic donor contribution from carotenoid even in these samples. Previous optical studies may have over-estimated carotenoid involvement [4,6]. In these investigations there was no direct measure of charge transfer (i.e. Q_A formation) and so carotenoid turnover was scaled to total absorbance rather than an internal reaction center count.

Previous work has also correlated either carotenoid and chlorophyll cation radical formation with the appearance of featureless EPR signal(s) at $g \sim 2$, of width 9.5–10.5 G [4,6,21]. Such an assignment may now require qualification, at least for minimally detergent-treated PS II samples as used here, since we observe a similar featureless photogenerated derivative EPR signal (~30% of $Y_{D^\bullet}$) in the absence of any chlorophyll or carotenoid oxidation. A non-pigment, non-tyrosine ('mystery', see below) donor may thus be present, which would be difficult to distinguish from Chl^+ or Car^+ radicals in conventional low field EPR.

4.1.2. Cytochrome/Q_A balance

The only donor oxidation that could be observed in optical spectroscopy was that of cytochrome b_{559}. By scaling to a dithionite-treated standard, where all cytochrome b_{559} is in its reduced form, the extent of cytochrome oxidation relative to reaction centers that undergo charge separation (as measured by Q_A formation) could be quantified. It was clear that cytochrome oxidation could not account for all illumination-induced Q_A formation. Similar quantification results were obtained via EPR spectroscopy. Furthermore, while Q_A was found to partially re-oxidize upon dark adaptation at 5 K, presumably via charge recombination pathways, oxidized cytochrome remained stably oxidized at 5 K. Subsequent sample re-illuminations generated no more oxidized cytochrome species. Therefore, while cytochrome oxidation is likely to be account for a substantial portion of PS II centers with stably reduced Q_A after illumination (Table 1), the decaying components of Q_A could not be accounted for by any donor species with a readily accessible optical signature.

4.1.3. Q_A decay-split signal involvement

Zhang et al. [36] demonstrated the S_1 split EPR signal of thermophilic cyanobacteria decayed together with the Q_AFe^{2+} resonance at $g\sim1.9$. As this signal is small and appears close to intense signals in the $g\sim2$ region, they also measured the $Q_A/Fe^{2+}/Q_B$ signal at $g\sim1.6$ [37], showing a similar effect. From this result they concluded that the split signal species was most likely a donor to $P680^+$, relaxing at 5 K via charge recombination.

Our experiments here on the signal using spinach PS II membranes confirm the observations of Zhang et al. [36]. Q_A decayed with the same half-life as the split signal resonance in approximately ~20% of centers that had undergone charge separation. This was consistent with our optical quantification (Fig. 2 and Table 1). We additionally found that the use of formate treatment [29] to enhance the Q_A/Fe^{2+} signal led to no changes in split signal formation. Apart from allowing more reliable quantification due to the enhanced intensity of the Q_A/Fe^{2+} signal, this observation is good evidence that the acceptor side of PS II, namely Q_A is not involved in the split signal. This can be compared to literature reports where formate alters the $Pheo_{D1}/Q_A$ spin–spin interaction, changing the splitting and signal width of the $Pheo_{D1}$ split signal [29].

4.1.4. New redox center (stable 'mystery donor')

An interesting finding from a correlation of our parallel optical and EPR measurements is that the featureless 10.5 G wide radical as seen by EPR has no obvious optical signature in the visible/near IR region. This radical was found to decay slowly during dark adaptation after its induction by cryogenic illumination, allowing it to be isolated from the faster decaying split signal. It was also found to undergo slow paramagnetic relaxation compared to (both components of) the split signal, and its $P_{1/2}$ value was comparable to that of $Y_{D^\bullet}$. These factors suggest that it is a magnetically isolated radical species in the protein matrix, possibly derived from an amino acid residue. The width of the EPR resonance suggests that it is a large molecule, and its g value (~2.002) and absence of characteristic proton hyperfine splitting features argue against an assignment to tyrosine. Another possible candidate is a tryptophan side chain, which should be detectable in the UV (<300 nm) region.

4.1.5. EPR of S_1 split signal; a 'tyrosine-like' component

The match between the fast phase of the Q_A^- decay kinetics and the split signal decay kinetics, together with the fact that a fast-relaxing, transient tyrosine radical was found by EPR spectroscopy in the $g\sim2$ region upon induction of the split signal, strongly suggest Y_Z involvement in the split signal. This is consistent with previous literature proposals, but is the first demonstration of the fact at those cryogenic temperatures (<10 K) at which the split species is directly observed.

The transient tyrosine signal may correspond to the '26 G fast decaying' signal first seen by [20]. This signal did not resolve a hyperfine coupling, but has approximately the same width and decay kinetics as the transient tyrosine signal observed here. It was reported that the '26 G' signal was not observed in samples containing 40% glycerol. As the addition of glycerol did not have any effect on S_1 split signal (shape or yield) for our PS II preparation, we suspect our samples resemble 'untreated PS II' as defined in [20] and therefore could potentially resolve a '26 G fast decaying' signal. However, we cannot exclude the possibility that this signal is separate from the '26 G signal', akin to the light-induced tyrosine signal observed in methanol containing samples.

Acknowledgements

The authors are grateful to Mr. K. Jackson for invaluable technical assistance. F. Ho acknowledges the financial support of the European Union Sixth Framework Programme Marie Curie Incoming International Fellowship (514817). S Styring acknowledges support from the Swedish Research Council and the Swedish Energy Agency. E. Krausz and R Pace acknowledge support from the Australian Research Council.

Appendix A. Supplementary data

Supplementary data associated with this article can be found, in the online version, at doi:10.1016/j.bbabio.2009.03.023.

References

[1] K. Ahrling, R.J. Pace, M.C.W. Evans, The Catalytic Manganese Cluster: Implications from Spectroscopy, Vol. 1, Springer, 2005.
[2] J.C. de Paula, J.B. Innes, G.W. Brudvig, Electron transfer in photosystem II at cryogenic temperatures, Biochemistry 24 (1985) 8114–8120.
[3] L.K. Thompson, G.W. Brudvig, Cytochrome *b*-559 may function to protect photosystem II from photoinhibition, Biochemistry 27 (1988) 6653–6658.
[4] P. Faller, A. Pascal, A.W. Rutherford, b-Carotene redox reactions in photosystem II: electron transfer pathway, Biochemistry 40 (2001) 6431–6440.
[5] J.S. Vrettos, D.H. Stewart, J.C. de Paula, G.W. Brudvig, Low-temperature optical and resonance raman spectra of a carotenoid cation radical in photosystem II, J. Phys. Chem. B 103 (1999) 6403–6406.
[6] J. Hanley, Y. Deligiannakis, A. Pascal, P. Faller, A.W. Rutherford, Carotenoid oxidation in photosystem II, Biochemistry 38 (1999) 8189–8195.
[7] C.A. Tracewell, G.W. Brudvig, Two redox-active b-carotene molecules in photosystem II, Biochemistry 42 (2003) 9127–9136.
[8] C.A. Tracewell, A. Cua, D.H. Stewart, D.F. Bocian, G.W. Brudvig, Characterization of carotenoid and chlorophyll photooxidation in photosystem II, Biochemistry 40 (2001) 193–203.
[9] C.A. Buser, L.K. Thompson, B.A. Diner, G. Brudvig, Electron-transfer reactions in manganese-depleted photosystem II, Biochemistry 29 (1990) 8977–8985.
[10] A. Cua, D.H. Stewart, G.W. Brudvig, D.F. Bocian, Selective resonance raman scattering from chlorophyll Z in photosystem II via excitation into the near-infrared absorption band of the cation, J. Am. Chem. Soc. 120 (1998) 4532–4533.
[11] K.V. Lakshmi, O.G. Poluektov, M.J. Reifler, A.M. Wagner, M.C. Thurnauer, G.W. Brudvig, Pulsed high-frequency EPR study on the location of carotenoid and chlorophyll cation radicals in photosystem II, J. Am. Chem. Soc. 125 (2003) 5005–5014.
[12] J.H.A. Nugent, P. Muhiuddin, M.C.W. Evans, Electron transfer from the water oxidizing complex at cryogenic temperatures: the S1 to S2 step, Biochemistry 41 (2002) 4117–4126.
[13] A. Boussac, J.-L. Zimmermann, A.W. Rutherford, EPR signals from modified charge accumulation states of the oxygen-evolving enzyme in Ca2+-deficient photosystem II, Biochemistry 28 (1989) 8984–8989.
[14] M. Sivaraja, J. Tso, G.C. Dismukes, A calcium specific site influences the structure of and activity of the manganese cluster responsible for photosynthetic water oxidation, Biochemistry 28 (1989) 9459–9464.
[15] D.J. Maclachlan, J.H.A. Nugent, Investigation of S3 electron paramagnetic resonance signals from the oxygen-evolving complex of photosystem 2: effect of inhibition of oxygen evolution by acetate, Biochemistry 32 (1993) 9772–9780.
[16] P. Dorlet, M.D. Valentin, G.T. Babcock, J.L. McCracken, Interaction of YZ with its environment in acetate-treated photosystem II membranes and reaction center cores, J. Phys. Chem. B 102 (1998) 8239–8247.
[17] K.V. Lakshmi, S.S. Eaton, G.R. Eaton, H.A. Frank, G.W. Brudvig, Analysis of dipolar and exchange interactions between manganese and tyrosine Z in the S2YZ; state of acetate-inhibited photosystem II via EPR spectral simulations at X- and Q-bands, J. Phys. Chem. B 102 (1998) 8327–8335.
[18] J.M. Peloquin, K.A. Campbell, R.D. Britt, 55 Mn pulsed ENDOR demonstrates that the photosystem II "split" EPR signal arises from a magnetically-coupled magnano-tyrosyl complex, J. Am. Chem. Soc. 120 (1998) 6840–6841.
[19] D. Koulougliotis, J.-R. Shen, N. Ioannidis, V. Petrouleas, Near-IR irradiation of the S2 state of the water oxidizing complex of photosystem II at liquid helium temperatures produces the metalloradical intermediate attributed to S1YZ, Biochemistry 42 (2003) 3045–3053.
[20] G. Sioros, D. Koulougliotis, G. Karapanagos, V. Petrouleas, The S1YZ; metalloradical EPR signal of photosystem II contains two distinct components that advance respectively to the multiline and $g=4.1$ conformations of S2, Biochemistry 46 (2007) 210–217.
[21] K.G.V. Havelius, J.-H. Su, Y. Feyziyev, F. Mamedov, S. Styring, Spectral resolution of the split EPR signals induced by illumination at 5 K from the S1, S3, and S0 states in photosystem II, Biochemistry 45 (2006) 9279–9290.
[22] J.H. Su, K.G.V. Havelius, F.M. Ho, G. Han, F. Mamedov, S. Styring, Formation spectra of the EPR split signals from the S0, S1, and S3 states in photosystem II induced by monochromatic light at 5 K, Biochemistry 46 (2007) 10703–10712.
[23] N. Ioannidis, G. Zahariou, V. Petrouleas, Trapping of the S2 to S3 state intermediate of the oxygen-evolving complex of photosystem II, Biochemistry 45 (2006) 6252–6259.
[24] T.M. Bricker, H.B. Pakrasi, L.A. Sherman, Characterization of a spinach photosystem II core preparation isolated by a simplified method, Arch. Biochem. Biophys. 237 (1985) 170–176.

[25] P.J. Smith, K.A. Ahrling, R.J. Pace, Nature of the S2 state electron paramagnetic resonance signals from the oxygen-evolving complex of photosystem II: Q-band and oriented X-band studies, J. Chem. Soc., Faraday Trans. 89 (1993) 2863–2868.
[26] P.J. Smith, S. Peterson, M. Masters, T. Wydrzynski, S. Styring, E. Krausz, R.J. Pace, Magneto-optical measurements of the pigments in fully active photosystem II core complexes from plants, Biochemistry 41 (2002) 1981–1989.
[27] J.L. Hughes, P. Smith, R. Pace, E. Krausz, Charge separation in photosystem II core complexes induced by 690–730 nm excitation at 1.7 K, Biochim. Biophys. Acta - Bioenergetics 1757 (2006) 841–851.
[28] S. Peterson, M. Masters, B.J. Prince, P.J. Smith, R.J. Pace, E. Krausz, Optical spectra of synechocystis and spinach photosystem II preparations at 1.7 K: identification of the D1-pheophytin energies and stark shifts, J. Am. Chem. Soc. 125 (2003) 13063–13074.
[29] A.W. Rutherford, J.L. Zimmermann, A new EPR signal attributed to the primary plastosemiquinone acceptor in photosystem II, Biochim. Biophys. Acta - Bioenergetics 767 (1984) 168–175.
[30] C. Zhang, S. Styring, Formation of split electron paramagnetic resonance signals in photosystem II suggests that tyrosine Z can be photooxidized at 5 K in the S0 and S1 states of the oxygen-evolving complex, Biochemistry 42 (2003) 8066–8076.
[31] D. Koulougliotis, C. Teutloff, Y. Sanakis, W. Lubitz, V. Petrouleas, The S1YZ. Metalloradical intermediate in photosystem II: an X- and W-band EPR study, Phys. Chem. Chem. Phys. 6 (2004) 4859–4863.
[32] J.-H. Su, K.G.V. Havelius, F. Mamedov, F.M. Ho, S. Styring, Split EPR signals from photosystem II are modified by methanol, reflecting S state-dependent binding and alterations in the magnetic coupling in the CaMn4 cluster, Biochemistry 45 (2006) 7617–7627.
[33] N. Ioannidis, G. Zahariou, V. Petrouleas, The EPR spectrum of tyrosine Z; and its decay kinetics in O2-evolving photosystem II preparations, Biochemistry 47 (2008) 6292–6300.
[34] G. Zahariou, N. Ioannidis, G. Sioros, V. Petrouleas, The collapse of the tyrosine Z-Mn spin–spin interaction above ~100 K reveals the spectrum of tyrosine Z. An application of rapid-scan EPR to the study of intermediates of the water splitting mechanism of photosystem II, Biochemistry 46 (2007) 14335–14341.
[35] R.G. Evelo, S. Styring, A.W. Rutherford, A.J. Hoff, EPR relaxation measurements of photosystem II reaction centers: influence of S-state oxidation and temperature, Biochim. Biophys. Acta 973 (1989) 428–442.
[36] C. Zhang, A. Boussac, A.W. Rutherford, Low-temperature electron transfer in photosystem II: a tyrosyl radical and semiquinone charge pair, Biochemistry 43 (2004) 13787–13795.
[37] B. Hallahan, S. Ruffle, S. Bowden, J.H.A. Nugent, Identification and characterisation of EPR signals involving QB semiquinone in plant Photosystem II, Biochim. Biophys. Acta 1059 (1991) 181–188.